Doctoral Thesis

# Theoretical studies on baryogenesis, neutrino mass, and dark matter in extended Higgs models


Kazuki Enomoto

*Department of Physics, Osaka University,*
*Toyonaka, Osaka, 560-0043, Japan*


大阪大学
OSAKA UNIVERSITY

OSAKA UNIVERSITY
School of Science
Graduate School of Science

# Acknowledgement

First of all, I would like to express my sincere gratitude to my supervisor, Prof. Shinya Kanemura for providing me with a lot of instruction to the research of particle physics. I would not have been able to complete this doctoral thesis without his guidance. I am also deeply thankful to the members of the doctoral thesis review committee, Prof. Tetsuya Onogi, Prof. Ryosuke Sato, Prof. Minoru Tanaka, and Prof. Hajime Nanjo for reading my thesis carefully and providing me with many useful comments. I am much obliged to my collaborators, Prof. Mayumi Aoki, Prof. Kei Yagyu, Prof. Hiroaki Sugiyama, Prof. Arindam Das, Dr. Kodai Sakurai, Mr. Kento Katayama, and Mr. Yushi Mura for our fruitful collaborations. I am grateful to the faculty members of the particle physics theory group at Osaka University, Prof. Hidenori Fukaya, Prof. Yutaka Hosotani, Prof. Satoshi Yamaguchi, and Prof. Norihiro Iizuka, and the secretaries, Ms. Satomi Suzuki and Ms. Kazumi Asano for their support of my research activities. I would also like to mention my thanks to the former faculty members of the group, Prof. Koji Hashimoto and Prof. Kinya Oda, and the former secretary, Ms. Mika Umetani for their support. I appreciate my colleagues in the group, Mr. Masashi Aiko, Mr. Naoki Kawai, Mr. Yoshiyuki Matsuki, and Mr. Masanori Tanaka for many exciting discussions and wonderful days. During a part of my Ph.D. program, I have been supported by the Sasakawa Scientific Research Grant from The Japan Science Society and JSPS KAKENHI Grant (No. JP21J11444). Finally, I would like to thank my family for their understanding and warm support.

# Abstract

Although the standard model in particle physics is a successful theory, it does not include the origins of some observed phenomena, for example, the baryon asymmetry of the universe, neutrino oscillations, and the existence of dark matter. Therefore, it is inevitable that physics beyond the standard model exists. In the standard model, the Higgs sector is assumed to be the minimal one without any theoretical principle. Then, it would be natural to consider that a non-minimal Higgs sector is realized in the physics beyond the standard model.

Several models including extended Higgs sectors have been studied. In some of them, the extended Higgs sector provides the origin of the unexplained phenomena. For example, electroweak baryogenesis, a mechanism for the production of the baryon asymmetry, can occur in some extended Higgs sectors with CP violation. The neutrino mass, which causes neutrino oscillations, can be generated by the quantum effects of additional scalar bosons. Furthermore, if a new scalar boson is electrically neutral and stable, it can be a candidate for dark matter.

Such models predict new particles whose mass scale is from the electroweak scale to the TeV scale. These are expected to be thoroughly tested in current and future experiments in the next few decades. Therefore, at the current stage of particle physics, they are quite interesting and important studies to examine the models with extended Higgs sector which includes the origins of the unexplained phenomena and to investigate how to test them by using various current and future experiments. In this doctoral thesis, I introduce two of our works based on this philosophy.

The first work is on electroweak baryogenesis in the two Higgs doublet model. In this model, the Higgs sector is extended by the second Higgs doublet. For successful electroweak baryogenesis, large enough CP violation and the strongly 1st order electroweak phase transition are essential, which are missing in the standard model. In the two Higgs doublet model, new CP-violating sources are supplied in the Higgs potential and the Yukawa interactions. In addition, the strongly 1st order phase transition can be realized by the non-decoupling effect of the additional scalar bosons.

Electroweak baryogenesis in the two Higgs doublet model has been investigated so far in some literature. However, it has been forced into a difficult situation as the experimental accuracy is improved. For example, the CP violation in the model is severely constrained by the measurements of the electric dipole moments. In addition, it has been revealed that the discovered Higgs boson behaves like the standard model one by the experimental result at the LHC so far.

In such a situation, a new scenario in the two Higgs doublet model was proposed. In this scenario, Yukawa interactions are assumed to be aligned to avoid dangerous flavor-changing neutral currents. To explain the observed nature of the Higgs boson, an alignment in the Higgs potential is also assumed so that coupling constants of the lightest Higgs boson coincide with those of the standard model Higgs boson at the tree level. Even under these simplifications, there are CP-violating phases in both the Higgs potential and the Yukawa interactions. By using the destructive interference between these CP-violating phases, it is possible to make the electric dipole moments small. Then, the severe experimental constraint on the electric dipole moments can be avoided while keeping each

CP-violating phase is large.

We investigate electroweak baryogenesis in this scenario. We find some benchmark scenarios where the observed baryon asymmetry can be reproduced under constraints from current experiments such as collider experiments, flavor experiments, and the measurements of the electric dipole moments. In these benchmark scenarios, the masses of the new scalar bosons are 300–400 GeV. They are expected to be directly produced in future high-energy colliders. In addition, in the benchmark scenarios, the prediction for the triple Higgs boson coupling is 35–55 % larger than the standard model prediction. This sizable deviation is expected to be detected in future Higgs precision measurements. We also discuss the verification of the scenarios by using other future experiments.

Next, we examine a TeV-scale extension of the two Higgs doublet model which can explain the origin of neutrino mass and the existence of dark matter in addition to the observed baryon asymmetry. In this model, a new $Z_2$ symmetry is imposed. The Higgs sector and the Yukawa interactions are further extended by new $Z_2$-odd particles: an isospin singlet charged scalar boson, a gauge singlet real scalar boson, and gauge singlet Majorana fermions.

New CP-violating sources are provided in the Higgs potential and the Yukawa interactions. The non-decoupling effect of the additional scalar bosons can make the electroweak phase transition strongly 1st order. Thus, baryon asymmetry can be produced by electroweak baryogenesis. Majorana-type masses of neutrinos are generated by the three-loop Feynman diagrams constituted by the additional scalar bosons and Majorana fermions. Furthermore, the real scalar boson or the lightest Majorana fermion can be the dark matter candidate.

As in the first work, we focus on the scenario, where the Higgs potential and the Yukawa interactions of the Higgs doublets are assumed to be aligned to explain the current experimental data. The severe constraints from the measurements of the electric dipole moments can be avoided by the destructive interference between the CP-violating phases in the Higgs potential and those in the Yukawa interactions.

We find a benchmark scenario in the model where all three phenomena can be simultaneously explained under the current experimental constraints such as collider experiments, flavor experiments, the measurements of the electric dipole moments, the direct search for dark matter, and the search for lepton flavor violation. The results of some numerical evaluations are shown. We also discuss the verification of the benchmark scenario by using various future experiments.

# Contents

# Chapter 1

# Introduction

The Standard Model (SM) in particle physics is a successful theory, which can explain many results in various experiments so far such as collider experiments, flavor experiments, and cosmological observations [1]. On the other hand, several phenomena have been observed that cannot be explained in the SM. For example, the Baryon Asymmetry of the Universe (BAU) [2, 3], neutrino oscillations [4–10], and the existence of Dark Matter (DM) [3]. Therefore, the SM is inherently an incomplete theory despite its success. There is no doubt about the existence of physics beyond the SM. Then, it is one of the most important issues in current particle physics to find out the nature of this new physics and to investigate how this is verified in current and future experiments.

The Higgs sector of the SM is the minimal one, where one isospin doublet scalar field, the Higgs doublet, is introduced [11, 12]. This is just a hypothesis, and there is no theoretical principle to guarantee its minimality. Although the Higgs sector has been partly revealed by the discovery of the Higgs boson in 2012 at the Large Hadron Collider (LHC) [13,14], the full structure of it is still unknown. There is thus still room to consider extensions of the Higgs sector by introducing new scalar bosons. Then, it would be natural to consider new models including extended Higgs sectors which have mechanisms to explain the observed mysterious phenomena such as the BAU, neutrino oscillation, and DM. In this thesis, we call such models *extended Higgs models*. Various extended Higgs models have been studied from this point of view. In the following, I introduce some examples.

The first example is extended Higgs models for the BAU. The evidence of nonzero BAU is given by the measurements of the cosmic abundance of light elements (deuteriums, heliums, and lithiums) [2] and the Cosmic Microwave Background (CMB) observation [3]. Considering cosmic inflation [15, 16], which is believed to have occurred in the early universe, the most plausible scenario to explain the observed BAU should be baryogenesis, where baryon number is produced in the baryon-symmetric universe after inflation. To realize baryogenesis, the three conditions which are known as Sakharov conditions have to be satisfied [17]; i) the existence of a baryon number violating process, ii) C and CP violation, and iii) departure from thermal equilibrium. Various mechanism to satisfy these conditions have been proposed so far, for example, GUT baryogenesis [18, 19], Affleck-Dine mechanism [20], Electroweak Baryogenesis (EWBG) [21], Leptogenesis [22], and so on.

Among these mechanisms, EWBG is especially important at the present stage of particle physics. In the scenario of EWBG, the baryon asymmetry is generated during the Electroweak Phase Transition (EWPT). Thus, it largely depends on the physics of the EWPT whether the observed baryon asymmetry can be reproduced in this scenario. The physics of the EWPT is expected to be thoroughly verified by using various experiments in the next few decades. Therefore, EWBG can be experimentally confirmed or excluded in the near future.

In the scenario of EWBG, the Sakharov conditions are satisfied as follows. The baryon number is violated in the weak Sphaleron transition at high temperatures [23]. C is broken by the electroweak gauge interactions. The source of CP violation is provided in the Higgs potential and/or Yukawa interactions. Departure from thermal equilibrium is realized by the strongly 1st order EWPT. By experiments so far, it has been revealed that EWBG cannot work in the SM because of two problems. First, the CP violation in the SM is not large enough for EWBG [24, 25]. Second, the EWPT in the SM is not strongly 1st order but the crossover transition [26–29]. Therefore, the extended Higgs sector including the source of CP violation is necessary for successful EWBG.

Many extended Higgs models for EWBG have been investigated so far. For example, EWPT and EWBG in the extended Higgs models with the isospin singlet with $Y = 0$, the isospin doublet with $Y = 1/2$, and the isospin triplet with $Y = 0$, where $Y$ denotes hypercharge are studied in Refs. [30–42], Refs. [43–58], and Refs. [59, 60], respectively.

Second, some extended Higgs models can explain the origin of tiny neutrino mass, which induces neutrino oscillations. To explain the observed neutrino oscillation data, at least two neutrinos must have tiny masses without degeneracy [4–10]. On the other hand, neutrinos are massless fermions in the SM since there are no right-handed neutrinos. In the case that right-handed neutrinos are added into the SM, neutrino mass is generated by the Vacuum Expectation Value (VEV) of the Higgs doublet. However, in this case, Yukawa couplings have to be unnaturally small. Therefore, a new mechanism to explain tiny neutrino masses is needed.

The most well-known one is the seesaw mechanism, in which Majorana-type masses of neutrinos are generated at tree level. There are three kinds of seesaw mechanisms, type-I, II, and III. In type-I seesaw mechanisms [61, 62], right-handed neutrinos with heavy Majorana mass are added into the SM. Then, neutrino mass is inversely proportional to the heavy neutrino mass. If the masses of heavy neutrinos are around the GUT scale ($\sim 10^{15}$ GeV), tiny neutrino mass can be explained while keeping $\mathcal{O}(1)$ Yukawa coupling. In type-II [62,63] and type-III [64] seesaw mechanisms, an isospin triplet scalar and isospin triplet fermions are added into the SM, respectively. If the masses of these new particles are around the GUT scale, tiny neutrino mass can be explained naturally.[1] Although the seesaw mechanism can naturally explain tiny neutrino mass, it is almost impossible to verify them experimentally because the scale of new particles is much higher than the scale of current collider experiments.

On the other hand, a different type model for neutrino mass was proposed by Zee [69]. In this model, the isospin singlet charged scalar boson and the second Higgs doublet are

[1]In type-II seesaw mechanism, tiny neutrino mass can also be explained by assuming a small scalar coupling. Then, the mass of the additional scalar bosons can be around the electroweak scale. Such a scenario is studied in Refs. [65–68].

added into the SM. Majorana neutrino mass is generated by a 1-loop Feynman diagram constituted by the additional scalar bosons. Then, the loop suppression factor and new coupling constants make neutrino mass small naturally. The mass scale of new particles is around the TeV scale. Therefore, it is expected that the additional scalar bosons can be tested in future experiments. Following this model, various models where Majorana neutrino masses are generated by the quantum effect of additional scalar bosons have been proposed so far [70–76]. Such models are often called *radiative seesaw models*.

Some radiative seesaw models can also explain the existence of DM by imposing a new $Z_2$ symmetry to stabilize the lightest $Z_2$-odd particle. Such a model was first proposed by Krauss, Nasri, and Trodden [74]. In this model, a $Z_2$-even singly charged scalar and a $Z_2$-odd one are added into the Higgs sector. In addition, $Z_2$-odd Majorana fermions are introduced. Majorana masses of these fermions provide the source of lepton number violation. Majorana neutrino mass is generated at the three-loop level. Furthermore, the lightest Majorana fermion is stable due to $Z_2$ symmetry. It can be the dark matter candidate. Various radiative seesaw models including the dark matter candidate have been proposed so far [73, 75, 76].

The extended Higgs models for Dirac neutrino masses have been also studied. In such models, although right-handed neutrinos are introduced to the SM, Yukawa interactions between right-handed neutrinos and the SM Higgs doublet are prohibited by the additional $Z_2$ or $U(1)$ symmetry. In the model proposed by Ref. [77], Dirac neutrino masses are generated at the tree level by the VEV of the additional isospin doublet scalar field. Assuming that this VEV is small enough, the generated Dirac neutrino mass can be as small as observed while keeping $\mathcal{O}(1)$ Yukawa couplings. Radiative seesaw models for the Dirac neutrino mass have been also studied so far [78–82]. In some of them [79–82], the DM candidate is included.

Finally, extended Higgs models are also investigated to explain the existence of DM. There are three simple cases for scalar DM; the gauge singlet DM [83–89], DM from an isospin doublet [90–94], and that from an isospin triplet with $Y = 0$ [95–97]. As mentioned above, they are also discussed with the BAU and/or neutrino mass. For example, EWBG in the $Z_2$-odd singlet scalar extension is discussed in Refs. [39–42]. The singlet scalar DM is included in some radiative seesaw models [75, 81]. The strongly 1st order EWPT caused by the doublet DM is discussed in Refs. [56–58]. Some radiative seesaw models [73,76,79,80,82] include such a DM candidate. The EWPT with an isospin triplet DM is investigated in Ref. [59].

As shown in the examples above, extended Higgs sectors are deeply related to the origin of unexplained phenomena, the BAU, neutrino mass, and DM. In addition, these extended Higgs models are expected to be tested by using current and future experiments. Consequently, it is an important and interesting work in current particle physics to consider such extended Higgs models and investigate how to verify them experimentally.

In this doctoral thesis, I introduce two of my works about extended Higgs models including the origin of unexplained phenomena. First, we evaluate the BAU generated via EWBG in a particular scenario of the CP-violating Two Higgs Doublet Model (THDM) [55]. In this scenario, we assume an alignment in the Yukawa interactions [98] to avoid dangerous Flavor Changing Neutral Currents (FCNCs). In addition, to satisfy the current constraints on the Higgs couplings at the LHC [99,100], we impose the assumption of the alignment in the Higgs potential [101] by which the lightest Higgs boson behaves like the SM one.

In Ref. [102], it has been shown that almost all parameter regions of the model can be tested by using the synergy of the direct search at the HL-LHC and the precision measurements of the Higgs boson couplings at the ILC with $\sqrt{s} = 250$ GeV together with discussions on perturbative unitarity and vacuum stability if this alignment is slightly broken. On the other hand, the alignment is kept exactly at the tree level, there are some regions that cannot be fully explored by the synergy of the HL-LHC and the ILC with $\sqrt{s} = 250$ GeV. Therefore, in the near future, the scenario with the alignment in the Higgs potential would be more important as experimental data are accumulated at collider experiments.

There are some references where the same scenario of the THDM is investigated. Constraints on the model from the Electric Dipole Moment (EDM) measurements have been studied in Ref. [101]. Collider phenomenology at hadron colliders and lepton colliders have been discussed in Ref. [103] and Ref. [104], respectively. On the other hand, we investigate whether the observed BAU can be reproduced via EWBG in the model under current experimental constraints.

We consider the charge transport scenario of top quarks, where the main source of CP violation is given by the Yukawa interactions between the top quark and the Higgs bosons [45,46]. The severe constraints from the electron EDM (eEDM) can be avoided by the destructive interference of the CP-violating phase in the Yukawa interaction and that in the Higgs potential [101]. The WKB method [105–109] is used to evaluate the BAU.

We provide benchmark scenarios of the model where the observed BAU can be reproduced with avoiding the theoretical bound from perturbative unitarity and vacuum stability and experimental constraints from the currently available data from EDM measurements, collider experiments, and flavor experiments.

Second, we study the TeV-scale extension of the model studied in the first one [110]. In this model, tiny neutrino mass and DM can also be explained in addition to the BAU. The model includes the additional $Z_2$ symmetry. Some $Z_2$-odd particles, charged scalar boson, real scalar boson, and Majorana fermions, are added. The real scalar boson or the lightest Majorana fermion can be the DM candidate. In addition, Majorana-type masses of neutrinos are generated at the three-loop level by a new Yukawa interaction and new scalar couplings.

The original idea of the model was proposed in Ref. [75]. However, in Ref. [75], CP violation in the Higgs potential is neglected for the sake of simplicity. Therefore, they only showed that the strongly 1st order EWPT can be realized while explaining data of neutrino oscillation and DM relic abundance under some experimental constraints at the time. We take into account the CP violation to investigate EWBG in the model. In addition, to avoid the severe constraints from the EDM measurements, we extend the original model in Ref. [75] according to the idea proposed in Ref. [101].

We show a benchmark scenario of the model where all the three problems can be explained simultaneously under various theoretically and experimentally constraints such as collider experiments, flavor experiments, the electric dipole measurements, the direct search of DM, and cosmological observables. Phenomenological consequences for the model are also discussed.

The paper of the first work is available on the arXiv and has been accepted by JHEP [55]. The second one is a work in progress and the paper is in preparation [110].

This thesis is organized as follows. In Chap. 2, some basic facts of the SM are shortly reviewed. In Chap. 3, the phenomena which cannot be explained in the SM, the BAU, neutrino oscillation, and DM are discussed. Chap. 4 and Chap. 5 are based on my works. In Chap. 4, EWBG is studied in the CP-violating THDM where both the Yukawa interactions and the Higgs potential of the model are aligned. In Chap. 5, the extension of the model studied in Chap. 4 is discussed. The summary of this thesis is provided In Chap. 6.

# Chapter 2

# Review of the standard model in particle physics

In this chapter, I review the SM in particle physics. In particular, I mainly discuss the electroweak interaction and the Higgs sector, which is known as the Glashow-Weinberg-Salam theory [11, 12, 111]. In the first section, I introduce the gauge groups and the fields in the model. In the second section, we discuss the mass generation for the gauge bosons by the Higgs mechanism [112–114], which is induced by the VEV of a scalar field. In the third section, I review that in the SM, the masses of fermions are also provided by the VEV of a scalar field. In the fourth section, we investigate the gauge interaction of fermions in the SM. In the last section, we discuss the CKM matrix and CPV phase.

## 2.1 Components of the Standard Model

The SM is described by a gauge theory that contains $\mathrm{SU}(3)_C \times \mathrm{SU}(2)_L \times \mathrm{U}(1)_Y$ gauge symmetries. The gauge group $\mathrm{SU}(3)_C$ provides color symmetry, and the gauge boson for the symmetry is gluon $G^a_\mu$ ($a$ =1–8) which mediates the strong interaction. On the other hand, $\mathrm{SU}(2)_L \times \mathrm{U}(1)_Y$ provides electroweak symmetry which is partly broken by the VEV of a scalar field as discussed in the next section. Symmetry represented by $\mathrm{SU}(2)_L$ is called the isospin symmetry. The gauge bosons for $\mathrm{SU}(2)_L$ and $\mathrm{U}(1)_Y$ gauge symmetries are denoted by $W^a_\mu$ ($a$ =1–3) and $B_\mu$, respectively.

Matter contents in the SM and their quantum numbers are shown in Table 2.1. Numbers in boldface mean a representation of each gauge group: **3** is a triplet, **2** is a doublet, and **1** is a singlet. The quantum number for $\mathrm{U}(1)_Y$ symmetry is called hypercharge. The index $i$ (=1–3) represents a flavor (generation) of fermions. The subscript $L$ ($R$) for each fermion means that the fermion has left-handed (right-handed) chirality.

The fermion fields in the SM can be divided into two categories. One is fermions which are triplets of $SU(3)_C$, and the other is color singlet fermions. A fermion in the former is called quark, and one in the latter is called lepton. Quarks interact with gluons, on the other hand, leptons do not.

There are two kinds of isospin doublet fermions in the SM: $Q'_{iL}$ and $L'_{iL}$ ($i$ =1–3).

They are parametrized as follows;

$$Q'_{iL} = \begin{pmatrix} u'_{iL} \\ d'_{iL} \end{pmatrix}, \quad L'_{iL} = \begin{pmatrix} \nu'_{iL} \\ \ell'_{iL} \end{pmatrix}. \tag{2.1.1}$$

All other fermions in the SM are isospin singlets.

A kinetic term for the fermion $f$ is given by

$$\mathcal{L}^f_{kin} = i\overline{f}\gamma^\mu D_\mu f, \tag{2.1.2}$$

where $D_\mu$ is a covariant derivative for $f$ and is given by

$$D_\mu = \partial_\mu - ig_C \boldsymbol{G}_\mu - ig_L \boldsymbol{W}_\mu - ig_Y Y B_\mu. \tag{2.1.3}$$

The symbols $\boldsymbol{G}_\mu$ and $\boldsymbol{W}_\mu$ are defined as

$$\boldsymbol{G}_\mu = \sum_{a=1}^{8} G^a_\mu T^a, \quad \boldsymbol{W}_\mu = \sum_{a=1}^{3} W^a_\mu \tau^a, \tag{2.1.4}$$

where $T^a$ and $\tau^a$ are generators for $\mathrm{SU}(3)_C$ and $\mathrm{SU}(2)_L$ group, respectively. For example, the generator $T^a$ for color triplets is given by $\lambda^a/2$, where $\lambda^a$ ($a$ =1–8) is Gell-Mann matrix, and the generator $\tau^a$ for isospin doublets is given by $\sigma^a/2$, where $\sigma^a$ ($a$ =1–3) is Pauli matrix. The symbol $Y$ in Eq. (2.1.3) means the hypercharge of the fermion $f$. In addition, the coupling constants for interaction with gauge bosons $G_\mu$, $W_\mu$, and $B_\mu$ are denoted by $g_C$, $g_L$, and $g_Y$, respectively in Eq. (2.1.3).

In the SM, there is only one scalar field $\phi$, which is a color singlet and an isospin doublet whose hypercharge is $Y = \frac{1}{2}$. This scalar field is called the Higgs field. Its kinetic term is given by

$$\mathcal{L}^\phi_{kin} = |D_\mu \phi|^2, \tag{2.1.5}$$

where $D_\mu$ is a covariant derivative defined in Eq. (2.1.3). By substituting the quantum numbers of $\phi$, the covariant derivative for $\phi$ is given by

$$D_\mu = \partial_\mu - \frac{1}{2}\begin{pmatrix} g_L W^3_\mu + g_Y B_\mu & g_L(W^1_\mu - iW^2_\mu) \\ g_L(W^1_\mu + iW^2_\mu) & -g_L W^3_\mu + g_Y B_\mu \end{pmatrix}. \tag{2.1.6}$$

| | $Q'_{iL}$ | $u'_{iR}$ | $d'_{iR}$ | $L'_{iL}$ | $\ell'_{iR}$ | $\phi$ |
|---|---|---|---|---|---|---|
| Spin | $\frac{1}{2}$ | $+\frac{1}{2}$ | $+\frac{1}{2}$ | $+\frac{1}{2}$ | $+\frac{1}{2}$ | 0 |
| $\mathrm{SU}(3)_C$ | **3** | **3** | **3** | **1** | **1** | **1** |
| $\mathrm{SU}(2)_L$ | **2** | **1** | **1** | **2** | **1** | **2** |
| $\mathrm{U}(1)_Y$ | $+\frac{1}{6}$ | $+\frac{2}{3}$ | $-\frac{1}{3}$ | $-\frac{1}{2}$ | $-1$ | $+\frac{1}{2}$ |

Table 2.1: Matter contents in the SM and their quantum numbers.

Before closing this section, we note that in the SM, the mass terms for gauge bosons and fermion are not allowed by the gauge symmetries. For example, the mass terms for gauge bosons $W^a_\mu$ have the following form.

$$\mathcal{L}^W_{mass} = \frac{1}{2}\sum_{a=1}^{3} W^a_\mu W^{a\mu}. \tag{2.1.7}$$

Obviously, these are not invariant under $\mathrm{SU}(2)_L \times \mathrm{U}(1)_Y$ gauge transformations. The mass terms for fermions are also forbidden because the left-handed fermions and right-handed fermions have different quantum numbers. However, we know that fermions and weak gauge bosons are massive particles from experimental results so far.[1] This contradiction can be solved by the VEV of the Higgs field as explained in the next section.

## 2.2 Higgs mechanism and masses of gauge bosons

### 2.2.1 Spontaneous symmetry breaking

In the SM, the Higgs potential is given by

$$V = \mu^2|\phi|^2 + \lambda|\phi|^4. \tag{2.2.1}$$

This can be rewritten as follow;

$$V = \lambda\Big(|\phi|^2 + \frac{\mu^2}{2\lambda}\Big)^2, \tag{2.2.2}$$

where we neglect the constant term. The coupling constant $\lambda$ has to be positive for the vacuum stability. Then, the shape of the Higgs potential changes by whether $\mu^2$ is positive or negative.

In the case that $\mu^2$ is positive, the point $|\phi|^2 = 0$ is a stationary point. On the other hand, in the case that $\mu^2$ is negative, the stationary point is not the origin but the point where the following condition is satisfied;

$$|\phi|^2 = -\frac{\mu^2}{2\lambda}. \tag{2.2.3}$$

In other words, at the vacuum, the Higgs field has a nonzero VEV in the case that $\mu^2 < 0$. In the following, we focus on this case.

Since the stationary condition is an invariant of $\mathrm{SU}(2)_L \times \mathrm{U}(1)_Y$ symmetry, it leads to a degenerated vacuum. In the case that $\phi$ obtains a nonzero VEV, it is convenient to introduce a new scalar field that represents a deviation from a vacuum for perturbative calculations. To do this, we need to choose one point satisfying Eq. (2.2.3) as the origin of perturbations from the degenerated vacuum. This choice breaks $\mathrm{SU}(2)_L \times \mathrm{U}(1)_Y$ symmetry, while $\mathrm{SU}(3)_C$ symmetry remains unbroken because the Higgs field is a color singlet. Such a phenomenon where a choice of vacuum breaks symmetry is called spontaneous symmetry breaking.

[1] As discussed later, the lightest neutrinos can be a massless particle.

To study this phenomenon furthermore, we parametrize the Higgs field $\phi$ as

$$\phi = \begin{pmatrix} G^+ \\ \frac{1}{\sqrt{2}}(v + h + iG^0) \end{pmatrix}, \tag{2.2.4}$$

where $v$ is VEV and satisfies the condition,

$$v^2 = -\frac{\mu^2}{\lambda}. \tag{2.2.5}$$

Since the Higgs potential is invariant of $\mathrm{SU}(2)_L \times \mathrm{U}(1)_Y$ transformations, we can choose this parametrization without loss of generality. By substituting Eq. (2.2.4) into Eq. (2.2.2), the Higgs potential is given by

$$\begin{aligned} V = {} & 4\lambda v^2 h^2 + 4v\lambda\big(h^3 + h(G^0)^2 + h|G^+|^2\big) \\ & + \lambda\big(h^4 + (G^0)^4 + |G^+|^4 + 2h^2(G^0)^2 + 2h^2|G^+|^2 + 2(G^0)^2|G^+|^2\big). \end{aligned} \tag{2.2.6}$$

This form of the potential no longer has $\mathrm{SU}(2)_L \times \mathrm{U}(1)_Y$ symmetry.

From Eq. (2.2.6), we can see that the real scalar field $h$ acquires a mass $m_h = 2\sqrt{\lambda}v$, while other scalar field $G^0$ and $G^\pm$ are massless scalar bosons. These massless modes are known as Nambu-Goldstone modes (NG modes) [115–117], which accompany spontaneous symmetry breaking of continuous symmetries.

In relativistic systems, the number of NG modes coincides with the number of broken generators of symmetry [118].[2] In the case of the SM, there are three NG modes, while the number of generators of $\mathrm{SU}(2)_L \times \mathrm{U}(1)_Y$ group is four. Therefore, there is unbroken $U(1)$ symmetry after $\phi$ obtain the VEV.

The generator for the unbroken $U(1)$ symmetry is given by $Q = \tau^3 + Y$. By this $U(1)$ rotation, the Higgs field transforms as follows;

$$\phi \to e^{i\theta(\frac{\sigma^3}{2}+Y)}\phi = \begin{pmatrix} e^{i\theta}G^+ \\ \frac{1}{\sqrt{2}}(v + h + iG^0) \end{pmatrix}, \tag{2.2.7}$$

where $\theta$ is an arbitrary angle. Since the lower element of $\phi$ does not change, the VEV $v$ is an invariant of this transformation and does not break the U(1) symmetry. In the SM, this residual U(1) symmetry is identified as the electromagnetic symmetry, and the generator $Q$ is the electric charge.

To summarize the results so far, in the SM, $\mathrm{SU}(2)_L \times \mathrm{U}(1)_Y$ symmetry is spontaneously broken into the electromagnetic symmetry $\mathrm{U}(1)_{\mathrm{em}}$ by the VEV of the Higgs field. It leads to one massive mode and three massless modes. The massive scalar boson $h$ is called the Higgs boson, and it was discovered in ATLAS [13] and CMS [14] experiments at the LHC in 2012.

If $\mathrm{SU}(2)_L \times \mathrm{U}(1)_Y$ symmetry is a global symmetry, three NG modes $G^0$ and $G^\pm$ are physical massless modes. However, in the case of gauge symmetry, they are not physical modes and are absorbed into the longitudinal modes of gauge bosons. In the next section, we discuss this issue.

[2] In non-relativistic systems, the number of NG modes is not necessarily the same as that of broken generators [119, 120].

### 2.2.2 Higgs mechanism

In this section, we discuss the consequences of the VEV of the Higgs field on the gauge sector. By substituting the VEV $\langle\phi\rangle = \frac{1}{\sqrt{2}}(0, v)^{\mathrm{T}}$ into the kinetic term of the Higgs field in Eq. (2.1.5), we obtain the following;

$$\begin{aligned}\mathcal{L}^{\phi}_{kin} &= \frac{1}{8}(0, v)\begin{pmatrix} g_L W^3_\mu + g_Y B_\mu & g_L(W^1_\mu - iW^2_\mu) \\ g_L(W^1_\mu + iW^2_\mu) & -g_L W^3_\mu + g_Y B_\mu \end{pmatrix}^2 \begin{pmatrix} 0 \\ v \end{pmatrix} \\ &= m_W^2 W^+_\mu W^{-\mu} + \frac{1}{2} m_Z^2 Z_\mu Z^\mu, \end{aligned} \tag{2.2.8}$$

where $W^\pm_\mu$, $Z_\mu$, $m_W$, and $m_Z$ are defined as

$$W^\pm_\mu = \frac{1}{\sqrt{2}}(W^1_\mu \mp iW^2_\mu), \quad Z_\mu = \cos\theta_{\mathrm{w}} W^3_\mu - \sin\theta_{\mathrm{w}} B_\mu, \tag{2.2.9}$$

$$m_W = \frac{1}{2} v g_L, \quad m_Z = \frac{1}{2} v g_Z. \tag{2.2.10}$$

The angle $\theta_{\mathrm{w}}$ in Eq. (2.2.9) is defined to satisfy the equation,

$$\tan\theta_{\mathrm{w}} = \frac{g_Y}{g_L}. \tag{2.2.11}$$

The coupling constant $g_Z$ in Eq. (2.2.10) is defined as $g_Z = \sqrt{g_L^2 + g_Y^2}$.

From Eq. (2.2.8), we can see that by the VEV $v$, the masses of gauge bosons $W^\pm_\mu$ and $Z_\mu$ are generated. This is an important result of the spontaneous breaking of gauge symmetry. This mechanism of the mass generation for gauge bosons is called Higgs mechanism [112–114]. In the Higgs mechanism, gauge bosons corresponding to broken generators of gauge symmetry acquire masses proportional to the VEV.

A gauge boson for an unbroken generator remains massless mode. In the SM, the unbroken generator is $Q = \tau^3 + Y$. Therefore, the massless gauge boson is given by

$$A_\mu = \sin\theta_{\mathrm{w}} W^3_\mu + \cos\theta_{\mathrm{w}} B_\mu. \tag{2.2.12}$$

This is orthogonal to $Z_\mu$;

$$\begin{pmatrix} Z_\mu \\ A_\mu \end{pmatrix} = \begin{pmatrix} \cos\theta_{\mathrm{w}} & -\sin\theta_{\mathrm{w}} \\ \sin\theta_{\mathrm{w}} & \cos\theta_{\mathrm{w}} \end{pmatrix} \begin{pmatrix} W^3_\mu \\ B_\mu \end{pmatrix}. \tag{2.2.13}$$

As mentioned in the previous section, the residual U(1) symmetry is identified as the electromagnetic symmetry. Thus, the massless gauge boson $A_\mu$ represents the photon.

By the Higgs mechanism, three gauge bosons $W^\pm_\mu$ and $Z_\mu$ acquire masses. The degree of freedom of massive gauge bosons is three, one longitudinal component and two transverse components. On the other hand, that of massless gauge bosons is two, only transverse components. The increased degree of freedom is provided by NG modes. The NG modes $G^\pm$ and $G^0$ are absorbed into the longitudinal components of $W^\pm_\mu$ and $Z_\mu$, respectively [121].

## 2.3 Masses of fermions

In this section, we discuss masses of fermions in the SM. As mentioned above, in the SM, since the left-handed fermions and the right-handed fermions have different quantum numbers, mass terms for the fermions are forbidden. This problem is also solved by the VEV of the Higgs field.

In the SM, the following Yukawa interactions exist;

$$\mathcal{L}_Y = -\sum_{i,j=1}^{3}\Big\{(y'_u)_{ij}\overline{Q'_{iL}}\tilde{\phi}u'_{jR} + (y'_d)_{ij}\overline{Q'_{iL}}\phi d'_{jR} + (y'_\ell)_{ij}\overline{L'_{iL}}\phi\ell'_{jR}.\Big\} + \text{h.c.}, \tag{2.3.1}$$

where the field $\tilde{\phi} = i\sigma^2\phi^*$ is an isospin doublet whose hypercharge is $Y = -1/2$. By substituting the VEV $\langle\phi\rangle = \frac{1}{\sqrt{2}}(0, v)^{\mathrm{T}}$ into the Yukawa interactions, we obtain the following;

$$\mathcal{L}^f_{mass} = -\frac{v}{\sqrt{2}}\sum_{i,j=1}^{3}\Big\{(y'_u)_{ij}\overline{u'_{iL}}u'_{jR} + (y'_d)_{ij}\overline{d'_{iL}}d'_{jR} + (y'_\ell)_{ij}\overline{\ell'_{iL}}\ell'_{jR}.\Big\} + \text{h.c.} \tag{2.3.2}$$

These are mass terms for the SM fermions. We note that neutrinos $\nu_{iL}$ $(i = 1, 2, 3)$ cannot acquire mass terms because right-handed neutrinos are not included in the SM.

To diagonalize the mass matrices, we use biunitary transformations [122], by which any $n \times n$ matrix $X$ can be diagonalized by two appropriate unitary matrices $U$ and $V$ so that all diagonal elements of $V^\dagger XU$ are non-negative valued. We transform the fermions as follows;

$$f'_{iL} \to f_{iL} = \sum_{j=1}^{3}(V_f^\dagger)_{ij}f'_{jL}, \quad f'_{iR} \to f_{iR} = \sum_{j=1}^{3}(U_f^\dagger)_{ij}f'_{jR}, \tag{2.3.3}$$

where $f = u, d, \ell$, and matrices $U_f$ and $V_f$ are $3 \times 3$ unitary matrices. After these transformations, the mass terms for the SM fermions are given by

$$\mathcal{L}^f_{mass} = -\frac{1}{\sqrt{2}}\sum_{i=1}^{3}\Big\{(y_u)_i\overline{u_{iL}}u_{iR} + (y_d)_i\overline{d_{iL}}d_{iR} + (y_\ell)_i\overline{\ell_{iL}}\ell_{iR}.\Big\} + \text{h.c.}, \tag{2.3.4}$$

where matrices $y_f$ $(f = u, d, \ell)$ are defined as $y_f = V_f^\dagger y'_f U_f$, and the diagonal elements of $y_f$ are positive valued.

Then, Dirac fermions defined as

$$f_i = f_{iL} + f_{iR}, \quad (f = u, d, \ell), \tag{2.3.5}$$

are mass eigenstates, and mass eigenvalue for $f_i$ is given by $m_{f_i} = v(y_f)_i/\sqrt{2}$.

## 2.4 Gauge interactions of fermions

In this section, we investigate the consequences of the redefinition of the fermions in Eq. (2.3.3) on the gauge interactions. Before the redefinition, all gauge interactions are diagonal for the fermion flavors. After the redefinition, the interaction with $A_\mu$ and $Z_\mu$

remain flavor-diagonal. On the other hand, the interactions between $W^\pm$ and the redefined fermions are given by

$$\mathcal{L}^f_{W^\pm} = \frac{g_L}{\sqrt{2}} W^+_\mu \sum_{i,j=1}^{3} \Big( \overline{\nu'_i}\gamma^\mu P_L (V_\ell)_{ij}\ell_j + \overline{u_i}\gamma^\mu P_L (V_u^\dagger V_d)_{ij} d_j \Big) + \text{h.c.} \tag{2.4.1}$$

The matrices $V_\ell$ and $V_u^\dagger V_d$ are generally non-diagonal matrices and seem to induce flavor violations. However, the charged current for leptons can be flavor diagonal by using the following unitary transformation;

$$\nu'_{iL} \to \nu_{iL} = \sum_{j=1}^{3} (V_\ell^\dagger)_{ij}\nu_{jL}. \tag{2.4.2}$$

This transformation is allowed because neutrinos are massless fermions in the SM. Therefore, lepton flavors are conserved in the SM.

In the case of quarks, since both up-type quarks and down-type quarks are massive fermions, the charged currents for quarks cannot be diagonalized for flavors. The unitary matrix $V = V_u^\dagger V_d$, which induces quark flavor violations, is called the Cabibbo-Kobayashi-Maskawa (CKM) matrix [123, 124].

We summarize the gauge interactions of the fermions in the SM. They are given by

$$\mathcal{L}^f_{gauge} = eA_\mu J^\mu_{\text{EM}} + g_L\big\{ (W^+_\mu J^{+\mu}_W + \text{h.c.}) + Z_\mu J^\mu_Z \big\}, \tag{2.4.3}$$

where $e = g_L \sin\theta_{\text{w}}$. The currents $J^\mu_{\text{EM}}$, $J^{+\mu}_W$, and $J^\mu_Z$ are defined as

$$J^\mu_{\text{EM}} = \sum_{i=1}^{3} \Big( -\overline{\ell_i}\gamma^\mu \ell_i + \frac{2}{3}\overline{u_i}\gamma^\mu u_i - \frac{1}{3}\overline{d_i}\gamma^\mu d_i \Big), \tag{2.4.4}$$

$$J^{+\mu}_W = \frac{1}{\sqrt{2}} \sum_{i=1}^{3} \Big( \overline{\nu_i}\gamma^\mu P_L \ell_i + \sum_{j=1}^{3} \overline{u_i}\gamma^\mu P_L V_{ij} d_j \Big), \tag{2.4.5}$$

$$\begin{aligned} J^\mu_Z = \frac{1}{\cos\theta_{\text{w}}} \sum_{i=1}^{3} \Big( &- \sin^2\theta_{\text{w}} J^\mu_{\text{EM}} + \frac{1}{2}(\overline{\nu_i}\gamma^\mu P_L \nu_i - \overline{\ell_i}\gamma^\mu P_L \ell_i) \\ &+ \frac{1}{2}(\overline{u_i}\gamma^\mu P_L u_i - \overline{d_i}\gamma^\mu P_L d_i) \Big), \end{aligned} \tag{2.4.6}$$

where $P_L = (1-\gamma_5)/2$ is a chirality projection operator for the left-handed chirality.

In the SM, all the neutral currents conserve lepton and quark flavors. The flavor-changing processes occur only by the charged currents. This is an important feature of the SM; there is no Flavor Changing Neutral Current (FCNC) at the tree level.

FCNCs can be generated by 1-loop diagrams in the SM. Contributions from these diagrams are proportional to a difference between squared masses of quarks. If masses of quarks degenerate, FCNCs vanish because of the unitarity of the CKM matrix. Therefore, FCNCs in the SM are strongly suppressed. This mechanism to suppress FCNCs is known as Glashow-Iliopoulos-Maiani (GIM) mechanism [125]. This suppression has a good agreement with experimental results. In fact, experiments so far have shown that the branching ratios of processes with FCNCs are very small, for example, $\text{Br}(D^0 \to \mu^-\mu^+) < 6.2 \times 10^{-9}$ and $\text{Br}(B^0 \to \mu^-\mu^+) = 1.6 \times 10^{-10}$.

## 2.5 The CKM matrix and CP-violation

In this section, we discuss the CPV phase in the CKM matrix. For a general discussion, we assume that the number of the quark flavor is $N$. Then, the CKM matrix is a $N \times N$ matrix and has $N^2$ real parameters. On the other hand, a $N \times N$ real orthogonal matrix has $N(N-1)/2$ real parameters. Thus, the CKM matrix has $N(N+1)/2$ phases.

Not all phases in the CKM matrix are physical. Some of them can be canceled by an appropriate redefinition of the phases of quark fields. However, if at least one phase is reft after the rephasing, it provides a source of CP violation.

In the case that we redefine $u_{iL}$ and $d_{iL}$ ($i = 1$–$N$) as

$$u_{iL} \to e^{i\theta_{u_i}} u_{iL}, \quad d_{iL} \to e^{i\theta_{d_i}} d_{iL}, \tag{2.5.1}$$

the charged current of quarks transforms as follows;

$$\mathcal{L}^f_{W^\pm} \propto \sum_{i,j=1}^{N} W^+_\mu \overline{u_{iL}} \gamma^\mu V_{ij} d_{jL} \to \sum_{i,j=1}^{N} W^+_\mu \overline{u_{iL}} \gamma^\mu (e^{i(\theta_{d_j} - \theta_{u_i})} V_{ij}) d_{jL} \tag{2.5.2}$$

We can see that $2N-1$ phases can be canceled by rephasing the quark fields. Therefore, the number of the CPV phases in the CKM matrix is given by

$$\frac{N(N+1)}{2} - (2N-1) = \frac{(N-1)(N-2)}{2}. \tag{2.5.3}$$

If the number of quark flavors is one or two, there is no CPV phase in the CKM matrix. In the SM ($N = 3$), there is one CPV phase, Kobayashi-Maskawa (KM) phase. Historically, the third quark flavor was proposed by Kobayashi and Masukawa [124] to explain the CP violation observed in the decay of K meson $K_L \to \pi^- \pi^+$.

The CKM matrix is represented by three rotation angles and the KM phase. The standard parametrization of it is given by

$$\begin{aligned} V &= \begin{pmatrix} 1 & 0 & 0 \\ 0 & c_{23} & s_{23} \\ 0 & -s_{23} & c_{23} \end{pmatrix} \begin{pmatrix} c_{13} & 0 & s_{13}e^{-i\delta} \\ 0 & 1 & 0 \\ -s_{13} & 0 & c_{13} \end{pmatrix} \begin{pmatrix} c_{12} & s_{12} & 0 \\ -s_{12} & c_{12} & 0 \\ 0 & 0 & 1 \end{pmatrix} \\ &= \begin{pmatrix} c_{12}c_{13} & s_{12}c_{13} & s_{13}e^{-i\delta} \\ -s_{12}c_{23} - c_{12}s_{23}s_{13}e^{i\delta} & c_{12}c_{23} - s_{12}s_{23}s_{13}e^{i\delta} & s_{23}c_{13} \\ s_{12}s_{23} - c_{12}c_{23}s_{13}e^{i\delta} & -c_{12}s_{23} - s_{12}c_{23}s_{13}e^{i\delta} & c_{23}c_{13} \end{pmatrix}, \end{aligned} \tag{2.5.4}$$

where $c_{ij}$ and $s_{ij}$ ($i, j = 1, 2, 3$) is defined as

$$c_{ij} = \cos\theta_{ij}, \quad s_{ij} = \sin\theta_{ij}. \tag{2.5.5}$$

The KM phase is denoted by $\delta$. The Majorana CPV phases is denoted by $\alpha_1$ and $\alpha_2$, and in the case of Dirac neutrinos, they equals to 0.

An important quantity when discussing CP violation in CKM matrices is the Jarlskog invariant [126]. To discuss it, we consider the quark mass matrix shown in Eq. (2.3.2);

$$\mathcal{L}^q_{mass} = -\sum_{i=1}^{3}\Big\{(m'_u)_{ij}\overline{u'_{iL}}u'_{jR} + (m'_d)_{ij}\overline{d'_{iL}}d'_{jR} + \text{h.c.}\Big\}, \tag{2.5.6}$$

where $m'_q$ ($q = u, d$) is defined as $m'_q = y'_q v/\sqrt{2}$. By an appropriate unitary rotation of the right-handed quarks, the mass matrix $m'_q$ can be a positive semidefinite hermitian matrix [127]. Let denote these matrices as $H_u$ and $H_d$, respectively. The mass matrices $H_u$ and $H_d$ are diagonalized as follows;

$$H_u = U^\dagger m_u U, \quad H_d = U'^\dagger m_d U', \tag{2.5.7}$$

where $U$ and $U'$ are unitary matrices, and $m_u$ and $m_d$ are diagonal mass matrices. In this basis, the CKM matrix is given by $V = UU'^\dagger$.

We define a hermitian matrix $C$ as $[H_u, H_d] = iC$. If $C = 0$, $H_u$ and $H_d$ are commutative, i.e. they are simultaneously diagonalized. By using equation $U' = V^\dagger U$, $C$ is represented by

$$C = -iU^\dagger[m_u, V m_d V^\dagger]U. \tag{2.5.8}$$

Therefore, the determinant of $C$ can be represented by using only the experimental observables: the elements of the CKM matrix and the masses of quarks. The determinant of $C$ is calculated as

$$\begin{aligned}\det C =& \det\Big(-i[H_u, H_d]\Big)\\ =& -2(m_t - m_c)(m_t - m_u)(m_c - m_u)(m_b - m_s)(m_b - m_d)(m_s - m_d)J,\end{aligned} \tag{2.5.9}$$

where $J$ is the Jarlskog invariant defined as

$$\mathrm{Im}[V_{ij}V_{kl}V^*_{il}V^*_{kj}] = J\sum_{m,n}\epsilon_{ikm}\epsilon_{jln}. \tag{2.5.10}$$

In the CP-conserving case, $J$ vanish. As discussed above, by the rotation $u_{iL} \to e^{i\theta_{u_i}}u_{iL}$, $d_{iL} \to e^{i\theta_{d_i}}d_{iL}$, the element of the CKM matrix is transformed as

$$V_{ij} \to e^{i(\theta_{d_j} - \theta_{u_i})}V_{ij}. \tag{2.5.11}$$

Therefore, the Jarlskog invariant $J$ is the CP-violating parameter in the CKM matrix, which is the invariant of the phase definition of the CKM matrix.

More generally, we consider the function of the $H_u$ and $H_d$;

$$f(H_u) = \sum_{n=1}^{\infty} a_n H_u^n, \quad g(H_d) = \sum_{m=1}^{\infty} b_m H_d^m. \tag{2.5.12}$$

We define the matrix $C(f, g)$ as $[f(H_u), g(H_d)] = iC(f, g)$. Since $H_u$ and $H_d$ are the hermitian matrices, the determinant of $C(f, g)$ is simply calculated as

$$\det C(f, g) = -2F[f(H_u)]G[g(H_d)]J, \tag{2.5.13}$$

where $F$ and $G$ are defined as

$$F[f(H_u)] = \big(f(m_t) - f(m_c)\big)\big(f(m_t) - f(m_u)\big)\big(f(m_c) - f(m_u)\big), \tag{2.5.14}$$

$$G[g(H_d)] = \big(g(m_b) - g(m_s)\big)\big(g(m_b) - g(m_d)\big)\big(g(m_s) - g(m_d)\big). \tag{2.5.15}$$

Even in this case, the determinant of $C(f, g)$ is proportional to the Jarlskog invariant $J$.

# Chapter 3

# Review of problems in the Standard Model and new physics

In this chapter, I review some phenomena which cannot be explained in the SM. In the first section, I discuss the problem of the BAU. In the second section, I review the problem of neutrino mass. In the last section, I discuss the problem of DM. In each section, I introduce some examples of new physics to explain these phenomena.

## 3.1 Baryon asymmetry of the universe

The evidence of the BAU is given by two kinds of experiments. First, from the observation of the cosmic abundance of the light elements (deuteriums, heliums, and lithiums) and the theory of the Big Bang Nucleosynthesis (BBN), the baryon-to-photon ratio $\eta_B$, which is the ratio of the current baryon number density to the photon density. The latest 95 % confidence interval of $\eta_B$ is observed as [2]

$$5.8 \times 10^{-10} \leq \eta_B \leq 6.5 \times 10^{-10} \quad \text{(BBN)}. \tag{3.1.1}$$

Second, from the observation of the CMB by Planck [3], the baryon density parameter is observed as $\Omega_b h^2 = 0.0224 \pm 0.0001$. This is translated into the 95 % confidence interval of $\eta_B$ as

$$6.04 \times 10^{-10} \leq \eta_B \leq 6.20 \times 10^{-10} \quad \text{(CMB)}. \tag{3.1.2}$$

Considering the inflation, which is believed to have occurred in the early universe, it is a plausible scenario that the observed baryon asymmetry has been created after the inflation. This scenario is called baryogenesis. To generate the baryon asymmetry, the following three conditions, which is called the Sakharov condition, have to be satisfied [17]:

(1) The existence of a baryon number violating process.

(2) Violation of $C$ and $CP$ symmetry.

(3) Departure from thermal equilibrium.

The necessity of the first condition is obvious. Let $A + B \to X + Y$ be a process that violates the baryon number conservation by $n$. If $C$ symmetry is respected, the $C$ conjugate of the process ($A^C + B^C \to X^C + Y^C$), where the superscript $C$ means the charge conjugation, occurs at the same probability as the process $A + B \to X + Y$. The process $A^C + B^C \to X^C + Y^C$ violates the baryon number conservation by $-n$. Therefore, in total, no baryon number asymmetry is created. The violation of $CP$ symmetry is needed for the same reason. In addition, if the system is in thermal equilibrium, even in the case that $C$ and $CP$ symmetry are violated, a particle and its anti-particle have the same equilibrium distribution. Consequently, all three conditions are necessary to generate baryon asymmetry.

Many scenarios satisfying the Sakharov conditions are proposed so far, for example, GUT baryogenesis [18, 19], Affleck-Dine mechanism [20], EWBG [21], Leptogenesis [22], and so on. Among these mechanisms, the scenario of EWBG has high testability because the EWBG is physics at the electroweak scale. Thus, EWBG can be experimentally tested by using various experiments in the next few decades such as colliders, flavor experiments, and cosmological observations. Therefore, investigating EWBG is especially important at the present stage of particle physics. From this point of view, we focus on EWBG in the following of this section.

### 3.1.1 Electroweak baryogenesis

In this section, we outline the scenario of EWBG. In the EWBG, the Sakharov conditions are satisfied as follows;

(1) The sphaleron transition at high temperature [23].

(2) $C$: SU(2) $\times$ U(1) gauge interactions,
$CP$: The CP-violating phase in the Higgs potential and/or the Yukawa interactions.

(3) The 1st order electroweak phase transition.

The sphaleron transition is a non-perturbative process where the baryon number $B$ and lepton number $L$ are not conserved, while the number of $B - L$ is conserved. The classical vacua of the gauge sector are infinitely degenerated, and each vacuum is labeled by an integer called Chern-Simons number $N_{CS}$. The sphaleron transition is the transition between vacua with different Chern-Simons numbers. The change of Chern-Simons number is accompanied by that of $B+L$; $\Delta N_{CS} = \Delta(B+L)$. This transition rate is exponentially small at zero temperature;

$$\Gamma_{ws} \propto e^{-\frac{4\pi}{\alpha_W}} \sim 10^{-165}, \tag{3.1.3}$$

where $\alpha_w$ is coupling constants for the weak interaction, $\alpha_w = g_L^2/4\pi$. Thus, the sphaleron transition is highly suppressed in the zero-temperature, and the baryon number is conserved at low energies in the SM. However, at high temperatures, this process occurs frequently enough and be in equilibrium [23].

If the electroweak phase transition is 1st order, bubbles of the true vacuum are created. The space is divided into the symmetric phase and the broken phase. The created bubble expands and collides with each other. After some time, the true vacuum covers the entire space.

When the bubble expands, the equilibrium state of particles in the bubble and that out of the bubble is different because the mass of the particles depends on the VEV of the Higgs doublet. Therefore, around the bubble wall, the particles are far from thermal equilibrium. The expanding bubble wall causes non-equilibrium states.

The baryon asymmetry is created via the expanding bubble wall in the so-called charge transport scenario [128]. If there are CP-violation in the interaction between the bubble walls and the particles, the rate of reflection for particles is different from that for anti-particles. Then, the current of hypercharge is generated around the bubble wall. Around the bubble wall, the hypercharge is accumulated in the broken phase, and the opposite sign hypercharge is accumulated in the symmetric phase. It is important to note that no baryon asymmetry is created at this stage because the interaction between the bubble wall and the particles are baryon number conserving.

The accumulated hypercharge generates the chemical potential for the Chern-Simons number. This chemical potential $\mu_{CS}$ causes the difference between the rates with increasing $N_{CS}$ ($\Gamma_+$) and those with decreasing $N_{CS}$ ($\Gamma_-$) [129];

$$\frac{\Gamma_+}{\Gamma_-} \simeq \exp\left(-\frac{\mu_{CS}}{2T}\right). \tag{3.1.4}$$

This difference translates the accumulated hypercharge into the baryon asymmetry.

To avoid washing out the generated baryon asymmetry in the bubbles, the rate of the sphaleron transition in the broken phase has to decouple rapidly. This condition can be represented by

$$\Gamma^{\rm br}_{\rm sph} < H(T_n), \tag{3.1.5}$$

where $\Gamma^{\rm br}_{\rm sph}$ is the rate of the sphaleron transition at the broken phase, and $H(T_n)$ is the Hubble parameter at $T = T_n$. The temperature $T_n$ is the nucleation temperature, at which one bubble of true vacuum is expected to be produced per one Hubble volume. This condition is roughly evaluated as $v_n/T_n \gtrsim 1$ [21], where $v_n$ is the VEV at $T = T_n$. The condition in Eq. (3.1.5) is called the sphaleron decoupling condition, and the electroweak phase transition satisfying this condition is said to be strongly 1st order. Consequently, the electroweak phase transition has to be strongly 1st order to generate the baryon asymmetry by EWBG.

If EWBG goes well in the SM, it is interesting and economic. However, it has been revealed that EWBG cannot be realized in the SM. There are two problems. One is the smallness of the CP-violation in the CKM matrix. The EWBG in the SM has been investigated in Refs. [24, 25, 130]. In these references, the strongly 1st order EWPT is assumed to occur. In Ref [25], the authors give a conservative upper bound on the magnitude of the baryon-to-entropy ratio as

$$\left|\frac{n_B}{s}\right| < 10^{-26}. \tag{3.1.6}$$

The observed value is $n_B/s \sim 10^{-11}$.[1] Consequently, CP-violation in the SM is too small to provide enough CPV source for successful EWBG.

[1]Assuming the standard cosmology, the baryon-to-entropy ratio and the baryon-to-photon ratio $\eta_B$ are related as $\eta_B \simeq 7.04 \times n_B/s$.

The second problem is the fact that the electroweak phase transition is not strongly 1st order in the SM [26–29]. By lattice calculations [28, 29], it is known that the Higgs boson has to be lighter than 80 GeV to realize the strongly 1st order electroweak phase transition in the SM. However, the observed Higgs boson mass is about 125 GeV. Then, the electroweak phase transition in the SM is a crossover transition, and departure from the thermal equilibrium cannot be satisfied.

As a result, EWBG cannot occur in the SM. Therefore, we need new physics to explain the observed baryon asymmetry. To make the successful EWBG, an extension of the Higgs sector is essential. In addition, to supply enough CPV, new physics have to contain a new CP-violating source.

### 3.1.2 Electroweak phase transition

As discussed in the above section, the strongly 1st order EWPT is required for EWBG. However, it cannot occur in the SM because the Higgs boson is too heavy. In this section, we discuss the EWPT and how strongly 1st order EWPT can be caused by the effects of new physics.

In the SM, the Higgs doublet acquires the VEV $v = 246$ GeV, and the electroweak symmetry is spontaneously broken. However, by the thermal effect, the electroweak symmetry can be restored [131–134]. In such a scenario, in the early universe with higher temperatures than the electroweak scale ($T > T_{EW} \sim 100$ GeV), the state with $\langle \phi_h \rangle = 0$ is the ground state, where $\phi_h$ is the Higgs doublet, and the electroweak symmetry is maintained. As the universe expands and the temperature cools, the energy of the state with the nonzero VEV decreases. At a certain temperature $T = T_c \sim T_{EW}$, the energy of the state with the nonzero VEV degenerates with that of the state with $\langle \phi_h \rangle = 0$. This temperature $T_c$ is called the critical temperature. At lower temperatures $T < T_c$, the state with the nonzero VEV is the ground state, and the electroweak symmetry is spontaneously broken. Therefore, the state of the medium changes from the symmetric phase into the broken phase as the universe cools. This transition phenomenon is called the EWPT, and it is believed to have occurred in the early universe.[2]

In the following, we discuss the phase transition induced by the VEV of the scalar field. Although the number of scalar fields which acquire the VEV can be more than one, in the following, we consider the case that only one scalar field $\phi$ acquires the VEV as in the SM for the sake of simplicity. The physics of the phase transition is investigated by using the Helmholtz free energy $F$. Assuming that the VEV is spatially uniform, the free energy $F$ is proportional to the spatial volume $\Omega$. Let $V_{eff}$ be the free energy density; $V_{eff} = F/\Omega$. Then, $V_{eff}$ is the function of the temperature $T$ and the uniform VEV $\varphi = \langle \phi \rangle_T$. The function $V_{eff}(T, \varphi)$ is called the effective potential.

In thermal equilibrium, the free energy is the minimum. Therefore, the VEV at temperature $T$ is the configuration that minimizes the effective potential $V_{eff}$. From this point of view, the effective potential at zero temperature and that at high temperature ($T > T_{EW}$) is given by Fig. 3.1.

[2] It is possible to consider the scenario where the electroweak symmetry is not restored even at high temperatures [133]. Models for such a scenario are studied in Refs. [135–138].

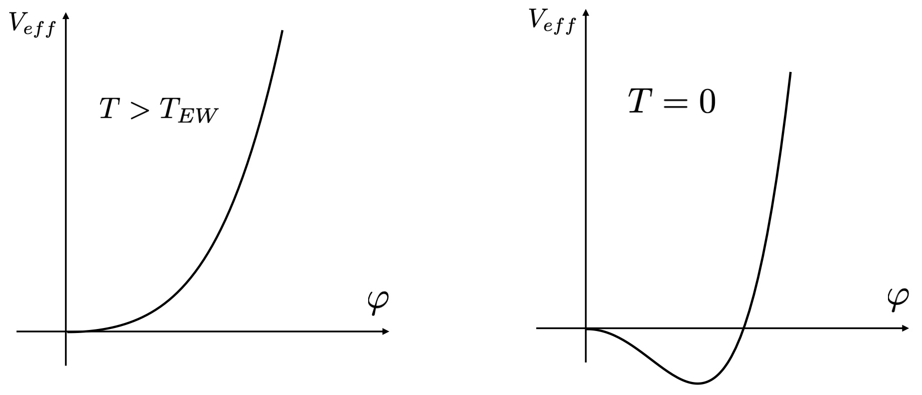


Figure 3.1: The effective potential at $T > T_{EW}$ (left) and $T = 0$ (right).

There are two main types of phase transitions; 2nd order phase transition and 1st order phase transition. The difference between them is the behavior of the transition from the symmetric phase (the left figure of Fig. 3.1) and the broken phase (the right one). In the 2nd order phase transition, the effective potential $V_{eff}$ changes with temperature as shown in the left figure of Fig. 3.2. The VEV changes slowly and homogeneously. On the other hand, the 1st order phase transition leads to the rapid change of the phase. The effective potential in the 1st order phase transition is shown in the right figure of Fig. 3.2. At the critical temperature $T = T_c$, there are two minima of the effective potential, and there is a barrier between the two configurations. At lower temperature $T < T_c$, the broken phase is the ground state and thermodynamically favorable. However, the transition to the broken phase is disturbed by the barrier and does not proceed homogeneously. Consequently, supercooling occurs, and a bubble of the true vacuum is locally generated. The 1st order phase transition proceeds via this nucleation and the expansion of the bubbles.

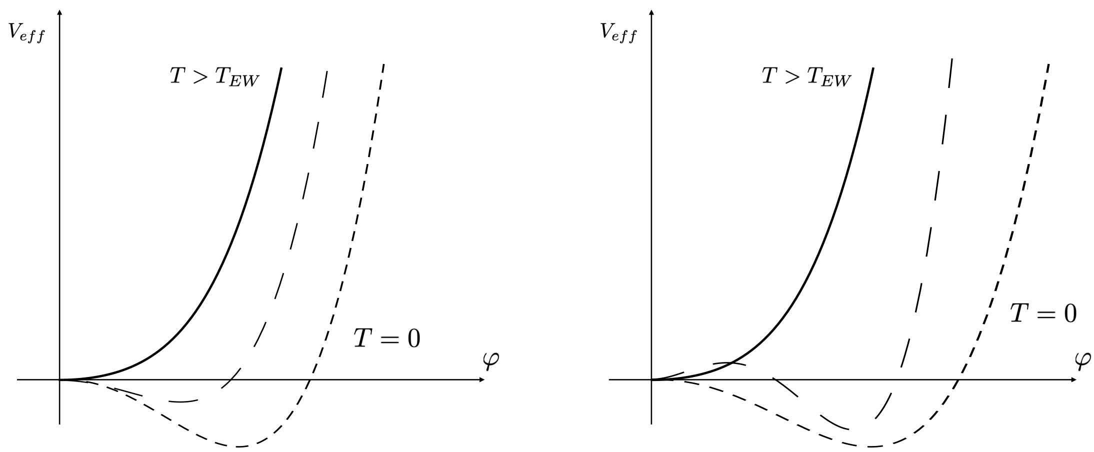


Figure 3.2: The behavior of the effective potential. The left (right) figure is for the 2nd (1st) order phase transition.

The behavior of the generated bubbles in the 1st order phase transition can be roughly understood by the following discussion. We consider the bubble nucleation at temperature $T$. The effective potential is defined as $V_{eff}(T, 0) = 0$, and we define $V_{min} = V_{eff}(T, \langle\phi\rangle) < 0$. Since the inside of the bubble is the broken phase, the gain of the free energy relative to the symmetric phase is given by

$$\Delta F = -\frac{4}{3}\pi R^3 |V_{min}|, \tag{3.1.7}$$

where $R$ is a radius of the bubble. On the other hand, since the configuration of $\phi$ has to be continuous, the effect of the surface tension increases the free energy. This effect is proportional to the surface area of the bubble. Thus, the total $\Delta F$ is given by

$$\Delta F = 4\pi R^2 \sigma - \frac{4}{3}\pi R^3 |V_{min}|, \tag{3.1.8}$$

where $\sigma$ is surface tension per unit area. The differential of $\Delta F$ by $R$ is calculated as

$$(\Delta F)' = \frac{\partial \Delta F}{\partial R} = 8\pi R\sigma - 4\pi R^2 |V_{min}| = 8\pi R\Big(\sigma - \frac{R}{2}|V_{min}|\Big). \tag{3.1.9}$$

Therefore, if the radius of the bubble is smaller than $R_c \equiv 2\sigma/|V_{min}|$, $(\Delta F)'$ is positive. The smaller $R$ is thermodynamically favorable, and the generated bubble collapses due to surface tension. On the other hand, if the radius of the bubble is bigger than $R_c$, $(\Delta F)'$ is negative. The bigger $R$ is thermodynamically favorable, and the generated bubble expands.

For EWBG, the 1st order phase transition is more important. We focus on this in the following. As discussed above, the barrier of the effective potential between the broken phase and the symmetric phase is needed to realize the 1st order phase transition. To discuss how this barrier is generated by the thermal effect, we consider the one-loop effective potential in SM-like models where the VEV of the Higgs doublet breaks the symmetry. Other particle contents are not fixed. It can be only the SM particles, or there can be additional particles. However, only the Higgs doublet acquire the VEV, and other scalar bosons do not (if they exist).

The tree-level Higgs potential is given by

$$V = -\mu^2 |\phi|^2 + \lambda |\phi|^4. \tag{3.1.10}$$

At zero temperature, the vacuum expectation value $v$ satisfies the following stationary condition;

$$\mu^2 = \lambda v^2. \tag{3.1.11}$$

The variable of the effective potential is defined as $\langle\phi\rangle = (0, v/\sqrt{2})^{\mathrm{T}}$. Neglecting the constant term, the tree level effective potential is given by

$$V_{eff}^{tree} = \frac{\lambda}{4}(\varphi^2 - v^2)^2. \tag{3.1.12}$$

The one-loop effective potential is given by [132]

$$V_{eff}^{1-loop} = \frac{\lambda}{4}(\varphi^2 - v^2)^2 - \delta\mu^2\varphi^2 + \delta\lambda\varphi^4 + \sum_{i=\text{bosons}} g_i I_{B_i} + \sum_{i=\text{fermions}} g_i I_{F_i}, \tag{3.1.13}$$

where $\delta\mu^2$ and $\delta\lambda$ are counterterms, and $g_i$ is the degree of freedom of each particle. The loop effect functions $I_B$ and $I_F$ are defined as

$$I_{B_i} = \int \frac{\mathrm{d}^3\mathrm{k}}{(2\pi)^3}\left\{\frac{E_i}{2} + \frac{1}{\beta}\log(1 - e^{-\beta E_i})\right\}, \tag{3.1.14}$$

$$I_{F_i} = -\int \frac{\mathrm{d}^3\mathrm{k}}{(2\pi)^3}\left\{\frac{E_i}{2} + \frac{1}{\beta}\log(1 + e^{-\beta E_i})\right\}, \tag{3.1.15}$$

where $E_i = \sqrt{k^2 + \tilde{m}_i^2}$ and $\tilde{m}_i(\varphi)$ is the field dependent mass of the particle $i$. The difference between $I_{B_i}$ and $I_{F_i}$ are caused by the statistical property of bosons and fermions. The first term of $I_{B_i}$ and $I_{F_i}$ are the quantum effect at $T = 0$.

To consider the thermal effect, we neglect the $\beta$ independent terms;

$$V_{eff}^{\beta} = \sum_{i=\text{bosons}} g_i I_{B_i}^{\beta} + \sum_{i=\text{fermions}} g_i I_{F_i}^{\beta}, \tag{3.1.16}$$

where

$$I_{B_i}^{\beta} = \frac{1}{\beta}\int \frac{\mathrm{d}^3\mathrm{k}}{(2\pi)^3}\log(1 - e^{-\beta E_i}), \quad I_{F_i}^{\beta} = -\frac{1}{\beta}\int \frac{\mathrm{d}^3\mathrm{k}}{(2\pi)^3}\frac{1}{\beta}\log(1 + e^{-\beta E_i}). \tag{3.1.17}$$

We consider the case of high temperature$m_i/T \ll 1$. Then, the thermal effect can be expanded as follows [30, 139];

$$V_{eff}^{\beta} = \frac{T^2}{24}\Big(\sum_{\text{bosons}} g_i \tilde{m}_i^2 + \frac{1}{2}\sum_{\text{fermions}} g_i \tilde{m}_i^2\Big). - \frac{T}{12\pi}\sum_{\text{bosons}} g_i \tilde{m}_i^3 + \mathcal{O}\Big(\tilde{m}_i^4 \log(\beta \tilde{m}_i)\Big). \tag{3.1.18}$$

Generally, the field-dependent mass $\tilde{m}_i^2$ is given by

$$\tilde{m}_i^2 = \frac{\lambda_i}{2}\varphi^2 + \mu_i^2, \tag{3.1.19}$$

where $m_i^2$ is the mass of particle $i$, $\mu_i^2$ is the invariant mass operator in Lagrangian, and the $\lambda_i$ is the coupling between the particle $i$ and the Higgs doublet. Then, the quadratic term of $\varphi^2$ comes from the first term of Eq. (3.1.18);

$$V_{eff}^{\beta} \ni \frac{T^2}{24}\frac{\varphi^2}{v^2}\Big(\sum_{\text{bosons}} g_i \lambda_i + \frac{1}{2}\sum_{\text{fermions}} g_i \lambda_i\Big). \tag{3.1.20}$$

This is the positive contribution and overcomes the tree level negative term $-\mu^2$ at a certain temperature. Consequently, the quadratic term of the effective potential is given by

$$V_{eff} \ni D(T^2 - T_0^2)\varphi^2, \tag{3.1.21}$$

where

$$D = \sum_{\text{bosons}} g_i \lambda_i + \frac{1}{2}\sum_{\text{fermions}} g_i \lambda_i. \tag{3.1.22}$$

At the temperature $T = T_0$, the thermal effect overcomes the tree-level potential. At higher temperature $T > T_0$, the quadratic term of the effective potential is positive.

The behavior of the second term in Eq. (3.1.18) is important for the 1st order phase transition. In the case that $m_i^2 \simeq \mu_i^2$, $\tilde{m}_i^3$ can be approximated by

$$\tilde{m}_i^3 \simeq \mu_i^3 + \frac{3}{2}\lambda_i \mu_i \varphi^2 + \mathcal{O}(\varphi^4). \tag{3.1.23}$$

Then, the effective potential is constituted by the quadratic term, the quartic term, and the higher term. Then, there is no barrier between the two phases. On the other hand, in the case that $m_i^2 \gg \mu_i^2$, the second term in Eq. (3.1.18) can be approximated by

$$V_{eff}^{\beta} \ni -\frac{T}{12\pi}\frac{\varphi^3}{v^3}\sum_{\text{bosons}} g_i m_i^3 \Big(1 - \frac{\mu_i^2}{m_i^2}\Big)^{\frac{3}{2}}. \tag{3.1.24}$$

Therefore, the cubic term in the effective potential is generated by the thermal effect of bosons in the case that $m_i^2 \gg \mu_i^2$. In such a case, the effective potential is given by

$$V_{eff} = D(T^2 - T_0^2)\varphi^2 - TE\varphi^3 + \lambda_T \varphi^4, \tag{3.1.25}$$

where $\lambda_T$ is the quartic coupling at temperature $T$, and the coefficient $E$ is defined as

$$E = \frac{1}{12\pi v^3}\sum_{\text{bosons}} g_i m_i^3 \Big(1 - \frac{\mu_i^2}{m_i^2}\Big)^{\frac{3}{2}}. \tag{3.1.26}$$

For successful EWBG, the strongly 1st order EWPT is required. We consider conditions for $D$, $E$, and $\lambda_T$ to realize the strongly 1st order EWPT. At the critical temperature $T_c$, two minima of the effective potential degenerate. One minimum is given by $\varphi = 0$. We define the other minimum as $\varphi = \varphi_c$. The following equation is derived as a condition for the point $\varphi = \varphi_c$ to give the local minimum;

$$\left.\frac{\partial V_{eff}}{\partial \varphi}\right|_{\varphi=\varphi_c} = 2D(T_c^2 - T_0^2)\varphi_c - 3T_c E\varphi_c^2 + 4\lambda_T \varphi_c^4 = 0. \tag{3.1.27}$$

Since the two minima degenerate, we obtain the condition,

$$V_{eff}(T_c, \varphi_c) = 4D(T_c^2 - T_0^2)\varphi_c^2 - 4T_c E\varphi_c^3 + 4\lambda_T \varphi_c^4 = 0. \tag{3.1.28}$$

By using these equations, the following relation is provided;

$$\frac{\varphi_c}{T_c} = \frac{E}{2\lambda_T}. \tag{3.1.29}$$

The sphaleron decoupling condition is given by $\varphi_n/T_n > 1$, where $T_n$ is the nucleation temperature and $\varphi_n$ is the VEV at $T = T_n$. Since the nucleation temperature and the critical temperature are close in most cases, the sphaleron decoupling condition is roughly evaluated as

$$\frac{\varphi_c}{T_c} = \frac{E}{2\lambda_T} > 1. \tag{3.1.30}$$

Therefore, for the strongly 1st order phase transition, the large $E$ is required.

An important property of the cubic term is that heavier $m_i$ induces the larger $E$. This is because we consider the case that $m_i^2 \gg \mu_i^2$. In this case, the heavier particle means the stronger coupling between the particle and the Higgs doublet. The effect of bosons does not decouple even in the heavier mass region. Such an effect is called the non-decoupling effect. Consequently, the non-decoupling effect of bosons induces the strongly 1st order phase transition. In the SM, there are gauge bosons and the Higgs bosons. However, it is known that the EWPT in the SM is not 1st order but a cross-over transition [28,29]. Therefore, to realize the strongly 1st order EWPT, the non-decoupling effect of the additional scalar bosons is necessary.

Before closing this section, we discuss the important consequences of the non-decoupling effect of the additional scalar bosons. It is known that the non-decoupling effect induces a sizable deviation of the triple Higgs boson coupling from the SM prediction [140–142]. To investigate them, we consider the zero temperature effective potential;

$$V_{eff}^{T=0} = \frac{\lambda}{4}(\varphi^2 - v^2)^2 - \delta\mu^2\varphi^2 + \delta\lambda\varphi^4 + \sum_{i=\text{Scalars}} g_i \int \frac{\mathrm{d}^3k}{(2\pi)^3}\frac{E_i}{2}. \tag{3.1.31}$$

We consider only the quantum effect of the additional scalar bosons because only the thermal effect by them is important. By using $\overline{\text{MS}}$ scheme, the integral is evaluated as

$$\int \frac{\mathrm{d}^3k}{(2\pi)^3}\frac{E_i}{2} = \frac{\tilde{m}_i^4}{64\pi^2}\log\left(\frac{\tilde{m}_i^2}{Q^2}\right), \tag{3.1.32}$$

where $Q$ is the renormalization scale. To determine the counterterms $\delta\mu^2$ and $\delta\lambda$, we impose the following renormalization conditions;

$$\left.\frac{\partial V_{eff}^{T=0}}{\partial\varphi}\right|_{\varphi=v} = 0, \qquad \left.\frac{\partial^2 V_{eff}^{T=0}}{\partial\varphi^2}\right|_{\varphi=v} = 2\lambda v^2. \tag{3.1.33}$$

The first and second equations fix the vacuum and the mass of the Higgs boson at one-loop level, respectively. Then, the contribution of the additional scalar bosons to the triple Higgs boson coupling is calculated as

$$\Delta\lambda_{hhh} = \frac{1}{3!}\left.\frac{\partial^3 V_{eff}^{T=0}}{\partial\varphi^3}\right|_{\varphi=v} = \sum_{\text{Scalars}} \frac{g_i}{24\pi^2 v^3}\frac{(m_i^2-\mu_i^2)^3}{m_i^2}. \tag{3.1.34}$$

The normalized deviation from the SM prediction is evaluated as [140, 141]

$$\Delta R = \frac{\Delta\lambda_{hhh}}{\lambda_{hhh}^{\text{SM}}} = \sum_{\text{Scalars}} \frac{g_i m_i^4}{12\pi^2 v^2 m_h^2}\left(1 - \frac{\mu_i^2}{m_i^2}\right)^3. \tag{3.1.35}$$

Therefore, in the case that $m_i^2 \gg \mu_i^2$, the effect of the additional scalar bosons does not decouple even in the heavy mass region. As a result, if the strongly 1st order EWPT is realized by the non-decoupling effect of the additional scalar bosons, $\Delta R$ is expected to be much larger than the SM prediction [143]. This is one of the effective ways to test the strongly 1st order EWPT.

### 3.1.3 WKB method for the charge transport scenario

In this section, I review the WKB method to calculate the charge accumulation in the charge transport scenario [105–109]. This approximation is valid in the case that the bubble wall width $L_w$ is larger than the typical interaction length of particles. At temperature $T$, the interaction length $\ell$ is roughly estimated as $\ell$ $1/T$. Therefore, the WKB method is applicable in the case of $L_w T > 1$.

#### WKB approximation and CP-violating force

When the bubble expands in the universe, the VEV of the Higgs doublet is not uniform in the entire space. At a point that is far from the vacuum bubble, the VEV remains zero although it is not thermodynamically stable. On the other hand, at the center of the bubble, the Higgs doublet acquires the nonzero VEV which minimizes the effective potential. In addition, at a point near the bubble wall, the VEV is different from that in the symmetric phase and from that in the broken phase because the configuration of the Higgs doublet is continuous. Therefore, the effect of the bubble generated in the 1st order EWPT can be described as the local VEV of the Higgs doublet. (See Fig. 3.3.)

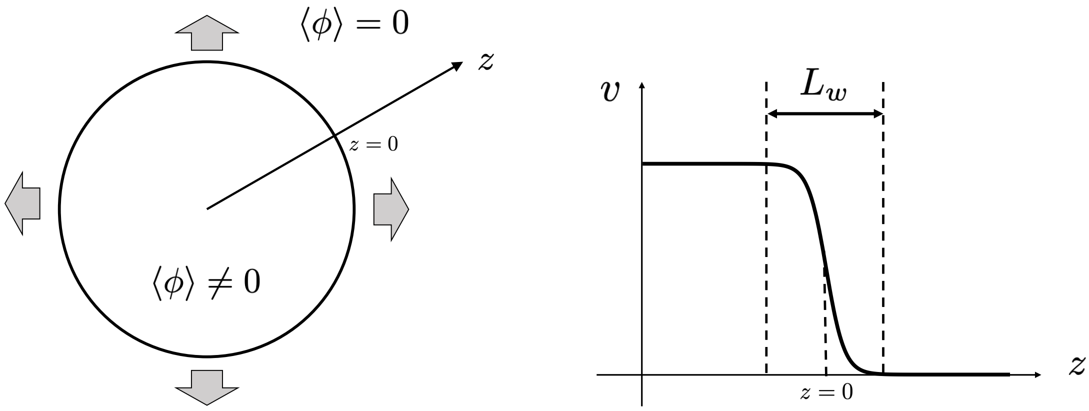


Figure 3.3: The definition of the coordinate $z$ in the wall frame (left) and the loccal VEV as a function of $z$ (right).

The SM particles acquire mass due to the Higgs mechanism. The local VEV means that the mass of the SM particles changes spatially. Therefore, the interaction between the expanding bubble wall and the particles can be described as the local mass of the particles.

To consider motions of the particles when the strongly 1st order EWPT occurs, we consider the Dirac equation for fermion $\psi$ which has the local mass. By solving the Dirac equation by using the WKB approximation, the force acting on the particles from the bubble wall is derived. We consider the problem in the wall frame, which is the coordinate where the radial direction of the bubble of true vacuum is set to be $z$ axis, and the bubble wall is stationary at $z = 0$ (See Fig. 3.3.) The negative direction of z is defined as pointing toward the center of the bubble.

The local mass is generally complex-valued. The mass term of the fermion $\psi$ is given by

$$\begin{aligned}\mathcal{L}_{\psi\text{-mass}} =& - M(z)\overline{\psi}P_R\psi + M(z)^*\overline{\psi}P_L\psi \\ =& \mathrm{Re}[M(z)]\overline{\psi}\psi + i\mathrm{Im}[M(z)]\overline{\psi}\gamma_5\psi. \end{aligned} \tag{3.1.36}$$

Since $\overline{\psi}\gamma_5\psi$ has odd-parity under the $P$ and $CP$ transformation, the imaginary part of the local mass is the source of P and CP violation.

The Dirac equation for $\psi$ is given by

$$(i\gamma^\mu\partial_\mu - M(z)P_R - M^*(z)P_L)\psi = 0, \tag{3.1.37}$$

where $M(z)$ is the local mass of the fermion $\psi$. The wave function of the positive energy state is given by

$$\psi_s = e^{-i\omega}\begin{pmatrix} L_s \\ R_s \end{pmatrix} \otimes \chi_s, \quad \sigma^3\chi_s = s\chi_s \tag{3.1.38}$$

where $s$ is spin along $z$ axis, and $\omega$ is the energy of $\psi$. By substituting $\psi_s$ into the Dirac equation, we obtain the following two equations;

$$(\omega - is\partial_z)L_s = MR_s, \tag{3.1.39}$$

$$(\omega + is\partial_z)R_s = M^*L_s. \tag{3.1.40}$$

By combing these equations to erase $R_s$, the equation for $L_s$ is given by

$$\Big((\omega + is\partial_z)\frac{1}{M}(\omega - is\partial_z) - M^*\Big)L_s = 0. \tag{3.1.41}$$

We assume that the mass term varies enough gradually along z. Then, the solution for $L_s$ under the WKB approximation is given by

$$L_s = \omega e^{i\int^z p_{cz}(z')\mathrm{d}z'}. \tag{3.1.42}$$

By substituting this formula into Eq. (3.1.41), the equations for $\omega$ and $p_{cz}$ are given as follows;

$$\begin{cases} \omega^2 - m^2 - p_{cz}^2 + (s\omega + p_{cz})\theta' - \frac{m'}{m}\frac{\omega'}{\omega} + \frac{\omega''}{\omega} = 0, \\ \\ 2p_{cz}\omega' + p_{cz}'\omega - \frac{m'}{m}(s\omega + p_{cz})\omega - \theta'\omega' = 0, \end{cases} \tag{3.1.43}$$

where the subscript $'$ means the derivative by $z$, and the functions $m(z)$ and $\theta(z)$ is defined as

$$m(z) = |M(z)|, \quad \theta(z) = \mathrm{arg}M(z). \tag{3.1.44}$$

Then, the solution for $p_{cz}$ up to the linear order of derivatives is calculated as

$$p_{cz} = p_{0z} \pm \frac{s\omega + p_{0z}}{2p_{0z}}\theta' + \alpha'(z), \tag{3.1.45}$$

where $\alpha(z)$ is an arbitrary function, and $p_{0z}$ is the solution at leading order and is given by

$$p_{0z} = \mathrm{sign}(p_{0z})\sqrt{\omega^2 - m^2}. \tag{3.1.46}$$

The sign of the second term of the right-hand side of Eq. (3.1.45) is + (−) for the particle (anti-particle). The energy of $\psi$ is given by

$$\omega = \sqrt{(p_{cz} - \alpha_{\mathrm{CP}})^2 + m^2} \mp \frac{s\theta'}{2}. \tag{3.1.47}$$

This is the dispersion relation in the frame where the particle $\psi$ does not have momentum in the direction parallel to the bubble wall. Boosting into the frame where $\psi$ has momentum in $x$ and $y$ direction, the dispersion relation is given by

$$\omega = \omega_0 \mp \frac{s\theta'}{2}\frac{\omega_{0z}}{\omega_0}, \tag{3.1.48}$$

where $\omega_0$ and $\omega_{0z}$ is defined as

$$\begin{aligned} \omega_0 &= \sqrt{p_x^2 + p_x^2 + (p_{cz} - \alpha_{\mathrm{CP}})^2 + m^2}, \\ \omega_{0z} &= \sqrt{(p_{cz} - \alpha_{\mathrm{CP}})^2 + m^2}. \end{aligned} \tag{3.1.49}$$

As suggested in Ref. [107, 144], the momentum $p_{cz}$ is the canonical momentum, not physical momentum because it includes the derivative of an arbitrary function. On the other hand, $p_x$ and $p_y$ are physical momenta because the morion in $x$ and $y$ direction is the same as that of free particles. The physical momentum in $z$ direction $p_z$ is calculated as $p_z = \omega v_{gz}$, where $v_{gz} = \partial\omega/\partial p_{cz}$ is a group velocity.

By using only physical quantity, the energy and the group velocity of the particle are represented as

$$E = E_0 \mp \Delta E, \tag{3.1.50}$$

$$v_{gz} = \frac{p_z}{E_0}\left(1 \pm \frac{s\theta'}{2}\frac{m^2}{E_0^2 E_{0z}}\right), \tag{3.1.51}$$

where $E$ is the energy $\omega$ which is represented by using $p_z$, and $E_0$, $E_{0z}$, and $\Delta E_0$ is defined as follows;

$$\Delta E = -\frac{sm^2\theta'}{2E_0 E_{0z}}, \tag{3.1.52}$$

$$E_0 = \sqrt{p_x^2 + p_y^2 + p_z^2 + m^2}, \tag{3.1.53}$$

$$E_{0z} = \sqrt{p_z^2 + m^2}. \tag{3.1.54}$$

Now, we are ready to find the forces acting on the particles. The force in $z$ direction $F_z$ is given by

$$F_z = \frac{\mathrm{d}p_z}{\mathrm{d}t} = \omega \dot{v}_{gz} = \omega\left\{v_{gz}\left(\frac{\partial v_{gz}}{\partial z}\right)_{p_{cz}} - \left(\frac{\partial\omega}{\partial z}\right)_{p_{cz}}\left(\frac{\partial v_{gz}}{\partial p_{cz}}\right)_z\right\}, \tag{3.1.55}$$

where we use the energy conservation $\dot{\omega} = 0$ and the canonical equations of motion. By substituting formulae for $\omega$ and $v_{gz}$, we obtain the following formula;

$$F_z = -\frac{(m^2)'}{2E_0} \pm \frac{s(m^2\theta')'}{2E_0 E_{0z}} \mp \frac{sm^2\theta'(m^2)'}{4E_0^3 E_{0z}}. \tag{3.1.56}$$

The sign of the second and third terms in the right-hand side of Eq. (3.1.56) change depending on whether the force act on the particle or the anti-particle. Therefore, they are CP-violating forces;

$$F_z^{\not{CP}} = \pm \frac{s(m^2\theta')'}{2E_0 E_{0z}} \mp \frac{sm^2\theta'(m^2)'}{4E_0^3 E_{0z}}. \tag{3.1.57}$$

This CP-violating force causes the difference between the motion of the particle and that of the anti-particle. The sign of CP-violating force $F_z^{\not{CP}}$ is changed by changing the helicity of $\psi$. It is because CP-violation and P-violation have the same origin, the imaginary part of the local mass.

**Transport equation**

In the above, we have derived the CP-violating force caused by the local mass. This induces the difference between the motion of the particle and that of its anti-particle around the bubble wall. This difference generates the current of the hypercharge, and the hypercharge is accumulated around the bubble wall. This charge accumulation is described by the chemical potential of the particle. Here, by using the Boltzmann equation and the CP-violating force, we derive a transport equation for the chemical potential. By solving this equation, we can obtain the distribution of the charge accumulation.

The Boltzmann equation in the wall frame for the distribution function $f_i(x, \boldsymbol{p})$ of the particle labeled by $i$ is given by

$$L[f_i] \equiv \left( v_{gz}\frac{\partial}{\partial z} + F_{iz}\frac{\partial}{\partial p_{iz}} \right) = C[f_i], \tag{3.1.58}$$

where $L[f_i]$ and $C[f_i]$ are the Liouville operator and the collision term for $f_i$, respectively. The force in the $z$ direction $F_{iz}$ includes both of the CP-even and CP-odd terms.

In the following, we assume that the state of fermion represented by the wave function in Eq. (3.1.42) behaves like a particle that has a kinetic momentum $(p_x, p_y, p_z)$ for the interactions whose mean free path $\Gamma^{-1}$ is less than the bubble wall width $L_w$. In other words, we assume that momenta are conserved in the scattering processes among the WKB states caused by interactions with $\Gamma^{-1} \ll L_w$, and the state behaves like a free particle at infinity. Therefore, in the calculation of the collision term in the Boltzmann equation, the usual Feynman rules can be used for the scattering among the WKB states.

Under this assumption, the thermal equilibrium distribution function in the wall frame of the WKB state is given by

$$f_i^{\mathrm{eq}}(x, \boldsymbol{p}) = \frac{1}{e^{\beta\gamma_w(E_{0i} \pm \Delta E_i + v_w p_{iz})} + 1}, \tag{3.1.59}$$

where $v_w$ is the wall velocity in the frame where the entire plasma is stationary. We parametrized the deviations from the thermal equilibrium as follows;

$$f_i(x,\boldsymbol{p}) = \frac{1}{e^{\beta[\gamma_w(E_{0i}\pm\Delta E_i+v_w p_{iz})-\mu_i(x)]}+1} + \delta f_i(x), \tag{3.1.60}$$

where the function $\delta f_i(x)$ is imposed not to affect the local number density of the particle $i$, i.e.

$$\int \mathrm{d}^3p\delta f_i = 0. \tag{3.1.61}$$

The chemical potential $\mu_i$ and the function $\delta f_i$ are parametrized as follows;

$$\mu_i = \mu_{\mathrm{i,1e}} + \mu_{\mathrm{i,2o}} + \mu_{\mathrm{i,2e}}, \quad \delta f_i = \delta f_{\mathrm{i,1e}} + \delta f_{\mathrm{i,2o}} + \delta f_{\mathrm{i,2e}}, \tag{3.1.62}$$

where the index 1 (2) shows the order of the perturbation, and CP-even (CP-odd) parts of each quantity have the index e (o). The CP-violating effect appears only in the second order of the perturbation. Then, the distribution function is expanded as

$$\begin{aligned} f_i \simeq\ & f_{i0,v_w} + f'_{i0,v_w}(\gamma_w\Delta E_i - \mu_{\mathrm{i,1e}} - \mu_{\mathrm{i,2o}} - \mu_{\mathrm{i,2e}}) \\ & + \frac{1}{2}f''_{i0,v_w}(\gamma_w^2(\Delta E)^2 - 2\gamma_w\Delta E\mu_{\mathrm{i,1e}}^2) + \delta f_{\mathrm{i,1e}} + \delta f_{\mathrm{i,2o}} + \delta f_{\mathrm{i,2e}}, \end{aligned} \tag{3.1.63}$$

where $f_{i0,v_w}$ is the unperturbed distribution function defined as

$$f_{i0,v_w} = \frac{1}{e^{\beta\gamma_w(E_{i0}+v_w p_{iz})}+1}. \tag{3.1.64}$$

By substituting Eq. (3.1.63) and the classical force in Eq. (3.1.56) into the Boltzmann equation, the CP-odd part of the Liouville operator is given by

$$\begin{aligned} \frac{1}{2}(L[f_i] - L[\overline{f_i}]) = \ & v_\omega f_{i0,v_w}\Big(\frac{s(m^2\theta')'}{2E_{i0}E_{i0z}} - \frac{s\theta' m^2(m^2)'}{4E_{i0}^3E_{i0z}}\Big) + v_\omega f''_{i0,v_\omega}\Big(\frac{s\theta' m^2(m^2)'}{4E_{i0}^2E_{i0z}}\Big) \\ & + \frac{(m^2)'\mu_{io}}{2E_{i0}\gamma_w}v_w f''_{i0,v_\omega} - \frac{p_{iz}\mu'_{io}}{E_{i0}\gamma_w}f'_{i0,v_w} + \frac{p_{iz}}{E_{i0}}(\partial_z\delta f_{io}) \\ & - \frac{(m^2)'}{2E_{i0}}(\partial_{p_{iz}}\delta f_{io}), \end{aligned} \tag{3.1.65}$$

where $\mu_{io}$ ($\delta f_{io}$) is the CP-odd part of $\mu_i$ ($\delta f_i$), and the function $f_{i0,v_\omega}$ is the unperturbed distribution function. In Eq. (3.1.65), we neglect the terms which is proportional to the CP-even part of $\mu_i$ or $\delta f_i$ because their effect on the baryon asymmetry is negligibly small [108]. The complete formula including the CP-even parts is shown in Ref. [45,108].

For simplicity, we assume that the wall velocity is enough small, and we expand $f_{i0,v_\omega}$ up to the linear order of $v_\omega$;

$$f_{i0,v_\omega} = f_{i0} + v_\omega p_{iz}f'_{i0} + \mathcal{O}(v_w^2), \tag{3.1.66}$$

where $f_{i0}$ and $f'_{i0}$ are defined as

$$f_{i0} = \frac{1}{e^{\beta E_{i0}} + 1}, \quad f'_{i0} = \frac{\mathrm{d}f_{i0}}{\mathrm{d}E_{i0}}. \tag{3.1.67}$$

In addition, we integrate Eq. (3.1.65) by three-momentum $\boldsymbol{p}_i$. Then, we obtain

$$\begin{aligned}\frac{1}{2}\left\langle L[f_i] - L[\overline{f}_i]\right\rangle &= \mu_{io} v_w (m^2)' \left\langle \frac{1}{2E_{i0}} f''_{i0} \right\rangle - \mu'_{io} v_\omega \left\langle \frac{p_{iz}^2}{E_{i0}} f''_{i0} \right\rangle \\ &+ \left\langle \frac{p_{iz}}{E_{i0}} (\partial_z \delta f_{io}) \right\rangle - (m^2)' \left\langle \frac{1}{2E_{i0}} (\partial_{p_{iz}} \delta f_{io}) \right\rangle, \end{aligned} \tag{3.1.68}$$

where the bracket $\langle \cdots \rangle$ is defined as

$$\langle X \rangle = \frac{\displaystyle\int \mathrm{d}^3 p_i \, X}{\displaystyle\int \mathrm{d}^3 p_i \, f'_{i0}(m_i = 0)}. \tag{3.1.69}$$

To perform the integrals including $\delta f_{io}$, we factorize it by using the plasma velocity $u_i$ defined as

$$u_i = \left\langle \frac{p_{iz}}{E_{i0}} \delta f_{io} \right\rangle. \tag{3.1.70}$$

In the other words, we evaluated the integral $\langle X \delta f_{io} \rangle$ as another integral $u_i \langle X E_{i0}/p_{iz} \rangle$.[3] Finally, we obtain the following result;

$$\frac{1}{2}\left\langle L[f_i] - L[\overline{f}_i]\right\rangle = v_w K_{i1} \mu'_{io} + v_w (m^2)' K_{i2} \mu_{io} + u'_i, \tag{3.1.71}$$

where $K_{i1}$ and $K_{i2}$ is given by [45, 108]

$$K_{i1} = \langle f'_{i0} \rangle, \quad K_{i2} = \left\langle \frac{1}{2E_{i0}} f''_{i0} \right\rangle. \tag{3.1.72}$$

In the same way, we can obtain the following equation;

$$\begin{aligned}\frac{1}{2}\left\langle \frac{p_{iz}}{E_{i0}} \left( L[f_{i0}] - L[\overline{f}_{i0}] \right) \right\rangle &= \lambda_i v_w (m^2\theta')' K_{i8} - \lambda_i v_w \theta' m^2 (m^2)' K_{i9} \\ &- \mu'_{io} K_{i4} + v_w (m^2)' u_i \tilde{K}_{i6} - v_w u'_i, \end{aligned} \tag{3.1.73}$$

where $\lambda_i$ is the helicity of the particle $i$. The functions $K_{i4}$, $\tilde{K}_{i6}$, $K_{i8}$, and $K_{i9}$ are defined in Ref. [45, 108] as

$$\begin{aligned} &K_{i4} = \left\langle \frac{p_{iz}^2}{E_{i0}^2} f'_{i0} \right\rangle, \quad \tilde{K_{i6}} = \left[ \frac{1}{2E_{i0}} f'_{i0} \right], \quad K_{i8} = \left\langle \frac{|p_{iz}| f'_{i0}}{2E_{i0}^2 E_{i0z}} \right\rangle, \\ &K_{i9} = \left\langle \frac{|p_{iz}|}{4E_{i0}^3 E_{i0z}} \left( \frac{f'_{i0}}{E_{i0}} - f''_{i0} \right) \right\rangle, \end{aligned} \tag{3.1.74}$$

[3] By this factorization, integrands of some integrals have the singularity at the origin because of $p_z$ in the denominator. In this case, we have to evaluate the integrals as Cauchy's principal values [109].

where the bracket $[\cdots]$ is given by

$$[X] = \frac{\displaystyle\int \mathrm{d}^3 p_i \, X}{\displaystyle\int \mathrm{d}^3 p_i \, f_{i0,v_w}}. \tag{3.1.75}$$

The integration of the collision term corresponding to Eqs. (3.1.71) and (3.1.73) is calculated in [107]. The results are given by

$$\begin{aligned}
&\frac{1}{2}\left\langle C[f_i] - C[\overline{f_i}]\right\rangle = \beta K_{i0} \sum_{\sigma\in\text{inela}} \Gamma_\sigma \sum_j s_j^\sigma \mu_{jo}, \\
&\frac{1}{2}\left\langle \frac{p_{iz}}{E_{i0}}(C[f_i] - C[\overline{f_i}])\right\rangle = \Gamma_{\text{tot}} u_i + v_w \beta K_{i0} \sum_{\sigma\in\text{inela}} \Gamma_\sigma \sum_j s_j^\sigma \mu_{jo},,
\end{aligned} \tag{3.1.76}$$

where $\Gamma_\sigma$ is the thermally averaged reaction rate for an inelastic scattering $\sigma$, and $\sum_{\sigma\in\text{inela}}$ means the sum for inelastic scattering processes $\sigma$. The symbol $s_j^\sigma$ is defined as $s_j^\sigma = 1$ ($s_j^\sigma = -1$) for $j$ in the initial (final) state of the process $\sigma$. The thermally averaged total reaction rate is denoted by $\Gamma_{\text{tot}}$ in Eq. (3.1.76). The function $K_{i0}$ in Eq. (3.1.76) is defined as

$$K_{i0} = -\left\langle f_{i0}\right\rangle. \tag{3.1.77}$$

Finally, By substituting Eqs. (3.1.71), (3.1.73), and (3.1.76) into the Boltzmann equation, we obtain the following two transport equations [45, 108];

$$\begin{cases}
u_i' + v_w K_{i1}\mu_{io}' + v_w (m^2)' K_{i2}\mu_{io} - \beta K_{i0} \sum_{\sigma\in\text{inela}} \Gamma_\sigma \sum_j s_j^\sigma \mu_{j0} = 0 \\
-\mu_{io}' K_{i4} - v_w u_i' + v_w (m^2)' \tilde{K}_{i6} u_i \\
\qquad\qquad\qquad + \Gamma_{\text{tot}} u_i + v_w \beta K_{i0} \sum_{\sigma\in\text{inela}} \Gamma_\sigma \sum_j s_j^\sigma \mu_{jo} = S_i.
\end{cases} \tag{3.1.78}$$

The source term $S_i$ is defined as

$$S_i = \lambda_i v_w \theta' m^2 (m^2)' K_{i9} - \lambda_i v_w (m^2 \theta')' K_{i8}. \tag{3.1.79}$$

In deriving Eq. (3.1.78), we have expanded $f_{i0,v_w}$ at linear order of $v_w$ for simplicity. The transport equation at full order of $v_w$ is investigated in Ref. [109]. According their results, an effect of the higher-order terms on the baryon asymmetry is negligibly small for $v_w$ less than 0.01. On the other hand, at $v_w = 0.1$, the effect of them can be estimated about 10–20 %, and the baryon asymmetry decreases due to the higher-order effect. As $v_w$ increases, the higher-order effects become larger. At $v_w \simeq 0.4$, the higher-order correction is about 50 %, and approximation would not be applicable.

### The formula for baryon asymmetry

By solving the above transport equations, the distributions of the chemical potentials are obtained. These are the distributions of the charge accumulation. However, at this stage, the baryon number asymmetry has not been produced yet because the interaction between the bubble wall and the particle is baryon number conserving.

The accumulated charge for the left-handed fermions provides the chemical potential of the Chern-Simons number $N_{CS}$. This chemical potential $\mu_{CS}$ causes the difference between the rates with increasing $N_{CS}$ ($\Gamma_+$) and those with decreasing $N_{CS}$ ($\Gamma_-$) [129];

$$\frac{\Gamma_+}{\Gamma_-} \simeq \exp\left(-\frac{\mu_{CS}}{2T}\right), \tag{3.1.80}$$

where $\beta = 1/T$ is the inverse temperature. Since the change of the Chern-Simons number $N_{CS}$ is the same as that of the $B + L$, i.e. $\Delta N_{CS} = \Delta(B + L)$, the difference between $\Gamma_+$ and $\Gamma_-$ produces baryon number asymmetry. Therefore, the accumulated charge described by the chemical potential provides the source of baryon asymmetry.

The change in the baryon number is described by the following differential equation [107];

$$\frac{\partial n_B}{\partial t} = \frac{3\Gamma_{sph}}{2}\Big(\mu_{q_L} T^2 - \frac{15}{2} n_B\Big). \tag{3.1.81}$$

The chemical potential $\mu_{q_L}$ is defined as

$$\mu_{q_L} = \frac{3}{2}(\mu_{u_L} + \mu_{d_L} + \mu_{c_L} + \mu_{s_L} + \mu_{t_L} + \mu_{b_L}), \tag{3.1.82}$$

where each chemical potential is given by solving the transport equations. The symbol $\Gamma_{sph}$ is the rate of the sphaleron transition in the symmetric phase. By lattice simulation, it is evaluated as $\Gamma_{ws} = 1.0 \times 10^{-6} T$ [145]. The first term of the right-hand side of the differential equation is the source term given by the charge accumulation. The second term represents the effect of the wash-out.

By solving the differential equation in the wall frame, the baryon asymmetry is given by

$$\frac{n_B}{s} = \frac{405\Gamma_{sph}}{4\pi^2 g_* v_w T}\int_0^\infty \mathrm{d}z\, \mu_{B_L} e^{-\nu z}, \tag{3.1.83}$$

where $\mu_{B_L} = \mu_{q_L}/3$ and $g_* = 106.75$ is the effective degree of freedom for entropy density at the EWPT. The symbol$\nu$ is defined as

$$\nu = \frac{45\Gamma_{sph}}{4v_w}. \tag{3.1.84}$$

The baryon-to-entropy ratio is determined by the chemical potential $\mu_{B_L}$ and the dimensionless parameter $A$ defined as

$$A = \frac{\Gamma_{sph}}{v_w T}. \tag{3.1.85}$$

Then baryon asymmetry is given by

$$\frac{n_B}{s} = \frac{405A}{4\pi^2 g_*}\int_0^\infty \mathrm{d}\hat{z}\, \left(\frac{\mu_{B_L}}{T}\right) e^{-\frac{45}{4}A\hat{z}}, \tag{3.1.86}$$

where $\hat{z} = zT$. In the limit of $A \to 0$ and $A \to \infty$, baryon asymmetry vanishes. This behavior can be interpreted as follows. The mean free path of the particle is roughly estimated as $\ell \sim 1/T$. Therefore, the charge accumulation is distributed in the $z \lesssim 1/T$. (See Fig. 3.4). The time it takes for the plasma in $z \lesssim 1/T$ to go inside the bubble is $\ell/v_w \sim 1/(v_w T)$. Therefore, the dimensionless quantity $A$ represents what times the sphaleron transition has occurred before the plasma in $z \lesssim \ell$ enters the bubble. If $A$ is too small, the accumulated charge is rarely converted to the baryon asymmetry. Thus, $n_B/s$ vanishes in the limit of $A \to 0$. On the other hand, in the limit of $A \to \infty$, the sphaleron transition occurs too frequently, and the baryon asymmetry vanishes due to the wash-out effect.

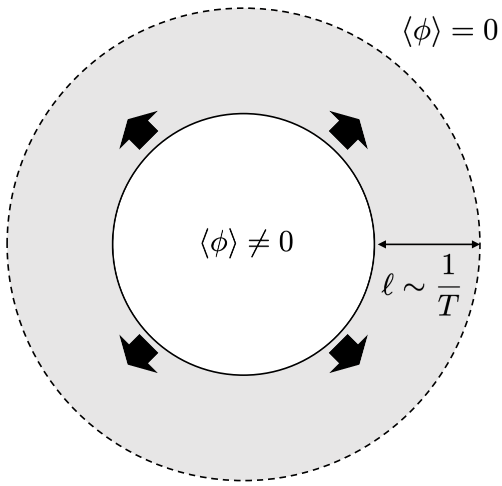


Figure 3.4: The charge accumulation out of the bubble. The circle with a solid line is the bubble wall. The gray region represents the accumulated charge out of the bubble. The width of the gray region is roughly estimated as $\ell \sim 1/T$.

## 3.2 Neutrino masses

By neutrino oscillation experiments so far, it has been shown that neutrinos have very small masses [4–6]. However, the origin of these tiny neutrino masses is still unknown. In this section, we discuss neutrino masses and their consequences. In addition, I introduce some new physics models for neutrino masses.

### 3.2.1 Neutrino masses and PMNS matrix

Neutrinos can have two kinds of mass terms. One is Dirac masses, which is constituted by left-handed fermion and right-handed fermion same with the other SM fermions. The other is Majorana masses, which contain only left-handed fermions (or only right-handed fermions). They are given by

$$\begin{aligned} &\text{Dirac mass} && (m'_\nu)_{ij}\overline{\nu_{iL}}\nu_{jR} + \text{h.c.} \\ &\text{Marjoana mass} && \frac{1}{2}(M'_\nu)_{ij}\overline{\nu^c_{ij}}\nu_{jL} + \text{h.c.}. \end{aligned} \tag{3.2.1}$$

To compose Dirac masses, it is necessary to introduce right-handed fermions to the SM. In the case that neutrinos have Dirac masses, neutrinos are Dirac fermions;

$$\nu_i = \nu_{iL} + \nu_{iR}. \tag{3.2.2}$$

On the other hand, in the case of Majorana masses, neutrinos are Majorana fermions;

$$\nu_i = \nu_{iL} + \nu_{iL}^c. \tag{3.2.3}$$

Majorana mass term is not invariant under a $U(1)$ rotation

$$\nu_{iL} \to e^{i\theta}\nu_{iL}. \tag{3.2.4}$$

This means that the number of neutrinos is not conserved. This is why the other SM fermions, which have electromagnetic charges, cannot have Majorana masses.

The Dirac mass matrix $m'_\nu$ is not generally diagonal to flavor. As mentioned in Sec. 2.3, it can be diagonalized by a bi-unitary transformation;

$$\nu_{iL} \to \nu_{aL} = \sum_{i=1}^{3} (U_\nu^\dagger)_{ai}\nu_{iL}, \tag{3.2.5}$$

$$\nu_{iR} \to \nu_{aR} = \sum_{i=1}^{3} (V_\nu^\dagger)_{ai}\nu_{iL}, \tag{3.2.6}$$

where $U_\nu$ and $V_\nu$ are appropriate unitary matrices, and then,

$$m'_\nu \to m_\nu = U_\nu^\dagger m_\nu V_\nu = \mathrm{diag}(m_{\nu_1}, m_{\nu_2}, m_{\nu_3}). \tag{3.2.7}$$

The Majorana mass matrix $M'_\nu$ is also not diagonal to flavor generally. However, it is a symmetric matrix. Then, it can be transformed into a diagonal matrix whose elements are non-negative valued by using an appropriate unitary matrix $\tilde{U}_\nu$ as follows [122].

$$\begin{aligned} \nu_{iL} &\to \nu_{aL} = \textstyle\sum_{i=1}^{3} (\tilde{U}_\nu^\dagger)_{ai}\nu_{iL}, \\ M'_\nu &\to M_\nu = \tilde{U}_\nu^{\mathrm{T}} M'_\nu \tilde{U} = \mathrm{diag}(M_{\nu_1}, M_{\nu_2}, M_{\nu_3}). \end{aligned} \tag{3.2.8}$$

An important point is that regardless of which type of masses neutrinos have, flavor eigenstates of neutrinos and mass eigenstates of them are related by a unitary matrix. This unitary matrix is called by Pontecorvo-Maki-Nakagawa-Sakata (PMNS) matrix [146,147]. In the following, the PMNS matrix is denoted by $U$, and flavor (mass) eigenstates of neutrinos are labeled by $i$, $j$, ... ($a$, $b$, ...);

$$\nu_\ell = \sum_{a=1}^{3} U_{\ell a}\nu_a. \tag{3.2.9}$$

Since the PMNS matrix is unitary, its elements are generally complex numbers. As in the case of the CKM matrix, not all of these phases are not physical, and some of them are canceled by rephasing of leptons.

In the case that neutrinos are Dirac fermions, the PMNS matrix includes $(N-1)(N-2)/2$ CPV phases, where $N$ is the number of lepton flavors, as discussed in the case of the CKM matrix. Thus, with three lepton flavors, the PMNS matrix has one CPV phase. This CPV phase is sometimes called the Dirac CPV phase.

In the case that neutrinos are Majorana fermions, we cannot change the phase of neutrinos because the Majorana mass terms are not invariant under the $U(1)$ rotation in Eq. (3.2.4). Therefore, only $N$ phases in the PMNS matrix are canceled by rephasing charged leptons. Then, the number of CPV phases in the PMNS matrix is $N(N-1)/2$, and it is three in the case of $N = 3$. The additional two phases are sometimes called Majorana CPV phases.

The PMNS matrix is parameterized as follows;

$$U = \begin{pmatrix} 1 & 0 & 0 \\ 0 & c_{23} & s_{23} \\ 0 & -s_{23} & c_{23} \end{pmatrix} \begin{pmatrix} c_{13} & 0 & s_{13}e^{-i\delta} \\ 0 & 1 & 0 \\ -s_{13} & 0 & c_{13} \end{pmatrix} \begin{pmatrix} c_{12} & s_{12} & 0 \\ -s_{12} & c_{12} & 0 \\ 0 & 0 & 1 \end{pmatrix} \begin{pmatrix} e^{i\alpha_1} & 0 & 0 \\ 0 & e^{i\alpha_2} & 0 \\ 0 & 0 & 1 \end{pmatrix}, \tag{3.2.10}$$

where $c_{ij}$ and $s_{ij}$ $(i, j = 1, 2, 3)$ is defined as

$$c_{ij} = \cos\theta_{ij}, \quad s_{ij} = \sin\theta_{ij}. \tag{3.2.11}$$

The Dirac CPV phase is denoted by $\delta$. The Majorana CPV phases is denoted by $\alpha_1$ and $\alpha_2$, and in the case of Dirac neutrinos, they equals to 0.

### 3.2.2 Phenomena induced by neutrino masses

In this section, I introduce some phenomena induced by neutrino masses.

#### Neutrino oscillation

Neutrino oscillation is a phenomenon where a flavor of neutrinos can change to another flavor, i.e.

$$\langle\nu_j|\nu_i(t)\rangle \neq 0, \quad i \neq j. \tag{3.2.12}$$

Here, I explain that neutrino masses induce this phenomenon. Discussion in this section is common to Dirac neutrinos and Majorana neutrinos.

We consider a neutrino which is a flavor eigenstate labeled by $i$ at the initial time $t = 0$. The amplitude to detect it as a different flavor eigenstate labeled by $j$ at the time $t$ is given by

$$\langle\nu_j|\nu_i(t)\rangle = \langle\nu_j| e^{-iHt} |\nu_i\rangle, \tag{3.2.13}$$

where $H$ is a Hamiltonian for neutrinos. In the case that the neutrino propagates as a free particle, then

$$|\nu_i(t)\rangle = \sum_{a=1}^{3} U_{ia} e^{-iE_a t} |\nu_a\rangle, \tag{3.2.14}$$

where $E_k = \sqrt{|\boldsymbol{p}|^2 + m_{\nu_a}^2}$ is an energy of the neutrino, and $\boldsymbol{p}$ is a three-momentum of it. Then, the amplitude is calculated as

$$\langle \nu_j | \nu_i(t) \rangle = \sum_{a=1}^{3} U_{ia} U_{ja}^* e^{-iE_a t}. \tag{3.2.15}$$

The probability of the transition $\nu_i \to \nu_j$ is given by

$$P_{\nu_i \to \nu_j} = \sum_{a,b=1}^{3} |U_{ia} U_{ja}^* U_{ib}^* U_{jb}| \cot\big((E_a - E_b)t - \varphi_{ij;ab}\big), \tag{3.2.16}$$

where $\varphi_{ij;ab} = \arg(U_{ia} U_{ja} U_{ib}^* U_{jb})$. By using the fact that neutrino masses are very small, the leading term of $P_{\nu_i \to \nu_j}$ is given by

$$P_{\nu_i \to \nu_j} \simeq \sum_{a,b=1}^{3} |U_{ia} U_{ja}^* U_{ib}^* U_{jb}| \cos\left( \frac{|\boldsymbol{p}| x}{2} \Delta m_{ab}^2 - \varphi_{ij;ab} \right), \tag{3.2.17}$$

where $\Delta m_{ab}^2 = m_{\nu_a}^2 - m_{\nu_b}^2$. In addition, in Eq. (3.2.17), we replace time $t$ with a propagation distance $x$ because neutrinos fly at almost the speed of light.

From Eq. (3.2.17), we can see that the probability of the process $\nu_i \to \nu_j$ is nonzero in the case that neutrinos are massive and not all their masses degenerate. Furthermore, it oscillates as a function of the propagation distance $x$.

In experiments, the distance from the source of neutrinos to detectors $x$ and the energy of neutrino beams $|\boldsymbol{p}|$ are fixed. Then, by measuring the probability $P_{\nu_i \to \nu_j}$, we can obtain information on the difference of squared masses $\Delta m_{ab}^2$ and the elements of the unitary matrix $U$. By fitting the combined data of results at various neutrino oscillation experiments, the following results are obtained [1].

$$\begin{aligned}
&\Delta m_{21}^2 = (7.53 \pm 0.18) \times 10^{-5}\ \mathrm{eV}^2, \\
&\Delta m_{32}^2 = (2.453 \pm 0.033) \times 10^{-3}, \quad \text{(Normal ordering)}, \\
&\Delta m_{32}^2 = (-2.536 \pm 0.034) \times 10^{-3}, \quad \text{(Inverted ordering)}, \\
&\sin^2\theta_{12} = 0.307 \pm 0.013, \\
&\sin^2\theta_{23} = 0.546 \pm 0.021, \quad \text{(Normal ordering)}, \\
&\sin^2\theta_{23} = 0.539 \pm 0.022, \quad \text{(Inverted ordering)}, \\
&\sin^3\theta_{13} = (2.20 \pm 0.07) \times 10^{-2}, \\
&\delta = 1.36^{+0.20}_{-0.16}\pi\ \mathrm{rad}.
\end{aligned} \tag{3.2.18}$$

The mass hierarchy between $\nu_2$ and $\nu_3$ is still not known. On the other hand, it is known that $\nu_2$ is heavier than $\nu_1$. The case that $m_{\nu_1} < m_{\nu_2} < m_{\nu_3}$ ($m_{\nu_3} < m_{\nu_1} < m_{\nu_2}$) is called the normal ordering (the inverted ordering). In Eq. (3.2.18), fitting values of $\Delta m_{23}$ and $\theta_{23}$ are different in the case of normal or inverted ordering. It is known that the probability of neutrino oscillations does not depend on the Majorana phases $\alpha_1$ and $\alpha_2$. Thus, they have not been measured yet.

**Lapton flavor violation**

Here, we discuss the effect of neutrino masses on the charged weak current. After the unitary transformation of neutrinos from flavor eigenstates to mass eigenstates, the interaction between $W^{\pm}$ and leptons are given by

$$\mathcal{L}^f \ni \frac{g_L}{\sqrt{2}} \sum_{i,a=1}^{3} \left( \overline{\nu_a} \gamma^\mu U^*_{\ell a} P_L \ell_i W^{+\mu} + \overline{\ell}_a \gamma^\mu U_{\ell a} P_L \nu_a W^{-\mu} \right). \tag{3.2.19}$$

These interactions induce Lepton Flavor Violation (LFV).

For example, the process $\mu \to e\gamma$ is generated via 1-loop diagrams [148]. The branching ratio for this process is given as follows

$$\mathrm{Br}(\mu \to e\gamma) = \frac{3}{32} \frac{\alpha}{\pi} \left| \sum_{a=1}^{3} U^*_{2a} U_{1a} \frac{m^2_{\nu_a}}{m^2_W} \right|^2 \sim 10^{-42}. \tag{3.2.20}$$

In the case of $m_{\nu_a} = 0$ $(a = 1, 2, 3)$, the branching ratio of $\mu \to e\gamma$ vanishes because the lepton flavor is conserved. Thus, the branching ratio for $\mu \to e\gamma$ via the PMNS matrix is so tiny.

The current upper limit of the process is given by $\mathrm{Br}(\mu \to e\gamma) \lesssim 4.2 \times 10^{-13}$. It is hopeless to measure the effect of neutrino masses in the current or near-future experiments. However, in some physics beyond the SM, there is another source of LFV, and larger LFV is expected. The observation of LFV processes such as $\mu \to e\gamma$ strongly constrains such new physics models.

**Lepton number violation**

As discussed in Sec. 3.2.1, the Majorana masses of neutrinos induce the conservation of the number of neutrinos. It causes the Lepton Number Violation (LNV). The lepton number is conserved in the SM and the case of Dirac neutrinos. Therefore, an observation of the LNV can be direct evidence of the Majorana nature of neutrinos.

The most effective way to verify the LNV is to observe neutrinoless double beta decay ($0\nu\beta\beta$). The most stringent limit on the half-life of the process is given by the KamLAND-Zen experiment as follows [149];

$$T_{1/2} > 1.07 \times 10^{26} \text{ years}. \tag{3.2.21}$$

. In this case that $0\nu\beta\beta$ is induced by the Majorana neutrino mass $M_\nu$, the $(1, 1)$ element of $M_\nu$ is constrained by KamLand-Zen results as

$$|(M_\nu)_{11}| < (61 - 165) \text{ meV}. \tag{3.2.22}$$

### 3.2.3 Seesaw mechanism

In the above, we have discussed the consequences of neutrino masses. From the results of neutrino oscillation experiments so far, it is unquestionable that neutrinos have masses. Then, what is the origin of the neutrino masses?

If neutrinos acquire masses from the VEV of the Higgs field in the same way as the other SM fermions, we have to introduce the right-handed neutrinos to the SM. Then, Dirac neutrino masses are given by

$$m_\nu = \frac{y_N}{\sqrt{2}} v, \tag{3.2.23}$$

where $y_N$ is the coupling constant of Yukawa interaction among left-handed lepton doublet, the Higgs field, and the right-handed neutrino. The VEV $v$ is measured as 246 GeV. On the other hand, it is known that neutrino masses are about $\mathcal{O}(0.1)$–$\mathcal{O}(0.01)$ eV. Then, to obtain the correct neutrino masses, we have to assume unnaturally small Yukawa coupling $y_N \simeq 10^{-(12\text{–}13)}$.

One of the more natural ways to explain tiny neutrino masses is given by seesaw mechanisms. In the mechanisms, physics at a high-energy scale provides the source of LNV, and it induces tiny neutrino masse at low energies. There are three types of seesaw mechanisms. In the following, they are explained in order.

### Type-I seesaw mechanism

In the Type-I seesaw mechanism, right-handed neutrinos $N_{aR}$ $(a = 1, 2, 3)$ are introduced to the SM. They have the following Majorana masses;

$$\mathcal{L}^N_{mass} = -\frac{1}{2} \sum_{a=1}^{3} M_{N_a} \overline{N^c_{aR}} N_{aR}, \tag{3.2.24}$$

where we fix the basis of the right-handed neutrinos so that the mass matrix for them is diagonal. The right-handed neutrinos have Yukawa interaction as follows;

$$\mathcal{L}_Y^{\text{Type-I}} = -\sum_{i,a=1}^{3} (y_N)_{ia} \overline{L_{iL}} \tilde{\phi} N_{aR} + \text{h.c.} \tag{3.2.25}$$

After the Higgs field obtains the VEV, the left-handed and right-handed neutrinos acquire the following neutrino mass matrix;

$$\mathcal{L}^{N\text{-}\nu}_{mass} = -\frac{1}{2} \overline{\boldsymbol{\nu}} \begin{pmatrix} 0 & m_\nu \\ m_\nu^{\mathrm{T}} & M_N \end{pmatrix} \boldsymbol{\nu} + \text{h.c.}, \tag{3.2.26}$$

where $\boldsymbol{\nu}$, $\overline{\boldsymbol{\nu}}$, and $m_\nu$ are defined as

$$\boldsymbol{\nu} = (\nu^c_{1L}, \nu^c_{2L}, \nu^c_{3L}, N_{1R}, N_{2R}, N_{3R})^{\mathrm{T}}, \tag{3.2.27}$$

$$\overline{\boldsymbol{\nu}} = (\overline{\nu^c_{1L}}, \overline{\nu^c_{2L}}, \overline{\nu^c_{3L}}, \overline{N_{1R}}, \overline{N_{2R}}, \overline{N_{3R}}), \tag{3.2.28}$$

$$m_\nu = \frac{v}{\sqrt{2}} y_\nu. \tag{3.2.29}$$

Under the assumption that $v \ll M_{N_a}$, Majorana mass matrix for light neutrinos are given by

$$M_\nu = -\frac{v^2}{2} y_N^* M_N^{-1} y_N^\dagger + \mathcal{O}\left(\frac{v^2}{M^2_{N_a}}\right). \tag{3.2.30}$$

Thus, in the case that $v/M_{N_a} \simeq 10^{-(12\text{-}13)}$, it is expected to obtain the correct neutrino masses with $\mathcal{O}(1)$ Yukawa couplings. Then, the scale of $M_{N_a}$ is about that of Grand Unified Theory (GUT);

$$M_{N_a} \simeq 10^{15}\ \text{GeV}. \tag{3.2.31}$$

**Type-II seesaw mechanism**

In the Type-II seesaw mechanism, an isospin triplet scalar field $\Delta$ whose hypercharge is 1 is introduced to the SM. The triplet scalar field $\Delta$ is parametrized as follows;

$$\Delta = \frac{1}{\sqrt{2}} \begin{pmatrix} \Delta^+ & \sqrt{2}\Delta^{++} \\ \sqrt{2}\Delta^0 & -\Delta^+ \end{pmatrix}. \tag{3.2.32}$$

The scalar potential is given by

$$V = -\mu^2|\phi|^2 + \lambda|\phi|^4 + m_\Delta^2 \text{Tr}[\Delta^\dagger\Delta] - \sigma\left(\phi^\dagger\Delta\phi^c\right) + \cdots , \tag{3.2.33}$$

where quartic couplings including $\Delta$ are omitted. The coupling $\sigma$ can be a real number by rephasing of $\Delta$.

Substituting the VEV of the Higgs field, the scalar potential is

$$V = -\sigma v^2 \text{Re}[\Delta^0] + m_\Delta^2|\Delta^0|^2 + \cdots \tag{3.2.34}$$

Then, the field $\Delta^0$ acquire the following VEV;

$$v_\Delta \equiv \left\langle \Delta^0 \right\rangle \simeq \frac{\sigma v^2}{2m_\Delta^2}, \tag{3.2.35}$$

where we assume that $m_\Delta > v$ and $\sigma \gg \langle\Delta^0\rangle$.

The triplet scalar field $\Delta$ interacts with lepton doublet via the Yukawa interaction

$$\mathcal{L}_Y^{\text{Type-II}} = \sum_{i,j=1}^{3} (Y_\Delta)_{ij} \overline{L_{iL}^c} \Delta L_{jL} + \text{h.c.} \tag{3.2.36}$$

By substituting the VEV of $\Delta^0$, Majorana neutrino masses are given by

$$M_\nu = \frac{\sigma v^2}{m_\Delta^2} Y_\Delta. \tag{3.2.37}$$

If $\sigma v/m_\Delta^2$ is about $10^{-(12\text{-}13)}$, it is expected that correct neutrino masses are realized with $\mathcal{O}(1)$ Yukawa couplings.

If we assume that $\sigma \simeq m_\Delta$, the scale of $m_\Delta$ is about GUT scale. On the other hand, if we assume that smaller $\sigma$ and smaller Yukawa couplings (but not unnaturally small), the scale of $M_\Delta$ can be the same order as $v$. Then, it would be expected to discover the additional scalar bosons $\Delta^{++}$, $\Delta^+$ and $\Delta^0$ at current or near-future collider experiments. By this phenomenological motivation, the scenario with $m_\Delta \simeq v$ has been investigated well [65–68].

Finally, we comment about a constrain on the VEV of $\Delta$. The VEV of the triplet scalar $v_\Delta$ violates the custodial symmetry [150–156] in the scalar potential. Then, the $\rho$ parameter is given by

$$\rho = \frac{1+2x^2}{1+4x^2}, \tag{3.2.38}$$

where $x = v_\Delta/v$. With the assumption that $x \ll 1$, $\rho$ is approximated by $\rho \simeq 1-2x^2$. The current constraint on $\rho-1$ from new physics contribution is given by $\delta\rho_{\rm new} = 0.05\pm0.06$ [1]. Then, the upper limit on $x$ is evaluated as $x \lesssim 0.3$ with 95 % C.L. Consequently, the VEV $v_\Delta$ is limited by about 70 GeV.

**Type-III seesaw mechanism**

In the Type-III seesaw mechanism, right-handed triplet fermions $\Sigma_{aR}$ $(a = 1, 2, 3)$ whose hypercharge is 0 are introduced to the SM. The triplet field is parameterized as

$$\Sigma_{aR} = \frac{1}{\sqrt{2}} \begin{pmatrix} \Sigma^0_{aR} & \sqrt{2}\Sigma^+_{aR} \\ \sqrt{2}\Sigma^-_{aR} & -\Sigma^0_{aR} \end{pmatrix}. \tag{3.2.39}$$

These fermions have Majorana masses;

$$\begin{aligned} \mathcal{L}^{\Sigma}_{mass} &= \sum_{a=1}^{3} -\frac{1}{2} M_{\Sigma_a} \mathrm{Tr}\left[\overline{\Sigma^c_{aR}}\Sigma_{aR}\right] + \text{h.c.} \\ &= \frac{1}{2}\sum_{a=1}^{3} M_{\Sigma_a}\left(\overline{\Sigma^{0c}_{aR}}\Sigma^0_{aR} + \text{h.c.}\right) \end{aligned} \tag{3.2.40}$$

The triplet fields interact with the lepton doublet and the Higgs field as follows;

$$\mathcal{L}^{\text{Type-III}}_{Y} = -\sum_{i,a=1}^{3} (Y_\Sigma)_{ai}\tilde{\phi}^\dagger \overline{\Sigma^c_{aR}} L_{iL} + \text{h.c.} \tag{3.2.41}$$

After the Higgs field obtain the VEV, the mass matrix for left-handed neutrinos $\nu_{iL}$ and right-handed triplet field $\Sigma^0_{aR}$ are given by

$$\mathcal{L}^{\Sigma\text{-}\nu}_{mass} = -\frac{1}{2}\overline{\tilde{\boldsymbol{\nu}}} \begin{pmatrix} 0 & \tilde{m}_\nu \\ \tilde{m}_\nu^{\rm T} & M_\Sigma \end{pmatrix} \tilde{\boldsymbol{\nu}} + \text{h.c.}, \tag{3.2.42}$$

where $\tilde{\boldsymbol{\nu}}$, $\overline{\tilde{\boldsymbol{\nu}}}$, and $\tilde{m}_\nu$ are defined as

$$\tilde{\boldsymbol{\nu}} = \left(\nu_{1L}, \nu_{2L}, \nu_{3L}, \Sigma^{0c}_{1R}, \Sigma^{0c}_{2R}, \Sigma^{0c}_{3R}\right)^{\rm T}, \tag{3.2.43}$$

$$\overline{\tilde{\boldsymbol{\nu}}} = \left(\overline{\nu_{1L}}, \overline{\nu_{2L}}, \overline{\nu_{3L}}, \overline{\Sigma^{0c}_{1R}}, \overline{\Sigma^{0c}_{1R}}, \overline{\Sigma^{0c}_{1R}}\right), \tag{3.2.44}$$

$$\tilde{m}_\nu = \frac{v}{2} Y_\Sigma. \tag{3.2.45}$$

Under the assumption that $v \ll M_{\Sigma_a} \ll v$, Majorana mass matrix for light neutrinos are given by

$$M_\nu = -\frac{v^2}{4} Y_\Sigma^{\mathrm{T}} M_\Sigma^{-1} Y_\Sigma + \mathcal{O}\left(\frac{v^2}{M_{\Sigma_a}^2}\right). \tag{3.2.46}$$

Thus, in the case that $v/M_{\Sigma_a} \simeq 10^{-(12\text{-}13)}$, it is expected to obtain the correct neutrino masses with $\mathcal{O}(1)$ Yukawa couplings, and the scale of $M_{\Sigma_a}$ is about the GUT scale.

In the Type-III seesaw mechanism, the left-handed charged lepton $\ell_{iL}$ are mixed with the singly charged fermion from the triplet $\Sigma_{aR}^+$;

$$\mathcal{L}_Y^{\text{Type-III}} \ni -\frac{v}{\sqrt{2}} \sum_{i,a=1}^{3} (Y_\Sigma)_{ai} \overline{\Sigma_{aR}^+} \ell_{jR} + \text{h.c.} \tag{3.2.47}$$

### 3.2.4 Radiative seesaw models

In the seesaw mechanisms, the typical scale of new physics is around the GUT scale. Thus, it is almost impossible to test them directly in future experiments. This difficulty is resolved by considering neutrino mass generation via loop diagrams. Then, the scale of new physics can be lowered by the loop suppression factor of the diagrams. Such models are often called *radiative seesaw models*. In this section, I introduce some radiative seesaw models.

#### Zee model

The first radiative seesaw model was proposed by A. Zee in 1980 [69]. The phenomenology of this model is investigated in Refs. [157,158]. In this model, the additional Higgs doublet $\phi_2$ and the singlet charged scalar boson $S^\pm$ are added into the SM. To avoid the dangerous FCNCs, the softly broken $Z_2$ symmetry is imposed where $\phi_2$ has odd parity and other scalar bosons have even parity.

The scalar potential of the model is given by

$$\begin{aligned} V_{\text{Zee}} =& -\mu_1^2|\phi_1|^2 - \mu_2^2|\phi_2|^2 - (\mu_{12}^2\phi_1^\dagger\phi_2 + \text{h.c.}) + \mu_s^2|S^+|^2 \\ &+ \frac{1}{2}\lambda_1|\phi_1|^4 + \frac{1}{2}\lambda_2|\phi_2|^4 + \lambda_3|\phi_1|^2|\phi_2|^2 + \lambda_4|\phi_1^\dagger\phi_2|^2 + \frac{1}{2}\Big(\lambda_5(\phi_1^\dagger\phi_2)^2 + \text{h.c.}\Big) \\ &- \sigma\Big(\tilde{\phi}_1^\dagger\phi_2 S^- + \text{h.c.}\Big) + \lambda_{1s}|\phi_1|^2|S^+|^2 + \lambda_{2s}|\phi_2|^2|S^+|^2 + \frac{1}{2}\lambda_s|S^+|^4. \end{aligned} \tag{3.2.48}$$

The interactions $\mu_{12}^2\phi_1^\dagger\phi_2$ and $\sigma\tilde{\phi}_1^\dagger\phi_2 S^-$ softly break $Z_2$ symmetry.

Both the Higgs doublets acquire the VEVs;

$$\langle\phi_a\rangle = \frac{1}{\sqrt{2}}\begin{pmatrix} 0 \\ v_a \end{pmatrix}, \quad (a = 1, 2). \tag{3.2.49}$$

The VEVs satisfy the condition $v = \sqrt{v_1^2 + v_2^2} = 246$ GeV. Let the Higgs doublets be represented by $\phi_a = (\phi_a^+, \phi_a^0)^{\mathrm{T}}$. Then, each element of the Higgs doublets and $S^+$ is represented by using the mass eigenstates of the CP-even Higgs bosons $h$ and $H$, the

CP-odd Higgs boson $A$, the charged Higgs bosons $S_1^+$ and $S_2^+$, and the NG bosons $G^0$ and $G^+$ as follows;

$$\begin{aligned}
\phi_1^0 &= \tfrac{1}{\sqrt{2}}\Big(v\cos\beta + H\cos\alpha - h\sin\alpha + i(G^0\cos\beta - A\sin\beta)\Big),\\
\phi_1^+ &= G^+\cos\beta - (S_1^+\cos\chi - S_2^+\sin\chi)\sin\beta,\\
\phi_2^0 &= \tfrac{1}{\sqrt{2}}\Big(v\sin\beta + H\cos\chi + h\cos\alpha + i(G^0\sin\beta - A\cos\beta)\Big),\\
\phi_2^+ &= G^+\sin\beta + (S_1^+\cos\chi - S_2^+\sin\chi)\cos\beta,\\
S^+ &= S_1^+\sin\chi + S_2^+\cos\chi.
\end{aligned} \tag{3.2.50}$$

The mixing angles $\alpha$, $\beta$, and $\chi$ are defined as

$$\begin{aligned}
\tan 2\alpha &= \frac{(M^2 - \lambda_{345}v^2)\tan 2\beta}{M^2 - (\lambda_1\cos^2\beta - \lambda_2\sin^2\beta)v^2/\cos 2\beta},\\
\tan\beta &= \frac{v_2}{v_1},\\
\tan 2\chi &= \frac{-\sqrt{2}\sigma v}{M^2 - \mu_s^2 - (\lambda_4 + \lambda_5 + \lambda_{1s}\cos^2\beta + \lambda_{2s}\sin^2\beta)v^2/2},
\end{aligned} \tag{3.2.51}$$

where $M^2 = \mu_{12}^2/(\sin\beta\cos\beta)$ and $\lambda_{345} = \lambda_3 + \lambda_4 + \lambda_5$.

The Yukawa interactions in the model are classified into four types Type-I, II, X, and Y depending on the $Z_2$ parities of the fermions [159–161]. The $Z_2$ parities of the fermions in each Type Yukawa interaction are shown in Table 3.1. In the following, we consider the case that all right-handed fermions have odd parity and all left-handed fermions have even parity. Then, all the SM fermions couples to only $\phi_2$, and $\phi_1$ does not interact with the SM fermions at tree level;

$$\mathcal{L}_{\phi ff}^{\text{Zee}} - \sum_{i,j=1}^{3}\Big\{(y_u')_{ij}\overline{Q_{iL}'}\tilde{\phi}_2 u_{jR}' + (y_d')_{ij}\overline{Q_{iL}'}\phi_2 d_{jR}' + (y_\ell')_{ij}\overline{L_{iL}'}\phi_2\ell_{jR}'.\Big\} + \text{h.c.} \tag{3.2.52}$$

In addition to these interactions, the left-handed lepton doublet interacts with the charged scalar boson $S^+$;

$$\mathcal{L}_{SLL}^{\text{Zee}} = \sum_{i,j=1}^{3}(Y_s)_{ij}\overline{L_{iL}}\tilde{L}_{jL}S^- + \text{h.c.}, \tag{3.2.53}$$

| | $u_{iR}$ | $d_{iR}$ | $\ell_{iR}$ |
|---|---|---|---|
| Type-I | − | − | − |
| Type-II | − | + | + |
| Type-X | − | − | + |
| Type-Y | − | + | − |

Table 3.1: $Z_2$-parity of the SM fermions. All the left-handed fermions are $Z_2$-even.

where $\tilde{L}_{jL} \equiv i\sigma_2 L^c_{jL}$. The matrix $Y_s$ is a complex anti-symmetric matrix and includes three complex phases. These phases can be 0 by rephasing the leptons. Thus, $Y_s$ is a real anti-symmetric matrix.

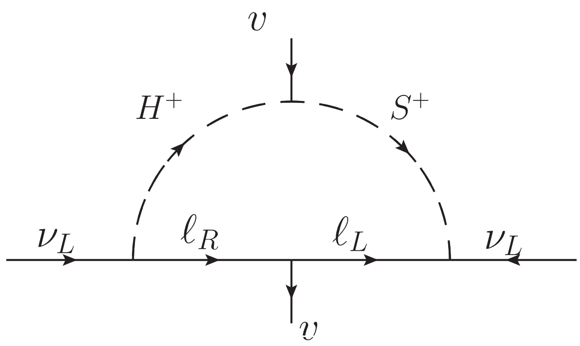


Figure 3.5: The Feynman diagram for neutrino mass in Zee model

The Majorana neutrino mass is generated via the 1-loop diagram shown in Fig. 3.5. It can be evaluated as

$$(m_\nu)_{ij} = \frac{1}{16\pi^2}(Y_s)_{ij}(m^2_{\ell_i} - m^2_{\ell_j})\sigma \cot\beta \frac{1}{m^2_{S_1} - m^2_{S_2}} \log\left(\frac{m^2_{S_1}}{m^2_{S_2}}\right). \tag{3.2.54}$$

**Ma model (Scotogenic model)**

Here, I introduce the model proposed E. Ma [73] as one example of radiative seesaw models including the DM candidate. This model is called Ma model or Scotogenic model. In this model, $Z_2$ symmetry is imposed, and $Z_2$-odd fields, an isospin doublet $\eta$ and three right-handed Majorana neutrinos $N_{aR}$ ($a = 1$–$3$) are introduced.[4]

The scalar potential is given by

$$\begin{aligned} V_{\mathrm{Ma}} =& -\mu_1^2|\phi|^2 + \mu_2^2|\eta|^2 \\ &+ \lambda_1|\phi|^4 + \lambda_2|\eta|^4 + \lambda_3|\phi|^2|\eta|^2 + \lambda_4|\phi^\dagger\eta|^2 + \lambda_5\big((\phi^\dagger\eta)^2 + \text{h.c.}\big). \end{aligned} \tag{3.2.55}$$

The coupling constant $\lambda_5$ is generally a complex number. However, it can be real by rephasing $\eta$. Therefore, there is no CP-violating phase in the Higgs potential.

Since the vacuum is assumed to respect $Z_2$ symmetry, only the Higgs doublet $\phi$ acquire the VEV;

$$\langle\phi\rangle = \frac{1}{\sqrt{2}}\begin{pmatrix} 0 \\ v \end{pmatrix} \tag{3.2.56}$$

Then, the stationary condition is given by

$$\mu_1^2 = \lambda_1 v^2. \tag{3.2.57}$$

[4]To explain neutrino oscillation data, at least two right-handed neutrinos are needed [162].

The additional scalar bosons come from the inert doublet $\eta$;

$$\eta = \begin{pmatrix} H^{\pm} \\ \frac{1}{\sqrt{2}}(H + iA) \end{pmatrix}. \tag{3.2.58}$$

Their masses are given by

$$m_{H^{\pm}} = \mu_2^2 + \frac{\lambda_3}{2}v^2, \tag{3.2.59}$$

$$m_H^2 = \mu_2^2 + \frac{1}{2}(\lambda_3 + \lambda_4 + \lambda_5)v^2, \tag{3.2.60}$$

$$m_A^2 = \mu_2^2 + \frac{1}{2}(\lambda_3 + \lambda_4 - \lambda_5)v^2. \tag{3.2.61}$$

Since there is no CP-violation in the Higgs potential, the CP-even scalar boson $H$ and the CP-odd scalar boson $A$ are not mixed at tree level.

In addition to the SM Yukawa interactions, the model has a new Yukawa interaction;

$$\mathcal{L}_{LN\eta} = (Y_\eta)_{ia}\overline{L_{iL}}\tilde{\eta}N_{aR} + \text{h.c.} \tag{3.2.62}$$

Then, Majorana neutrino mass is generated at the one-loop level via the Feynman diagram shown in Fig. 3.6. The formula for neutrino mass is given by

$$(m_\nu)_{ij} = \frac{1}{16\pi^2}\sum_a (Y_\eta)^*_{ia}(Y_\eta)^*_{ja}M_{N_a}\left\{\frac{m_H^2}{m_H^2 - M_{N_a}^2}\log\left(\frac{m_H^2}{M_{N_a}^2}\right) - \frac{m_A^2}{m_A^2 - M_{N_a}^2}\log\left(\frac{m_A^2}{M_{N_a}^2}\right)\right\}, \tag{3.2.63}$$

where $M_{N_a}$ is Majorana mass of $N_a$.

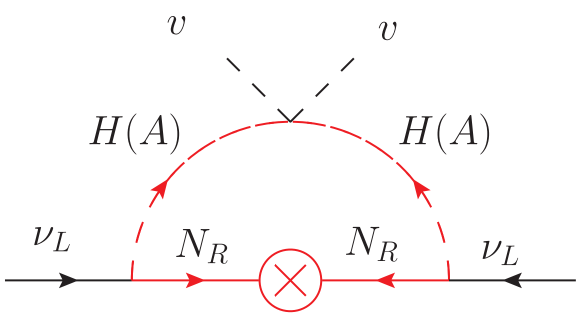


Figure 3.6: The Feynman diagram for neutrino mass in Ma model. The symbol $\otimes$ represents Majorana mass for $N_{aR}$.

## 3.3 Dark matter

DM is first proposed by Fritz Zwicky to explain the motion of galaxies in a galaxy cluster in 1933 [163]. Since then, the existence of DM has been supported by various experimental results, for example, the observation of the CMB, the weak gravitational lensing, and so on. DM also plays an essentially important role in the theory of structure formation in the universe.

By the latest Planck data [3], it has been found that DM makes up about 27 % of the current universe. Thus, DM should be stable and electrically neutral. However, other natures of DM have not been revealed yet. In other words, we know hardly anything about what DM is.

The attractive scenario in particle physics is that DM is an elementary particle. In the SM, neutrinos are stable and electrically neutral. Thus, they were considered to be DM candidates. However, it has been revealed that if neutrinos are a major component of DM, it is not possible to explain the formation of the observed structure in the universe such as galaxies, galaxy clusters, and so on. Consequently, the existence of DM cannot be explained in the SM. A new particle is needed to explain the existence of DM.

### 3.3.1 Freeze-out mechanism

One of the most plausible scenarios to explain the relic abundance of DM in the universe is the scenario utilizing the freeze-out mechanism. In this scenario, we consider a particle that is stable and electrically neutral as DM. This particle does not decay, while a pair of them can annihilate into lighter particles, in particular into the SM fermions. In the early universe, the particles are in thermal equilibrium with other particles. As the universe is cooled down, at some time, the reaction rate of the pair annihilation becomes smaller than the expansion rate of the universe, i.e. the annihilation process freezes out. Then, the density of the particle is also frozen, and it is the observed relic density.

The number density of the DM particle satisfies the Boltzmann equation [164],

$$\frac{\mathrm{d}n_\alpha}{dt} + 3\frac{\dot{a}}{a}n_\alpha = 2\int \frac{g_\alpha}{(2\pi)^3}\frac{\mathrm{d}^3p_\alpha}{2E_\alpha}C[f_\alpha], \tag{3.3.1}$$

where $\alpha$ is a label for the kind of particles and $n_\alpha$, $E_\alpha$, and $\boldsymbol{p}_\alpha$ is the number density, the energy, and the three-momentum of the DM particle $\alpha$. The scale factor is denoted by $a$ in Eq. (3.3.1), and $\dot{a}$ is a time derivative of it. The symbol $C[f_\alpha]$ is the scattering term for the distribution function of the DM particle $f_\alpha$. For the process $\alpha\beta \leftrightarrow ij$, the Boltzmann equation is given by

$$\frac{\mathrm{d}n_\alpha}{dt} + 3\frac{\dot{a}}{a}n_\alpha = -\langle\sigma v\rangle\left(n_\alpha n_\beta - n_\alpha^{\mathrm{eq}} n_\beta^{\mathrm{eq}}\right), \tag{3.3.2}$$

where $\langle\sigma v\rangle$ is a thermal averaged scattering cross section for the process $\alpha\alpha \to ij$ defined as follows;

$$\langle\sigma v\rangle = \frac{\displaystyle\int \mathrm{d}n_\alpha^{\mathrm{eq}}\,\mathrm{d}n_\beta^{\mathrm{eq}}\,\sigma v}{\displaystyle\int \mathrm{d}n_\alpha^{\mathrm{eq}}\,\mathrm{d}n_\beta^{\mathrm{eq}}}, \tag{3.3.3}$$

where $n_\alpha^{\mathrm{eq}}$ ($n_\beta^{\mathrm{eq}}$) is the thermal equilibrium distribution of the particle $\alpha$ ($\beta$). The symbol $\sigma$ is the scattering cross section of the process $\alpha\beta \to ij$, and $v$ is the Møller velocity []. In deriving Eq. (3.3.2), we assume $C$ and $CP$ symmetry in the process $\alpha\beta \to ij$.

In the case of $\beta$ is an anti-particle of $\alpha$, we can set $n_\alpha^{(\mathrm{eq})} = n_\beta^{(\mathrm{eq})}$, and we obtain

$$\frac{\mathrm{d}n_\alpha}{dt} + 3\frac{\dot{a}}{a}n_\alpha = -\langle\sigma v\rangle\left(n_\alpha^2 - (n_\alpha^{\mathrm{eq}})^2\right), \tag{3.3.4}$$

In the case that $\alpha$ is identical to $\beta$, the symmetry factor $1/2$ is needed on the right-hand side of the equation. However, this factor is canceled by factor 2 caused by the fact that the number of created or annihilated $\alpha$ is twice as much as that in the case of $\alpha \neq \beta$. Therefore, Eq. (3.3.4) can be used in the case of $\alpha = \beta$.

Since the entropy in a Hubble volume is conserved, the following equation is derived from Eq. (3.3.4) by using the assumption that the number density of $\alpha$ freezes out at radiation-dominated era;

$$\frac{\mathrm{d}Y_\alpha}{\mathrm{d}x} = -\frac{s}{xH}\langle\sigma v\rangle\left(Y_\alpha^2 - (Y_\alpha^{\mathrm{eq}})^2\right), \tag{3.3.5}$$

where $Y_\alpha^{(\mathrm{eq})} = n_\alpha^{(\mathrm{eq})}/s$ and $s$ is the entropy density. The variable $x$ is defined as $x = m_\alpha/T$, where $m_\alpha$ is mass of the particle $\alpha$ and $T$ is temperature. The symbol $H$ is the Hubble parameter; $H = \dot{a}/a$.

In the case of $\langle\sigma v\rangle$ is proportional to $x^{-n}$, where $n$ is any non-negative integer, we can approximately solve the above equation. By using this approximated solution, the density parameter for the DM particle $\alpha$ is given by

$$\Omega_{\alpha 0}h^2 = 1.04 \times 10^9 \times \left(\frac{m_{\mathrm{pl}}}{\mathrm{GeV}}\right)^{-1}\left(\frac{\langle\sigma v\rangle}{\mathrm{GeV}^{-2}}\right)^{-1} \times \frac{1}{\sqrt{g_*}}(n+1)x_f^{n+1}, \tag{3.3.6}$$

where $m_{\mathrm{pl}} \simeq 1.2 \times 10^{19}$ GeV is the Planck mass, and $g_* \simeq 106.75$ is the effective degree of freedom for the energy (entropy) density in the radiation-dominated era. The freeze-out temperature $x_f$ can be approximately evaluated as [164]

$$\begin{aligned} x_f =& \log\left[0.038(n+1)\frac{g_\alpha}{\sqrt{g_*}}m_{\mathrm{pl}}m_\alpha\langle\sigma v\rangle|_{x=1}\right] \\ &- \left(n+\frac{1}{2}\right)\log\left[\log\left[0.038(n+1)\frac{g_\alpha}{\sqrt{g_*}}m_{\mathrm{pl}}m_\alpha\langle\sigma v\rangle|_{x=1}\right]\right], \end{aligned} \tag{3.3.7}$$

where $g_\alpha$ is the degree of freedom of the DM particle $\alpha$. The cosmological parameter for DM is observed by Planck collaboration as [3]

$$\Omega_{\mathrm{DM}0}h^2 = 0.120 \pm 0.001 \tag{3.3.8}$$

# Chapter 4

# Electroweak baryogenesis in the aligned two Higgs doublet model

In this chapter, I introduce one of our work [55]. In this work, we investigate electroweak baryogenesis in the CP-violating two Higgs doublet model. In this model, the additional CP-violating sources for baryogenesis are supplied by the Yukawa interactions and the Higgs potential. We consider the scenario where severe constraints from the current electric dipole measurements can be avoided by destructive interference between CP-violating phases in the Yukawa interactions and the Higgs potential [101]. We show that the observed baryon asymmetry can be obtained under various experimental and theoretical constraints, and the typical mass scale of the additional Higgs bosons is 300–400 GeV. We also discuss how to test this scenario at various future experiments.

## 4.1 Lagrangian of the model

In this model, there are two isospin doublets $\phi_1$ and $\phi_2$ whose hypercharge is 1/2. The fermion contents and gauge symmetries are the same as those in the SM. The scalar potential is given by

$$\begin{aligned}
V_{\mathrm{THDM}} = &-\mu_1'^2|\phi_1|^2 - \mu_2'^2|\phi_2|^2 - \left\{\mu_{12}'^2\phi_1^\dagger\phi_2 + \mathrm{h.c.}\right\} \\
&+ \frac{\lambda_1'}{2}|\phi_1|^4 + \frac{\lambda_2'}{2}|\phi_2|^4 + \lambda_3'|\phi_1|^2|\phi_2|^2 + \lambda_4'|\phi_1^\dagger\phi_2|^2 \\
&+ \left\{\frac{\lambda_5'}{2}(\phi_1^\dagger\phi_2)^2 + \lambda_6'|\phi_1|^2(\phi_1^\dagger\phi_2) + \lambda_7'|\phi_2|^2(\phi_1^\dagger\phi_2) + \mathrm{h.c.}\right\}.
\end{aligned} \tag{4.1.1}$$

In general, the coupling constants $\mu_{12}'^2$, $\lambda_5$, $\lambda_6$, and $\lambda_7$ are complex valued.

Both doublets can acquire the VEVs, and each VEV is defined as

$$\langle\phi_\alpha\rangle = \frac{1}{\sqrt{2}}\begin{pmatrix} 0 \\ v_\alpha \end{pmatrix}, \quad \alpha = 1, 2, \tag{4.1.2}$$

where $v_\alpha$ are complex numbers generally. By an appropriate $U(2)$ transformation between the doublets $\phi_1$ and $\phi_2$, we can always move on the so-called Higgs basis, where only one of the doublets obtain the real-valued VEV [165]. Such a unitary transformation is generally given by

$$\begin{pmatrix} \Phi_1 \\ \Phi_2 \end{pmatrix} = \frac{1}{v} \begin{pmatrix} v_1^* & v_2^* \\ -v_2 e^{i\phi} & v_1 e^{i\phi} \end{pmatrix} \begin{pmatrix} \phi_1 \\ \phi_2 \end{pmatrix}, \tag{4.1.3}$$

where $v = \sqrt{|v_1|^2 + |v_2|^2} = 246$ GeV is the total electroweak symmetry breaking VEV. In this basis, only $\Phi_1$ obtains the VEV;

$$\langle \Phi_1 \rangle = \frac{1}{\sqrt{2}} \begin{pmatrix} 0 \\ v \end{pmatrix}, \quad \langle \Phi_2 \rangle = \begin{pmatrix} 0 \\ 0 \end{pmatrix}. \tag{4.1.4}$$

The angle in Eq. (A.1) is an arbitrary phase and means the degree of freedom of choosing the phase of $\Phi_2$. In the following, we discuss consider the issue on this basis.

The Higgs potential in the Higgs basis is given by

$$\begin{aligned} V_{\mathrm{THDM}} = &-\mu_1^2|\Phi_1|^2 - \mu_2^2|\Phi_2|^2 - \left\{\mu_{12}^2 \Phi_1^\dagger \Phi_2 + \mathrm{h.c.}\right\} \\ &+ \frac{\lambda_1}{2}|\Phi_1|^4 + \frac{\lambda_2}{2}|\Phi_2|^4 + \lambda_3|\Phi_1|^2|\Phi_2|^2 + \lambda_4|\Phi_1^\dagger\Phi_2|^2 \\ &+ \left\{\frac{\lambda_5}{2}(\Phi_1^\dagger\Phi_2)^2 + \lambda_6|\Phi_1|^2(\Phi_1^\dagger\Phi_2) + \lambda_7|\Phi_2|^2(\Phi_1^\dagger\Phi_2) + \mathrm{h.c.}\right\} \end{aligned} \tag{4.1.5}$$

The relations between coupling constants in the Higgs potential and those in Eq. (4.1.1) are shown in Appendix A. The coupling constants $\mu_{12}^2$, $\lambda_5$, $\lambda_6$, and $\lambda_7$ can be complex number. By rephrasing $\Phi_2$, one of their phases can be zero. Therefore, there are three CP-violating couplings in the Higgs potential.

The elements of each doublet are parametrized as follows;

$$\Phi_1 = \begin{pmatrix} G^+ \\ \frac{1}{\sqrt{2}}(v + h_1 + iG^0) \end{pmatrix}, \quad \Phi_1 = \begin{pmatrix} H^+ \\ \frac{1}{\sqrt{2}}(h_2 + ih_3) \end{pmatrix}. \tag{4.1.6}$$

By substituting Eq. (4.1.6) into the Higgs potential, we obtain the following stationary conditions;

$$\mu_1^2 = -\frac{1}{2}\lambda_1 v^2, \quad \mu_{12}^2 = -\frac{1}{2}\lambda_6 v^2. \tag{4.1.7}$$

The phase of $\mu_{12}^2$ and that of $\lambda_6$ are related by the second equation. Thus, the number of independent CP-violating phases is two in the Higgs potential.

By using the stationary conditions, the mass terms for the Higgs bosons are given by

$$\mathcal{L}_{\mathrm{mass}} = m_{H^\pm}^2|H^\pm|^2 + \frac{1}{2}\sum_{\alpha,\beta=1}^{3} h_\alpha (M_h^2)_{\alpha\beta} h_\beta. \tag{4.1.8}$$

The mass for the charged Higgs boson $H^\pm$ is given by

$$m_{H^\pm}^2 = M^2 + \frac{1}{2}\lambda_3 v^2, \tag{4.1.9}$$

where $M^2 = -\mu_2^2$. The other charged scalar boson $G^\pm$ do not have the mass term, and it is the NG boson.

The neutral scalar bosons are mixed by the mass matrix $M_h^2$ defined as

$$M_h^2 = v^2 \begin{pmatrix} \lambda_1 & \mathrm{Re}[\lambda_6] & -\mathrm{Im}[\lambda_6] \\ \mathrm{Re}[\lambda_6] & \frac{M^2}{v^2} + \frac{1}{2}(\lambda_3 + \lambda_4 + \mathrm{Re}[\lambda_5]) & -\frac{1}{2}\mathrm{Im}[\lambda_5] \\ -\mathrm{Im}[\lambda_6] & -\frac{1}{2}\mathrm{Im}[\lambda_5] & \frac{M^2}{v^2} + \frac{1}{2}(\lambda_3 + \lambda_4 - \mathrm{Re}[\lambda_5]) \end{pmatrix}. \tag{4.1.10}$$

The mixings among the neutral scalar states are caused by $\lambda_6$ and $\mathrm{Im}[\lambda_5]$. As mentioned above, $\mathrm{Im}[\lambda_5]$ can be zero by an appropriating rephasing of $\Phi_2$. In this case, only $\lambda_6$ is the source of the mixings. For simplicity, we consider this case, and $\lambda_5$ is a real number in the following.

The mass eigenstates of the $Z_2$-even neutral scalar states $(H_1, H_2, H_3)$ are defined by using a real $3 \times 3$ orthogonal matrix $R$ as

$$H_\alpha = \sum_{\beta=1}^{3} R_{\alpha\beta} h_\beta, \tag{4.1.11}$$

where the matrix $R$ diagonalizes the mass matrix $M_h^2$ as $R^{\mathrm{T}} M_h^2 R = \mathrm{diag}(m_{H_1}^2, m_{H_2}^2, m_{H_3}^2)$. The non-diagonal elements $R_{21}$ and $R_{31}$ induce the deviations of the Higgs boson couplings from the SM ones at tree level. To avoid them, we assume that $\lambda_6 = 0$ for simplicity [101]. Then, $\mu_{12}^2$ is also 0 by the stationary condition in Eq. (5.1.4).

Under this assumption, the matrix $R$ is an identity matrix ($R_{\alpha\beta} = \delta_{\alpha\beta}$), and the neutral Higgs bosons are aligned. The masses of $H_1$, $H_2$, and $H_3$ is given by

$$m_{H_1}^2 = \lambda_1 v^2, \tag{4.1.12}$$

$$m_{H_2}^2 = M^2 + \frac{1}{2}v^2(\lambda_3 + \lambda_4 + \lambda_5), \tag{4.1.13}$$

$$m_{H_3}^2 = M^2 + \frac{1}{2}v^2(\lambda_3 + \lambda_4 - \lambda_5). \tag{4.1.14}$$

Then, the scalar boson $H_1$ $(= h_1)$ is the SM Higgs boson whose mass is $m_{H_1} = 125$ GeV. By using Eqs. (4.1.13) and (4.1.14), we can obtain the relations between the scalar coupling and the mass of the additional Higgs bosons.

$$\lambda_3 = \frac{2}{v^2}(m_{H^\pm}^2 - M^2), \tag{4.1.15}$$

$$\lambda_4 = \frac{1}{v^2}(m_{H_2}^2 + m_{H_3}^2 - 2m_{H^\pm}^2), \tag{4.1.16}$$

$$\lambda_5 = \frac{1}{v^2}(m_{H_2}^2 - m_{H_3}^2). \tag{4.1.17}$$

As a result, the real free parameters in the Higgs potential are $M^2(= -\mu_2^2)$, $m_{H^\pm}$, $m_{H_2}$, $m_{H_3}$, $\lambda_2$, $|\lambda_7|$, and $\theta_7(= \arg[\lambda_7])$. The angle $\theta_7 \in [0, 2\pi)$ is the CP-violating parameter in the Higgs potential.

The Yukawa interactions in the model are given by

$$\mathcal{L}_Y = -\sum_{\alpha=1}^{2}\sum_{i,j=1}^{3}\left\{(y_u^{a\prime})_{ij}\overline{Q'_{iL}}\tilde{\Phi}_a u'_{jR} + (y_d^{a\prime})_{ij}\overline{Q'_{iL}}\Phi_a d'_{jR} + (y_\ell^{a\prime})_{ij}\overline{L'_{iL}}\Phi_a \ell_{jR}\right\} + \text{h.c.} \quad (4.1.18)$$

The VEV $\langle\Phi_1\rangle$ generates the mass matrices of the SM fermions;

$$m'_f = \frac{v}{\sqrt{2}}(y_f^{1\prime}), \quad f = u, d, \ell, \quad (4.1.19)$$

which are not generally diagonal matrices. To diagonalize $m'_f$, we redefine the fermions by unitary matrices as in the SM;

$$L'_{iL} = \sum_{j=1}^{3}(V_\ell)_{ij}L_{jL}, \quad \ell'_{iR} = \sum_{j=1}^{3}(U_\ell)_{ij}\ell_{jR}, \quad (4.1.20)$$

$$q'_{iL} = \sum_{j=1}^{3}(V_q)_{ij}q_{jL}, \quad q'_{iR} = \sum_{j=1}^{3}(U_q)_{ij}q_{jR}, \quad \text{for } q = u, d, \quad (4.1.21)$$

where matrices $V_f$ and $U_f$ ($f = u, d, \ell$) are unitary matrices that diagonalize the Yukawa couplings as

$$(V_f^\dagger y_f^{1\prime} U_f)_{ij} = (y_f^1)_i \delta_{ij}. \quad (4.1.22)$$

Then, the up-type quarks $(u_1, u_2, u_3) = (u, c, t)$, the down-type quarks $(d_1, d_2, d_3) = (d, s, b)$, and the charged leptons $(\ell_1, \ell_2, \ell_3) = (e, \mu, \tau)$ are mass eigenstates. The neutrinos $(\nu_1, \nu_2, \nu_3) = (\nu_e, \nu_\mu, \nu_\tau)$ are massless fermions.

In general, the matrices $y_f^{1\prime}$ and $y_f^{2\prime}$ are independent of each other, and $y_f^{2\prime}$ is not diagonalized by the redefinitions of the fermions in Eqs. (4.1.20) and (4.1.21). Then, the Yukawa interactions between the additional neutral scalar state ($H_2$ and $H_3$) and the SM fermions are given by

$$\begin{aligned}\mathcal{L}_Y \ni -\frac{1}{\sqrt{2}}\sum_{i,j=1}^{3}\Big\{&(y_u^2)_{ij}\overline{u_{iL}}u_{iR}(H_2 - iH_3) + (y_d^2)_{ij}\overline{d_{iL}}d_{iR}(H_2 + iH_3) \\ &+ (y_\ell^2)_{ij}\overline{\ell_{iL}}\ell_{iR}(H_2 + iH_3)\Big\} + \text{h.c.},\end{aligned} \quad (4.1.23)$$

where

$$(y_f^2)_{ij} \equiv (V_f^\dagger y_f^{2\prime} U_f)_{ij}, \quad f = u, d, \ell. \quad (4.1.24)$$

The non-diagonal elements of $y_f^2$ cause the dangerous FCNCs at tree level. To avoid them, we simply assume the Yukawa alignment condition proposed in Ref. [98], where the Yukawa matrices $y_f^{1\prime}$ and $y_f^{2\prime}$ are proportional to each other;

$$y_u^{2\prime} = \zeta_u^* y_u^{1\prime}, \quad y_d^{2\prime} = \zeta_d y_d^{1\prime}, \quad y_\ell^{2\prime} = \zeta_\ell y_\ell^{1\prime}, \quad (4.1.25)$$

where $\zeta_f$ ($f = u, d, \ell$) is a complex number. Then, the matrices $y_f^{1\prime}$ and $y_f^{2\prime}$ can be simultaneously diagonalized by the redefinitions of the fermions in Eqs. (4.1.20) and (4.1.21). In the Yukawa interactions, there are three CP-violating phases $\theta_f = \arg[\zeta_f]$ ($f = u, d, e$).

The Yukawa interactions between the charged Higgs boson $H^\pm$ and the SM fermions are given by

$$\mathcal{L}_Y \ni -\frac{\sqrt{2}}{v}H^+\sum_{i,j=1}^{3}\left\{\overline{u_i}V_{ij}(\zeta_d m_{d_j}P_R-\zeta_u m_{u_i}P_L)d_j+\zeta_\ell m_{\ell_i}\delta_{ij}\overline{\nu_i}P_R\ell_j\right\}, \tag{4.1.26}$$

where the matrix $V$ is the CKM matrix, and $m_f$ is the mass of fermion $f$. The neutral Higgs bosons ($H_1$, $H_2$, and $H_3$) interact with the SM fermions as follows;

$$\mathcal{L}_Y \ni -\sum_{i=1}^{3}\sum_{f=u,d,\ell}\frac{m_{f_i}}{v}\left\{H_1\overline{f}_if_i+\sum_{\alpha=2}^{3}H_\alpha\overline{f}_i(\kappa^\alpha_{S,f}+\kappa^\alpha_{P,f}\gamma_5)f_i\right\}. \tag{4.1.27}$$

The coefficients of the scalar and pseudo-scalar couplings for $H_2$ and $H_3$ are defined as

$$\kappa^2_{S,f}=\mathrm{Re}[\zeta_f],\quad \kappa^3_{S,f}=-\mathrm{Im}[\zeta_f],\quad \kappa^2_{P,f}=i(-1)^f\,\mathrm{Im}[\zeta_f],\quad \kappa^3_{P,f}=i(-1)^f\,\mathrm{Re}[\zeta_f], \tag{4.1.28}$$

where

$$(-1)^f=\begin{cases}1 & (f=d,\ell),\\ -1 & (f=u).\end{cases} \tag{4.1.29}$$

## 4.2 Constraints on the model

In this section, we discuss some experimental and theoretical constraints on the model. In the following, we consider the case that $|\zeta_u|=|\zeta_d|=|\zeta_\ell|$. Then, the Yukawa interactions in the model are the same as those in Type-I THDM [159–161] except for the CP-violating phases.

First, we consider constraints from the direct searches for the charged Higgs boson according to Refs [102, 166, 167]. At the LEP experiment, the charged Higgs boson is produced by $e^+e^-\to H^+H^-$. By assuming that two decay channels $H^\pm\to cs$ and $H^\pm\to\tau\nu$ exhaust the $H^\pm$ decay width, the lower bound on $m_{H^\pm}$ is given by 80 GeV at 95 % C.L., which is almost independent of the values of $\zeta_f$ ($f=u,d,\ell$) [168].[1] On the other hand, at the LHC experiment, the main production channel for $H^\pm$ depends on its mass. If $H^\pm$ is lighter than top quarks, they are produced mainly via the top quark decay $t\to H^\pm b$ [169]. In this case, by using the latest CMS results [170], the upper bound on $|\zeta_f|$ is given by about 0.07 (0.27) for $m_{H^\pm}=80$ GeV (160 GeV). If the decay $t\to H^\pm b$ are not kinematically allowed, the main production channel of $H^\pm$ is the associated production with the bottom quark $gg\to H^\pm tb$ ($gb\to tH^\pm$) [169]. In this case, by using the latest data at the ATLAS experiment [171], the upper bound on $|\zeta_f|$ is given by about 0.5 (0.6) for $m_{H^\pm}=200$ GeV (400 GeV).

Second, we consider constraints from the direct searches for the additional neutral Higgs bosons according to Refs. [102, 167]. As shown in Eq. (4.1.27), the couplings

[1] For small $\zeta_f$ couplings, the decays $H^\pm\to W^{\pm *}H_{2,3}$ can be dominant if the masses of $H_{2,3}$ are enough small. The lower bound on $m_{H^\pm}$ from the search for these decay channels is investigated in Ref. [168]. It slightly changed by the value of $|\zeta_f|$ and is about from 70 to 90 GeV.

between the SM and the additional neutral Higgs bosons depend on the CP-violating phases of $\zeta_f$ couplings. Here, we neglect the effects of CP violation for simplicity. At the LHC, $H_{2,3}$ are dominantly produced via the top quark loop unless the value of $|\zeta_f|$ is too small [169].[2] In the case that masses of the additional Higgs bosons are degenerate, the branching ratios of $H_{2,3} \to t\bar{t}$ are almost 100 % regardless of the value of $|\zeta_f|$ if they are kinematically allowed [102]. Then, by using the latest data at the ATLAS experiment [172], the constraints on $|\zeta_f|$ from the search for $H_{2,3} \to t\bar{t}$ is given as $|\zeta_f| \lesssim 0.67$ for $m_{H_{2,3}} = 400$ GeV [102, 167]. If $m_{H_{2,3}} < 2m_t$, the strong constraint is given by the search for $H_{2,3} \to \tau\overline{\tau}$ [102, 167]. By camparing the latest results at the ATLAS experiment [173] and the results in Refs. [102, 167], the upper bound on $|\zeta_f|$ can be estimated to be about 0.35 for $m_{H_{2,3}} = 200$ GeV.

Third, we consider constraints from the flavor experiments. These constraints for softly $Z_2$ symmetric THDMs are investigated in Refs. [167, 174, 175]. According to Ref. [175], in the case that $|\zeta_u| = |\zeta_d| = |\zeta_e|$, the current stringent constraint is given by the searches for $B^0 \to \mu^+\mu^-$ [176, 177]. The upper bound on $|\zeta_f|$ is about 0.33 (0.5) for $m_{H^\pm} = 100$ GeV (400 GeV) at 95 % C.L. [175].

Fourth, we consider the constraints from the experiments for EDM measurements. The EDM of a fermion $f$ ($d_f$) is defined as

$$\mathcal{L}_{\rm EDM} = -\frac{d_f}{2}\overline{f}\sigma^{\mu\nu}(i\gamma_5)fF_{\mu\nu}. \tag{4.2.1}$$

From the latest results of the electron EDM (eEDM) measurement at the ACME experiments [178], the constraint on $d_e$ is given by $|d_d + kC_s| < 1.1 \times 10^{-29}$ e cm, where $C_s$ is the coefficient of the interaction between electrons and nucleons; $C_s(\overline{e}i\gamma_5 e)(\overline{N}N)$, and the constant $k$ is about $\mathcal{O}(10^{-15})$ GeV$^2$ e cm. As discussed in Refs. [101, 179, 180], the second term is typically two orders smaller than the current constraint in the parameter region that we discussed later. Therefore, we require that $|d_e| < 1.0 \times 10^{-29}$ e cm as the current constraint from ACME experiment [178].

Figure 4.1: Barr-Zee type diagrams with fermion loop (left) and with scalar loop (right).

In the model, $d_e$ is generated via 2-loop Barr-Zee type diagrams [181]. The 1-loop diagrams via the Yukawa interaction with the additional Higgs bosons are negligibly small because of the electron mass suppression [179]. There are two kinds of Barr-Zee type diagrams shown in Fig. 4.1. One is the diagrams including a fermion loop (left

[2]If we consider the case that $|\zeta_d|$ is much larger than $|\zeta_u|$, for example MSSM with large $\tan\beta$, the bottom associated production $gg \to H_{2,3}b\overline{b}$ is also important [169]. However, in the case that $|\zeta_u| = |\zeta_d| = |\zeta_\ell|$, it is about two orders smaller than the top quark loop contribution [102].

figure), and the other is those including a scalar loop (right figure). In the case that $|\zeta_u| = |\zeta_d| = |\zeta_e|$, the top quark loop gives the largest contribution in the diagrams with a fermion loop. Then, the contribution from fermion loop diagrams are approximately proportional to $\sin(\theta_u - \theta_e)$. On the other hand, the scalar loop diagrams are proportional to $\sin(\theta_7 - \theta_e)$. Therefore, by using the destructive interference between $\theta_u - \theta_e$ and $\theta_7 - \theta_e$, the current eEDM constraint can be avoided without assuming very small CP-violating phases [101].

The latest constraints from the measurement of the neutron EDM (nEDM) is given by the NEDM collaboration as $|d_n| < 1.8 \times 10^{-26}$ e cm at 90 % C.L. [182]. According to Refs. [183–186], $d_n$ can be evaluated as follows by using the QCD sum rule;

$$d_n = 0.79 d_d - 0.20 d_u + e(0.59 d_d^C + 0.30 d_u^C)/g_C, \tag{4.2.2}$$

where $g_C$ is the gauge coupling constant for the strong interaction, and $d_q^C$ $(q = u, d)$ is chromo EDM. Other operators such as Weinberg operator [187, 188] and four Fermi interactions [189] also contribute to the nEDM. In the parameter region that we discussed later, the contribution from the four Fermi interactions is negligibly small [179]. Thus, in the following, we consider only the contributions from $d_n$ and the Weinberg operator.

Fifth, we consider the oblique parameters S, T, and U [190]. Here, the $T$ parameter is discussed in particular. In the scalar potential where the alignment for neutral Higgs bosons is assumed, $\lambda_4 - \lambda_5$ and $\mathrm{Im}[\lambda_7]$ violate the custodial symmetry [150–156] and induce the deviation of the $T$ parameter from the SM prediction. At the one-loop level, $\mathrm{Im}[\lambda_7]$ does not contribute to the $T$ parameter [152, 154]. Thus, the contribution to the $T$ parameter from the additional Higgs bosons is proportional to $\lambda_4 - \lambda_5$ at the 1-loop level. By using mass formulae in Eqs. (4.1.9) and (4.1.14), we obtain the equation

$$\lambda_4 - \lambda_5 = \frac{2(m_{H_3}^2 - m_{H^\pm}^2)}{v^2}. \tag{4.2.3}$$

Consequently, it is found that in the case that $m_{H_3} = m_{H^\pm}$, the additional Higgs bosons do not contribute to the $T$ parameter at the one-loop level.

Finally, the extended Higgs sector in the model is constrained theoretically by the perturbative unitarity [191–194] and the vacuum stability [195–197]. In our analysis, we use conditions for these constraints in Refs. [194] and [197].

## 4.3 The effective potential

In this section, we consider the effective potential for neutral elements of the isospin doublets $\Phi_1$ and $\Phi_2$ at the one-loop level. By choosing an appropriate gauge, the classical fields can be parametrized as

$$\Phi_1 = \frac{1}{\sqrt{2}} \begin{pmatrix} 0 \\ \varphi_1 \end{pmatrix}, \quad \Phi_2 = \frac{1}{\sqrt{2}} \begin{pmatrix} 0 \\ \varphi_2 + i\varphi_3 \end{pmatrix}. \tag{4.3.1}$$

By substituting these classical fields into the Higgs potential, we can obtain the tree-level effective potential $V_0$ as follows.

$$\begin{aligned} V_0(\varphi_1, \varphi_2, \varphi_3) = & \frac{\mu_1^2}{2}\varphi_1^2 + \frac{\mu_2^2}{2}(\varphi_2^2 + \varphi_3^2) + \frac{\lambda_1}{8}\varphi_1^4 + \frac{\lambda_2}{8}(\varphi_2^4 + 2\varphi_2^2\varphi_3^2 + \varphi_3^4) \\ & + \frac{1}{4}(\lambda_3 + \lambda_4 + \lambda_5)\varphi_1^2\varphi_2^2 + \frac{1}{4}(\lambda_3 + \lambda_4 - \lambda_5)\varphi_1^2\varphi_3^2 \\ & + \frac{1}{2}\mathrm{Re}[\lambda_7]\varphi_1\varphi_2(\varphi_2^2 + \varphi_3^2) - \frac{1}{2}\mathrm{Im}[\lambda_7]\varphi_1\varphi_3(\varphi_2^2 + \varphi_3^2), \end{aligned} \tag{4.3.2}$$

where we use the Higgs alignment assumption $\lambda_6 = 0$ at tree level and the tree level stationary conditions in Eq. (5.1.4).

The one-loop level effective potential is given by

$$V_1 = V_0 + V_{\mathrm{CW}} + V_{\mathrm{c.t.}}, \tag{4.3.3}$$

where $V_{\mathrm{CW}}$ is the Coleman-Weinberg potential [198], and $V_{\mathrm{c.t.}}$ is the counterterms. We evaluate the one-loop diagrams in the Landau gauge. Then, the Coleman-Weinberg potential is given by

$$V_{\mathrm{CW}} = \sum_\alpha (-1)^{s_\alpha} \frac{n_\alpha}{64\pi^2}\tilde{m}_\alpha^4 \left[\log\frac{\tilde{m}_\alpha^2}{Q^2} - \frac{3}{2}\right], \tag{4.3.4}$$

where $Q$ is the renormalization scale, and the index $\alpha$ represents the kinds of particles in the loop diagrams; $\alpha = t$, $W^\pm$, $Z$, $\gamma$, $G^\pm$, $G^0$, $H^\pm$, $H_1$, $H_2$, and $H_3$. The field-dependent masses for the particle $\alpha$ are denoted by $\tilde{m}_\alpha^2$. Formulae for $\tilde{m}_\alpha^2$ are shown in Appendix C. The symbol $n_\alpha$ and $(-1)^{s_\alpha}$ in Eq. (5.5.4) are the degrees of freedom and the statistical factor for particle $\alpha$, respectively. The statistical factor is defined as

$$(-1)^{s_\alpha} = \begin{cases} 1 & (\alpha \text{ is a boson}), \\ -1 & (\alpha \text{ is a fermion}). \end{cases} \tag{4.3.5}$$

In Eq. (5.5.4), the contributions from the fermions except for the top quark are not included because their contributions are negligibly small.

To determine the counterterms, we impose the following renormalization conditions at the vacuum at zero temperature;

$$\frac{\partial V_1}{\partial \varphi_i} = 0 \quad (i = 1, 2, 3), \tag{4.3.6}$$

$$\frac{\partial^2 V_1}{\partial \varphi_i \partial \varphi_j} = (M_h^2)_{ij} \quad (i, j = 1, 2, 3), \tag{4.3.7}$$

where $M_h^2$ is the mass matrix for the neutral Higgs bosons defined in Eq. (4.1.10). The second derivatives in the conditions include IR divergences caused by the NG bosons. To avoid them, we replace the NG boson mass at the vacuum with the IR cutoff scalar 1 GeV [199]. The first (second) renormalization condition provides three (six) independent equations. By using these equations, counterterms for $\mu_1^2$, $\mu_3^2$, $\lambda_1$, $\lambda_3$, $\lambda_4$, $\lambda_5$, and $\lambda_6$ are determined. We use the $\overline{\mathrm{MS}}$ scheme to fix the counterterms for $\mu_2^2$, $\lambda_2$, and $\lambda_7$.

At finite temperature, the effective potential is given by

$$V_{\text{eff}}(\varphi_i, T) = V_1 + V_T. \tag{4.3.8}$$

where $V_T$ is the thermal effects at the one-loop level with daisy resummations. For the resummations, we employ the Parwani scheme [200]. Then, the thermal correction at the one-loop level is given as follows [132, 200];

$$V_T = \sum_\alpha (-1)^\alpha \frac{n_k}{2\pi^2\beta^4} \int_0^\infty \mathrm{d}x \, \log\Big(1 - (-1)^{s_k} \exp(-\sqrt{x^2 + \beta^2(\tilde{m}_\alpha^\beta)^2})\Big), \tag{4.3.9}$$

where $(\tilde{m}_\alpha^\beta)^2$ is the field-dependent masses including thermal corrections if $\alpha$ is the gauge bosons or the scalar bosons. For the top quark, it is the same as $\tilde{m}_t^2$. The formulae for $(\tilde{m}_\alpha^\beta)^2$ for each particle are shown in Appendix C.

In the model, the strongly 1st order EWPT can be realized by the non-decoupling effects of the additional scalar bosons. In such a case, the Higgs triple coupling can deviate sizably from the prediction in the SM [140, 141, 143]. By using the effective potential at zero temperature, this deviation in the model is evaluated as

$$\begin{aligned} \Delta R \equiv& \frac{\lambda_{hhh} - \lambda_{hhh}^{\text{SM}}}{\lambda_{hhh}^{\text{SM}}} \\ =& \frac{1}{12\pi^2 v^2 m_{H_1}^2} \Big\{ \frac{2(m_{H^\pm}^2 - \mu_2^2)^3}{m_{H^\pm}^2} + \frac{(m_{H_2}^2 - \mu_2^2)^3}{m_{H_2}^2} + \frac{(m_{H_3}^2 - \mu_2^2)^3}{m_{H_3}^2} \Big\}. \end{aligned} \tag{4.3.10}$$

## 4.4 Electroweak baryogenesis

In this section, we provide the transport equations and the formulae to evaluate the generated baryon asymmetry. The charge transport mechanism by the top quarks in the THDMs is investigated in Refs. [45, 46]. We consider the same situation in these references. We discuss the issue in the wall frame, where the bubble wall is stationary. The radial direction of the bubble is denoted by the $z$-axis. The bubble wall is fixed at $z = 0$, and the negative direction of $z$ is the inside of the bubble (the broken phase).

Since we consider the case that the main source of CP violation is provided by top quarks via the charge transport mechanism, the effects of leptons are expected to be small and are neglected. We consider the transport equations for only quarks and the Higgs. In deriving the transport equation, we use the WKB approximation method [105–109]. In the transport equation, we consider only the baryon number conserving processes; the strong sphaleron process [201, 202], the W scattering, the top Yukawa interaction, the top helicity flips, and the Higgs number violation, and the thermally averaged reaction rate for each process is denoted by $\Gamma_{ss}$, $\Gamma_W$, $\Gamma_y$, $\Gamma_m$, and $\Gamma_h$, respectively. In addition, we neglect the masses of the quarks except for the top quark and the Higgs.

Then, the transport equations for the quarks in the first and second generations and the right-handed bottom quarks can be solved analytically [107]. Their chemical potentials can be represented by using those of the top quark and the left-handed bottom quark. By using these solutions, the transport equations for the left-handed top quark ($t$), the charge conjugation of the right-handed top quark ($t^c$), the left-handed bottom quark ($b$), and the Higgs ($h$) is given as follows [45, 108, 109];

- Left-handed top quarks ($t$)

$$v_w K_{1,t}\mu_t' + v_w K_{2,t}(M_t^2)'\mu_t + u_t' - K_{0,t}\overline{\Gamma}_t = 0, \tag{4.4.1}$$
$$-K_{4,t}\mu_t' - v_w u_t' + v_w \tilde{K}_{6,t}(M_t^2)'u_t + \Gamma^t_{\mathrm{tot}} u_t + v_w K_{0,t}\overline{\Gamma}_t = -S_t. \tag{4.4.2}$$

- Charge conjugation of right-hand top quarks ($t^c$)

$$v_w K_{1,t}\mu_{t^c}' + v_w K_{2,t}(M_t^2)'\mu_{t^c} + u_{t^c}' - K_{0,t}\overline{\Gamma}_{t^c} = 0, \tag{4.4.3}$$
$$-K_{4,t}\mu_{t^c}' - v_w u_{t^c}' + v_w \tilde{K}_{6,t}(M_t^2)'u_{t^c} + \Gamma^t_{\mathrm{tot}} u_{t^c} + v_w K_{0,t}\overline{\Gamma}_{t^c} = -S_t. \tag{4.4.4}$$

- left-hand bottom quarks ($b$)

$$v_w K_{1,b}\mu_b' + u_b' - K_{0,b}\overline{\Gamma}_b = 0, \tag{4.4.5}$$
$$-K_{4,b}\mu_b' - v_w u_b' + \Gamma^b_{\mathrm{tot}} u_b + v_w K_{0,b}\overline{\Gamma}_b = 0, \tag{4.4.6}$$

- Higgs ($h$)

$$v_w K_{1,h}\mu_h' + u_h' - K_{0,h}\overline{\Gamma}_h = 0, \tag{4.4.7}$$
$$-K_{4,h}\mu_h' - v_w u_h' + \Gamma^h_{\mathrm{tot}} u_h + v_w K_{0,h}\overline{\Gamma}_h = 0, \tag{4.4.8}$$

where $S_t$ in Eqs. (4.4.2) and (4.4.4) is defined as

$$S_t = -v_w K_{8,t}(M_t^2\theta_t')' + v_w K_{9,t}\theta' M_t^2 (M_t^2)', \tag{4.4.9}$$

where the functions $M_t$ and $\theta_t$ are the absolute value and the phase of the localized top masses. The localized top masses can be calculated by using the solutions of the bounce equations for $\varphi_1$, $\varphi_2$, and $\varphi_3$. Let $\hat{\varphi}_i(z)$ $(i = 1, 2, 3)$ be these solutions. Then, $M_t(z)$ and $\theta(z)$ are evaluated as [46]

$$M_t(z) = \frac{m_t}{v}\left(\hat{\varphi}_1^2 + 2|\zeta_u|\hat{\varphi}_1\hat{\varphi}_H\cos(\theta_H + \theta_u) + |\zeta_u|^2\hat{\varphi}_H^2\right)^{1/2}, \tag{4.4.10}$$
$$\partial_z\theta_t(z) = -\frac{\hat{\varphi}_H^2}{\hat{\varphi}_1^2 + \hat{\varphi}_H^2}\partial_z\theta_H + \partial_z \mathrm{Tan}^{-1}\left(\frac{\hat{\varphi}_H|\zeta_u|\sin(\theta_H + \theta_u)}{\hat{\varphi}_1 + \hat{\varphi}_H|\zeta_u|\cos(\theta_H + \theta_u)}\right), \tag{4.4.11}$$

where $\hat{\varphi}_H(z) = \sqrt{\hat{\varphi}_2^2 + \hat{\varphi}_3^2}$ and $\theta_H(z) = \mathrm{Tan}^{-1}(\hat{\varphi}_3/\hat{\varphi}_2)$.

We explain the definitions of undefined parameters in Eqs. (4.4.1)-(4.4.9) in order. The symbol $\mu_i$ ($u_i$) for $i = t$, $t^c$, $b$, and $h$ is CP-odd parts of the local chemical potential (the plasma velocity) of the particle $i$, which is a function of the radial coordinate $z$. The prime in the equations denotes the derivative by $z$. For the definitions of the functions $K_{a,i}$ ($a = 0$–$9$, $i = t, b, h$), see Sec. 3.1.3 of this thesis. The symbol $\Gamma^i_{\mathrm{tot}}$ is the thermally averaged total reaction rate for the particle $i$, and $\overline{\Gamma}_i$ denotes the effect from the inelastic scatterings for $i$ which is given by

$$\begin{aligned}\overline{\Gamma}_t &= \Gamma_{ss}\Big((1+9K_{1,t})\mu_{t_L} + (1+9K_{1,b})\mu_b + (1-9K_{1,t})\mu_{t^c}\Big)\\ &\quad + \Gamma_W(\mu_t - \mu_b) + \Gamma_y(\mu_t + \mu_h + \mu_{t^c}) + \Gamma_m(\mu_t + \mu_{t^c}), \qquad (4.4.12)\\ \overline{\Gamma}_{t^c} &= \Gamma_{ss}\Big((1-K_{1,t})\mu_{t^c} + (1+9K_{1,t})\mu_t + (1+9K_{1,b})\mu_b\Big)\\ &\quad + \Gamma_m(\mu_{t^c} + \mu_t) + \Gamma_y(2\mu_{t^c} + \mu_t + \mu_b + 2\mu_h), \qquad (4.4.13)\\ \overline{\Gamma}_b &= \Gamma_{ss}\big((1+9K_{1,t})\mu_t + (1+9K_{1,b})\mu b + (1-9K_{1,t})\mu_{t^c}\big)\\ &\quad + \Gamma_W(\mu_b - \mu_t) + \Gamma_y(\mu_b + \mu_h + \mu_{t^c}), \qquad (4.4.14)\\ \overline{\Gamma}_h &= \Gamma_y(2\mu_h + \mu_t + \mu_b + 2\mu_{t^c}) + \Gamma_h\mu_h. \qquad (4.4.15)\end{aligned}$$

By solving the above transport equations with the boundary conditions $\mu_i(z = \pm\infty) = 0$ $(i = t, t^c, b, h)$, the distribution of the CP-odd chemical potential can be obtained. Then, the baryon asymmetry $\eta_B \equiv n_B/s$, where $n_B$ is the baryon number density and $s$ is the entropy density, can be evaluated by the following formula [46, 107];

$$\eta_B = \frac{405\Gamma_{\rm sph}}{4\pi^2 v_w g_* T}\int_0^\infty {\rm d}z\, \mu_{B_L} f_{\rm sph} \exp\Big(-\frac{45\Gamma_{\rm sph} z}{4v_w}\Big), \qquad (4.4.16)$$

where $g_* = 106.75$ is the effective degree of freedom for the entropy density at the electroweak phase transition. The symbol $\Gamma_{\rm sph}$ denotes the rate of the weak sphaleron. The integrand $\mu_{B_L}$ is defined by using the solution of the transport equations as follows:

$$\mu_{B_L} = \frac{1}{2}(1+4K_{1,t})\mu_t + \frac{1}{2}(1+4K_{1,b})\mu_b - 2K_{1,t}\mu_{t^c}. \qquad (4.4.17)$$

In addition, the function $f_{\rm sph}(z)$ is given by

$$f_{\rm sph} = \min\Big(1,\ \frac{2.4T}{\Gamma_{\rm sph}} e^{-40v(z)/T}\Big), \qquad (4.4.18)$$

where $v(z) = \sqrt{\hat\varphi_1^2(z) + \hat\varphi_2^2(z) + \hat\varphi_3^2(z)}$. This function represents the the suppression of the weak sphaleron rate for $z > 0$ caused by the non-zero VEVs [46].

## 4.5 Numerical evaluations

In this section, we show the results of numerical evaluations for the EWPT and EWBG. In the evaluations, we use the values shown in Table 4.1, which are the SM parameters at the scale of the mass of the Z boson. Some quantities about the EWPT such as nucleation temperature $T_n$ are evaluated by using CosmoTransitions [203], which is a set of python modules.

As discussed in Sec. 3.1.1, for successful electroweak baryogenesis, the condition $v_n/T_n \gtrsim 1$, where $v_n$ is the total electroweak symmetry breaking VEV at the nucleation temperature, i.e.,

$$v_n = \sqrt{\langle\Phi_1\rangle^2 + \langle\Phi_2\rangle^2}\,\Big|_{T=T_n}. \qquad (4.5.1)$$

In the model, this condition can be satisfied due to the non-decoupling effects of the additional scalar bosons $H^{\pm}$, $H_2$, and $H_3$. In such a case, a sizable deviation of the triple Higgs boson coupling from the SM prediction ($\Delta R$) is expected [140,141,143]. In Fig. 4.2, $v_n/T_n$ and $\Delta R$ are shown for some values of the additional Higgs bosons masses. Input parameters for Fig. 4.2 are as follows;

$$\begin{aligned} &M = 30\ \text{GeV}, \quad \lambda_2 = 0.1, \quad |\lambda_7| = 0.8, \quad \theta_7 = 0.9, \\ &|\zeta_e| = |\zeta_u| = |\zeta_d| = 0.14, \quad \theta_u = \theta_d = 2.8, \quad \delta \equiv \theta_u - \theta_e = 0.05. \end{aligned} \tag{4.5.2}$$

We have used CosmoTransitions to evaluate $v_n/T_n$, and $\Delta R$ is calculated by using Eq. (4.3.10). We have checked that all the theoretical and experimental constraints in Sec. 4.2 are sat-

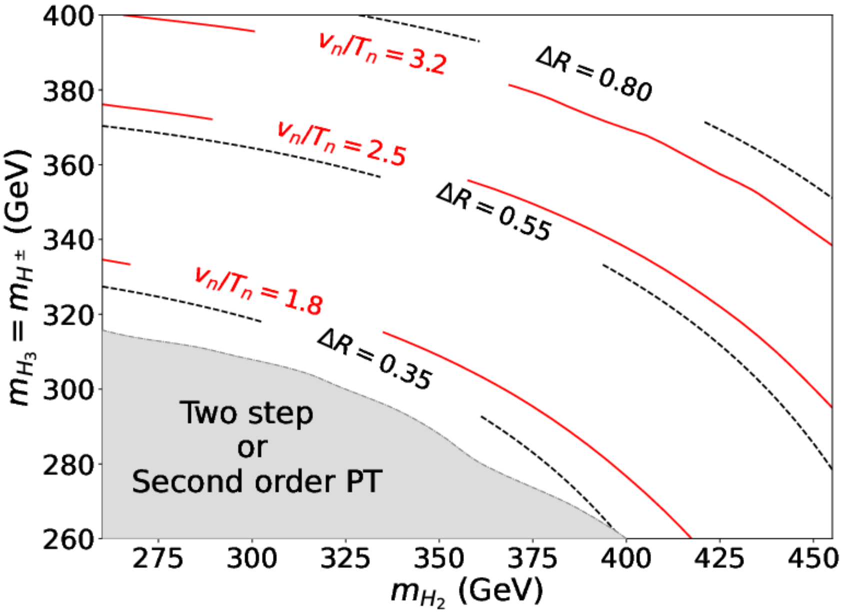


Figure 4.2: Contour plots of $v_n/T_n$ (red lines) and $\Delta R$ (black lines). The input parameters are shown in Eq. (4.5.2).

| | | | |
|---|---|---|---|
| $m_u = 1.29 \times 10^{-3}$, | $m_c = 0.619$, | $m_t = 171.7$, | $m_W = 80.379$ |
| $m_d = 2.93 \times 10^{-3}$, | $m_s = 0.055$, | $m_b = 2.89$, | $m_Z = 91.1876$ |
| $m_e = 4.87 \times 10^{-4}$, | $m_\mu = 0.103$, | $m_\tau = 1.746$. | (in GeV) |
| $\alpha = 1/127.955$, | $\alpha_S = 0.1179$. | | |

Table 4.1: The input parameters of the SM parameters [191]. The masses of fermions and gauge bosons are given in GeV. The coupling constants $\alpha$ and $\alpha_S$ are the fine structure constant of QED and QCD, respectively.

isfied for all the regions in Fig. 4.2.

In the gray region in Fig. 4.2, the EWPT is the two-step one or the 2nd order one. It is found that in the region where the 1st order phase transition occurs, $v_n/T_n$ is large enough for successful EWBG. In such a parameter region, $\Delta R$ is expected to be about 30–80 %. Since the invariant mass $M$ is fixed, the non-decoupling effect is enhanced in the heavy mass region. Therefore, $v_n/T_n$ and $\Delta R$ increase as the additional Higgs boson is heavier. In Fig. 4.3, produced baryon asymmetry via EWBG is shown. The

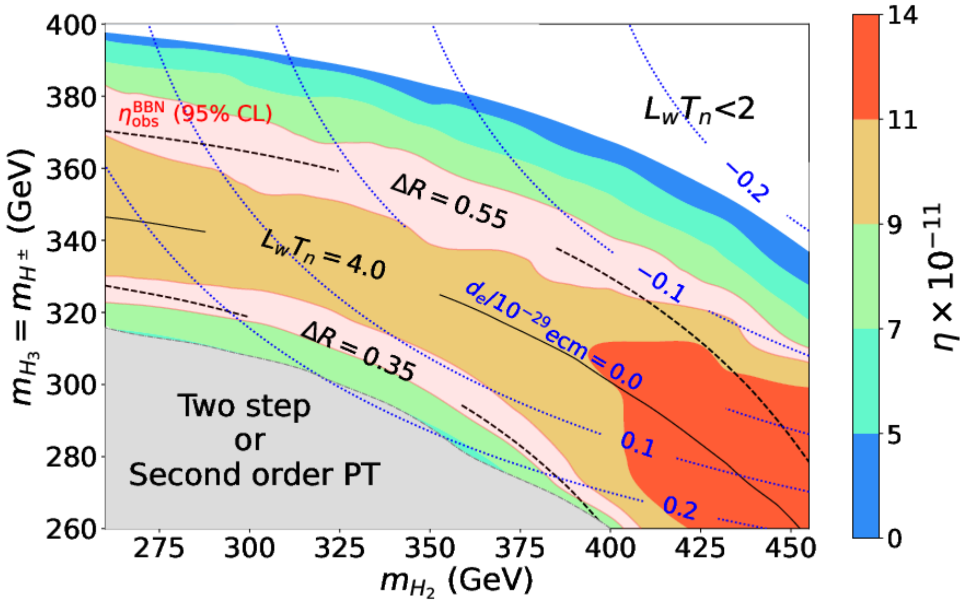


Figure 4.3: The generated baryon asymmetry is shown. Input parameters are shown in Eq. (4.5.2). On the point in the pink regions, the observed baryon asymmetry can be obtained.

input parameters are in Eq. (4.5.2). In solving the transport equations, we assum that $v_w = 0.1$ and use the following values for the reaction rates; $\Gamma_{ss} = 4.9\times10^{-4}T$ [204], $\Gamma_W = \Gamma^h_{\rm tot}$ [45, 108], $\Gamma_y = 4.2\times10^{-3}T$ [205], $\Gamma_m = M_t^2/(63T)$ [205], and $\Gamma_h = \hat{m}_W^2/(50T)$ [205], where $\hat{m}_W$ is the localized W boson mass defined as $\hat{m}_W^2(z) = g_L^2(\hat{\varphi}_1^2+\hat{\varphi}_2^2+\hat{\varphi}_3^2)/4$. The thermally averaged total reaction rates are evaluated as $\Gamma^i_{\rm tot} = K_{4,i}/(K_{1,i}D_i)$, where $D_i$ is the diffusion coefficient for the particle $i$ and is given by [107, 205]

$$D_t = D_b \equiv D_q = \frac{6}{T}, \quad D_h = \frac{20}{T}. \tag{4.5.3}$$

The gray region in Fig 4.3 is the same as that in Fig. 4.2. The black line in the figure is the contour for $L_wT_n = 4.0$, where $L_w$ is the width of the bubble wall. It is determined by fitting the solutions of the bounce equation $v(z) \equiv \sqrt{\hat{\varphi}_1^2+\hat{\varphi}_2^2+\hat{\varphi}_3^2}$ with $\frac{v_n}{2}(1-\tanh\frac{z}{L_w})$. In the region below the line for $L_wT_n = 4.0$, the produced baryon asymmetry increases as the additional Higgs boson is heavier. It is because the EWPT is stronger in the heavier mass region as shown in Fig. 4.2. On the other hand, in the region above the line $L_w T_n = 4.0$, the produced baryon asymmetry decreases as the masses of the Higgs bosons increase. This is due to the fact that $L_w T_n$ is smaller as the phase transition is stronger. This behavior is discussed in Ref. [206]. In addition, for too small $L_w T_n$, the WKB approximation method is not an appropriate [105–107].

In the two pink regions in Fig. 4.3, the observed baryon asymmetry can be explained within 95 % C.L. In these regions, the sizable $\Delta R$ is expected (30–50 %). It would be tested at future collider experiments such as HL-LHC [207], the upgraded ILC [208,209], and CLIC [210]. In the orange and red regions, the produced baryon asymmetry is larger than the observed one.

The blue dotted lines in Fig. 4.3 are contour plots for the eEDM $d_e/|d_e^{\rm exp}| = 0, \pm 0.1$, and $\pm 0.2$, where $|d_e^{\rm exp}| = 1.0 \times 10^{-29}$ (e cm) is the current upper limit given by the ACME result [178]. On the line $d_e/|d_e^{\rm exp}| = 0$, fermion loop diagrams and scalar loop diagrams shown Fig. 4.1 cancel each other due to the destructive interference between CP-violating phases [104]. The contour for the current upper limit $d_e/|d_e^{\rm exp}| = \pm 1.0$ is outside the figure. Therefore, it is found that in all the pink regions, the observed baryon asymmetry can be reproduced under the current severe constraint from the eEDM measurements. At future eEDM experiments, the one-order magnitude improvement of the upper limit on $d_e$ is expected [178]. Then, the region except for one sandwiched between the lines $d_e/|d_e^{\rm exp} = \pm 0.1$ will be excluded. Therefore, almost all the lower pink regions would be tested by the future eEDM measurements.

In the mass region in Fig. 4.3, the nEDM is about four orders smaller than the current upper limit. It is because we assume that $\theta_u = \theta_d$, and the leading contribution to nEDM is proportional to $\sin(\theta_u - \theta_d)$ as discussed in Sec. 4.2. If we consider the case that $\theta_d \neq \theta_u$, the nEDM can be enhanced. In such a case, the nEDM is about one order smaller than the current upper limit. In the future, the one-order magnitude improvement of the nEDM measurement is expected [211]. Thus, some parameter regions in Fig. 4.3 would be tested by future nEDM measurements in the case that $\theta_u \neq \theta_d$.

In Fig. 4.4, the eEDM and the baryon asymmetry are shown for various values of $\lambda_7$. In the upper, the lower left, and the lower right figures, we assume that $\delta (\equiv \theta_u - \theta_e) = 0$, 0.05, and $-0.05$, respectively. In addition, we assume the following input parameters;

$$\begin{aligned} &m_{H_2} = m_{H_3} = m_{H^\pm} = 330 \text{ GeV}, \quad M = 30 \text{ GeV}, \quad \lambda_2 = 0.1, \\ &|\zeta_u| = |\zeta_d| = |\zeta_e| = 0.15, \quad \theta_u = \theta_d = 1.2. \end{aligned} \tag{4.5.4}$$

In the black regions in Fig. 4.4, the EWBG occurs in multiple steps. Such regions are neglected for the sake of simplicity. In the pink regions, the observed baryon asymmetry can be reproduced within 95 % C.L. The typical value of $v_n/T_n$ in these regions are about 2.0. Since we fixed the value of $\zeta_u$, the pink regions in the three figures are almost the same.

The blue lines in Fig. 4.4 are contour plot for the eEDM $d_e/|d_e^{\rm exp}| = 0$ and $\pm 0.1$. The yellow regions are excluded by the ACME result [178]. In the upper figure ($\delta = 0$), the top quark loop diagrams vanish because $\sin \delta = 0$. Then, the eEDM is generated via only the scalar loop diagrams at two-loop levels. Therefore, $d_e$ equals to zero on the line $\theta_7 - \theta_e = 0$ and $\pi$. In this case, almost all regions for the correct baryon asymmetry are excluded by the current eEDM data and will be completely excluded by the one-order magnitude improvement in the near future [178].

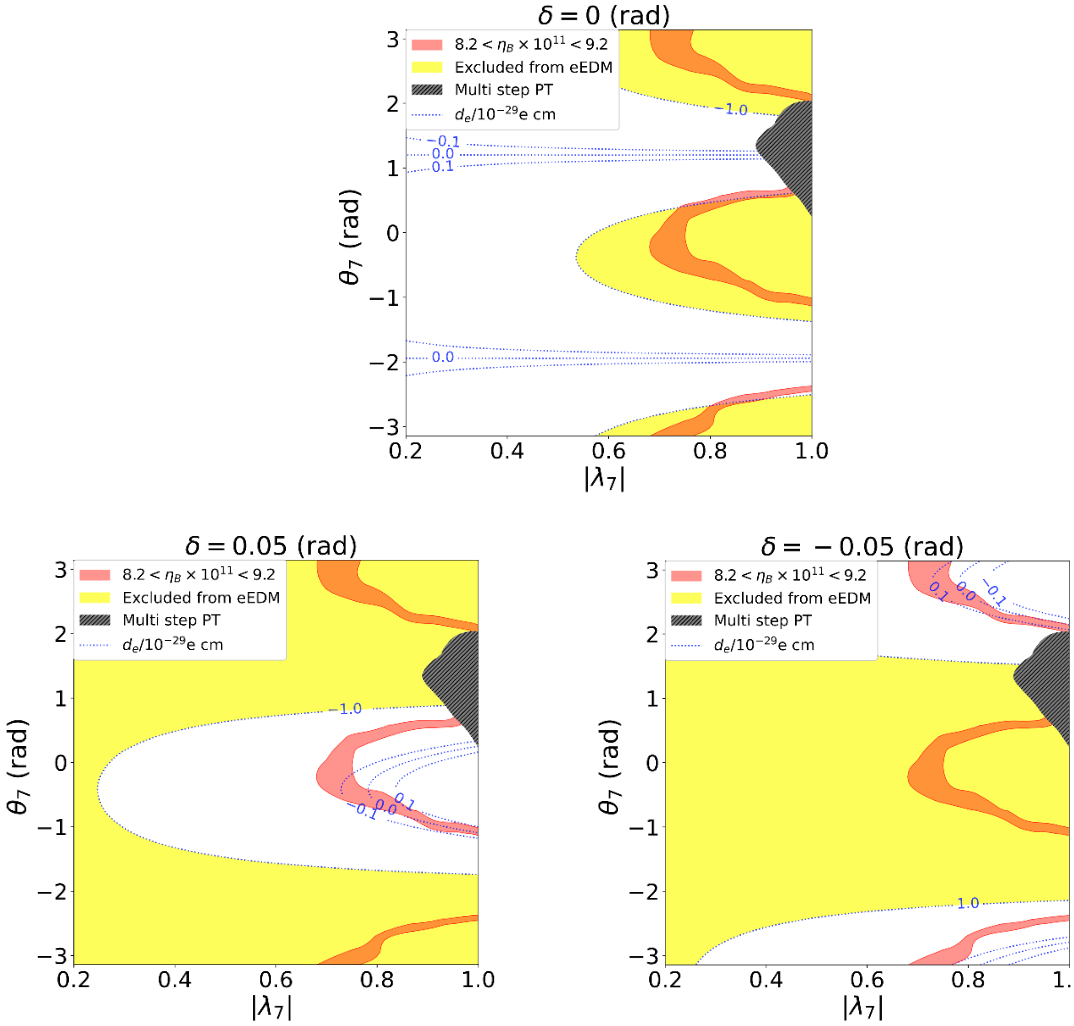


Figure 4.4: Dependence on $\lambda_7$ of the eEDM and that of the baryon asymmetry for $\delta = 0$ (upper), $\delta = 0.05$ (lower left) and $\delta = -0.05$ (lower right). Input parameters are shown in Eq. (4.5.4). On the points in the pink regions, the observed baryon asymmetry can be obtained.

In the lower-left figure ($\delta = 0.05$), the excluded yellow regions are drastically changed because the top quark loop diagrams give large contributions to the eEDM. Even in this case, there is a line on which $d_e$ at two-loop level vanish due to the destructive interference between the CP-violating phases in the region $|\lambda_7| \gtrsim 0.8$. In the pink region between the lines $\theta_7 = \pm 1$, the observed baryon asymmetry can be reproduced under the current eEDM constraint. By the one-order magnitude improvement of the eEDM measurements, the wide part of this pink region will be tested.

In the case that $\delta = -0.05$ (lower right figure), the sign of the top quark loop diagram is opposite from that in the lower left figure ($\delta = 0.05$). The allowed region is thus shifted by $\pi$ in the direction of $\theta_7$ from that in the figure for $\delta = 0.05$. Then, the pink region between the lines $\theta_7 = \pm 1$ is excluded by the current ACME result. On the other hand, in the other two pink regions, the eEDM constraint is avoided, and we can obtain the observed baryon asymmetry within 95 % C.L. The wide part of these pink regions will be tested by the one-order magnitude improvement.

## 4.6 Discussions and predictions

In this section, we comment on the evaluation of the baryon asymmetry. The testability of the model in future experiments is also discussed in the latter of this section.

**Comments on the evaluation of the baryon asymmetry**

In the above analyses, we assume that $|\zeta_u| = |\zeta_d| = |\zeta_e|$ for the sake of simplicity. In this case, the top quarks couple most strongly to the Higgs boson among the SM fermions, and the main source of the CP violation is supplied by the charged transport mechanism by the top quarks. If we relax the condition $|\zeta_u| = |\zeta_d| = |\zeta_e|$, the main source of the CP violation can be changed. For example, if we consider the case that $|\zeta_u| \ll |\zeta_e|$, the tau leptons can provide a larger CP violation effect than the top quarks [212–214]. Similarly, in the case that $|\zeta_u| \ll |\zeta_d|$, the bottom quarks can play an essential role for EWBG [53]. These situations are also interesting, and they will be investigated elsewhere [215].

In addition, we can consider relaxing the assumption of the Yukawa alignment [98]. Then, the additional Higgs bosons have the flavor non-diagonal Yukawa interactions. These flavor non-diagonal interactions are strongly constrained by the current flavor experiments. Even in such a case, some of the non-diagonal interactions can be an important piece of the source of CP violation. For example, the effect of $t$-$c$ ($\tau$-$\nu$) mixing coupling in EWBG is investigated in Ref. [52] (Refs. [50, 51]). This extension of the Yukawa interactions can also be considered in our model. The effects of the flavor non-diagonal interactions in our model will be investigated in the future [215].

In our evaluation of the baryon asymmetry, we have considered the issue at the linear order of $v_w$. In Ref. [109], it is investigated how the neglected higher-order terms change the result. According to this reference, in the case that $v_w = 0.1$, it is expected that the produced baryon asymmetry is reduced by 10–20 %. Thus, if we take into account the relativistic effect of the bubble wall velocity, the regions for overproduction in Fig. 4.3 and Fig. 4.4 would be suitable to reproduce the observed baryon asymmetry.

While we have used the WKB approximation method in deriving the transport equations, there is another method to evaluate the baryon asymmetry produced by EWBG, the VEV Insertion Approximation (VIA) [216]. In Refs. [54, 109, 206], these two methods are compared, and they have found that the produced baryon asymmetry evaluated by the VIA method is orders of magnitude larger than that evaluated by using the WKB approximation. Therefore, in the case that the VIA is used to evaluate the baryon asymmetry in our model, the regions for the successful baryogenesis in Fig. 4.3 and Fig. 4.4 are drastically changed. Even in such a case, by taking $|\zeta_u|$ and $|\lambda_7|$ to be smaller with keeping the destructive interference, it would be able to reproduce the observed baryon asymmetry by taking under the current eEDM constraint.

**Testability of the model at future experiments**

Next, we discuss the testability of the model at various future experiments. In our model, new scalar bosons $H^\pm$, $H_{2,3}$ are included. As shown in Fig. 4.3, the observed baryon asymmetry is reproduced by the effects of the additional Higgs bosons whose masses are 300–400 GeV. These additional Higgs bosons would be tested at the HL-LHC [102].

According to Ref. [102], in the case that $|\zeta_u| = |\zeta_d| = |\zeta_e|$, the pseudo scalar Higgs boson $H_3$ whose mass is in 200 GeV $\lesssim m_{H_3} \lesssim$ 350 GeV is expected to be tested by searching for $H_3 \to \tau\overline{\tau}$ at the HL-LHC with the integrated luminosity $L = 3000$ fb$^{-1}$ unless $|\zeta_u|$ is smaller than about 0.17. Heavier $H_3$ can be tested by searching for $H_3 \to t\bar{t}$. The testable mass region depends on the value of $|\zeta_u|$. In the case that $|\zeta_u| = 0.33$ (0.5), $H_3$ which is lighter than about 600 GeV (800 GeV) can be tested at the HL-LHC with $L = 3000$ fb$^{-1}$ [102]. The searching for the signal from $H^\pm \to tb$ is also an important test of our model. At the HL-LHC with $L = 3000$ fb$^{-1}$, $H^\pm$ which is lighter than 600 GeV (800 GeV) is expected to be tested in the case that $|\zeta_u| = 0.33$ (0.5) [102].

The testability of the additional Higgs bosons at the HL-LHC strongly depends on the values of $\zeta_f$ couplings. For example, in the case that $|\zeta_u| = 1/|\zeta_d| = 1/|\zeta_e|$, where the model has the same Yukawa structure as that in Type-II THDM [159–161], the bottom associated production of $H_{2,3}$ are enhanced in small $|\zeta_u|$ regions. Thus, $H_3$ which is lighter than about 500 GeV can be tested by combing the searches for $H_3 \to \tau\overline{\tau}$ and $H_3 \to t\bar{t}$ regardless of the value of $|\zeta_u|$ [102]. The charged Higgs boson is also thoroughly tested by using the searches for $H^\pm \to tb$ and $H^\pm \to \tau\nu$ at the HL-LHC [102].

Recently, the test of the additional Higgs boson in our model at hadron colliders has been studied in Ref. [103]. The authors have considered the case that decays $H_{2,3} \to t\bar{t}$ and $H^\pm \to tb$ are kinematically prohibited and have investigated the following pair production of the additional Higgs bosons with the CP-conserving Yukawa interactions; $pp \to H_2H_3$, $pp \to H_2H^\pm$, $pp \to H_3H^\pm$, and $pp \to H^+H^-$. They have found that in such a case, the additional Higgs bosons are strongly constrained by using the search for multi-lepton final states. For example, in the case that $(m_{H_2}, m_{H_3}, m_{H^\pm}) = (230, 280, 280)$ GeV and $\zeta_u = 0.1$, $\zeta_e$ is expected to be tested at the HL-LHC up to $\zeta_e = 0.15$ (1.8) for $\zeta_d = 0.1$ (1.0).

In the above analyses, we assume the alignment in the Higgs potential ($\lambda_6 = 0$). If we consider the case that this alignment is broken, the decays of the additional Higgs boson into a pair of gauge bosons and a pair of a gauge boson and the SM Higgs boson are generated at tree-level. Therefore, even in the case that the deviation from the alignment is slight, the branching ratios of the additional Higgs bosons drastically change. Then, the testability of the model can be greatly enhanced [102].

The additional Higgs bosons can also be tested at future flavor experiments such as Belle-II [217] and LHCb [218] by observing the processes like $B \to X_s\gamma$, $B^0 \to \mu^+\mu^-$, and the $B^0$-$\overline{B}^0$ mixing. Furthermore, the future flavor experiments are expected to be also effective to test the CP-violating phases of $\zeta_u$, $\zeta_d$, and $\zeta_e$. For example, by searching for the asymmetry between the CP violation in $B^- \to X_s^-\gamma$ and that in $B^0 \to X_s^0\gamma$, these phases would be tested [53, 219, 220].

The CP-violating phases in the model can be also tested by future EDM measurements as discussed in Sec. 4.5. In next-generation experiments for both the eEDM and the nEDM, the upper limits are expected to be improved by a one-order magnitude [178,211]. These improvements are expected to be effective to explore the regions for successful EWBG in Fig. 4.3 and 4.4.

Furthermore, the CP-violating phase of $\zeta_e$ can be tested at future lepton colliders by observing the azimuthal angle distribution of the hadronic decays of the tau leptons from the decay of $H_2, H_3$ [104, 221]. In Ref. [104], this testability in our model has been investigated. The authors have found that it would be possible to distinguish the CP-violating case ($\sin\theta_e \neq 0$) and the CP-conserving case by looking at the azimuthal angle distribution at the future upgraded ILC with $L = 3000$ fb$^{-1}$ unless the additional Higgs bosons are too heavy and $\theta_e$ is too small. This test would be particularly effective in the case that $|\zeta_e| \gg |\zeta_u|, |\zeta_d|$ and $\theta_e = \mathcal{O}(1)$.

In the model, the strongly 1st order phase transition is caused by the non-decoupling effect of the additional Higgs bosons. This non-decoupling effect can be tested by the measurements of the triple Higgs bosons coupling [140, 141, 143] via the di-Higgs production at future high-energy colliders [208, 222–229]. At the HL-HLC and the upgraded ILC with $\sqrt{s} = 500$ GeV (1 TeV), the triple Higgs boson coupling is expected to be measured with the accuracies 50 % [207, 208] and 27 % (10 %) [209]. As discussed in Sec. 4.5, in the regions for the successful EWBG in Figs. 4.3 and 4.4, $\Delta R$ is about 30–50 %. These deviations would be tested at the HL-LHC and the future upgraded ILC.

Finally, GW can be produced by the 1st order EWPT in extended Higgs sectors [230–232]. They would be detectable at future space-based GW detectors such as LISA [233], DECIGO [234], and BBO [235]. This testability of our model will be investigated elsewhere [215].

## 4.7 Summary of Chapter 4

In this chapter, I have introduced one of my works in Ref. [55]. In this work, we have investigated EWBG in the CP-violating two Higgs doublet model, where the Yukawa interactions are aligned to avoid the FCNCs, and coupling constants of the lightest Higgs boson coincide with those in the SM at tree level. In the analyses, we have focused on the parameter regions where the severe constraints from the current eEDM measurement can be satisfied by the destructive interferences between the CP-violating phases in the Yukawa interactions and that in the Higgs potential. We have some benchmark scenarios where the observed baryon number asymmetry can be reproduced under the various experimental and theoretical constraints. These benchmark scenarios can be tested by various future experiments. The typical value of the additional Higgs bosons is 300–400 GeV for the successful EWBG. These would be tested at the HL-LHC and flavor experiments such as Belle-II and LHCb. The CP-violating phases which are essential to the successful EWBG would be tested by future EDM measurements, flavor experiments, and linear colliders. In addition, the strongly 1st order EWPT in the model can be tested by measuring the triple Higgs boson coupling. The typical value in the benchmark scenarios is 35–55 %. This would be tested by the HL-LHC and the future upgraded ILC. In addition, the strongly 1st order EWPT in the model might be able to be tested by observing the GWs. This possibility will be investigated in the future.

# Chapter 5

# The model for tiny neutrino masses, dark matter and baryon asymmetry of the universe

In this chapter, I introduce another of my work [110]. In this work, we investigate a new model which can explain tiny neutrino masses, DM, and the BAU. This model includes two isospin doublets. Thus, the Higgs potential in this model is an extension of that in the THDMs discussed in Chapter 4.

The original idea of the model was proposed by Aoki, Kanemura, and Seto in 2009 [75] (in the following, this reference is denoted by AKS09). However, in AKS09, the authors neglected CP violation for the sake of simplicity. They only showed that the strongly 1st order EWPT can be realized while explaining data of neutrino oscillation and DM relic abundance under some experimental constraints at the time.

We take into account the CP violation to investigate EWBG in the model. In addition, to avoid the severe constraints from the EDM measurements, we extend the original model in AKS09 according to the idea proposed in Ref. [101], which is discussed in the previous chapter. We show a benchmark scenario where neutrino masses, DM, and the BAU can be explained simultaneously with satisfying constraints from current experiments. We also discuss how to test these benchmark scenarios at the near-future experiments.

## 5.1 The model

### 5.1.1 Lagrangian of the model

In Table 5.1, fermion and scalar fields in the model are shown. In addition to the fields in the SM, there are three gauge-singlet right-handed fermions $N_{aR}$ ($a = 1, 2, 3$) and three kinds of scalar fields, the isospin doublet $\Phi_2$, the singly charged isospin singlet $S^{\pm}$, and the gauge singlet real scalar $\eta$. We impose a new exact $Z_2$ symmetry on the model. The fields $N'_{aR}$, $S^{\pm}$, and $\eta$ have odd-parity under $Z_2$ transformation. The $Z_2$-odd fermions

$N_{aR}$ $(a = 1, 2, 3)$ have Majorana-type masses,

$$\mathcal{L}^N_{mass} = -\frac{1}{2}\sum_{a=1}^{3}(M_{N_a})\overline{N^c_{aR}}N_{aR} + \text{h.c.}, \tag{5.1.1}$$

where we define the basis of $N_{aR}$ so that the mass matrix is diagonal.

We assume that the isospin doublets are in the Higgs basis discussed in Sec. 4.1. Then, the Higgs potential in the model is given by

$$\begin{aligned}
V = &-\mu_1^2|\Phi_1|^2 - \mu_2^2|\Phi_2|^2 - \left\{\mu_{12}^2\Phi_1^\dagger\Phi_2 + \text{h.c.}\right\} + \mu_s^2|S^+|^2 + \frac{\mu_\eta^2}{2}\eta^2 \\
&+ \frac{\lambda_1}{2}|\Phi_1|^4 + \frac{\lambda_2}{2}|\Phi_2|^4 + \lambda_3|\Phi_1|^2|\Phi_2|^2 + \lambda_4|\Phi_1^\dagger\Phi_2|^2 \\
&+ \left\{\frac{\lambda_5}{2}(\Phi_1^\dagger\Phi_2)^2 + \lambda_6|\Phi_1|^2(\Phi_1^\dagger\Phi_2) + \lambda_7|\Phi_2|^2(\Phi_1^\dagger\Phi_2) + \text{h.c.}\right\} \\
&+ \rho_1|\Phi_1|^2|S^+|^2 + \rho_2|\Phi_2|^2|S^+|^2 + \left\{\rho_{12}(\Phi_1^\dagger\Phi_2)|S^+|^2 + \text{h.c.}\right\} \\
&+ \frac{\sigma_1}{2}|\Phi_1|^2\eta^2 + \frac{\sigma_2}{2}|\Phi_2|^2\eta^2 + \left\{\frac{\sigma_{12}}{2}(\Phi_1^\dagger\Phi_2)\eta^2 + \text{h.c.}\right\} \\
&+ \left\{\sum_{\alpha,\beta=1}^{2}\kappa(\epsilon_{\alpha\beta}\widetilde{\Phi}_\alpha^\dagger\Phi_\beta)S^-\eta + \text{h.c.}\right\} + \frac{\lambda_s}{4}|S^+|^4 + \frac{\lambda_\eta}{4!}\eta^4 + \frac{\xi}{2}|S^+|^2\eta^2.
\end{aligned} \tag{5.1.2}$$

The relations between the coupling constants in the Higgs basis and those in any other basis are shown in Appendix A. In general, the coupling constants $\mu_{12}^2$, $\lambda_5$, $\lambda_6$, $\lambda_7$, $\rho_{12}$, $\sigma_{12}$, and $\kappa$ are complex number. As discussed in Sec. 4.1, one of $\mu_{12}^2$, $\lambda_5$, $\lambda_6$, $\lambda_7$ can be a real parameter by rephasing $\Phi_2$ appropriately. In addition, rephasing of $S^\pm$ can remove the phase of $\kappa$. As a result, there are five CP-violating couplings in the Higgs potential.

Since we consider the case that $Z_2$ symmetry is not broken at the vacuum, only isospin doublets $\Phi_1$ and $\Phi_2$ can acquire the VEVs. Since we consider the issues in the Higgs basis, the elements of $\Phi_1$ and $\Phi_2$ are parametrized as follows;

$$\Phi_1 = \begin{pmatrix} G^+ \\ \frac{1}{\sqrt{2}}(v + h_1 + iG^0) \end{pmatrix}, \quad \Phi_2 = \begin{pmatrix} H^+ \\ \frac{1}{\sqrt{2}}(h_2 + ih_3) \end{pmatrix}. \tag{5.1.3}$$

| | Fermion fields | | | | | | Scalar fields | | | |
|---|---|---|---|---|---|---|---|---|---|---|
| | $Q'_{iL}$ | $u'_{iR}$ | $d'_{iR}$ | $L'_{iL}$ | $\ell'_{iR}$ | $N_{aR}$ | $\Phi_1$ | $\Phi_2$ | $S^+$ | $\eta$ |
| $\mathrm{SU(3)_C}$ | **3** | **3** | **3** | **1** | **1** | **1** | **1** | **1** | **1** | **1** |
| $\mathrm{SU(2)_L}$ | **2** | **1** | **1** | **2** | **1** | **1** | **2** | **2** | **1** | **1** |
| $\mathrm{U(1)_Y}$ | 1/6 | 2/3 | −1/3 | −1/2 | −1 | 0 | +1/2 | +1/2 | +1 | 0 |
| $Z_2$ | + | | | | | − | + | | − | |

Table 5.1: Table of the fields in the model and quantum numbers for them.

By substituting Eq. (5.1.3) into the Higgs potential, we obtain the same stationary conditions as those in the THDM.

$$\mu_1^2 = \frac{1}{2}\lambda_1 v^2, \quad \mu_{12}^2 = \frac{1}{2}\lambda_6 v^2. \tag{5.1.4}$$

The phase of $\mu_{12}^2$ and that of $\lambda_6$ relate to each other by the second stationary condition. Thus, there are four independent CPV phases in the Higgs potential.

By using the stationary conditions, we obtain the following mass terms for the scalar bosons;

$$\mathcal{L}^s_{mass} = m^2_{H^\pm}|H^+|^2 + m_S^2|S^+|^2 + \frac{1}{2}\sum_{\alpha,\beta=1}^{3} h_\alpha (M_h^2)_{\alpha\beta} h_\beta + \frac{1}{2}m_\eta^2\eta^2. \tag{5.1.5}$$

The scalar bosons $G^\pm$ and $G^0$ do not have mass terms, and they are the NG bosons. The charged scalar bosons ($H^\pm$ and $S^\pm$) and the real scar boson ($\eta$) are mass eigenstates without mixing, and their masses are given by

$$m^2_{H^\pm} = M^2 + \frac{1}{2}\lambda_3 v^2, \tag{5.1.6}$$

$$m_S^2 = \mu_s^2 + \frac{1}{2}\rho_1 v^2, \tag{5.1.7}$$

$$m_\eta^2 = \mu_\eta^2 + \frac{1}{2}\sigma_1 v^2, \tag{5.1.8}$$

where $M^2 = -\mu_2^2$. The neutral Higgs bosons are mixed by the mass matrix defined as

$$M_h^2 = v^2 \begin{pmatrix} \lambda_1 & \mathrm{Re}[\lambda_6] & -\mathrm{Im}[\lambda_6] \\ \mathrm{Re}[\lambda_6] & \frac{M^2}{v^2} + \frac{1}{2}(\lambda_3+\lambda_4+\mathrm{Re}[\lambda_5]) & -\frac{1}{2}\mathrm{Im}[\lambda_5] \\ -\mathrm{Im}[\lambda_6] & -\frac{1}{2}\mathrm{Im}[\lambda_5] & \frac{M^2}{v^2} + \frac{1}{2}(\lambda_3+\lambda_4-\mathrm{Re}[\lambda_5]) \end{pmatrix}. \tag{5.1.9}$$

This is the same as that in Sec. 4.1. For the sake of simplicity, we choose the phase of $\Phi_2$ so that $\lambda_5$ is a real number. Then, mixings among the neutral Higgs bosons caused by only one CP-violating parameter $\lambda_6$.

As discussed in Sec. 4.1, nonzero $\lambda_6$ induce the deviations of the Higgs boson couplings from the SM ones at tree level. To avoid them, we simply assume the alignment in the Higgs potential, i.e. $\lambda_6 = 0$ [101]. Then, the mass matrix $M_h^2$ is a diagonal matrix, and the masses of the neutral Higgs bosons are given by

$$m^2_{H_1} = \lambda_1 v^2, \tag{5.1.10}$$

$$m^2_{H_2} = M^2 + \frac{1}{2}v^2(\lambda_3+\lambda_4+\lambda_5), \tag{5.1.11}$$

$$m^2_{H_3} = M^2 + \frac{1}{2}v^2(\lambda_3+\lambda_4-\lambda_5). \tag{5.1.12}$$

They are the same formulae in the THDM discussed in Sec. 4.1. We also obtain the same relations between the scalar couplings and masses of the additional Higgs bosons;

$$\lambda_3 = \frac{2}{v^2}(m_{H^\pm}^2 - \mu_2^2), \tag{5.1.13}$$

$$\lambda_4 = \frac{1}{v^2}(m_{H_2}^2 + m_{H_3}^2 - 2m_{H^\pm}^2), \tag{5.1.14}$$

$$\lambda_5 = \frac{1}{v^2}(m_{H_2}^2 - m_{H_3}^2). \tag{5.1.15}$$

By the alignment assumption in the Higgs potential, the CP-violating parameters $\lambda_6$ and $\mu_{12}^2$ are set to be zero. As a result, there are three CP-violating phases in the Higgs potential $\theta_7 = \arg[\lambda_7]$, $\theta_\rho = \arg[\rho_{12}]$, and $\theta_\sigma = \arg[\sigma_{12}]$.

The Yukawa interactions in the model are given by

$$\begin{aligned}\mathcal{L}_Y = &-\sum_{\alpha=1}^{2}\sum_{i,j=1}^{3}\left\{(y_u^{a\prime})_{ij}\overline{Q'_{iL}}\tilde{\Phi}_a u'_{jR} + (y_d^{a\prime})_{ij}\overline{Q'_{iL}}\Phi_a d'_{jR} + (y_\ell^{a\prime})_{ij}\overline{L_{iL}}\Phi_a \ell'_{jR}\right\}\\ &-\sum_{ia=1}^{3}(Y'_N)_{ai}\overline{N_{aR}^c}\ell'_{iR}S^+ + \text{h.c.}.\end{aligned} \tag{5.1.16}$$

First, we discuss the Yukawa interactions between the Higgs doublets $\Phi_\alpha$ ($\alpha = 1, 2$) and the SM fermions, which are the same as those in the THDM discussed in Chap. 4. The VEV of $\Phi_1$ generates the mass matrices of the SM fermions;

$$m'_f = \frac{v}{\sqrt{2}}(y_f^{1\prime}), \quad f = u, d, \ell, \tag{5.1.17}$$

which are not generally diagonal matrices. To diagonalize $m'_f$, we redefine the fermions by unitary matrices as in the SM;

$$L'_{iL} = \sum_{j=1}^{3}(V_\ell)_{ij}L_{jL}, \quad \ell'_{iR} = \sum_{j=1}^{3}(U_\ell)_{ij}\ell_{jR}, \tag{5.1.18}$$

$$q'_{iL} = \sum_{j=1}^{3}(V_q)_{ij}q_{jL}, \quad q'_{iR} = \sum_{j=1}^{3}(U_q)_{ij}q_{jR}, \quad \text{for } q = u, d, \tag{5.1.19}$$

where matrices $V_f$ and $U_f$ ($f = u, d, \ell$) are unitary matrices that diagonalize the Yukawa couplings as

$$(V_f^\dagger y_f^{1\prime} U_f)_{ij} = (y_f^1)_i \delta_{ij}. \tag{5.1.20}$$

Then, the up-type quarks $(u_1, u_2, u_3) = (u, c, t)$, the down-type quarks $(d_1, d_2, d_3) = (d, s, b)$, and the charged leptons $(\ell_1, \ell_2, \ell_3) = (e, \mu, \tau)$ are mass eigenstates. The neutrinos $(\nu_1, \nu_2, \nu_3) = (\nu_e, \nu_\mu, \nu_\tau)$ are massless fermions.

As discussed in Sec. 4.1, if $y_f^{1'}$ and $y_f^{2\prime}$ cannot be diagonalized simultaneously, the flavor-changing neutral currents are induced at the tree level. To avoid them, we assume the following conditions;

$$y_u^{2'} = \zeta_u^* y_u^{1'}, \quad y_d^{2'} = \zeta_d y_d^{1'}, \quad y_\ell^{2'} = V_\ell \zeta_\ell V_\ell^\dagger y_\ell^{1'}, \tag{5.1.21}$$

where $\zeta_u$ and $\zeta_d$ are complex numbers, whereas $\zeta_\ell$ is a complex diagonal matrix defined as

$$\zeta_\ell = \begin{pmatrix} \zeta_e & 0 & 0 \\ 0 & \zeta_\mu & 0 \\ 0 & 0 & \zeta_\tau \end{pmatrix}, \quad (\zeta_e,\ \zeta_\mu,\ \zeta_\tau \in \mathbb{C}). \tag{5.1.22}$$

Under this assumption, $y_\ell^{2\prime}$ is diagonalized as follows;

$$\begin{aligned} y_\ell^{2\prime} \to V_\ell^\dagger y_\ell^{2\prime} U_\ell = (V_\ell^\dagger V_\ell)\zeta_\ell (V_\ell^\dagger y_\ell^{1\prime} U_\ell) = \zeta_\ell y_\ell^1 \\ = \frac{\sqrt{2}}{v} \mathrm{diag}(\zeta_e m_e,\ \zeta_\mu m_\mu,\ \zeta_\tau m_\tau). \end{aligned} \tag{5.1.23}$$

In the case that $\zeta_e = \zeta_\mu = \zeta_\tau$, the assumption in Eq. (5.1.21) is the same as the Yukawa alignment condition proposed by Pich and Tuzon [98]. Consequently, there are five CP-violating phases in the Yukawa interactions between the Higgs bosons and the SM fermions: $\theta_u = \arg[\zeta_u]$, $\theta_d = \arg[\zeta_d]$, $\theta_e = \arg[\zeta_e]$, $\theta_\mu = \arg[\zeta_\mu]$, and $\theta_\tau = \arg[\zeta_\tau]$. In the following of this chapter, we call Eq. (5.1.21) the Yukawa alignment condition, not only the case that $\zeta_e = \zeta_\mu = \zeta_\tau$.

By using the Yukawa alignment condition, the Yukawa interactions between the Higgs bosons and the SM fermions are given as follows;

$$\begin{aligned} \mathcal{L}_Y \ni & -\frac{\sqrt{2}}{v} H^+ \sum_{i,j=1}^{3} \Big\{ \overline{u_i} V_{ij} (\zeta_d m_{d_j} P_R - \zeta_u m_{u_i} P_L) d_j + \zeta_{\ell_i} m_{\ell_i} \delta_{ij} \overline{\nu_i} P_R \ell_j \Big\} \\ & - \sum_{i=1}^{3} \sum_{f=u,d,\ell} \sum_{\alpha=1}^{3} \frac{m_{f_i}}{v} \overline{f_i} (\kappa_{S,f_i}^\alpha + \kappa_{P,f_i}^\alpha \gamma_5) f_i H_\alpha, \end{aligned} \tag{5.1.24}$$

where $(\zeta_{\ell_1}, \zeta_{\ell_2}, \zeta_{\ell_3}) = (\zeta_e, \zeta_\mu, \zeta_\tau)$. The coefficients for the scalar coupling $\kappa_{S,f_i}^\alpha$ are defined as

$$\begin{aligned} &\kappa_{S,u_i}^1 = 1, && \kappa_{S,d_i}^1 = 1, && \kappa_{S,\ell_i}^1 = 1, \\ &\kappa_{S,u_i}^2 = \mathrm{Re}[\zeta_u], && \kappa_{S,d_i}^2 = \mathrm{Re}[\zeta_d], && \kappa_{S,\ell_i}^2 = \mathrm{Re}[\zeta_{\ell_i}], \\ &\kappa_{S,u_i}^3 = -\mathrm{Im}[\zeta_u], && \kappa_{S,di_i}^3 = -\mathrm{Im}[\zeta_d], && \kappa_{S,\ell_i} = -\mathrm{Im}[\zeta_{\ell_i}]. \end{aligned} \tag{5.1.25}$$

The coefficients for the pseudo-scalar coupling $\kappa_{P,f_i}^\alpha$ are defined as

$$\begin{aligned} &\kappa_{P,u_i}^1 = 0, && \kappa_{P,d_i}^1 = 0, && \kappa_{P,\ell_i}^1 = 0, \\ &\kappa_{P,u_i}^2 = -i\mathrm{Im}[\zeta_u], && \kappa_{P,d_i}^2 = i\mathrm{Im}[\zeta_d], && \kappa_{P,\ell_i}^2 = i\mathrm{Im}[\zeta_{\ell_i}], \\ &\kappa_{P,u_i}^3 = -i\mathrm{Re}[\zeta_u], && \kappa_{P,d_i}^3 = i\mathrm{Re}[\zeta_d], && \kappa_{P,\ell_i}^3 = i\mathrm{Re}[\zeta_{\ell_i}]. \end{aligned} \tag{5.1.26}$$

Next, we discuss the Yukawa interactions between $S^\pm$ and the charged leptons in the second row of Eq.(5.1.16). In the mass eigenstate basis of the right-handed charged leptons, we define the new Yukawa coupling matrix $Y_N$ as follows;

$$\mathcal{L}_Y \ni -(Y_N)_{ai} \overline{N_{aR}^c} \ell_{iR} S^+ + \mathrm{h.c.} \tag{5.1.27}$$

The relation between $Y'_N$ and $Y_N$ is given by $(Y_N)_{ij} = (Y'_N U_\ell)_{ij}$, where $U_\ell$ is the unitary matrix defined in Eq.(4.1.20).

### 5.1.2 Constraints on the model

In this section, we discuss some experimental and theoretical constraints on the model. The part in common with the THDM is omitted, which has been discussed in Chapter 4.

First, we consider the constraints from collider experiments. For the constraints on $H^\pm$, $H_{2,3}$, see discussion in Sec. 4.2. The $Z_2$-odd charged scalar boson $S^\pm$ and Majorana fermions $N_a$ $(a = 1, 2, 3)$ interact with right-handed charged leptons via the Yukawa interaction in Eq. (5.1.27). Therefore, at hadron colliders, a pair of $S^+S^-$ is generated via gauge interaction, and they decay into Majorana fermions and the charged leptons if the lightest Majorana fermion is lighter than $S^\pm$. In the case that the produced Majorana fermion (or decay products of this Majorana fermion) is detected as the missing momentums, the final state of this process is two charged leptons and missing momentums. The new physics search by exploring this process is well investigated. According to the latest results at the ATLAS experiment [236–238], assuming that $S^\pm$ decays into a lepton and $N_a$ with a 100 % branching ratio, the lower bound on $m_S$ is given by about 700 GeV for the massless Majorana fermion. In the case that mass of the Majorana fermion is 100 GeV (200 GeV), the mass regions $100 \lesssim m_S \lesssim 140$ GeV and $160 \lesssim m_S \lesssim 700$ GeV ($200 \lesssim m_S \lesssim 220$ GeV and 260 GeV $\lesssim m_S \lesssim 700$ GeV) are excluded.

| Processes | Upper limits | Processes | Upper limits |
|---|---|---|---|
| $\mu \to e\gamma$ | $4.2 \times 10^{-13}$ [239] | $\mu \to 3e$ | $1.0 \times 10^{-12}$ [241] |
| $\tau \to e\gamma$ | $3.3 \times 10^{-8}$ [240] | $\tau \to 3e$ | $2.7 \times 10^{-8}$ [242] |
| $\tau \to \mu\gamma$ | $4.4 \times 10^{-8}$ [240] | $\tau \to 3\mu$ | $2.1 \times 10^{-8}$ [242] |

| Processes | Upper limits |
|---|---|
| $\tau \to e\mu\bar{e}$ | $1.8 \times 10^{-8}$ [242] |
| $\tau \to \mu\mu\bar{e}$ | $1.7 \times 10^{-8}$ [242] |
| $\tau \to ee\overline{\mu}$ | $1.5 \times 10^{-8}$ [242] |
| $\tau \to e\mu\overline{\mu}$ | $2.7 \times 10^{-8}$ [242] |

Table 5.2: The current upper limits on the branching ratios for the lepton flavor violating processes

Second, we consider the constraint from flavor experiments. For the constraints on $H^\pm$, $H_{2,3}$, see discussion in Sec. 4.2. The Yukawa interaction in Eq. (5.1.27) provides the source of Lepton Flavor Violation (LFV). Therefore, the masses of $S^\pm$ and $N_a$ and the Yukawa coupling constants $(Y_N)_{a\ell}$ are constrained by the searches for lepton flavor violating processes. In this thesis, we consider two kinds of the lepton flavor violating decays, $\ell_i \to \ell_j\gamma$ and $\ell_i \to \ell_j\ell_k\overline{\ell}_m$ $(i,j,k,m = 1,2,3)$. Current upper limits on the branching ratio for these processes are shown in Table 5.2. In particular, $\mu \to e\gamma$ and $\mu \to 3e$ give the severe constraint. Although other lepton flavor violating processes are explored [243–245], their constraints are expected to be weaker than those of $\ell_i \to \ell_j\gamma$ and $\ell_i \to \ell_j\ell_k\overline{\ell}_m$ in our model [246].

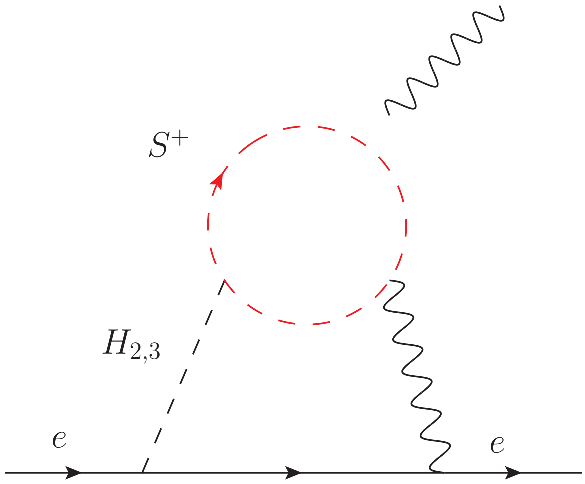


Figure 5.1: A Barr-Zee type diagram including the $S^\pm$ loop.

Third, we consider the constraint from the EDM measurements. The contribution to the eEDM and nEDM from the additional Higgs bosons are discussed in Sec. 4.2. In addition to these contributions, there are Barr-Zee type diagrams that include a $S^\pm$ loop shown in Fig. 5.1. These diagrams are proportional to $\sin(\theta_f - \theta_\rho)$, where $f$ is the fermion in the external line. We impose the eEDM and nEDM in the model to satisfy $|d_e| < 1.0 \times 10^{-29}$ e m [178] and $|d_n| < 1.8 \times 10^{-26}$ e cm [182], respectively.

Finally, the extended Higgs sector in the model is constrained theoretically by the vacuum stability. Conditions for the Higgs potential to be bounded from below are given by Ref. [247]. In our analyses, we employ these conditions.

## 5.2 Neutrino masses

In this section, the formulae for neutrino masses are provided. In the model, Majorana-type masses of neutrinos are generated via 3-loop Feynman diagrams shown in Fig. 5.2. By using the approximation that the charged leptons in the internal lines are thought to be massless, the mass matrix is calculated as

$$(M_\nu)_{ij} = 4\left(\frac{1}{16\pi^2}\right)^3 \kappa^2(\zeta^*_{\ell_i} m_{\ell_i})(\zeta^*_{\ell_j} m_{\ell_j}) \sum_{a=1}^{3} (Y_N)_{aj} M_{N_a} (Y_N)_{ai} \Big(F_{1a} + F_{2a}\Big). \qquad (5.2.1)$$

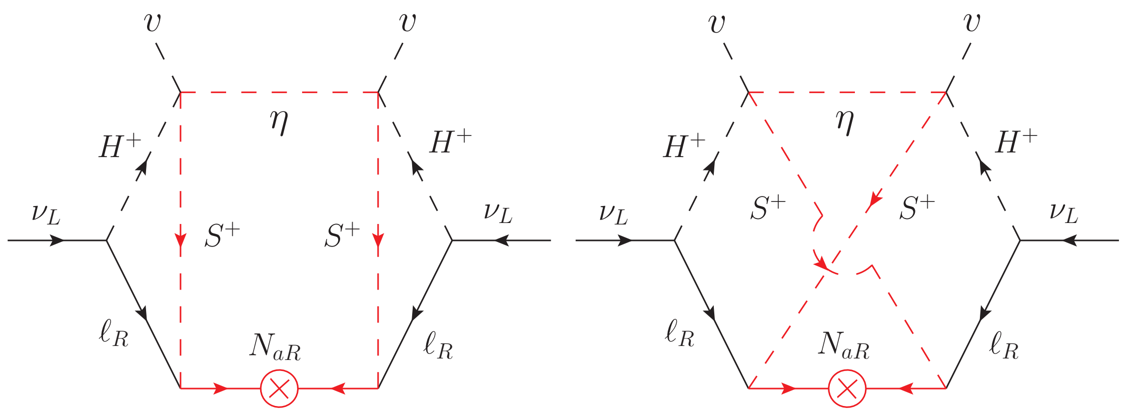


Figure 5.2: Feynman diagrams for neutrino masses. Red lines are $Z_2$-odd fields. The symbol $\otimes$ means the Majorana masses of $N_{aR}$.

The loop functions $F_{ka}$ $(k = 1, 2)$ are given by

$$F_{ka} = \int_0^1 \tilde{\mathrm{d}}^4x \int_0^\infty \mathrm{d}u \int_0^\infty \mathrm{d}v \, \frac{2\sqrt{uv}}{(u + m_{H^+}^2)(v + m_{H^+}^2)} \frac{1}{B_k^3} \left( \sqrt{A_k^2 - B_k^2} + \frac{A_k^2}{\sqrt{A_k^2 - B_k^2}} - 2A_k \right), \tag{5.2.2}$$

where the integral $\int \tilde{\mathrm{d}}^4x$ is defined as

$$\int \tilde{\mathrm{d}}^4x \equiv \int_0^1 \mathrm{d}x \int_0^1 \mathrm{d}y \int_0^1 \mathrm{d}z \int_0^1 \mathrm{d}\omega \, \delta(1 - x - y - z - \omega), \tag{5.2.3}$$

and $A_k$ and $B_k$ are provided as

$$\begin{cases} A_1 = (y+z)m_S^2 + xM_{N_a}^2 + \omega m_\eta^2 + (y+\omega)(x+z)u + (x+y)(z+\omega)v, \\ B_1 = 2(yz - x\omega)\sqrt{uv}, \end{cases} \tag{5.2.4}$$

$$\begin{cases} A_2 = (y+z)m_S^2 + xM_{N_a}^2 + \omega m_\eta^2 + y(1-y)u + z(1-z)v, \\ B_2 = 2yz\sqrt{uv}. \end{cases} \tag{5.2.5}$$

The loop functions $F_{1a}$ and $F_{2a}$ in Eq. (5.2.1) correspond to the left diagram and the right one in Fig. 5.2, respectively. The detailed calculation of the loop functions is shown in Appendix B.

The function $A_k$ defined in Eqs. (5.2.4) and (5.2.5) are nonzero in all domain of the integrals in Eq. (5.2.2). On the other hand, $B_k$ can be 0 on some points in the domain. As $B_k$ goes to 0, the integrand in Eq. (5.2.2) converges to 0;

$$\lim_{B_k \to 0} \frac{1}{B_k^3} \left( \sqrt{A_k^2 - B_k^2} + \frac{A_k^2}{\sqrt{A_k^2 - B_k^2}} - 2A_k \right) = 0, \tag{5.2.6}$$

although each term in the above equation does not converge to 0 as $B_k \to 0$. This cancellation leads to a serious deterioration of the accuracy in the numerical evaluation of the loop functions. Therefore, in the domain where $B_k$ is close to 0, the linear expanded formula $B_k/(4A_k^3)$ should be used alternatively.

The loop function $F_{1a}$ can also be represented in a different formula [75]. This formula is given by

$$F_{1a} = \frac{1}{m_{H^+}^4} \frac{1}{M_{N_a}^2 - m_\eta^2} \times \int_0^\infty \mathrm{d}x\, x \left( \frac{M_{N_a}^2}{x + M_{N_a}^2} - \frac{m_\eta^2}{x + m_\eta^2} \right) \Big( B_1(m_{H^+}, m_S; -x) - B_1(0, m_S; -x) \Big)^2, \tag{5.2.7}$$

where the function $B_1$ is the coefficient function for 1-loop integrals in the Passarino-Veltman reduction formula [248]. The formula in Eq. (5.2.7) can be understood by the topological property of the left figure in Fig. 5.2 that the diagram can be separated into the two one-loop diagrams by cutting the internal lines of $N_{aR}$ and $\eta$. The derivation of Eq. (5.2.7) is shown in Appendix B.

Before closing this section, we give comments about the discrepancy between the results in the above and that in AKS09. The loop function $F_{1a}$ in Eqs. (5.2.2) and (5.2.7) is the same as that in AKS09. On the other hand, the loop function $F_{2a}$ is different. In AKS09, $F_{1a}$ and $F_{2a}$ have the same formula. Therefore, the entire contribution of the loop diagrams is twice as much as $F_{1a}$. However, using the formulae in Eq. (5.2.2), the value of $F_{2a}$ is typically one order smaller than $F_{1a}$. Then, the entire contribution of the loop diagrams is approximately the same as $F_{1a}$. Consequently, the formula of neutrino mass matrix in the above gives about a half value of that in AKS09.

## 5.3 Lepton Flavor Violating processes

As in the previous section, the Yukawa interactions between $S^\pm$ and charged leptons are indispensable to generate neutrino masses. On the other hand, they lead to LFV processes, which are strongly constrained by experiments. We consider two kinds of LFV decay processes $\ell_i \to \ell_j\gamma$ and $\ell_i \to \ell_j\ell_k\overline{\ell}_m$.

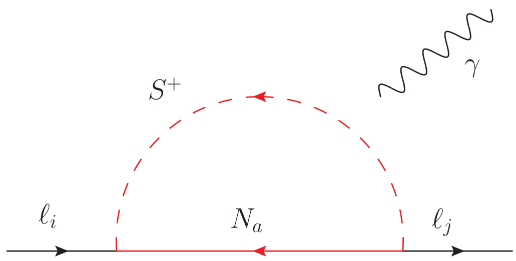


Figure 5.3: The Feynman diagram for $\ell_i \to \ell_j\gamma$

First, the process $\ell_i \to \ell_j\gamma$ are generated via 1-loop diagram shown in Fig. 5.3. The ratio of $\mathrm{Br}(\ell_i \to \ell_j\gamma)$ to $\mathrm{Br}(\ell_i \to \ell_j\nu_{\ell_i}\overline{\nu}_{\ell_j})$, where $\mathrm{Br}(X)$ means the branching ratio of the process $X$, is given by

$$\frac{\mathrm{Br}(\ell_i \to \ell_j\gamma)}{\mathrm{Br}(\ell_i \to \ell_j\nu_{\ell_i}\overline{\nu}_{\ell_j})} = \frac{3\alpha}{64\pi G_F^2}\frac{1}{m_S^4}\left|\sum_a (Y_N)^*_{aj}(Y_N)_{ai}f_1(r_a)\right|^2, \tag{5.3.1}$$

where $r_a = M_{N_a}^2/m_S^2$ and the function $f_1(x)$ is defined as

$$f_1(x) = \frac{1-6x+3x^2+2x^3-6x^2\log x}{6(-1+x)^4}. \tag{5.3.2}$$

In Eq. (5.3.1), we neglect the mass of the charged lepton in the final state.

Second, the process $\ell_i \to \ell_j\ell_k\overline{\ell}_m$ is generated via two kinds of box diagrams shown in Fig. 5.4.[1] The ratio of $\mathrm{Br}(\ell_i \to \ell_j\ell_k\overline{\ell}_m)$ to $\mathrm{Br}(\ell_i \to \ell_j\nu_{\ell_i}\overline{\nu}_{\ell_j})$ is as follows;

$$\frac{\mathrm{Br}(\ell_i \to \ell_j\ell_k\overline{\ell}_m)}{\mathrm{Br}(\ell_i \to \ell_j\nu_{\ell_i}\overline{\nu}_{\ell_j})} = \frac{S}{16G_F^2}\left(\frac{1}{16\pi^2}\right)^2\left|A_{ijkm}+B_{ijkm}\right|^2, \tag{5.3.3}$$

where $A_{ijkm}$ and $B_{ijkm}$ are contributions from the left diagram in Fig. 5.4 and the right one, respectively. They are given by

$$A_{ijkm} = \sum_{a,b}(Y_N)_{ai}(Y_N)^*_{aj}(Y_N)^*_{bk}(Y_N)_{bm}\frac{1}{m_S^2}\frac{f_2(r_a)-f_2(r_b)}{r_a-r_b} + (j \leftrightarrow k), \tag{5.3.4}$$

$$B_{ijkm} = \sum_{a,b}(Y_N)_{ai}(Y_N)^*_{bj}(Y_N)^*_{bk}(Y_N)_{am}\frac{\sqrt{r_ar_b}}{m_S^2}\frac{f_3(r_a)-f_3(r_b)}{r_a-r_b} + (j \leftrightarrow k), \tag{5.3.5}$$

where the functions $f_2(x)$ and $f_3(x)$ are defined as

$$f_2(x) = \frac{1}{2}\left\{\frac{x^2}{(1-x)^2}\log x + \frac{1}{1-x}\right\}, \tag{5.3.6}$$

$$f_3(x) = \frac{1}{2}\left\{\frac{x}{(1-x)^2}\log x + \frac{1}{1-x}\right\}. \tag{5.3.7}$$

The symbol $S$ in Eq. (5.3.3) is a symmetry factor defined as follows;

$$S = \begin{cases} 2 & (j \neq k), \\ 1 & (j = k). \end{cases} \tag{5.3.8}$$

## 5.4 Dark matter

In the model, $Z_2$ symmetry is imposed and we assume that the vacuum respect this symmetry. Then, the lightest $Z_2$-odd particle is stable. If it is a neutral particle, it is a candidate of DM. There are two kinds of $Z_2$-odd neutral particles in the model, the Majorana fermions $N_a$ and the real scalar $\eta$. We consider the case that $\eta$ is the lightest $Z_2$-odd particle.

[1] The photon penguin diagrams also contribute to the process $\ell_i \to \ell_j\ell_k\overline{\ell}_m$. In the case of large Yukawa couplings, the contribution from the box diagrams is dominant. In the benchmark scenario, which is discussed later, the Yukawa couplings between $S^\pm$ and electrons are large. Thus, we consider only the contribution from the box diagrams.

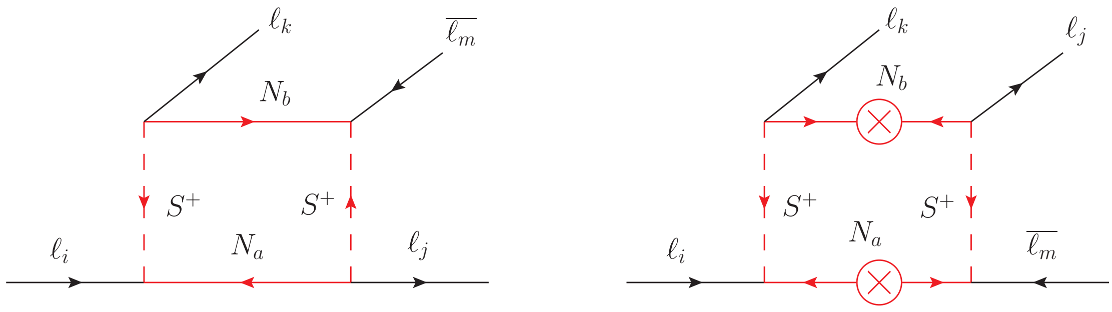


Figure 5.4: Feynman diagrams for $\ell_i \to \ell_j \ell_k \overline{\ell}_m$. The symbol $\otimes$ represents Majorana mass of $N_a$.

### 5.4.1 Relic abundance

In this section, we give some formulae for the relic abundance of $\eta$ via the freeze-out mechanism. We consider only the following DM annihilations processes;

$$\eta\eta \to f_i\overline{f_i}, \quad \eta\eta \to W^+W^-, \quad \eta\eta \to ZZ, \tag{5.4.1}$$

where $f$ $(= u, d, e)$ represents a kind of fermions and $i$ $(= 1, 2, 3)$ is the flavor index. We do not consider the DM annihilation into photons $\eta\eta \to \gamma\gamma$ and that into gluons $\eta\eta \to gg$ because it occurs at the loop level. In addition, we neglect DM annihilations into the scalar boson pairs and those into three or higher body systems.

First, we investigate the annihilation processes into the SM fermions $\eta\eta \to f_i\overline{f_i}$. These processes are mediated by $H_1$, $H_2$, and $H_3$. The three-point interactions between a pair of $\eta$ and the neutral Higgs bosons are given by

$$\mathcal{L}_{\eta\eta H} = -\sum_{\alpha=1}^{3} \frac{v}{2}\lambda_{\eta\eta\alpha}\eta^2 H_\alpha, \tag{5.4.2}$$

where coupling constants $\lambda_{\eta\eta\alpha}$ are defined as

$$\lambda_{\eta\eta 1} = \sigma_1, \quad \lambda_{\eta\eta 2} = \mathrm{Re}[\sigma_{12}], \quad \lambda_{\eta\eta 3} = \mathrm{Im}[\sigma_{12}]. \tag{5.4.3}$$

Then, the scattering cross section for $\eta\eta \to f_i\overline{f_i}$ is given by

$$\begin{aligned}\sigma_{f_i\overline{f_i}} = \frac{N_c^f m_{f_i}^2}{8\pi s}\sqrt{\frac{s-4m_{f_i}^2}{s-4m_\eta^2}}\Bigg((s-4m_{f_i}^2)\left|\sum_{\alpha=1}^{3}\frac{\lambda_{\eta\eta\alpha}\kappa_{S,f_i}^{\alpha}}{s-m_{H_\alpha}^2+im_{H_\alpha}\Gamma_{H_\alpha}}\right|^2 \\ + s\left|\sum_{\alpha=1}^{3}\frac{\lambda_{\eta\eta\alpha}\kappa_{P,f_i}^{\alpha}}{s-m_{H_\alpha}^2+im_{H_\alpha}\Gamma_{H_\alpha}}\right|^2\Bigg),\end{aligned} \tag{5.4.4}$$

where $s$ is one of the Mandelstam variables, and $N_c^f$ is a color factor of the fermion $f_i$. The coupling constants $\kappa_{S,f_i}^{\alpha}$ and $\kappa_{P,f_i}^{\alpha}$ are defined in Eqs. (5.1.25) and (5.1.26), respectively. The decay width for $H_\alpha$ is denoted by $\Gamma_{H_\alpha}$ in Eq. (5.4.4).

At the leading order of the relative velocity $v$, the thermally averaged cross section [249, 250] for $\eta\eta \to f_i\overline{f_i}$ is given by

$$\langle\sigma_{f_i\overline{f_i}}v\rangle \simeq \frac{N_c m_{f_i}^2}{64\pi m_\eta^4}\sqrt{1-\frac{m_{f_i}^2}{m_\eta^2}}\left\{\left(1-4\frac{m_{f_i}^2}{m_\eta^2}\right)\left|\sum_{\alpha=1}^{3}\frac{\lambda_{\eta\eta\alpha}\kappa_{S,f}^{\alpha}}{1-R_\alpha^2+iR_\alpha R_{\Gamma_\alpha}}\right|^2 + \left|\sum_{\alpha=1}^{3}\frac{\lambda_{\eta\eta\alpha}\kappa_{P,f}^{\alpha}}{1-R_\alpha^2+iR_\alpha R_{\Gamma_\alpha}}\right|^2\right\}, \tag{5.4.5}$$

where we define the following;

$$R_\alpha = \frac{m_{H_\alpha}}{2m_\eta}, \quad R_{\Gamma_\alpha} = \frac{\Gamma_{H_\alpha}}{2m_\eta}; \quad \alpha = 1,2,3. \tag{5.4.6}$$

Second, we consider the annihilation processes into the electroweak gauge bosons. The processes $\eta\eta \to W^+W^-$ and $\eta\eta \to ZZ$ occur at tree level mediated by the SM Higgs boson $H_1$. Since we assume the alignment condition in the Higgs potential ($\lambda_6 = 0$), the additional Higgs bosons do not contribute to this process at the tree level.

The scattering cross section for $\eta\eta \to VV$ ($V = W^\pm$ or $Z$) is given by

$$\sigma_{VV} = \frac{\sigma_1^2 S_V}{32\pi s}\sqrt{\frac{s-4m_V^2}{s-4m_\eta^2}}\frac{1}{(s-m_{H_1}^2)^2+m_{H_1}^2\Gamma_{h_1}^2}\left((s-2m_V^2)^2+8m_V^4\right), \tag{5.4.7}$$

where $m_V$ is the mass of the gauge boson $V$ and $S_V$ is a symmetry factor defined as

$$S_V \equiv \begin{cases} 2 & (V = W^\pm), \\ 1 & (V = Z). \end{cases} \tag{5.4.8}$$

At the leading order of $v$, the thermally averaged cross section for $\eta\eta \to VV$ is given by

$$\langle\sigma_{VV}v\rangle \simeq \frac{\sigma_1^2 S_V}{64\pi m_\eta^2}\sqrt{1-\frac{m_V^2}{m_\eta^2}}\frac{1}{(1-R_1^2)^2+R_1^2R_{\Gamma_1}^2}\left\{\left(1-\frac{m_V^2}{2m_\eta^2}\right)^2+\frac{m_V^4}{2m_\eta^4}\right\}. \tag{5.4.9}$$

By using the above thermally averaged cross sections, the relic abundance $\eta$ is approximately evaluated by

$$\Omega_{\eta 0}h^2 = 1.04\times 10^9 \times \frac{x_f}{\sqrt{g_*}}\left(\frac{m_{\rm pl}}{\rm GeV}\right)^{-1}\left(\frac{\langle\sigma_{\rm all}v\rangle}{\rm GeV^{-2}}\right)^{-1}, \tag{5.4.10}$$

where $m_{\rm pl}$ is the Planck mass, and $g_* \simeq 106.75$ is the effective degree of freedom in the radiation dominated era [249, 250]. The symbol $\langle\sigma_{\rm all}v\rangle$ in Eq. (5.4.10) is the sum of the thermally averaged cross sections of all processes in Eq. (5.4.1);

$$\langle\sigma_{\rm all}v\rangle = \langle\sigma_{WW}v\rangle + \langle\sigma_{ZZ}v\rangle + \sum_{f=u,d,e}\sum_{i=1}^{3}\langle\sigma_{f_i\overline{f_i}}v\rangle \tag{5.4.11}$$

The freeze-out temperature $x_f$ in Eq. (5.4.10) is approximately evaluated as follows [164]

$$x_f = \log\left[0.038\frac{m_\eta}{\sqrt{g_*}}m_{\rm pl}\langle\sigma_{\rm all}v\rangle\right] - \frac{1}{2}\log\left[\log\left[0.038\frac{m_\eta}{\sqrt{g_*}}m_{\rm pl}\langle\sigma_{\rm all}v\rangle\right]\right]. \tag{5.4.12}$$

### 5.4.2 Direct detection

In this section, the formula for the scattering cross section of the DM scattering $\eta N \to \eta N$ is provided, where $N$ is the proton ($N = p$) or the neutron ($N = n$). This scattering occurs via the t-channel diagrams mediated by the neutral Higgs bosons $H_1$, $H_2$, and $H_3$. Here, we neglect contributions from $H_2$ and $H_3$ for the sake of simplicity.

The effective coupling of the interaction between $H_1$ and nucleons $N$ is given by

$$g_N = \frac{1}{v}\sum_q \langle N|m_q\overline{q}q|N\rangle\,, \tag{5.4.13}$$

where $\sum_q$ means the sum for quarks. According to Refs. [251], $g_N$ is evaluated as

$$g_N \simeq 1.1 \times 10^{-3}. \tag{5.4.14}$$

Since the typical momentum exchange between DM and the nucleon is $\mathcal{O}(100\text{ MeV})$, we neglect it in the calculation of the scattering cross section. Then, the cross section $\sigma_{\eta N}$ is given by

$$\sigma_{\eta N} \simeq \frac{\sigma_1^2 g_N^2}{16\pi m_{H_1}^4}\frac{v^2 m_N^2}{(m_\eta + m_N)^2}. \tag{5.4.15}$$

## 5.5 Baryon asymmetry of the universe

In this section, some formulae necessary to calculate the baryon asymmetry generated via electroweak baryogenesis are provided. First, we investigate the effective potential of the model. The formulae for the one-loop level effective potential at zero and finite temperatures are shown. The formula for the one-loop correction on the Higgs triple coupling is also shown.

Second, we investigate EWBG in the model via the charge transport mechanisms by top quarks. The transport equations and the formula for the generated baryon asymmetry via the sphaleron transition are shown.

### 5.5.1 The effective potential

We consider the effective potential for neutral elements of the doublets $\Phi_1$ and $\Phi_2$. By choosing an appropriate gauge, the classical fields can be parametrized as

$$\Phi_1 = \frac{1}{\sqrt{2}}\begin{pmatrix} 0 \\ \varphi_1 \end{pmatrix}, \quad \Phi_2 = \frac{1}{\sqrt{2}}\begin{pmatrix} 0 \\ \varphi_2 + i\varphi_3 \end{pmatrix}. \tag{5.5.1}$$

By substituting these classical fields into the Higgs potential, we can obtain the tree-level effective potential $V_0$ as follows.

$$
\begin{aligned}
V_0(\varphi_1, \varphi_2, \varphi_3) = &\frac{\mu_1^2}{2}\varphi_1^2 + \frac{\mu_2^2}{2}(\varphi_2^2 + \varphi_3^2) + \frac{\lambda_1}{8}\varphi_1^4 + \frac{\lambda_2}{8}(\varphi_2^4 + 2\varphi_2^2\varphi_3^2 + \varphi_3^4) \\
&+ \frac{1}{4}(\lambda_3 + \lambda_4 + \lambda_5)\varphi_1^2\varphi_2^2 + \frac{1}{4}(\lambda_3 + \lambda_4 - \lambda_5)\varphi_1^2\varphi_3^2 \\
&+ \frac{1}{2}\mathrm{Re}[\lambda_7]\varphi_1\varphi_2(\varphi_2^2 + \varphi_3^2) - \frac{1}{2}\mathrm{Im}[\lambda_7]\varphi_1\varphi_3(\varphi_2^2 + \varphi_3^2),
\end{aligned}
\tag{5.5.2}
$$

where we use the Higgs alignment assumption $\lambda_6 = 0$ at tree level and the tree level stationary conditions in Eq. (5.1.4).

The 1-loop level effective potential is given by

$$
V_1 = V_0 + V_{\mathrm{CW}} + V_{\mathrm{c.t.}}, \tag{5.5.3}
$$

where $V_{\mathrm{CW}}$ is the Coleman-Weinberg potential [198], and $V_{\mathrm{c.t.}}$ is the counterterms. The Coleman-Weinberg potential in Landau gauge is given by

$$
V_{\mathrm{CW}} = \sum_\alpha (-1)^{s_\alpha} \frac{n_\alpha}{64\pi^2}\tilde{m}_\alpha^4 \Big[\log\frac{\tilde{m}_\alpha^2}{Q^2} - \frac{3}{2}\Big], \tag{5.5.4}
$$

where $Q$ is the renormalization scale, and the index $\alpha$ represents the kinds of particles in the loop diagrams; $\alpha = t$, $W^\pm$, $Z$, $\gamma$, $G^\pm$, $G^0$, $H^\pm$, $H_1$, $H_2$, $H_3$, $S^\pm$, and $\eta$. The field-dependent masses for the particle $\alpha$ are denoted by $\tilde{m}_\alpha^2$. Formulae for $\tilde{m}_\alpha^2$ are shown in Appendix C. The symbol $n_\alpha$ and $(-1)^{s_\alpha}$ in Eq. (5.5.4) are the degrees of freedom and the statistical factor for particle $\alpha$, respectively. The statistical factor is defined as

$$
(-1)^{s_\alpha} = \begin{cases} 1 & (\alpha \text{ is a boson}), \\ -1 & (\alpha \text{ is a fermion}). \end{cases} \tag{5.5.5}
$$

In Eq. (5.5.4), the contributions from the SM fermions except for the top quark are not included because their contributions are negligibly small. On the other hand, the Majorana fermions $N_a$ does not contribute to the effective potential at the one-loop level.

To determine the counterterms, we impose the following renormalization conditions at the point $\varphi_1 = v$, $\varphi_{2,3} = 0$;

$$
\frac{\partial V_1}{\partial \varphi_i} = 0 \quad (i = 1, 2, 3), \tag{5.5.6}
$$

$$
\frac{\partial^2 V_1}{\partial \varphi_i \partial \varphi_j} = (M_h^2)_{ij} \quad (i, j = 1, 2, 3), \tag{5.5.7}
$$

where $M_h^2$ is the mass matrix for the neutral Higgs bosons defined in Eq. (5.1.9). The second derivatives in the conditions have IR divergences caused by the NG bosons. To avoid them, we replace the NG boson mass at the vacuum with the IR cutoff scalar 1 GeV [199].

The first (second) renormalization condition provides three (six) independent equations. By using these equations, counterterms for $\mu_1^2$, $\mu_3^2$, $\lambda_1$, $\lambda_3$, $\lambda_4$, $\lambda_5$, and $\lambda_6$ are determined. We use the $\overline{\mathrm{MS}}$ scheme to fix the counterterms for $\mu_2^2$, $\lambda_2$, and $\lambda_7$. The counterterms for other scalar couplings do not contribute to the effective potential at the one-loop level.

At finite temperature, the effective potential is given by

$$V_{\mathrm{eff}}(\varphi_i, T) = V_1 + V_T. \tag{5.5.8}$$

where $V_T$ is the thermal effects at the one-loop level with daisy resummation. For the resummation, we employ the Parwani scheme [200]. Then, the thermal correction at the one-loop level is given as follows [132];

$$V_T = \sum_\alpha (-1)^\alpha \frac{n_k}{2\pi^2\beta^4}\int_0^\infty \mathrm{d}x\, \log\Big(1-(-1)^{s_k}\exp(-\sqrt{x^2+\beta^2(\tilde{m}_\alpha^\beta)^2})\Big), \tag{5.5.9}$$

where $(\tilde{m}_\alpha^\beta)^2$ is the field-dependent masses including thermal corrections if $\alpha$ is the gauge bosons or the scalar bosons. For the top quark, it is the same as $\tilde{m}_t^2$. The formulae for $(\tilde{m}_\alpha^\beta)^2$ for each particle are shown in Appendix C.

In the model, the strongly 1st order EWPT can be realized by the non-decoupling effects of the additional scalar bosons. In such a case, the Higgs triple coupling can deviate sizably from the prediction in the SM [140, 141, 143]. By using the effective potential at zero temperature, this deviation in the model is evaluated as

$$\begin{aligned}\Delta R \equiv \frac{\lambda_{hhh}-\lambda_{hhh}^{\mathrm{SM}}}{\lambda_{hhh}^{\mathrm{SM}}} =& \frac{1}{12\pi^2 v^2 m_{H_1}^2}\Big\{\frac{2(m_{H^\pm}^2-\mu_2^2)^3}{m_{H^\pm}^2}+\frac{(m_{H_2}^2-\mu_2^2)^3}{m_{H_2}^2}+\frac{(m_{H_3}^2-\mu_2^2)^3}{m_{H_3}^2}\\ &+\frac{2(m_S^2-\mu_S^2)^3}{m_S^2}+\frac{(m_\eta^2-\mu_\eta^2)^3}{m_\eta^2}\Big\}.\end{aligned} \tag{5.5.10}$$

### 5.5.2 Electroweak baryogenesis

Here, we investigate EWBG via the charge transport mechanism by top quarks based on discussions in Refs. [45, 46, 108]. We discuss the issue in the wall frame, where the bubble wall is stationary. The radial direction of the bubble is denoted by the $z$-axis. The bubble wall is fixed at $z = 0$, and the negative direction of $z$ is the inside of the bubble (the broken phase).

#### The transport equation

The transport equations in the wall frame are given as follows [45, 108]

$$\begin{cases} u_i' + v_w K_{i1}\mu_{io}' + v_w (m^2)' K_{i2}\mu_{io} - \beta K_{i0}\sum_{\sigma\in\mathrm{inela}}\Gamma_\sigma \sum_j s_j^\sigma \mu_{j0} = 0 \\ -\mu_{io}' K_{i4} - v_w u_i' + v_w (m^2)'\tilde{K}_{i6} u_i \\ \qquad\qquad +\Gamma_{\mathrm{tot}} u_i + v_w \beta K_{i0}\sum_{\sigma\in\mathrm{inela}}\Gamma_\sigma \sum_j s_j^\sigma \mu_{jo} = S_i, \end{cases} \tag{5.5.11}$$

where $\mu_i$ and $u_i$ are the chemical potential and the plasma velocity of the particle $i$, respectively. The definitions of other quantities in Eq. (5.5.11) are shown in Sec. (3.1.3).

The transport equation for each species is a pair of first-order differential equations. These can be transformed into the following single second-order differential equation by removing $u_i$. At the linear order of $v_w$, this differential equation is given by

$$D_i \mathcal{J}_{iA} \xi_i'' + \left( D_i \mathcal{J}_{iA}' + v_\omega \mathcal{J}_{i1} \right) \xi_i' + v_\omega a_i' \mathcal{J}_{i2} \xi_i - \mathcal{J}_{i0} \sum_\sigma \gamma_\sigma \sum_j s_j^\sigma \xi_j = -D_i \mathcal{J}_{iS}, \tag{5.5.12}$$

where we define the following dimensionless quantities;

$$\begin{aligned}
&\xi_i \equiv \beta \mu_{i2}, \quad a_i \equiv \beta^2 m_i^2, \quad \gamma_{\text{tot}} \equiv \beta \Gamma_{\text{ tot}}, \quad \gamma_\sigma \equiv \beta \Gamma_\sigma, \\
&\mathcal{J}_{i0} \equiv \beta K_{i0}, \quad \mathcal{J}_{i1} \equiv K_{i1}, \quad \mathcal{J}_{i2} \equiv \beta^{-2} K_{i2}, \quad \mathcal{J}_{i3} \equiv K_{i4}, \\
&\mathcal{J}_{i4} \equiv \beta^{-2} \tilde{K}_{i6}, \quad \mathcal{J}_{i5} \equiv \beta^{-2} K_{i8}, \quad \mathcal{J}_{i6} \equiv \beta^{-2} m_i^2 K_{i9},
\end{aligned} \tag{5.5.13}$$

and the functions $\mathcal{J}_{iA}$ and $\mathcal{J}_{iS}$ is given by

$$\mathcal{J}_{iA} = \mathcal{J}_{i1} \left( 1 - v_\omega D_i \frac{a_i' \mathcal{J}_{i1} \mathcal{J}_{i4}}{\mathcal{J}_{i3}} \right), \quad \mathcal{J}_{iS} = \frac{\mathcal{J}_{i1} \mathcal{S}_i}{\mathcal{J}_{i3}}, \tag{5.5.14}$$

The symbol $D_i$ in Eq. (5.5.12) is a diemensionless diffusion coefficient normalized $\beta$ defined as

$$D_i = \frac{\mathcal{J}_{i3}}{\mathcal{J}_{i1} \gamma_{\text{tot}}}. \tag{5.5.15}$$

The quantities with the superscript $'$ represent derivatives by $z$ of them. The formulae for each $\mathcal{J}$ function are given by

$$\begin{aligned}
&\mathcal{J}_{i0} = \frac{6}{\pi^2} \int_0^\infty \mathrm{d}x \, \frac{x^2}{e^{\epsilon_i} + 1}, \quad \mathcal{J}_{i1} = \frac{6}{\pi^2} \int_0^\infty \mathrm{d}x \, \frac{x^2 e^{\epsilon_i}}{(e^{\epsilon_i} + 1)^2}, \quad \mathcal{J}_{i2} = -\frac{3}{\pi^2} \int_0^\infty \mathrm{d}x \, \frac{e^{\epsilon_i}}{(e^{\epsilon_i} + 1)^2}, \\
&\mathcal{J}_{i3} = \frac{2}{\pi^2} \int_0^\infty \mathrm{d}x \, \frac{x^4}{\epsilon_i^2} \frac{e^{\epsilon_i}}{(e^{\epsilon_i} + 1)^2}, \quad \mathcal{J}_{i4} = -\frac{1}{2} \frac{\displaystyle\int_0^\infty \mathrm{d}x \, \frac{1}{e^{\epsilon_i} + 1}}{\displaystyle\int_0^\infty \mathrm{d}x \, \frac{x^2}{e^{\epsilon_i} + 1}}, \\
&\mathcal{J}_{i5} = \frac{3}{\pi^2} \int_{\sqrt{a_i}}^\infty \mathrm{d}x \frac{e^x}{(e^x + 1)^2} \left( 1 - \frac{\sqrt{a_i}}{x} \right), \quad \mathcal{J}_{i6} = \frac{3}{2\pi^2} a_i^{\frac{3}{2}} \int_{\sqrt{a_i}}^\infty \mathrm{d}x \, \frac{1}{\epsilon_i^3} \frac{e^x}{(e^x + 1)^2},
\end{aligned} \tag{5.5.16}$$

where $\epsilon_i = \sqrt{x^2 + a_i}$. The derivation of these formulae are shown in Appendix D.

We consider only the transport equations of quarks and Higgs. We assume that the impacts of other species are enough small. Following discussions in Refs. [45, 108], the following baron number conserved processes are considered as inelastic processes in the transport equations; the top Yukawa interaction, the strong sphaleron [201, 202], the top helicity flips, and the Higgs number violation.

In this case, the transport equations for light quarks (quarks in the first and second generations and right-handed bottom quarks) can be solved analytically [107]. The dimensionless chemical potential $\xi_{q_L}$ ($\xi_{q_R}$) for a left-handed (right-handed) light quark can be represented by using those of top quarks and left-handed bottom quarks as follows [107];

$$\xi_{q_L} = -\xi_{q_R} = \mathcal{J}_{b1}\xi_{b_L} + \mathcal{J}_{t1}(\xi_{t_L} + \xi_{t_R}). \tag{5.5.17}$$

By using this formula, the transport equations for the chemical potentials of left-handed top quarks ($\xi_{t_L}$), right-handed top quarks ($\xi_{t_R}$), left-handed bottom quarks ($\xi_{b_L}$), and Higgs doublet ($h$) are given by

$$\begin{cases} D_q\mathcal{J}_{tA}\xi''_{t_L} + \big(D_q\mathcal{J}'_{tA} + v_\omega\mathcal{J}_{t1}\big)\xi'_{t_L} + v_\omega a'_t\mathcal{J}_{t2}\xi_{t_L} - \mathcal{J}_{t0}\gamma_{t_L} = -D_q\mathcal{J}'_{tS}, \\ D_q\mathcal{J}_{tA}\xi''_{t_R} + \big(D_q\mathcal{J}'_{tA} + v_\omega\mathcal{J}_{t1}\big)\xi'_{t_R} + v_\omega a'_t\mathcal{J}_{t2}\xi_{t_R} - \mathcal{J}_{t0}\gamma_{t_R} = D_q\mathcal{J}'_{tS}, \\ D_q\xi''_{b_L} + v_\omega\xi'_{b_L} - \mathcal{J}_0\gamma_{b_L} = 0, \\ D_h\xi''_h + v_\omega\xi'_h - \mathcal{J}_0\gamma_h = 0, \end{cases} \tag{5.5.18}$$

where we neglect the masses of the bottom quarks and the Higgs because their effect is negligibly small [45, 108]. The function $\mathcal{J}_0$ is $\mathcal{J}_{i0}$ for massless particles $i$. The symbol $D_q$ and $D_h$ denote the dimensionless diffusion coefficient for quarks and that for the Higgs, respectively.

In Eq. (5.5.18), the effects of inelastic scattering processes for each species are represented by $\gamma_{t_L}$, $\gamma_{t_R}$, $\gamma_{b_L}$, and $\gamma_h$. They are defined as;

$$\begin{aligned}\gamma_{t_L} = {} & \gamma_m(\xi_{t_L} - \xi_{t_R}) + \gamma_W(\xi_{t_L} - \xi_{b_L}) + \gamma_y(\xi_{t_L} + \xi_h - \xi_{t_R}) \\ & + \gamma_{ss}\big\{(1 + 9\mathcal{J}_{t1})\xi_{t_L} + 10\xi_{b_L} - (1 - 9\mathcal{J}_{t1})\xi_{t_R}\big\},\end{aligned} \tag{5.5.19}$$

$$\begin{aligned}\gamma_{t_R} = {} & \gamma_m(\xi_{t_R} - \xi_{t_L}) + \gamma_y(2\xi_{t_R} - \xi_{t_L} - \xi_{b_L} - 2\xi_h) \\ & + \gamma_{ss}\big\{(1 - 9\mathcal{J}_{t1})\xi_{t_R} - (1 + 9\mathcal{J}_{t1})\xi_{t_L} - 10\xi_{b_L}\big\},\end{aligned} \tag{5.5.20}$$

$$\begin{aligned}\gamma_{b_L} = {} & \gamma_W(\xi_{b_L} - \xi_{t_L}) + \gamma_y(\xi_{b_L} + \xi_h - \xi_{t_R}) \\ & + \gamma_{ss}\big\{(1 + 9\mathcal{J}_{1t})\xi_{t_L} + 10\xi_{b_L} - (1 - 9\mathcal{J}_{1t})\xi_{t_R}\big\},\end{aligned} \tag{5.5.21}$$

$$\gamma_h = \gamma_y(2\xi_h + \xi_{t_L} + \xi_{b_L} - 2\xi_{t_R}) + \gamma_h\xi_h, \tag{5.5.22}$$

where $\gamma_y$, $\gamma_{ss}$, $\gamma_m$, and $\gamma_h$ are thermally averaged reaction rates normalized by $T$ of the top Yukawa interaction, the strong sphaleron, the top helicity flips, and the Higgs number violation, respectively.

### The baryon number density

By solving the above transport equation, the distributions of the chemical potentials around the bubble wall are obtained. By using these chemical potentials, we can evaluate the baryon asymmetry as follows [45, 107, 108];

$$\frac{n_B}{s} = \frac{405\Gamma^{\rm s}_{\rm sph}}{4\pi^2 g_{*s} T}\int_0^\infty {\rm d}z\ f_{\rm sph}(z)\xi_{B_L} e^{-\nu z}, \tag{5.5.23}$$

where $s$ and $g_{*s}$ are the entropy density and the effective degree of freedom for the entropy density, respectively, and $\xi_{B_L}$ and $\nu$ are defined as

$$\xi_{B_L} = \frac{1}{2}\Big\{(1+4\mathcal{J}_{t1})\xi_{t_L} + 5\xi_{b_L} + 4\mathcal{J}_{t1}\xi_{t_R}\Big\}, \tag{5.5.24}$$

$$\nu = \frac{3\Gamma^{\rm s}_{\rm sph}A}{2v_w} = \frac{45\Gamma^{\rm s}_{\rm sph}}{4v_w}. \tag{5.5.25}$$

The symbol $\Gamma^{\rm s}_{\rm sph}$ denotes the weak sphaleron rate in the symmetric phase. The function $f_{\rm sph}(z)$ in Eq. (5.5.23) represents the correction for the weak sphaleron rate caused by the nonzero VEV $v(z)$ in $z > 0$. According to Ref. [46], it can be evaluated as

$$f_{\rm sph}(z) = \min\left\{1,\quad \frac{2.4T}{\Gamma^{\rm s}_{\rm sph}} e^{-40v(z)/T}\right\}. \tag{5.5.26}$$

## 5.6 Benchmark scenario

In this section, I introduce a benchmark scenario of the model where baryon asymmetry, neutrino masses, and DM can be explained simultaneously under the constraints of the current experiments. The prediction of this benchmark scenario and some discussions are also provided.

### 5.6.1 Numerical evaluations in the benchmark scenario

In the benchmark scenario, we assume the following input parameters.

**Masses of particles**

$$\begin{aligned}
&m_{H_1} = 125\ \text{GeV},\quad m_{H_2} = 420\ \text{GeV},\quad m_{H_3} = m_{H^\pm} = 250\ \text{GeV},\\
&m_S = 400\ \text{GeV},\quad m_\eta = 63\ \text{GeV},\\
&(M_{N_1}, M_{N_2}, M_{N_3}) = (2000, 2500, 3000)\ \text{GeV}.
\end{aligned} \tag{5.6.1}$$

**The Higgs potential**

$$\begin{aligned}
&v = 246\ \text{GeV},\quad M^2(\equiv -\mu_2^2) = (50\ \text{GeV})^2,\quad \mu_S^2 = (320\ \text{GeV})^2,\\
&\lambda_2 = 0.1,\quad |\lambda_7| = 0.8,\quad |\rho_{12}| = 0.1,\quad \rho_2 = 0.1,\\
&\sigma_1 = |\sigma_{12}| = 1.1\times 10^{-3},\quad \sigma_2 = 0.1,\quad \lambda_s = 0.1,\quad \xi = 0.1,\quad \kappa = 1.0,\\
&\theta_7 = 0.779,\quad \theta_\rho = 0.20,\quad \theta_\sigma = 0.
\end{aligned} \tag{5.6.2}$$

**The Yukawa interactions**

$$
\begin{aligned}
&|\zeta_e| = 80, \quad |\zeta_\mu| = 0.5, \quad |\zeta_\tau| = |\zeta_u| = |\zeta_d| = 0.246,\\
&\theta_u = -2.9 \quad \theta_d = 0.0, \quad \theta_e = \theta_\rho = 0.20,\\
&Y_N = \begin{pmatrix} -0.0622 - 0.0638i & 1.38 - 0.762i & 0.417 - 0.0432i \\ -0.383 + 1.49i & 2.01 - 0.703i & 0.267 + 0.270i \\ -0.404 - 0.105i & -0.108 - 0.166i & 0.188 - 0.275i \end{pmatrix}.
\end{aligned} \tag{5.6.3}
$$

The remaining parameters in the Higgs potential are determined by the input parameters as follows;

$$\lambda_1 \simeq 0.258, \quad \lambda_3 \simeq 1.98, \quad \lambda_4 = \lambda_5 \simeq 1.88, \quad \rho_1 \simeq 1.90, \quad \mu_\eta^2 \simeq (62.8\ \mathrm{GeV})^2. \tag{5.6.4}$$

By using the neutrino mass formula in Eq. (5.2.1), the neutrino mass and the PMNS matrix elements in the benchmark scenario are calculated as

$$(m_{\nu_1}, m_{\nu_2}, m_{\nu_3}) = (2.3,\ 9.0,\ 50)\ \mathrm{meV}, \tag{5.6.5}$$

$$\sin^2\theta_{12} = 0.304, \quad \sin^2\theta_{13} = 2.20 \times 10^{-2}, \quad \sin^2\theta_{23} = 0.543, \tag{5.6.6}$$

$$\delta = -1.90, \quad \alpha_1 = 1.89, \quad \alpha_2 = 0.325, \tag{5.6.7}$$

where $\theta_{ij}$ $(i, j = 1, 2, 3)$, $\delta$, $\alpha_1$, and $\alpha_2$ are the parameters in the PMNS matrix in Eq. (3.2.10). These values are consistent with the current neutrino oscillation data for the normal ordering mass hierarchy [1]. In addition, the sum of the neutrino masses are evaluated as

$$\sum_{i=1}^{3} m_{\nu_i} = 62\ \mathrm{meV}. \tag{5.6.8}$$

This is smaller than the upper limit from the latest Planck data [3]; $\sum m_{\nu_i} < 102$ meV.

The branching ratios for the lepton flavor violating processes in the benchmark scenario are shown in Table 5.3. It is found that all the processes satisfy the current upper limit.

Next, we consider the eEDM in the benchmark scenario. In the benchmark scenario, we assume that $\theta_e = \theta_\rho$ for simplicity. Then, the contribution from the $S^\pm$ loop diagram shown in Fig. 5.1 vanish. The severe constraint from the eEDM measurement is avoided by the destructive interference between the top quark loop diagrams and the scalar loop diagrams including $H_{2,3}$ and $H^\pm$. This is the same situation as the model discussed in Chapter 4. The prediction of $d_e$ in the benchmark scenario is given by

$$d_e = -1.6 \times 10^{-30}\ \mathrm{e\,cm}. \tag{5.6.9}$$

This is the one-order magnitude smaller than the current upper limit.

In the benchmark scenario, the lightest $Z_2$-odd particle is the real singlet scalar boson $\eta$. Thus, $\eta$ is the DM particle in the benchmark scenario. With the input parameters shown in Eqs. (5.6.1)–(5.6.3), the relic abundance of $\eta$ is calculated as

$$\Omega_\eta h^2 = 0.12. \tag{5.6.10}$$

| Processes | BR | Upper limits |
|---|---|---|
| $\mu \to e\gamma$ | $7.18 \times 10^{-16}$ | $4.2 \times 10^{-13}$ |
| $\tau \to e\gamma$ | $2.37 \times 10^{-12}$ | $3.3 \times 10^{-8}$ |
| $\tau \to \mu\gamma$ | $1.31 \times 10^{-11}$ | $4.4 \times 10^{-8}$ |

| Processes | BR | Upper limits |
|---|---|---|
| $\mu \to 3e$ | $1.35 \times 10^{-15}$ | $1.0 \times 10^{-12}$ |
| $\tau \to 3e$ | $1.68 \times 10^{-11}$ | $2.7 \times 10^{-8}$ |
| $\tau \to 3\mu$ | $5.14 \times 10^{-15}$ | $2.1 \times 10^{-8}$ |

| Processes | BR | Upper limits |
|---|---|---|
| $\tau \to e\mu\bar{e}$ | $4.11 \times 10^{-10}$ | $1.8 \times 10^{-8}$ |
| $\tau \to \mu\mu\bar{e}$ | $2.60 \times 10^{-13}$ | $1.7 \times 10^{-8}$ |
| $\tau \to ee\bar{\mu}$ | $7.17 \times 10^{-14}$ | $1.5 \times 10^{-8}$ |
| $\tau \to e\mu\bar{\mu}$ | $7.63 \times 10^{-13}$ | $2.7 \times 10^{-8}$ |

Table 5.3: Branching ratios for the lepton flavor violating processes in the benchmark scenario and the current upper limit on them

Thus, in the benchmark scenario, the observed relic density of DM can be explained [3]. On the other hand, by using Eq. (5.4.15), the scattering cross section for $\eta N \to \eta N$ is evaluated as

$$\sigma_{\eta N} \simeq 2.3 \times 10^{-48}\ \mathrm{cm}^2. \tag{5.6.11}$$

The current upper limit for $\sigma_{\eta N}$ is given by the XENON1T experiment [252]. In the case that the mass of DM particle is 63 GeV, the upper limit is about $10^{-27}$ cm$^2$. Therefore, the benchmark scenario can explain the DM relic density under the constraints from the DM direct search.

Finally, we consider EWBG in the benchmark scenario. In Fig. 5.5, the $\Delta R$ in Eq. (5.5.10) and $v_n/T_n$ for various values of $m_{H_2}$, $m_{H_3} = m_{H^\pm}$ are shown. In the evaluation of $T_n$ and $v_n$, we have used CosmoTransitions [203]. The values of the parameters except for $m_{H_2}$, $m_{H_3}$, and $m_{H^\pm}$ are the same as those in the benchmark scenario. Since we fix the value of the invariant mass parameter $M^2$, the non-decoupling effect of $H_2$, $H_3$, and $H^\pm$ is stronger as the masses of them increase. Thus, in Fig. 5.5, we can see that the EWPT is stronger in the heavier mass regions.

The blue point in Fig. 5.5 corresponds to the benchmark scenario. On this point, the nucleation temperature is evaluated as $T_n = 100$ GeV, and $v_n/T_n$ is given by $v_n/T_n = 1.74$. Therefore, the strongly 1st order EWPT can be realized in the benchmark scenario. In addition, the prediction for $\Delta R$ in the benchmark scenario is $\Delta R = 38$ %. This deviation is expected to be verified in the future upgraded ILC with $\sqrt{s} = 500$ GeV and 1 TeV.

In Fig. 5.6, we show the distribution of the dimensionless chemical potentials $\xi_i$ ($i = t_L$, $t_R^c$, $b_L$, $\phi$) which is given by solving the transport equations in Eq. (5.5.18). The horizontal axis in Fig. 5.6 is the radial coordinate perpendicular to the bubble wall which is normalized by $T_n$. The positive (negative) direction of the horizontal axis is the broken (symmetric) phase. We can see that the left-handed and right-handed top quarks provide large contributions. The chemical potentials of the bottom quark and the Higgs are

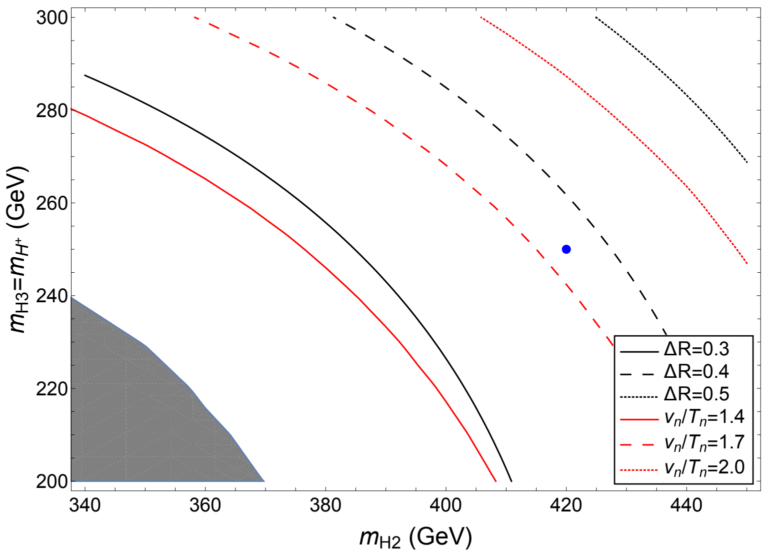


Figure 5.5: The $\Delta R$ in Eq. (5.5.10) and $v_n/T_n$ in the model. The values of parameters except for $m_{H_2}$, $m_{H_3}$, and $m_{H^\pm}$ is the same as those in the benchmark scenario. The blue point represents the benchmark scenario ($m_{H_2} = 420$ GeV, $m_{H_3} = m_{H^\pm} = 250$ GeV).

negligibly small.

The chemical potentials for the left-handed fermions in $z > 0$ can be converted into the baryon asymmetry by the weak Sphaleron transition. By using the formula in Eq. (5.5.23), the produced baryon asymmetry in the benchmark scenario is evaluated as

$$\frac{n_B}{s} = 8.65 \times 10^{-11}, \tag{5.6.12}$$

where $n_B$ is the number density of baryon and $s$ is the entropy density.

The observed quantity for the baryon asymmetry is the baryon-to-photon ratio $\eta_B$, which is the ratio of the number density of the baryon and that of the photon. In the standard cosmology, $\eta_B$ can be evaluated as $\eta_B \simeq 7.04 \times (n_B/s)$. By using this equation, $\eta_B$ in the benchmark scenario is given by

$$\eta_B \simeq 7.04 \times \frac{n_B}{s} = 6.1 \times 10^{-10}. \tag{5.6.13}$$

The 95 % C.L. interval of $\eta_B$ is provided by the observations related to BBN [?] as well as the latest Planck data [3] as follows;

$$\begin{aligned} &5.8 \times 10^{-10} \leq \eta_B \leq 6.5 \times 10^{-10} \quad &&\text{(BBN)}, \\ &6.04 \times 10^{-10} \leq \eta_B \leq 6.20 \times 10^{-10} \quad &&\text{(Planck)}. \end{aligned} \tag{5.6.14}$$

Therefore, in the benchmark scenario, the observed baryon asymmetry can be explained within 95 % C.L. As a result, the baryon asymmetry, neutrino mass, and DM relic density can be explained simultaneously in the benchmark scenario under the experimental constraints discussed in Sec. 5.1.2.

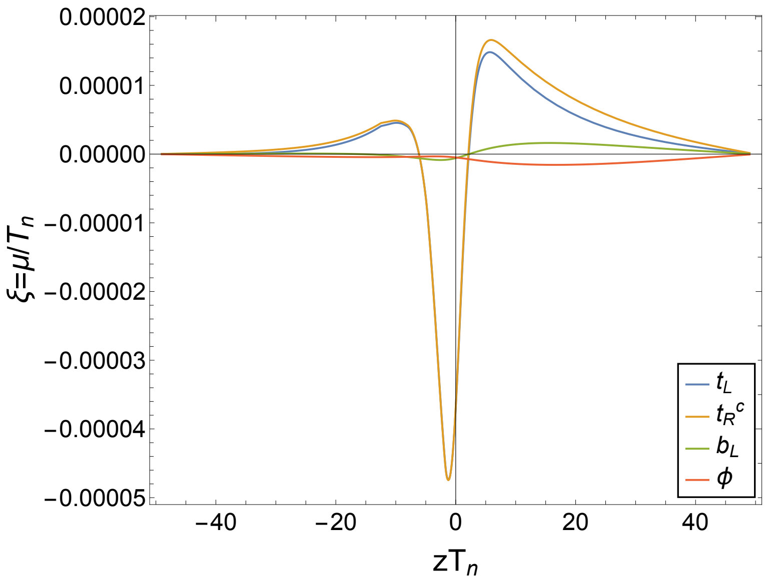


Figure 5.6: The distribution of the chemical potential in the benchmark scenario. The bubble wall is at the origin.

### 5.6.2 Predictions

In this section, we discuss distinctive predictions of the benchmark scenario. First, we consider the future direct searches of the additional Higgs bosons at the HL-LHC. In the benchmark scenario, $\zeta$ couplings are set to be

$$|\zeta_u| = |\zeta_d| = |\zeta_\tau| = 0.246, \quad |\zeta_\mu| = 0.5, \quad |\zeta_e| = 80. \tag{5.6.15}$$

Although, $|\zeta_e|$ and $|\zeta_\mu|$ is larger than the other $\zeta$ couplings, the hierarchy of the lepton's Yukawa couplings is given by

$$m_\tau|\zeta_\tau| : m_\mu|\zeta_\mu| : m_e|\zeta_e| \simeq 1 : 0.12 : 0.092. \tag{5.6.16}$$

Therefore, the decays of the additional Higgs bosons are almost the same as those in the Type-I THDM, where all $\zeta$ couplings are real and have the same value. Then, the charged Higgs boson in the benchmark scenario is produced via the process $gg \to H^\pm tb$ and decays into $tb$ at almost 100 %. The expected upper limit on $|\zeta_u|$ from the search for this process at the HL-HLC with the integrated luminosity $L = 3000$ fb$^{-1}$ is given by $|\zeta_u| \lesssim 0.2$ at 95 % C.L. [102]. Thus, the signal of this process in the benchmark scenario is expected to be detected at the HL-LHC.

The additional neutral scalars can be also produced at the HL-LHC. The dominated single production channel is the gluon fusion process $gg \to H_{2,3}$ [169]. In the benchmark scenario, $H_2$ decays into a pair of top quarks at almost 100 %. On the other hand, $H_3 \to t\bar{t}$ is kinematically prohibited, thus $H_3$ decays into $b\bar{b}$, $gg$, and $\tau\bar{\tau}$. Therefore, the signal of the process $gg \to H_2 \to t\bar{t}$ and $gg \to H_3 \to \tau\bar{\tau}$ would be detected at the HL-LHC [102].[2]

[2]In Ref. [102], the CP-conserving case is investigated, and the expected upper limit on $|\zeta_u|$ from the search for these signals at the Hl-LHC is provided. In our benchmark scenario, $\zeta_u$ has the CP-violating phase, and it would be affect the production cross sections of $H_2$ and $H_3$.

Next, we discuss the future direct search for $S^\pm$. At the hadron collider, a pair of $S^+S^-$ is produced by $q\overline{q} \to Z^*/\gamma^* \to S^+S^-$. Since $S^\pm$ is lighter than the Majorana fermions, the final states of it has to include DM particle $\eta$. The main decay mode is $S^\pm \to H^\pm \eta$ via the scalar coupling $\kappa(\tilde{\Phi}_1^\dagger \Phi_2)S^-\eta$. The charged Higgs boson decays into $tb$ at almost 100 %. The DM particle $\eta$ is stable, and it is missing energy at the detector. Therefore, the signal of the production of $S^+S^-$ pair is $pp \to S^+S^- \to 2t2b\not{E} \to 4b2j\not{E}$ or $pp \to S^+S^- \to 2t2b\not{E} \to 4b2\ell\not{E}$ in the benchmark scenario. At the HL-LHC, this channel would be useful to search for $S^\pm$ in the benchmark scenario.

The charged scalar $S^\pm$ is also produced at $e^+$-$e^-$ colliders if it is kinematically allowed. In addition to the s-channel diagram $e^+e^- \to Z^*/\gamma^* \to S^+S^-$, there is t-channel diagram $e^+e^- \to S^+S^-$ via the Yukawa interaction $Y_N$. For $S^\pm$ in the benchmark scenario, the t-channel diagram gives the leading contribution, and the production cross section can reach about 100 fb for $m_S = 400$ GeV at $\sqrt{s} = 1$ TeV in the case of $\mathcal{O}(1)$ Yukawa couplings [75]. Therefore, it would be possible to explore $S^\pm$ at the future upgraded ILC with the beam energy higher than 800 GeV.

The Yukawa interaction among $S^\pm$, $N_a$, and charged leptons induce the lepton flavor violating processes. At the future experiments, the upper limits for these processes are expected to be improved by one or a few order. In Table 5.4, we show the benchmark scenario's prediction and the expected upper limit for these processes are shown. In

| Processes | Benchmark scenario | Expected limits | Experiments |
|---|---|---|---|
| $\mu \to e\gamma$ | $7.18 \times 10^{-16}$ | $6 \times 10^{-14}$ | MEG-II [253] |
| $\tau \to e\gamma$ | $2.37 \times 10^{-12}$ | $3 \times 10^{-9}$ | Belle-II [217] |
| $\tau \to \mu\gamma$ | $1.31 \times 10^{-11}$ | $1 \times 10^{-9}$ | Belle-II [217] |
| $\mu \to 3e$ | $1.35 \times 10^{-15}$ | $1 \times 10^{-16}$ | Mu3e [254, 255] |
| $\tau \to 3e$ | $1.68 \times 10^{-11}$ | $4 \times 10^{-10}$ | Belle-II [217] |
| $\tau \to 3\mu$ | $5.14 \times 10^{-15}$ | $3 \times 10^{-10}$ | Belle-II [217] |
| $\tau \to e\mu\overline{e}$ | $4.11 \times 10^{-10}$ | $3 \times 10^{-10}$ | Belle-II [217] |
| $\tau \to \mu\mu\overline{e}$ | $2.60 \times 10^{-13}$ | $3 \times 10^{-10}$ | Belle-II [217] |
| $\tau \to ee\overline{\mu}$ | $7.17 \times 10^{-14}$ | $1 \times 10^{-10}$ | Belle-II [217] |
| $\tau \to e\mu\overline{\mu}$ | $7.63 \times 10^{-13}$ | $4 \times 10^{-10}$ | Belle-II [217] |

Table 5.4: Predictions in the benchmark scenario and the expected upper limit at 90 % C.L. for each lepton flavor violating process.

the MEG-II experiment, the upper limit on $\mu \to e\gamma$ is expected to be improved up to $6 \times 10^{-14}$ [253]. However, in the benchmark scenario, the branching ratio for it is predicted to be two orders smaller than the expected upper limit at the MEG-II experiment. The Mu3e experiment is planned to run in two phases. In phase I, the Mu3e experiment aims to measure or exclude the branching ratio for $\mu \to 3e$ up to $2 \times 10^{-15}$ [254, 255]. In phase

II, the upper limit for $\mu \to 3e$ is expected to be improved up to $1 \times 10^{-16}$ [254, 255]. In phase II, the prediction for the process in the benchmark scenario would be confirmed or excluded. The expected upper limits on other processes are given by the Belle-II experiment. The value in Table 5.4 assumes the integrated luminosity $L = 50$ ab$^{-1}$. In the benchmark scenario, the prediction for $\tau \to e\mu\bar{e}$ would be tested at the Belle-II experiment with $L = 50$ ab$^{-1}$.

The structure of the Yukawa coupling $Y_N$ will also be explored by future neutrino oscillation experiments. At the future T2K experiment using Hyper-Kamiokande [256], some PMNS matrix parameters are expected to be measured with higher accuracy. This improvement would provide more precise information on the structure of $Y_N$. In particular, the precision measurement of the Dirac phase of the PMNS matrix would give a hint of the CP-violating structure of $Y_N$.

In the benchmark scenario, the eEDM is predicted to be $d_e = -1.6 \times 10^{-30}$ e cm. This is a one-order magnitude smaller than the current upper limit and would be tested by the future one-order improvement of the eEDM measurement [178]. In addition, the CP-violation in the model would be tested at future flavor experiments such as Belle-II [217] and LHCb [218] by searching for the asymmetry between the CP violation in $B^- \to X_s^- \gamma$ and that in $B^0 \to X_s^0 \gamma$ [53, 219, 220]. Furthermore, it would be possible to measure the CP-violating phase of $\zeta_e$ at future lepton colliders by looking at the azimuthal angle distribution of the hadronic decays of the tau leptons from the decay of $H_2, H_3$ [104, 221].

The scattering cross section of the process $\eta N \to \eta N$ is predicted to be $\sigma_{\eta N} = 2.3 \times 10^{-48}$ cm$^2$ in the benchmark scenario, which is about one-order smaller than the current upper limit from the XENON experiment [252]. The signal of this DM scattering would be detected at the future LZ experiment [257]. Furthermore, the DARWIN experiment [258] aims to explore the entire accessible WIMP parameter space. The DM $\eta$ would be thoroughly tested by these future experiments.

The strongly 1st order EWPT can be tested by the future Higgs precision measurements. The non-decoupling effect of the additional scalar bosons leads to a sizable $\Delta R$ [140, 141, 143]. This deviation can be measured in the precision measurement of the di-Higgs production at future high-energy colliders [208, 222–229]. At the HL-HLC and the upgraded ILC with $\sqrt{s} = 500$ GeV (1 TeV), the triple Higgs boson coupling is expected to be measured with the accuracies 50 % [207, 208] and 27 % (10 %) [209]. In the benchmark scenario, the Higgs triple coupling is predicted to be deviated by 38 % from the SM prediction. This prediction would be verified at the future upgraded ILC.

Finally, GW can be produced by the 1st order EWPT in extended Higgs sectors [230–232]. They would be detectable at future space-based GW detectors such as LISA [233], DECIGO [234], and BBO [235].

## 5.7 Summary of Chapter 5

In this chapter, I introduce one of my works [110]. In this work, we investigate a new model which can explain tiny neutrino masses, DM, and the BAU simultaneously. In the model, Majorana masses of neutrinos are generated by three-loop diagrams. The DM candidate is $Z_2$-odd real scalar boson or the lightest Majorana fermion. The EWPT in the model can be the strongly 1st order phase transition due to the non-decoupling effect of the additional scalar bosons. Then, the baryon asymmetry of the universe is produced via EWBG. I have introduced the benchmark scenario of the model, where all three problems can be explained under the current constraints from various experimental data. In particular, the severe constraint from the eEDM measurement is avoided by the destructive interference between the CP-violating phases in the Higgs potential and the Yukawa interaction. In the benchmark scenario, the masses of new scalar bosons are $m_{H_3} = m_{H^\pm} = 250$ GeV, $m_{H_2} = 420$ GeV, $m_S = 400$ GeV, and $m_\eta = 63$ GeV. They would be produced and tested at future collider experiments. The lepton flavor violating coupling $Y_N$ would be explored by future flavor experiments and neutrino oscillation experiments. The CP violation in the model would be verified by the eEDM measurements, the flavor experiments, and the lepton colliders. The DM nature would be tested at future DM direct detection experiments. In addition, the strongly 1st order EWPT can be tested by the measurements of the Higgs triple coupling and future GW observations.

# Chapter 6

# Grand Summary

In this chapter, we summarize this doctoral thesis. In Chap. 2, some basic facts of the SM have been shortly reviewed. In the SM, the mass terms of gauge bosons are prohibited by gauge symmetry. In addition, the fermions cannot also have mass terms since the left-handed fermions and right-handed fermions have different quantum numbers. We have shown that in the SM, the mass of the gauge bosons and the fermions are provided by the VEV of the isospin doublet scalar field, the Higgs doublet. We have also shown that the CP violation is caused by the phase of the CKM matrix. For this phase to be a physical CP-violating phase, the number of fermion flavors must be three or larger.

In Chap. 3, we have discussed some phenomena which cannot be explained in the SM. First, we have discussed the BAU and EWBG [21]. To produce the BAU, the Sakharov conditions [17] have to be satisfied. In the SM, they are not satisfied since CP-violation is too small and the EWPT is not the strongly 1st order. Therefore, for successful EWBG, the extended Higgs sector including a new CP-violating source is needed. The WKB method [105–109], which is one of the approximation methods to evaluate the BAU generated by EWBG, has been reviewed.

Second, we have discussed neutrino oscillations and neutrino mass. To explain the observed neutrino oscillation data, at least two neutrinos have to be massive particles. However, in the SM, all of them are massless fermions. Therefore, new physics is needed to explain neutrino mass. Since the neutrinos are electrically neutral, they can have two types of mass terms; Dirac-type mass and Majorana-type mass. Neutrino mass induces the LFV via the PMNS matrix regardless of which type of mass term neutrinos have. This causes the neutrino oscillation, and other lepton flavor violating processes such as $\mu \to e\gamma$. However, the branching ratio of $\mu \to e\gamma$ via neutrino mass is much smaller than the current experimental upper limit. Thus, it would be difficult to detect the effect of neutrino mass by measuring $\mu \to e\gamma$. If neutrinos are Majorana fermions, lepton number conservation is broken. This nature of Majorana neutrinos can be tested by the observation of $0\nu\beta\beta$. Type-I, II, III seesaw mechanisms have been introduced as examples of new physics to explain neutrino mass.

Third, we have discussed the DM. The freeze-out mechanism which is one of the scenarios to obtain the observed relic density of DM has been reviewed. Some formulae to evaluate DM relic abundance are provided.

In Chap. 4, I have introduced one of my works [55]. We have investigated EWBG in the CP-violating two Higgs doublet model, where the Yukawa interactions are aligned to avoid the FCNCs, and coupling constants of the lightest Higgs boson coincide with those in the SM at tree level. In the analyses, we have focused on the parameter regions where the severe constraints from the current eEDM measurement can be satisfied by the destructive interferences between the CP-violating phases in the Yukawa interactions and that in the Higgs potential. We have some benchmark scenarios where the observed baryon number asymmetry can be reproduced under the various experimental and theoretical constraints. These benchmark scenarios can be tested by various future experiments. The typical value of the additional Higgs bosons is 300–400 GeV for the successful EWBG. These would be tested at the HL-LHC and flavor experiments such as Belle-II and LHCb. The CP-violating phases which are essential to the successful EWBG would be tested by future EDM measurements, flavor experiments, and linear colliders. In addition, the strongly 1st order EWPT in the model can be tested by measuring the triple Higgs boson coupling. The typical value in the benchmark scenarios is 35–55 %. This would be tested by the HL-LHC and the future upgraded ILC. In addition, the strongly 1st order EWPT in the model might be able to be tested by observing the GWs. This possibility will be investigated in the future.

In Chap. 5, I have introduced an extension of the model studied in Chap. 4 [110]. In this model, the BAU, neutrino mass, and DM can be explained simultaneously by the extended Higgs sector and right-handed neutrinos. The EWPT in the model can be the strongly 1st order phase transition due to the non-decoupling effect of the additional scalar bosons. Then, the baryon asymmetry of the universe is produced via EWBG. Majorana masses of neutrinos are generated by three-loop diagrams. The DM candidate is $Z_2$-odd real scalar boson or the lightest Majorana fermion. I have introduced the benchmark scenario of the model, where all three problems can be explained under the current constraints from various experimental data. In particular, the severe constraint from the eEDM measurement is avoided by the destructive interference between the CP-violating phases in the Higgs potential and the Yukawa interaction. In the benchmark scenario, the masses of new scalar bosons are $m_{H_3} = m_{H^\pm} = 250$ GeV, $m_{H_2} = 420$ GeV, $m_S = 400$ GeV, and $m_\eta = 63$ GeV. They would be produced and tested at future collider experiments. The lepton flavor violating coupling $Y_N$ would be explored by future flavor experiments and neutrino oscillation experiments. The CP violation in the model would be verified by the eEDM measurements, the flavor experiments, and the lepton colliders. The DM nature would be tested at future DM direct detection experiments. In addition, the strongly 1st order EWPT can be tested by the measurements of the Higgs triple coupling and future GW observations.

# Appendix A

# Relations among scalar coupling constants in two bases

In this Appendix, the relations among the scalar couplings in the Higgs basis and those in any other basis. The Higgs doublets in the Higgs basis are denoted by $(\Phi_1, \Phi_2)$, and those in any other basis are denoted by $(\phi_1, \phi_2)$. The relation of them is given by

$$\begin{pmatrix} \Phi_1 \\ \Phi_2 \end{pmatrix} = \frac{1}{v} \begin{pmatrix} v_1^* & v_2^* \\ -v_2 e^{i\phi} & v_1 e^{i\phi} \end{pmatrix} \begin{pmatrix} \phi_1 \\ \phi_2 \end{pmatrix}, \tag{A.1}$$

where $v_1$ and $v_2$ are the VEVs of $\phi_1$ and $\phi_2$, respectively. Then, the VEV of $\Phi_1$ is given by $v = \sqrt{v_1^2 + v_2^2}$. The VEVs $v_1$ and $v_2$ are generally complex number, and the arguments of them are denoted by $\theta_1$ and $\theta_2$, respectively. The phase $\phi$ is an arbitrary phase corresponding to the degree of freedom of rephasing $\Phi_2$.

By using this relation, we can obtain the following relations for the scalar couplings in the THDM discussed in Chap. 4.

$$\mu_1^2 = \mu_1'^2 c_\beta^2 + \mu_2'^2 s_\beta^2 + 2\mathrm{Re}[\mu_{12}'^2 e^{-i\theta_{12}}] c_\beta s_\beta, \tag{A.2}$$

$$\mu_2^2 = \mu_2'^2 s_\beta^2 + \mu_2'^2 c_\beta^2 - 2\mathrm{Re}[\mu_{12}'^2 e^{-i\theta_{12}}] c_\beta s_\beta, \tag{A.3}$$

$$\mu_{12}^2 = e^{-i(\theta_1+\theta_2+\phi)} \big( -\mu_1'^2 c_\beta s_\beta + \mu_2'^2 c_\beta s_\beta + \mathrm{Re}[\mu_{12}'^2 e^{-i\theta_{12}}](c_\beta^2 - s_\beta^2) + i\mathrm{Im}[\mu_{12}'^2 e^{-i\theta_{12}}] \big), \tag{A.4}$$

$$\lambda_1 = \lambda_1' c_\beta^4 + \lambda_2' s_\beta^4 + 2\lambda_{345}' c_\beta^2 s_\beta^2 + 4\big( \mathrm{Re}[\lambda_6' e^{-i\theta_{12}}] c_\beta^2 + \mathrm{Re}[\lambda_7' e^{-i\theta_{12}}] s_\beta^2 \big) c_\beta s_\beta, \tag{A.5}$$

$$\lambda_2 = \lambda_1' s_\beta^4 + \lambda_2' c_\beta^4 + 2\lambda_{345}' c_\beta^2 s_\beta^2 - 4\big( \mathrm{Re}[\lambda_6' e^{-i\theta_{12}}] s_\beta^2 + \mathrm{Re}[\lambda_7' e^{-i\theta_{12}}] c_\beta^2 \big) c_\beta s_\beta, \tag{A.6}$$

$$\lambda_3 = \lambda_3' + (\lambda_1' + \lambda_2' - 2\lambda_{345}') c_\beta^2 s_\beta^2 - 2\big( \mathrm{Re}[\lambda_6' e^{-i\theta_{12}}] - \mathrm{Re}[\lambda_7' e^{-i\theta_{12}}] \big)(c_\beta^2 - s_\beta^2) c_\beta s_\beta, \tag{A.7}$$

$$\lambda_4 = \lambda_4' + (\lambda_1' + \lambda_2' - 2\lambda_{345}') c_\beta^2 s_\beta^2 - 2\big( \mathrm{Re}[\lambda_6' e^{-i\theta_{12}}] - \mathrm{Re}[\lambda_7' e^{-i\theta_{12}}] \big)(c_\beta^2 - s_\beta^2) c_\beta s_\beta. \tag{A.8}$$

$$\begin{aligned}\lambda_5 = e^{-2i(\theta_1+\theta_2+\phi)}\Big\{&\mathrm{Re}[\lambda_5' e^{-2i\theta_{12}}] + (\lambda_1' + \lambda_2' - 2\lambda_{345}')c_\beta^2 s_\beta^2 \\ &- 2\big(\mathrm{Re}[\lambda_6' e^{-i\theta_{12}}] - \mathrm{Re}[\lambda_7' e^{-i\theta_{12}}]\big)(c_\beta^2 - s_\beta^2)c_\beta s_\beta + i\mathrm{Im}[\lambda_5' e^{-2i\theta_{12}}](c_\beta^2 - s_\beta^2) \\ &- 2i\big(\mathrm{Im}[\lambda_6' e^{-i\theta_{12}}] - \mathrm{Im}[\lambda_7' e^{-i\theta_{12}}]\big)c_\beta s_\beta\Big\}, \end{aligned} \tag{A.9}$$

$$\begin{aligned}\lambda_6 = e^{-i(\theta_1+\theta_2+\phi)}\Big\{&-\big(\lambda_1' c_\beta^2 - \lambda_2' s_\beta^2 - \lambda_{345}'(c_\beta^2 - s_\beta^2)\big)c_\beta s_\beta \\ &+ \mathrm{Re}[\lambda_6' e^{-i\theta_{12}}]c_\beta^2(c_\beta^2 - 3s_\beta^2) - \mathrm{Re}[\lambda_7' e^{-i\theta_{12}}]s_\beta^2(s_\beta^2 - 3c_\beta^2) \\ &+ i\mathrm{Im}[\lambda_5' e^{-2i\theta_{12}}]c_\beta s_\beta + i\mathrm{Im}[\lambda_6' e^{-i\theta_{12}}]s_\beta^2 + i\mathrm{Im}[\lambda_7' e^{-i\theta_{12}}]c_\beta^2\Big\}, \end{aligned} \tag{A.10}$$

$$\begin{aligned}\lambda_7 = e^{-i(\theta_1+\theta_2+\phi)}\Big\{&-\big(\lambda_1' s_\beta^2 - \lambda_2' c_\beta^2 + \lambda_{345}'(c_\beta^2 - s_\beta^2)\big)c_\beta s_\beta \\ &- \mathrm{Re}[\lambda_6' e^{-i\theta_{12}}]s_\beta^2(s_\beta^2 - 3c_\beta^2) + \mathrm{Re}[\lambda_7' e^{-i\theta_{12}}]c_\beta^2(c_\beta^2 - 3s_\beta^2) \\ &- i\mathrm{Im}[\lambda_5' e^{-2i\theta_{12}}]c_\beta s_\beta + i\mathrm{Im}[\lambda_6' e^{-i\theta_{12}}]s_\beta^2 + i\mathrm{Im}[\lambda_7' e^{-i\theta_{12}}]c_\beta^2\Big\}. \end{aligned} \tag{A.11}$$

These results are consistent with those in Ref. [101], in which the phase $\phi$ is fixed at $\phi = -\theta_1 + \theta_2$.

In the same way, the coupling relations for the model discussed in Chap. 5 are founded. They are given by Eqs. (A.2)-(A.11) and the following equations;

$$\rho_1 = \rho_1' c_\beta^2 + \rho_2' s_\beta^2 + 2c_\beta s_\beta \mathrm{Re}[\rho_{12}' e^{-i\theta_{12}}], \tag{A.12}$$

$$\rho_2 = \rho_1' s_\beta^2 + \rho_2' c_\beta^2 - 2c_\beta s_\beta \mathrm{Re}[\rho_{12}' e^{-i\theta_{12}}], \tag{A.13}$$

$$\rho_{12} = e^{-i(\theta_1+\theta_2)}\Big\{(\rho_2' - \rho_1')c_\beta s_\beta + \mathrm{Re}[\rho_{12}' e^{-i\theta_{12}}](c_\beta^2 - s_\beta^2) + i\mathrm{Im}[\rho_{12}' e^{-i\theta_{12}}]\Big\}, \tag{A.14}$$

$$\sigma_1 = \sigma_1' c_\beta^2 + \sigma_2' s_\beta^2 + 2c_\beta s_\beta \mathrm{Re}[\sigma_{12}' e^{-i\theta_{12}}], \tag{A.15}$$

$$\sigma_2 = \sigma_1' s_\beta^2 + \sigma_2' c_\beta^2 - 2c_\beta s_\beta \mathrm{Re}[\sigma_{12}' e^{-i\theta_{12}}], \tag{A.16}$$

$$\sigma_{12} = e^{-i(\theta_1+\theta_2+\phi)}\Big\{(\sigma_2' - \sigma_1')c_\beta s_\beta + \mathrm{Re}[\sigma_{12}' e^{-i\theta_{12}}](c_\beta^2 - s_\beta^2) + i\mathrm{Im}[\sigma_{12}' e^{-i\theta_{12}}]\Big\}, \tag{A.17}$$

$$\kappa = (\det U_H)^* \kappa' = e^{-i\phi}\kappa'. \tag{A.18}$$

The rest of the scalar couplings ($\lambda_s$, $\lambda_\eta$, and $\xi$) do not change by selecting the basis.

# Appendix B

# The loop functions in the formula for the neutrino mass matrix

In this Appendix, the calculations of the loop functions in the formula for the neutrino mass matrix in Sec. 5.2. The amputated correlation function corresponding to the left diagram in Fig. 5.2 is calculated as

$$i\Sigma^1_{ij} = -4i\left(\frac{1}{16\pi^2}\right)^3 (\kappa\zeta^*_\ell)^2 m_{\ell_i} m_{\ell_j} \sum_{a=1}^{3} (Y_N)_{aj} M_{N_a} (Y_N)_{ai} F_{1a}, \tag{B.1}$$

where the momentum of the external neutrinos is 0. By using an approximation where masses of the charged leptons in the internal lines are neglected, the loop function $F_1$ is given by

$$\begin{aligned} F_{1a} =& (16\pi^2)^3 \frac{1}{i} \int \frac{\mathrm{d}^4 p}{(2\pi)^4} \int \frac{\mathrm{d}^4 q}{(2\pi)^4} \int \frac{\mathrm{d}^4 k}{(2\pi)^4} \frac{1}{p^2} \frac{1}{q^2} \frac{1}{p^2 - m_{H^\pm}^2} \frac{1}{q^2 - m_{H^\pm}^2} \\ & \times \frac{1}{k^2 - m_\eta^2} \frac{1}{k^2 - M_{N_a}^2} \frac{1}{(k-p)^2 - m_S^2} \frac{1}{(k-q)^2 - m_S^2} \not{q}\not{p}. \end{aligned} \tag{B.2}$$

The integral by $k^\mu$ can be performed by using Feynman parametrization as follows;

$$\begin{aligned} & \int \frac{\mathrm{d}^4 k}{(2\pi)^4} \frac{1}{k^2 - m_\eta^2} \frac{1}{k^2 - M_{N_a}^2} \frac{1}{(k-p)^2 - m_S^2} \frac{1}{(k-q)^2 - m_S^2} \\ =& \int_0^1 \tilde{\mathrm{d}}^4 x \int \frac{\mathrm{d}^4 k}{(2\pi)^4} \frac{3!}{(k^2 - D)^4} = \frac{i}{16\pi^2} \int_0^1 \tilde{\mathrm{d}}^4 x \frac{1}{D^2}, \end{aligned} \tag{B.3}$$

where the integral $\int_0^1 \tilde{\mathrm{d}}^4 x$ is defined as

$$\int_0^1 \tilde{\mathrm{d}}^4 x \equiv \int_0^1 \mathrm{d}x \int_0^1 \mathrm{d}y \int_0^1 \mathrm{d}z \int_0^1 \mathrm{d}\omega\, \delta(1 - x - y - z - \omega), \tag{B.4}$$

and $D$ is given by

$$D = x M_{N_a}^2 + (y+z) m_S^2 + \omega m_\eta^2 - y(1-y)p^2 - z(1-z)q^2 + 2yz p\cdot q. \tag{B.5}$$

Since the integrand is symmetric with respect to the interchange $p^\mu \leftrightarrow q^\mu$, the gamma matrices $\not{q}\not{p}$ can be replaced with $q \cdot p = q_\mu p^\mu$. Now, we use Wick rotations for $p^\mu$ and $q^\mu$ and define the momentums $P^\mu$ and $Q^\mu$ in four-dimensional Euclidean space as

$$P^0 = -ip^0,, \quad P^k = p^k, \quad Q^0 = -iq^0, \quad Q^k = q^k, \quad (k = 1, 2, 3). \tag{B.6}$$

Then, the loop function $F_{1a}$ is given by

$$\begin{aligned} F_{1a} = &\frac{1}{\pi^4} \int_0^1 \tilde{\mathrm{d}}^4 x \int \mathrm{d}^4 P \int \mathrm{d}^4 Q \, \frac{1}{P^2} \frac{1}{Q^2} \frac{1}{P^2 + m_{H^\pm}^2} \frac{1}{Q^2 + m_{H^\pm}^2} \\ &\times \frac{P \cdot Q}{(x M_{N_a}^2 + (y+z) m_S^2 + \omega m_\eta^2 + y(1-y) P^2 + z(1-z) Q^2 - 2yz P \cdot Q)^2}. \end{aligned} \tag{B.7}$$

We define the 0th axis in the $P^\mu$ coordinate as the direction of the vector $Q^\mu$ and rewrite Eq. (B.7) in the following polar coordinate;

$$\begin{cases} P^0 = P_r \cos\theta \cos\phi, \\ P^1 = P_r \cos\theta \sin\phi, \\ P^2 = P_r \sin\theta \cos\chi, \\ P^3 = P_r \sin\theta \sin\chi. \end{cases} \qquad \left( \begin{array}{l} 0 \le P_r \le \infty, \\ 0 \le \theta \le \pi/2, \\ 0 \le \phi \le 2\pi, \\ 0 \le \chi \le 2\pi. \end{array} \right) \tag{B.8}$$

Then, the integrals by $P^\mu$ and $Q^\mu$ can be written as

$$\int \mathrm{d}^4 P \int \mathrm{d}^4 Q = \frac{\pi^2}{2} \int_0^\infty \mathrm{d}u \int_0^\infty \mathrm{d}v \int_0^{2\pi} \mathrm{d}\phi \int_0^{2\pi} \mathrm{d}\chi \int_0^1 \mathrm{d}t \, uvt, \tag{B.9}$$

where $u \equiv P^2$, $v \equiv Q^2$, and $t \equiv \cos\theta$. The loop function $F_{1a}$ is given by

$$F_{1a} = \frac{1}{\pi} \int_0^1 \tilde{\mathrm{d}}^4 x \int_0^\infty \mathrm{d}u \int_0^\infty \mathrm{d}v \int_0^{2\pi} \mathrm{d}\phi \int_0^1 \mathrm{d}t \frac{1}{u + m_{H^\pm}^2} \frac{1}{v + m_{H^\pm}^2} \frac{\sqrt{uv} t^2 \cos\phi}{(A_1 - B_1 t \cos\phi)^2}, \tag{B.10}$$

where

$$A_1 = x M_{N_a}^2 + (y+z) m_S^2 + \omega m_\eta^2 + y(1-y) u + z(1-z) v, \tag{B.11}$$

$$B_1 = 2yz\sqrt{uv}. \tag{B.12}$$

In all domains of the integrals, the function $A_1$ is always positive, and the following inequality is satisfied;

$$0 \le \frac{|B_1| t}{A_1} < 1. \tag{B.13}$$

Then, the integral by $\phi$ can be performed by using the residue theorem, and we obtain the following result;

$$F_{1a} = 2 \int_0^1 \tilde{\mathrm{d}}^4 x \int_0^\infty \mathrm{d}u \int_0^\infty \mathrm{d}v \frac{1}{u + m_{H^\pm}^2} \frac{1}{v + m_{H^\pm}^2} \sqrt{uv} \frac{B_1}{A_1^3} \int_0^1 \mathrm{d}t \frac{t^3}{\left(1 - \frac{B_1^2 t^2}{A_1^2}\right)^{3/2}}. \tag{B.14}$$

The integral by $t$ can be easily calculated by changing the integral variable into $s \equiv t^2$. Consequently, we obtain the formula for the loop function $F_{1a}$ as follows;

$$F_{1a} = \int_0^1 \tilde{\mathrm{d}}^4 x \int_0^\infty \mathrm{d}u \int_0^\infty \mathrm{d}v \frac{2\sqrt{uv}}{(u+m_{H^\pm}^2)(v+m_{H^\pm}^2)} \frac{1}{B_1^3} \Big( \sqrt{A_1^2 - B_1^2} + \frac{A_1^2}{\sqrt{A_1^2 - B_1^2}} - 2A_1 \Big). \tag{B.15}$$

This formula is the same as that in Eq. (5.2.2) in Sec. 5.2. The loop function $F_{2a}$ can be calculated in the same way.

Next, we derive the simple formula for $F_{1a}$ in Eq. (5.2.7) in Sec. 5.2. First, we change the integral variables in Eq. (B.2) as follows;

$$\begin{aligned} F_{1a} = (16\pi^2)^3 \frac{1}{i} \int \frac{\mathrm{d}^4 p}{(2\pi)^4} \int \frac{\mathrm{d}^4 q}{(2\pi)^4} \int \frac{\mathrm{d}^4 k}{(2\pi)^4} \frac{1}{p^2 - M_{N_a}^2} \frac{1}{p^2 - m_\eta^2} \\ \times \frac{1}{q^2 - m_{H^+}^2} \frac{1}{q^2} \frac{1}{(p+q)^2 - m_S^2} \frac{1}{k^2 - m_{H^+}^2} \frac{1}{k^2} \frac{1}{(p+k)^2 - m_S^2} (q \cdot k), \end{aligned} \tag{B.16}$$

where the gamma matrices $\not{q}\not{k}$ is replaced into $q \cdot k$ since the integrand is symmetric with respect to $q \leftrightarrow k$.

Then $F_{1a}$ can be calculated as follows;

$$\begin{aligned} F_{1a} &= \frac{(16\pi^2)^3}{i m_{H^+}^4} \int \frac{\mathrm{d}^4 p}{(2\pi)^4} \int \frac{\mathrm{d}^4 q}{(2\pi)^4} \int \frac{\mathrm{d}^4 k}{(2\pi)^4} \frac{1}{p^2 - M_{N_a}^2} \frac{1}{p^2 - m_\eta^2} \\ &\qquad \times \left( \frac{1}{q^2 - m_{H^+}^2} - \frac{1}{q^2} \right) \frac{q^\mu}{(p+q)^2 - m_S^2} \left( \frac{1}{k^2 - m_{H^+}^2} - \frac{1}{k^2} \right) \frac{k_\mu}{(p+k)^2 - m_S^2} \\ &= -\frac{16\pi^2}{i m_{H^\pm}^4} \int \frac{\mathrm{d}^4 p}{(2\pi)^4} \frac{1}{p^2 - M_{N_a}^2} \frac{1}{p^2 - m_\eta^2} p^2 \Big( B_1(m_{H^+}, m_S; p^2) - B_1(0, m_S; p^2) \Big)^2, \end{aligned} \tag{B.17}$$

where $B_1$ is the Passarino-Veltman function for 1-loop integrals [248]. By using the Wick rotation, we obtain the follwing result;

$$\begin{aligned} F_{1a} =& \frac{1}{m_{H^\pm}^4} \frac{1}{M_{N_a}^2 - m_\eta^2} \\ & \times \int_0^\infty \mathrm{d}x\, x \left( \frac{M_{N_a}^2}{x + M_{N_a}^2} - \frac{m_\eta^2}{x + m_\eta^2} \right) \Big( B_1(m_{H^+}, m_S; -x) - B_1(0, m_S; -x) \Big)^2. \end{aligned} \tag{B.18}$$

This formula is the same as that in Eq. (5.2.7).

# Appendix C

# Formulae for the field-dependent masses

In this appendix, we show the formulae for the field-dependent masses which is necessary to evaluate the effective potential shown in Sec. 5.5.1. We show $(\tilde{m}_\alpha^\beta)^2$ for each particle, which includes the thermal corrections if $\alpha$ is the gauge bosons or the scalar bosons. The field-dependent masses at zero-temperature $\tilde{m}_\alpha^2$ can be obtained by taking $T = 0$ in the formulae for $(\tilde{m}_\alpha^\beta)^2$. For the top quark, $(m_\alpha^\beta)^2$ and $\tilde{m}_\alpha^2$ is the same.

We define the classical field for the Higgs doublets as follows;

$$\Phi_1 = \frac{1}{\sqrt{2}} \begin{pmatrix} 0 \\ \varphi_1 \end{pmatrix}, \quad \Phi_2 = \frac{1}{\sqrt{2}} \begin{pmatrix} 0 \\ \varphi_2 + i\varphi_3 \end{pmatrix}. \tag{C.1}$$

In the following results, we assume the alignment in the Higgs potential; $\lambda_6 = \mu_3^2 = 0$. In addition, we consider the case that $\lambda_5$ is a real number by an appropriate rephasing of $\Phi_2$.

First, the field-dependent masses for $G^\pm$ and $H^\pm$ are given by the eigenvalues of a $2 \times 2$ hermitian matrix $\tilde{M}_\pm^2$. Each element of $\tilde{M}_\pm^2$ is given by

$$\begin{aligned}(\tilde{M}_\pm^2)_{G^+G^-} = \mu_1^2 + \frac{\lambda_1}{2}\varphi_1^2 + \frac{\lambda_3}{2}(\varphi_2^2 + \varphi_3^2) \\ + \frac{T^2}{24}\Big(6\lambda_1 + 4\lambda_3 + 2\lambda_4 + 2\rho_1 + \sigma_1 + 6y_t^2 + \frac{9g_L^2}{2} + \frac{3g_Y^2}{2}\Big),\end{aligned} \tag{C.2}$$

$$\begin{aligned}(\tilde{M}_\pm^2)_{G^+H^-} = (\tilde{M}_\pm^2)^*_{H^+G^-} = \frac{1}{2}(\lambda_4 + \lambda_5)\varphi_2 + \frac{i}{2}(\lambda_4 - \lambda_5)\varphi_3 + \frac{\lambda_7^*}{2}(\varphi_2^2 + \varphi_3^2) \\ + \frac{T^2}{24}\Big(6\lambda_7^* + 2\rho_{12} + \sigma_{12} + 6y_t^2\zeta_u^*\Big),\end{aligned} \tag{C.3}$$

$$\begin{aligned}(\tilde{M}_\pm^2)_{H^+H^-} = \mu_2^2 + \frac{\lambda_2}{2}(\varphi_2^2 + \varphi_3^2) + \frac{\lambda_3}{2}\varphi_1^2 + \mathrm{Re}[\lambda_7]\varphi_1\varphi_2 - \mathrm{Im}[\lambda_7]\varphi_1\varphi_3 \\ + \frac{T^2}{24}\Big(6\lambda_2 + 4\lambda_3 + 2\lambda_4 + 2\rho_2 + \sigma_2 + 6y_t^2|\zeta_u|^2 + \frac{9g_L^2}{2} + \frac{3g_Y^2}{2}\Big),\end{aligned} \tag{C.4}$$

where $y_t$ is defined as $y_t = \sqrt{2}m_t/v$.

Second, the field-dependent masses for the neutral scalar bosons $H_1$, $H_2$, $H_3$, and $G^0$ are given by the eigenvalues of a $4 \times 4$ real symmetric matrix $\tilde{M}_0^2$. Each element of $\tilde{M}_0^2$ is given by

$$(\tilde{M}_0^2)_{G^0G^0} = \mu_1^2 + \frac{\lambda_1}{2}\varphi_1^2 + \frac{1}{2}(\lambda_3 + \lambda_4 - \lambda_5)\varphi_2^2 + \frac{1}{2}(\lambda_3 + \lambda_4 + \lambda_5)\varphi_3^2 + \frac{T^2}{24}\Big(6\lambda_1 + 4\lambda_3 + 2\lambda_4 + 2\rho_1 + \sigma_1 + 6y_t^2 + \frac{9g_L^2}{2} + \frac{3g_Y^2}{2}\Big), \tag{C.5}$$

$$(\tilde{M}_0^2)_{H_1H_1} = \mu_1^2 + \frac{3}{2}\lambda_1\varphi_1^2 + \frac{1}{2}(\lambda_3 + \lambda_4 + \lambda_5)\varphi_2^2 + \frac{1}{2}(\lambda_3 + \lambda_4 - \lambda_5)\varphi_3^2 + \frac{T^2}{24}\Big(6\lambda_1 + 4\lambda_3 + 2\lambda_4 + 2\rho_1 + \sigma_1 + 6y_t^2 + \frac{9g_L^2}{2} + \frac{3g_Y^2}{2}\Big), \tag{C.6}$$

$$(\tilde{M}_0^2)_{H_2H_2} = \mu_2^2 + \frac{\lambda_2}{2}(3\varphi_2^2 + \varphi_3^2) + \frac{1}{2}(\lambda_3 + \lambda_4 + \lambda_5)\varphi_1^2 + 3\mathrm{Re}[\lambda_7]\varphi_1\varphi_2 - \mathrm{Im}[\lambda_7]\varphi_1\varphi_3 + \frac{T^2}{24}\Big(6\lambda_2 + 4\lambda_3 + 2\lambda_4 + 2\rho_2 + \sigma_2 + 6y_t^2|\zeta_u|^2 + \frac{9g_L^2}{2} + \frac{3g_Y^2}{2}\Big), \tag{C.7}$$

$$(\tilde{M}_0^2)_{H_3H_3} = \mu_2^2 + \frac{\lambda_2}{2}(3\varphi_2^2 + \varphi_3^2) + \frac{1}{2}(\lambda_3 + \lambda_4 - \lambda_5)\varphi_1^2 + \mathrm{Re}[\lambda_7]\varphi_1\varphi_2 - 3\mathrm{Im}[\lambda_7]\varphi_1\varphi_3 + \frac{T^2}{24}\Big(6\lambda_2 + 4\lambda_3 + 2\lambda_4 + 2\rho_2 + \sigma_2 + 6y_t^2|\zeta_u|^2 + \frac{9g_L^2}{2} + \frac{3g_Y^2}{2}\Big), \tag{C.8}$$

$$(\tilde{M}_0^2)_{G^0H_1} = (\tilde{M}_0^2)_{H_1G^0} = \lambda_5\varphi_2\varphi_3, \tag{C.9}$$

$$(\tilde{M}_0^2)_{G^0H_2} = (\tilde{M}_0^2)_{H_2G^0} = \lambda_5\varphi_1\varphi_3 + \mathrm{Re}[\lambda_7]\varphi_2\varphi_3 + \frac{1}{2}\mathrm{Im}[\lambda_7](3\varphi_2^2 + \varphi_3^2) + \frac{T^2}{24}\Big(6\mathrm{Im}[\lambda_7] + 2\mathrm{Im}[\rho_{12}] + \mathrm{Im}[\sigma_{12}] - 6y_t^2\mathrm{Im}[\zeta_u]\Big), \tag{C.10}$$

$$(\tilde{M}_0^2)_{G^0H_3} = (\tilde{M}_0^2)_{H_3G^0} = \lambda_5\varphi_1\varphi_2 + \frac{1}{2}\mathrm{Re}[\lambda_7](\varphi_2^2 + 3\varphi_3^2) + \mathrm{Im}[\lambda_7]\varphi_2\varphi_3 + \frac{T^2}{24}\Big(6\mathrm{Re}[\lambda_7] + 2\mathrm{Re}[\rho_{12}] + \mathrm{Re}[\sigma_{12}] + 6y_t^2\mathrm{Re}[\zeta_u]\Big), \tag{C.11}$$

$$(\tilde{M}_0^2)_{H_1H_2} = (\tilde{M}_0^2)_{H_2H_1} = (\lambda_3 + \lambda_4 + \lambda_5)\varphi_1\varphi_2 + \frac{1}{2}\mathrm{Re}[\lambda_7](3\varphi_2^2 + \varphi_3^2) - \mathrm{Im}[\lambda_7]\varphi_2\varphi_3 + \frac{T^2}{24}\Big(6\mathrm{Re}[\lambda_7] + 2\mathrm{Re}[\rho_{12}] + \mathrm{Re}[\sigma_{12}] + 6y_t^2\mathrm{Re}[\zeta_u]\Big), \tag{C.12}$$

$$(\tilde{M}_0^2)_{H_1H_3} = (\tilde{M}_0^2)_{H_3H_1} = (\lambda_3 + \lambda_4 - \lambda_5)\varphi_1\varphi_3 - \frac{1}{2}\mathrm{Im}[\lambda_7](\varphi_2^2 + 3\varphi_3^2) + \mathrm{Re}[\lambda_7]\varphi_2\varphi_3 + \frac{T^2}{24}\Big(-6\mathrm{Im}[\lambda_7] - 2\mathrm{Im}[\rho_{12}] - \mathrm{Im}[\sigma_{12}] + 6y_t^2\mathrm{Im}[\zeta_u]\Big), \tag{C.13}$$

$$(\tilde{M}_0^2)_{H_2H_3} = (\tilde{M}_0^2)_{H_3H_2} = \lambda_2\varphi_2\varphi_3 + \mathrm{Re}[\lambda_7]\varphi_1\varphi_3 - \mathrm{Im}[\lambda_7]\varphi_1\varphi_2. \tag{C.14}$$

Third, the field-dependent masses for the $Z_2$-odd scalar bosons $S^{\pm}$ and $\eta$ are given by

$$(\tilde{m}_S^{\beta})^2 = \mu_S^2 + \frac{\rho_1}{2}\varphi_1^2 + \frac{\rho_2}{2}(\varphi_2^2+\varphi_3^2) + \mathrm{Re}[\rho_{12}]\varphi_1\varphi_2 - \mathrm{Im}[\rho_{12}]\varphi_1\varphi_3 + \frac{T^2}{6}(\rho_1+\rho_2+6g_Y^2), \tag{C.15}$$

$$(\tilde{m}_\eta^{\beta})^2 = \mu_\eta^2 + \frac{\sigma_1}{2}\varphi_1^2 + \frac{\sigma_2}{2}(\varphi_2^2+\varphi_3^2) + \mathrm{Re}[\sigma_{12}]\varphi_1\varphi_2 - \mathrm{Im}[\sigma_{12}]\varphi_1\varphi_3 + \frac{T^2}{6}(\sigma_1+\sigma_2). \tag{C.16}$$

Fourth, we consider the field-dependent masses for the gauge bosons. The field-dependent masses for the gauge bosons $W_\mu^a$ $(a = 1,2,3)$ and $B_\mu$ are given by a $2\times 2$ real symmetric matrix $(\tilde{M}_V^2)$ whose elements are defined as follows;

$$(\tilde{M}_V^2)_{W_\mu^a W_\nu^b} = \Big(\frac{g_L^2}{4}\varphi^2 + 2g_L^2T^2\delta_{\mu,||}\Big)\delta_{a,b}\delta_{\mu,\nu}, \tag{C.17}$$

$$(\tilde{M}_V^2)_{W_\mu^3 B_\nu} = \frac{1}{4}g_L g_Y\varphi^2\delta_{\mu,\nu}, \tag{C.18}$$

$$(\tilde{M}_V^2)_{B_\mu B_\nu} = \Big(\frac{g_Y^2}{4}\varphi^2 + \frac{8}{3}g_Y^2T^2\delta_{\mu,||}\Big)\delta_{\mu,\nu}, \tag{C.19}$$

where $\varphi^2$ is the total VEV; $\varphi^2 = \varphi_1^2+\varphi_2^2+\varphi_3^2$. The symbol $\delta_{\mu,||}$ means that only the longitudinal components of the gauge bosons receive the thermal corrections at this order [259].

Finally, we consider the field-dependent masses of the top quark. We do not consider the thermal resummation for the top quark since thermal fermion loops do not have the infrared problems caused by zero modes of Matsubara frequency [132]. Then, the field-dependent masses of the top quark is given by

$$\begin{aligned}(\tilde{m}_t^{\beta})^2 = \tilde{m}_t^2 = \frac{m_t^2}{v^2}\Big\{&\big(\varphi_1+\varphi_2|\zeta_u|\cos\theta_u - \varphi_3|\zeta_u|\sin\theta_u\big)^2\\ &+\big(\varphi_2|\zeta_u|\sin\theta_u+\varphi_3|\zeta_u|\cos\theta_u\big)^2\Big\}.\end{aligned} \tag{C.20}$$

# Appendix D

# Formulae for the $\mathcal{J}$ functions in the transport equation

In this appendix, we show the details of the derivation of the integral expressions for the $\mathcal{J}$ functions shown in Eq. (5.5.18). First, we consider the normalization factor $N_0$, which is the denominator of the right-hand side of Eq. (3.1.69);

$$N_0 \equiv \int \mathrm{d}^3p\, f'_{0+}(m=0) = -\beta \int \mathrm{d}^3p\, \frac{e^{\beta|\boldsymbol{p}|}}{(e^{\beta|\boldsymbol{p}|}+1)^2}. \tag{D.1}$$

By using polar coordinate and changing the integral variable to the dimensionless variable $x = \beta|\boldsymbol{p}|$, it is calculated as

$$N_0 = -4\pi\beta^{-2} \int_0^\infty \mathrm{d}x\, \frac{x^2 e^x}{(e^x+1)^2} = -\frac{2\pi^3}{3}\beta^{-2}. \tag{D.2}$$

Next, we consider the function $\mathcal{J}_{i0}$;

$$\mathcal{J}_{i0} = -\frac{\beta}{N_{i0}} \int \mathrm{d}^3p\, \frac{1}{e^{\beta\sqrt{\boldsymbol{p}^2+m_i^2}}+1} = \frac{6\beta^3}{\pi^2} \int_0^\infty \mathrm{d}p\, \frac{p^2}{e^{\beta\sqrt{p^2+m_i^2}}+1}. \tag{D.3}$$

By using the integral variable $x = \beta|\boldsymbol{p}|$, we obtain the following integral representation for $\mathcal{J}_{i0}$;

$$\mathcal{J}_{i0} = \frac{6}{\pi^2} \int_0^\infty \mathrm{d}x\, \frac{x^2}{e^{\epsilon_i}+1}, \tag{D.4}$$

where $\epsilon_i \equiv \sqrt{x^2+a_i}$ and $a_i = \beta^2 m_i^2$. This is the formula in Eq. (5.5.16). The formulae for $\mathcal{J}_{i1}$-$\mathcal{J}_{i4}$ can be obtain in the same way.

To derive the formulae for $\mathcal{J}_{i5}$ and $\mathcal{J}_{i6}$, a little more complicated calculation is needed. Here, we show only the calculation of $\mathcal{J}_{i5}$, and $\mathcal{J}_{i6}$ can be obtained in the same way. The function $\mathcal{J}_{i5}$ is defined as

$$\mathcal{J}_{i5} = \frac{\beta^{-2}}{N_0} \int \mathrm{d}^3p\, \frac{|p_{iz}|f'_{i0}}{2E_{i0}^2 E_{i0z}} = -\frac{3}{4\pi^3} \int \mathrm{d}^3p\, \frac{|p_{iz}|f'_{i0}}{(\boldsymbol{p}_i^2+m_i^2)\sqrt{p_{iz}^2+m_i^2}}. \tag{D.5}$$

For the massless particle ($m_i^2 = 0$), this integral is easily calculated;

$$\mathcal{J}_{i5}(m_i^2=0) = \frac{3}{4\pi^2} \int \frac{\mathrm{d}^3p}{\boldsymbol{p}_i^2} \frac{\beta e^{|\boldsymbol{p}_i|}}{(e^{|\boldsymbol{p}_i|}+1)^2} = \frac{3}{\pi^2} \int_0^\infty \mathrm{d}x \frac{e^x}{(e^x+1)^2} = \frac{3}{2\pi^2}. \tag{D.6}$$

Therefore, in the following, we consider the case that $\sqrt{a_i} \neq 0$.

We define dimensionless integral variables $(x_1, x_2, x_3) = (p_{ix}, p_{iy}, p_{iz})$. By using the two dimensional polar coordinate $x_1 = r\cos\theta$ and $x_2 = r\sin\theta$, $\mathcal{J}_{i5}$ is represented by

$$\mathcal{J}_{i5} = -\frac{3}{2\pi^2}\int_0^\infty \mathrm{d}r \int_{-\infty}^\infty \mathrm{d}x_3 \frac{r|x_3|}{(r^2 + x_3^2 + a_i)\sqrt{x_3^2 + a_i}} \frac{\partial f_{i0}}{\partial \epsilon_i}. \tag{D.7}$$

By changing the integral variable $r$ to $\epsilon_i = \sqrt{r^2 + x_3^2 + a_i}$, $\mathcal{J}_{i5}$ is calculated as follows;

$$\begin{aligned}
\mathcal{J}_{i5} =& -\frac{3}{2\pi^2}\int_{-\infty}^\infty \mathrm{d}x_3 \ \frac{|x_3|}{\sqrt{x_3^2 + a_i}} \int_{\epsilon_{iz}}^\infty \frac{\mathrm{d}\epsilon_i}{\epsilon_i}\frac{\partial f_{i0}}{\partial \epsilon_i} \\
=& -\frac{3}{\pi^2}\int_0^\infty \mathrm{d}x_3 \ \frac{\partial \epsilon_{iz}}{\partial x_3} \int_{\epsilon_{iz}}^\infty \frac{\mathrm{d}\epsilon_i}{\epsilon_i}\frac{\partial f_{i0}}{\partial \epsilon_i} \\
=& -\frac{3}{\pi^2}\left\{\left[\epsilon_{iz}\int_{\epsilon_{iz}}^\infty \frac{\mathrm{d}\epsilon_i}{\epsilon_i}\frac{\partial f_{i0}}{\partial \epsilon_i}\right]_{x_3=0}^{x_3=\infty} + \int_0^\infty \mathrm{d}x_3 \ \frac{x_3}{\epsilon_{iz}} \ \frac{\partial f_{i0}}{\partial \epsilon_i}\bigg|_{\epsilon_i=\epsilon_{iz}}\right\} \\
=& -\frac{3}{\pi^2}\left\{-\sqrt{a_i}\int_{\sqrt{a_i}}^\infty \frac{\mathrm{d}\epsilon_i}{\epsilon_i}\frac{\partial f_{i0}}{\partial \epsilon_i} + \int_{\sqrt{a_i}}^\infty \mathrm{d}\epsilon_i \ \frac{\partial f_{i0}}{\partial \epsilon_i}\right\} \\
=& \ \frac{3}{\pi^2}\int_{\sqrt{a_i}}^\infty \mathrm{d}x \frac{e^x}{(e^x+1)^2}\Big(1 - \frac{\sqrt{a_i}}{x}\Big),
\end{aligned} \tag{D.8}$$

where $\epsilon_{iz} = \sqrt{x_3^2 + a_i}$. In the transformation from the second line to the third line, the partial integration for $x_3$ is used. This is the formula in Eq. (5.5.16). In the limit that $a_i \to 0$, this formula reproduce the result for massless particle in Eq. (D.7).

# Bibliography


[1] P. A. Zyla *et al.* [Particle Data Group], "Review of Particle Physics," PTEP **2020**, no.8, 083C01 (2020).

[2] B. D. Fields, K. A. Olive, T. H. Yeh and C. Young, JCAP **03**, 010 (2020) [erratum: JCAP **11**, E02 (2020)] [arXiv:1912.01132 [astro-ph.CO]].

[3] N. Aghanim *et al.* [Planck], "Planck 2018 results. VI. Cosmological parameters," Astron. Astrophys. **641**, A6 (2020) [erratum: Astron. Astrophys. **652**, C4 (2021)] [arXiv:1807.06209 [astro-ph.CO]].

[4] Y. Fukuda *et al.* [Super-Kamiokande], "Evidence for oscillation of atmospheric neutrinos," Phys. Rev. Lett. **81**, 1562-1567 (1998) [arXiv:hep-ex/9807003 [hep-ex]].

[5] Q. R. Ahmad *et al.* [SNO], "Measurement of the rate of $\nu_e + d \to p + p + e^-$ interactions produced by $^8$B solar neutrinos at the Sudbury Neutrino Observatory," Phys. Rev. Lett. **87**, 071301 (2001) [arXiv:nucl-ex/0106015 [nucl-ex]].

[6] Q. R. Ahmad *et al.* [SNO], "Direct evidence for neutrino flavor transformation from neutral current interactions in the Sudbury Neutrino Observatory," Phys. Rev. Lett. **89**, 011301 (2002) [arXiv:nucl-ex/0204008 [nucl-ex]].

[7] K. Abe *et al.* [T2K], "Improved constraints on neutrino mixing from the T2K experiment with $\mathbf{3.13 \times 10^{21}}$ protons on target," Phys. Rev. D **103**, no.11, 112008 (2021) [arXiv:2101.03779 [hep-ex]].

[8] M. A. Acero *et al.* [NOvA], "An Improved Measurement of Neutrino Oscillation Parameters by the NOvA Experiment," [arXiv:2108.08219 [hep-ex]].

[9] D. Adey *et al.* [Daya Bay], "Measurement of the Electron Antineutrino Oscillation with 1958 Days of Operation at Daya Bay," Phys. Rev. Lett. **121**, no.24, 241805 (2018) [arXiv:1809.02261 [hep-ex]].

[10] B. Aharmim *et al.* [SNO], Phys. Rev. C **88**, 025501 (2013) doi:10.1103/PhysRevC.88.025501 [arXiv:1109.0763 [nucl-ex]].

[11] S. Weinberg, "A Model of Leptons," Phys. Rev. Lett. **19**, 1264-1266 (1967)

[12] A. Salam, "Weak and Electromagnetic Interactions," Conf. Proc. C **680519**, 367-377 (1968)

[13] G. Aad *et al.* [ATLAS], "Observation of a new particle in the search for the Standard Model Higgs boson with the ATLAS detector at the LHC," Phys. Lett. B **716**, 1-29 (2012) [arXiv:1207.7214 [hep-ex]].

[14] S. Chatrchyan *et al.* [CMS], "Observation of a New Boson at a Mass of 125 GeV with the CMS Experiment at the LHC," Phys. Lett. B **716**, 30-61 (2012) [arXiv:1207.7235 [hep-ex]].

[15] A. H. Guth, "The Inflationary Universe: A Possible Solution to the Horizon and Flatness Problems," Phys. Rev. D **23**, 347-356 (1981)

[16] K. Sato, "First Order Phase Transition of a Vacuum and Expansion of the Universe," Mon. Not. Roy. Astron. Soc. **195**, 467-479 (1981) NORDITA-80-29.

[17] A. D. Sakharov, "Violation of CP Invariance, C asymmetry, and baryon asymmetry of the universe," Pisma Zh. Eksp. Teor. Fiz. **5**, 32-35 (1967)

[18] M. Yoshimura, "Unified Gauge Theories and the Baryon Number of the Universe," Phys. Rev. Lett. **41**, 281-284 (1978) [erratum: Phys. Rev. Lett. **42**, 746 (1979)]

[19] S. Weinberg, "Cosmological Production of Baryons," Phys. Rev. Lett. **42**, 850-853 (1979)

[20] I. Affleck and M. Dine, "A New Mechanism for Baryogenesis," Nucl. Phys. B **249**, 361-380 (1985)

[21] V. A. Kuzmin, V. A. Rubakov and M. E. Shaposhnikov, "On the Anomalous Electroweak Baryon Number Nonconservation in the Early Universe," Phys. Lett. B **155**, 36 (1985)

[22] M. Fukugita and T. Yanagida, "Baryogenesis Without Grand Unification," Phys. Lett. B **174**, 45-47 (1986)

[23] F. R. Klinkhamer and N. S. Manton, "A Saddle Point Solution in the Weinberg-Salam Theory," Phys. Rev. D **30**, 2212 (1984)

[24] M. B. Gavela, P. Hernandez, J. Orloff and O. Pene, "Standard model CP violation and baryon asymmetry," Mod. Phys. Lett. A **9**, 795-810 (1994) [arXiv:hep-ph/9312215 [hep-ph]]; M. B. Gavela, M. Lozano, J. Orloff and O. Pene, Nucl. Phys. B **430**, 345-381 (1994) [arXiv:hep-ph/9406288 [hep-ph]]; M. B. Gavela, P. Hernandez, J. Orloff, O. Pene and C. Quimbay, "Standard model CP violation and baryon asymmetry. Part 2: Finite temperature," *ibid* **430**, 382-426 (1994) [arXiv:hep-ph/9406289 [hep-ph]].

[25] P. Huet and E. Sather, "Electroweak baryogenesis and standard model CP violation," Phys. Rev. D **51**, 379-394 (1995) [arXiv:hep-ph/9404302 [hep-ph]].

[26] M. E. Shaposhnikov, "Baryon Asymmetry of the Universe in Standard Electroweak Theory," Nucl. Phys. B **287**, 757-775 (1987)

[27] A. I. Bochkarev and M. E. Shaposhnikov, "Electroweak Production of Baryon Asymmetry and Upper Bounds on the Higgs and Top Masses," Mod. Phys. Lett. A **2**, 417 (1987)

[28] K. Kajantie, M. Laine, K. Rummukainen and M. E. Shaposhnikov, "Is there a hot electroweak phase transition at $m_H \gtrsim m_W$?," Phys. Rev. Lett. **77**, 2887-2890 (1996) [arXiv:hep-ph/9605288 [hep-ph]];

[29] M. D'Onofrio and K. Rummukainen, "Standard model cross-over on the lattice," Phys. Rev. D **93**, no.2, 025003 (2016) [arXiv:1508.07161 [hep-ph]].

[30] G. W. Anderson and L. J. Hall, "The Electroweak phase transition and baryogenesis," Phys. Rev. D **45**, 2685-2698 (1992)

[31] J. R. Espinosa and M. Quiros, "The Electroweak phase transition with a singlet," Phys. Lett. B **305**, 98-105 (1993) [arXiv:hep-ph/9301285 [hep-ph]].

[32] J. Choi and R. R. Volkas, "Real Higgs singlet and the electroweak phase transition in the Standard Model," Phys. Lett. B **317**, 385-391 (1993) [arXiv:hep-ph/9308234 [hep-ph]].

[33] S. W. Ham, Y. S. Jeong and S. K. Oh, "Electroweak phase transition in an extension of the standard model with a real Higgs singlet," J. Phys. G **31**, no.8, 857-871 (2005) [arXiv:hep-ph/0411352 [hep-ph]].

[34] S. J. Huber, T. Konstandin, T. Prokopec and M. G. Schmidt, "Electroweak Phase Transition and Baryogenesis in the nMSSM," Nucl. Phys. B **757**, 172-196 (2006) [arXiv:hep-ph/0606298 [hep-ph]].

[35] A. Ahriche, "What is the criterion for a strong first order electroweak phase transition in singlet models?," Phys. Rev. D **75**, 083522 (2007) [arXiv:hep-ph/0701192 [hep-ph]].

[36] J. M. Cline, G. Laporte, H. Yamashita and S. Kraml, "Electroweak Phase Transition and LHC Signatures in the Singlet Majoron Model," JHEP **07**, 040 (2009) [arXiv:0905.2559 [hep-ph]].

[37] J. R. Espinosa, T. Konstandin and F. Riva, "Strong Electroweak Phase Transitions in the Standard Model with a Singlet," Nucl. Phys. B **854**, 592-630 (2012) [arXiv:1107.5441 [hep-ph]].

[38] J. R. Espinosa, B. Gripaios, T. Konstandin and F. Riva, "Electroweak Baryogenesis in Non-minimal Composite Higgs Models," JCAP **01**, 012 (2012) [arXiv:1110.2876 [hep-ph]].

[39] J. McDonald, "Electroweak baryogenesis and dark matter via a gauge singlet scalar," Phys. Lett. B **323**, 339-346 (1994)

[40] S. Profumo, M. J. Ramsey-Musolf and G. Shaughnessy, "Singlet Higgs phenomenology and the electroweak phase transition," JHEP **08**, 010 (2007) [arXiv:0705.2425 [hep-ph]].

[41] V. Barger, P. Langacker, M. McCaskey, M. Ramsey-Musolf and G. Shaughnessy, "Complex Singlet Extension of the Standard Model," Phys. Rev. D **79**, 015018 (2009) [arXiv:0811.0393 [hep-ph]].

[42] J. M. Cline and K. Kainulainen, "Electroweak baryogenesis and dark matter from a singlet Higgs," JCAP **01**, 012 (2013) [arXiv:1210.4196 [hep-ph]].

[43] N. Turok and J. Zadrozny, "Electroweak baryogenesis in the two doublet model," Nucl. Phys. B **358**, 471-493 (1991)

[44] J. M. Cline, K. Kainulainen and A. P. Vischer, "Dynamics of two Higgs doublet CP violation and baryogenesis at the electroweak phase transition," Phys. Rev. D **54**, 2451-2472 (1996) [arXiv:hep-ph/9506284 [hep-ph]].

[45] L. Fromme, S. J. Huber and M. Seniuch, "Baryogenesis in the two-Higgs doublet model," JHEP **11**, 038 (2006) [arXiv:hep-ph/0605242 [hep-ph]].

[46] J. M. Cline, K. Kainulainen and M. Trott, "Electroweak Baryogenesis in Two Higgs Doublet Models and B meson anomalies," JHEP **11**, 089 (2011) [arXiv:1107.3559 [hep-ph]].

[47] S. Tulin and P. Winslow, Phys. Rev. D **84**, 034013 (2011) doi:10.1103/PhysRevD.84.034013 [arXiv:1105.2848 [hep-ph]].

[48] T. Liu, M. J. Ramsey-Musolf and J. Shu, "Electroweak Beautygenesis: From b \to s CP-violation to the Cosmic Baryon Asymmetry," Phys. Rev. Lett. **108**, 221301 (2012) [arXiv:1109.4145 [hep-ph]].

[49] M. Ahmadvand, "Baryogenesis within the two-Higgs-doublet model in the Electroweak scale," Int. J. Mod. Phys. A **29**, no.20, 1450090 (2014) [arXiv:1308.3767 [hep-ph]].

[50] C. W. Chiang, K. Fuyuto and E. Senaha, "Electroweak Baryogenesis with Lepton Flavor Violation," Phys. Lett. B **762**, 315-320 (2016) [arXiv:1607.07316 [hep-ph]].

[51] H. K. Guo, Y. Y. Li, T. Liu, M. Ramsey-Musolf and J. Shu, "Lepton-Flavored Electroweak Baryogenesis," Phys. Rev. D **96**, no.11, 115034 (2017) [arXiv:1609.09849 [hep-ph]].

[52] K. Fuyuto, W. S. Hou and E. Senaha, "Electroweak baryogenesis driven by extra top Yukawa couplings," Phys. Lett. B **776**, 402-406 (2018) [arXiv:1705.05034 [hep-ph]]; "Cancellation mechanism for the electron electric dipole moment connected with the baryon asymmetry of the Universe," Phys. Rev. D **101**, no.1, 011901 (2020) [arXiv:1910.12404 [hep-ph]].

[53] T. Modak and E. Senaha, "Electroweak baryogenesis via bottom transport," Phys. Rev. D **99**, no.11, 115022 (2019) [arXiv:1811.08088 [hep-ph]]; "Probing Electroweak Baryogenesis induced by extra bottom Yukawa coupling via EDMs and collider signatures," JHEP **11**, 025 (2020) [arXiv:2005.09928 [hep-ph]]; "Electroweak baryogenesis via bottom transport: Complementarity between LHC and future lepton collider probes," Phys. Lett. B **822**, 136695 (2021) [arXiv:2107.12789 [hep-ph]].

[54] P. Basler, M. Mühlleitner and J. Müller, "Electroweak Baryogenesis in the CP-Violating Two-Higgs Doublet Model," [arXiv:2108.03580 [hep-ph]].

[55] K. Enomoto, S. Kanemura and Y. Mura, "Electroweak baryogenesis in aligned two Higgs doublet models," JHEP **01**, 104 (2022) [arXiv:2111.13079 [hep-ph]].

[56] T. A. Chowdhury, M. Nemevsek, G. Senjanovic and Y. Zhang, "Dark Matter as the Trigger of Strong Electroweak Phase Transition," JCAP **02**, 029 (2012) [arXiv:1110.5334 [hep-ph]].

[57] D. Borah and J. M. Cline, "Inert Doublet Dark Matter with Strong Electroweak Phase Transition," Phys. Rev. D **86**, 055001 (2012) [arXiv:1204.4722 [hep-ph]].

[58] G. Gil, P. Chankowski and M. Krawczyk, "Inert Dark Matter and Strong Electroweak Phase Transition," Phys. Lett. B **717**, 396-402 (2012) [arXiv:1207.0084 [hep-ph]].

[59] H. H. Patel and M. J. Ramsey-Musolf, "Stepping Into Electroweak Symmetry Breaking: Phase Transitions and Higgs Phenomenology," Phys. Rev. D **88**, 035013 (2013) [arXiv:1212.5652 [hep-ph]].

[60] C. W. Chiang and T. Yamada, "Electroweak phase transition in Georgi–Machacek model," Phys. Lett. B **735**, 295-300 (2014) [arXiv:1404.5182 [hep-ph]].

[61] P. Minkowski, "$\mu \to e\gamma$ at a Rate of One Out of $10^9$ Muon Decays?," Phys. Lett. B **67**, 421-428 (1977); T. Yanagida, "Horizontal gauge symmetry and masses of neutrinos," Conf. Proc. C **7902131**, 95-99 (1979); "Horizontal Symmetry and Masses of Neutrinos," Prog. Theor. Phys. **64**, 1103 (1980); M. Gell-Mann, P. Ramond and R. Slansky, "Complex Spinors and Unified Theories," Conf. Proc. C **790927**, 315-321 (1979) [arXiv:1306.4669 [hep-th]];

[62] R. N. Mohapatra and G. Senjanovic, "Neutrino Mass and Spontaneous Parity Nonconservation," Phys. Rev. Lett. **44**, 912 (1980). J. Schechter and J. W. F. Valle, "Neutrino Masses in SU(2) x U(1) Theories," Phys. Rev. D **22**, 2227 (1980)

[63] W. Konetschny and W. Kummer, "Nonconservation of Total Lepton Number with Scalar Bosons," Phys. Lett. B **70**, 433-435 (1977); M. Magg and C. Wetterich, Phys. Lett. B **94**, 61-64 (1980); G. Lazarides, Q. Shafi and C. Wetterich, Nucl. Phys. B **181**, 287-300 (1981).

[64] R. Foot, H. Lew, X. G. He and G. C. Joshi, "Seesaw Neutrino Masses Induced by a Triplet of Leptons," Z. Phys. C **44**, 441 (1989)

[65] A. G. Akeroyd and M. Aoki, "Single and pair production of doubly charged Higgs bosons at hadron colliders," Phys. Rev. D **72**, 035011 (2005) [arXiv:hep-ph/0506176 [hep-ph]].

[66] A. G. Akeroyd, M. Aoki and H. Sugiyama, "Lepton Flavour Violating Decays tau $\rightarrow$ anti-l ll and mu $\rightarrow$ e gamma in the Higgs Triplet Model," Phys. Rev. D **79**, 113010 (2009) [arXiv:0904.3640 [hep-ph]].

[67] A. G. Akeroyd and H. Sugiyama, "Production of doubly charged scalars from the decay of singly charged scalars in the Higgs Triplet Model," Phys. Rev. D **84**, 035010 (2011) [arXiv:1105.2209 [hep-ph]].

[68] M. Aoki, S. Kanemura and K. Yagyu, "Testing the Higgs triplet model with the mass difference at the LHC," Phys. Rev. D **85**, 055007 (2012) [arXiv:1110.4625 [hep-ph]].

[69] A. Zee, "A Theory of Lepton Number Violation, Neutrino Majorana Mass, and Oscillation," Phys. Lett. B **93**, 389 (1980) [erratum: Phys. Lett. B **95**, 461 (1980)]

[70] T. P. Cheng and L. F. Li, "Neutrino Masses, Mixings and Oscillations in SU(2) x U(1) Models of Electroweak Interactions," Phys. Rev. D **22**, 2860 (1980)

[71] A. Zee, "Quantum Numbers of Majorana Neutrino Masses," Nucl. Phys. B **264**, 99-110 (1986)

[72] K. S. Babu, "Model of 'Calculable' Majorana Neutrino Masses," Phys. Lett. B **203**, 132-136 (1988)

[73] E. Ma, "Verifiable radiative seesaw mechanism of neutrino mass and dark matter," Phys. Rev. D **73**, 077301 (2006) [arXiv:hep-ph/0601225 [hep-ph]].

[74] L. M. Krauss, S. Nasri and M. Trodden, "A Model for neutrino masses and dark matter," Phys. Rev. D **67**, 085002 (2003) [arXiv:hep-ph/0210389 [hep-ph]].

[75] M. Aoki, S. Kanemura and O. Seto, "Neutrino mass, Dark Matter and Baryon Asymmetry via TeV-Scale Physics without Fine-Tuning," Phys. Rev. Lett. **102**, 051805 (2009) [arXiv:0807.0361 [hep-ph]]; "A Model of TeV Scale Physics for Neutrino Mass, Dark Matter and Baryon Asymmetry and its Phenomenology," Phys. Rev. D **80**, 033007 (2009) [arXiv:0904.3829 [hep-ph]].

[76] M. Gustafsson, J. M. No and M. A. Rivera, "Predictive Model for Radiatively Induced Neutrino Masses and Mixings with Dark Matter," Phys. Rev. Lett. **110**, no.21, 211802 (2013) [erratum: Phys. Rev. Lett. **112**, no.25, 259902 (2014)] [arXiv:1212.4806 [hep-ph]]; "Radiative neutrino mass generation linked to neutrino mixing and $0\nu\beta\beta$-decay predictions," Phys. Rev. D **90**, no.1, 013012 (2014) [arXiv:1402.0515 [hep-ph]];

[77] S. M. Davidson and H. E. Logan, "Dirac neutrinos from a second Higgs doublet," Phys. Rev. D **80**, 095008 (2009) [arXiv:0906.3335 [hep-ph]].

[78] S. Nasri and S. Moussa, "Model for small neutrino masses at the TeV scale," Mod. Phys. Lett. A **17**, 771-778 (2002) [arXiv:hep-ph/0106107 [hep-ph]]; S. Kanemura, T. Nabeshima and H. Sugiyama, Phys. Lett. B **703**, 66-70 (2011) [arXiv:1106.2480 [hep-ph]].

[79] P. H. Gu and U. Sarkar, "Radiative Neutrino Mass, Dark Matter and Leptogenesis," Phys. Rev. D **77**, 105031 (2008) [arXiv:0712.2933 [hep-ph]].

[80] S. Kanemura, K. Sakurai and H. Sugiyama, "Probing Models of Dirac Neutrino Masses via the Flavor Structure of the Mass Matrix," Phys. Lett. B **758**, 465-472 (2016) [arXiv:1603.08679 [hep-ph]].

[81] S. Kanemura, K. Sakurai and H. Sugiyama, "Neutrino mass without lepton number violation, dark matter; and a strongly first-order phase transition," Phys. Rev. D **96**, no.9, 095024 (2017) [arXiv:1705.07040 [hep-ph]].

[82] K. Enomoto, S. Kanemura, K. Sakurai and H. Sugiyama, "New model for radiatively generated Dirac neutrino masses and lepton flavor violating decays of the Higgs boson," Phys. Rev. D **100**, no.1, 015044 (2019) [arXiv:1904.07039 [hep-ph]].

[83] V. Silveira and A. Zee, "SCALAR PHANTOMS," Phys. Lett. B **161**, 136-140 (1985)

[84] J. McDonald, "Gauge singlet scalars as cold dark matter," Phys. Rev. D **50**, 3637-3649 (1994) [arXiv:hep-ph/0702143 [hep-ph]].

[85] C. P. Burgess, M. Pospelov and T. ter Veldhuis, "The Minimal model of nonbaryonic dark matter: A Singlet scalar," Nucl. Phys. B **619**, 709-728 (2001) [arXiv:hep-ph/0011335 [hep-ph]].

[86] R. N. Lerner and J. McDonald, "Gauge singlet scalar as inflaton and thermal relic dark matter," Phys. Rev. D **80**, 123507 (2009) [arXiv:0909.0520 [hep-ph]].

[87] S. Kanemura, S. Matsumoto, T. Nabeshima and N. Okada, "Can WIMP Dark Matter overcome the Nightmare Scenario?," Phys. Rev. D **82**, 055026 (2010) [arXiv:1005.5651 [hep-ph]].

[88] J. M. Cline, K. Kainulainen, P. Scott and C. Weniger, "Update on scalar singlet dark matter," Phys. Rev. D **88**, 055025 (2013) [erratum: Phys. Rev. D **92**, no.3, 039906 (2015)] [arXiv:1306.4710 [hep-ph]].

[89] P. Athron *et al.* [GAMBIT], "Status of the scalar singlet dark matter model," Eur. Phys. J. C **77**, no.8, 568 (2017) [arXiv:1705.07931 [hep-ph]].

[90] N. G. Deshpande and E. Ma, "Pattern of Symmetry Breaking with Two Higgs Doublets," Phys. Rev. D **18**, 2574 (1978)

[91] R. Barbieri, L. J. Hall and V. S. Rychkov, "Improved naturalness with a heavy Higgs: An Alternative road to LHC physics," Phys. Rev. D **74**, 015007 (2006) [arXiv:hep-ph/0603188 [hep-ph]].

[92] L. Lopez Honorez, E. Nezri, J. F. Oliver and M. H. G. Tytgat, "The Inert Doublet Model: An Archetype for Dark Matter," JCAP **02**, 028 (2007) [arXiv:hep-ph/0612275 [hep-ph]].

[93] A. Goudelis, B. Herrmann and O. Stål, "Dark matter in the Inert Doublet Model after the discovery of a Higgs-like boson at the LHC," JHEP **09**, 106 (2013) [arXiv:1303.3010 [hep-ph]].

[94] S. Kanemura, M. Kikuchi and K. Sakurai, "Testing the dark matter scenario in the inert doublet model by future precision measurements of the Higgs boson couplings," Phys. Rev. D **94**, no.11, 115011 (2016) [arXiv:1605.08520 [hep-ph]].

[95] M. Cirelli, N. Fornengo and A. Strumia, "Minimal dark matter," Nucl. Phys. B **753**, 178-194 (2006) [arXiv:hep-ph/0512090 [hep-ph]].

[96] M. Cirelli, A. Strumia and M. Tamburini, "Cosmology and Astrophysics of Minimal Dark Matter," Nucl. Phys. B **787**, 152-175 (2007) [arXiv:0706.4071 [hep-ph]].

[97] P. Fileviez Perez, H. H. Patel, M. J. Ramsey-Musolf and K. Wang, "Triplet Scalars and Dark Matter at the LHC," Phys. Rev. D **79**, 055024 (2009) [arXiv:0811.3957 [hep-ph]].

[98] A. Pich and P. Tuzon, "Yukawa Alignment in the Two-Higgs-Doublet Model," Phys. Rev. D **80**, 091702 (2009) [arXiv:0908.1554 [hep-ph]].

[99] A. M. Sirunyan *et al.* [CMS], "Combined measurements of Higgs boson couplings in proton–proton collisions at $\sqrt{s} = 13\,\mathrm{TeV}$," Eur. Phys. J. C **79**, no.5, 421 (2019) [arXiv:1809.10733 [hep-ex]].

[100] G. Aad *et al.* [ATLAS], "Combined measurements of Higgs boson production and decay using up to 80 $\mathrm{fb}^{-1}$ of proton-proton collision data at $\sqrt{s} = 13$ TeV collected with the ATLAS experiment," Phys. Rev. D **101**, no.1, 012002 (2020) [arXiv:1909.02845 [hep-ex]].

[101] S. Kanemura, M. Kubota and K. Yagyu, "Aligned CP-violating Higgs sector canceling the electric dipole moment," JHEP **08**, 026 (2020) [arXiv:2004.03943 [hep-ph]].

[102] M. Aiko, S. Kanemura, M. Kikuchi, K. Mawatari, K. Sakurai and K. Yagyu, "Probing extended Higgs sectors by the synergy between direct searches at the LHC and precision tests at future lepton colliders," Nucl. Phys. B **966**, 115375 (2021) [arXiv:2010.15057 [hep-ph]].

[103] S. Kanemura, M. Takeuchi and K. Yagyu, "Probing double-aligned two Higgs doublet models at LHC," [arXiv:2112.13679 [hep-ph]].

[104] S. Kanemura, M. Kubota and K. Yagyu, "Testing aligned CP-violating Higgs sector at future lepton colliders," JHEP **04**, 144 (2021) [arXiv:2101.03702 [hep-ph]].

[105] M. Joyce, T. Prokopec and N. Turok, "Electroweak baryogenesis from a classical force," Phys. Rev. Lett. **75**, 1695-1698 (1995) [erratum: Phys. Rev. Lett. **75**, 3375 (1995)] [arXiv:hep-ph/9408339 [hep-ph]].

[106] M. Joyce, T. Prokopec and N. Turok, "Nonlocal electroweak baryogenesis. Part 1: Thin wall regime," Phys. Rev. D **53**, 2930-2957 (1996) [arXiv:hep-ph/9410281 [hep-ph]]; "Nonlocal electroweak baryogenesis. Part 2: The Classical regime," Phys. Rev. D **53**, 2958-2980 (1996) [arXiv:hep-ph/9410282 [hep-ph]].

[107] J. M. Cline, M. Joyce and K. Kainulainen, "Supersymmetric electroweak baryogenesis," JHEP **07**, 018 (2000) [arXiv:hep-ph/0006119 [hep-ph]].

[108] L. Fromme and S. J. Huber, "Top transport in electroweak baryogenesis," JHEP **03**, 049 (2007) [arXiv:hep-ph/0604159 [hep-ph]].

[109] J. M. Cline and K. Kainulainen, "Electroweak baryogenesis at high bubble wall velocities," Phys. Rev. D **101**, no.6, 063525 (2020) [arXiv:2001.00568 [hep-ph]].

[110] M. Aoki, K. Enomoto, S. Kanemura, in preparation.

[111] S. L. Glashow, "Partial Symmetries of Weak Interactions," Nucl. Phys. **22**, 579-588 (1961).

[112] P. W. Higgs, "Broken symmetries, massless particles and gauge fields," Phys. Lett. **12**, 132-133 (1964); "Broken Symmetries and the Masses of Gauge Bosons," Phys. Rev. Lett. **13**, 508-509 (1964); "Spontaneous Symmetry Breakdown without Massless Bosons," Phys. Rev. **145**, 1156-1163 (1966).

[113] F. Englert and R. Brout, "Broken Symmetry and the Mass of Gauge Vector Mesons," Phys. Rev. Lett. **13**, 321-323 (1964)

[114] G. S. Guralnik, C. R. Hagen and T. W. B. Kibble, "Global Conservation Laws and Massless Particles," Phys. Rev. Lett. **13**, 585-587 (1964)

[115] Y. Nambu, "Quasiparticles and Gauge Invariance in the Theory of Superconductivity," Phys. Rev. **117**, 648-663 (1960)

[116] J. Goldstone, "Field Theories with Superconductor Solutions," Nuovo Cim. **19**, 154-164 (1961)

[117] Y. Nambu and G. Jona-Lasinio, "Dynamical Model of Elementary Particles Based on an Analogy with Superconductivity. 1.," Phys. Rev. **122**, 345-358 (1961); "Dynamical Model of Elementary Particles Based on an Analogy with Superconductivity. 2.," Phys. Rev. **124**, 246-254 (1961).

[118] J. Goldstone, A. Salam and S. Weinberg, "Broken Symmetries," Phys. Rev. **127**, 965-970 (1962)

[119] H. Watanabe and H. Murayama, "Unified Description of Nambu-Goldstone Bosons without Lorentz Invariance," Phys. Rev. Lett. **108**, 251602 (2012) [arXiv:1203.0609 [hep-th]].

[120] Y. Hidaka, "Counting rule for Nambu-Goldstone modes in nonrelativistic systems," Phys. Rev. Lett. **110**, no.9, 091601 (2013) [arXiv:1203.1494 [hep-th]].

[121] See, for example, S. Weinberg, "Quantum theory of fields II", Cambridge University Press.

[122] See, for example, R. N. Mohapatra, P. B. Pal, "Massive neutrinos in physics and astrophysics", World Scientific.

[123] N. Cabibbo, "Unitary Symmetry and Leptonic Decays," Phys. Rev. Lett. **10**, 531-533 (1963)

[124] M. Kobayashi and T. Maskawa, "CP Violation in the Renormalizable Theory of Weak Interaction," Prog. Theor. Phys. **49**, 652-657 (1973)

[125] S. L. Glashow, J. Iliopoulos and L. Maiani, "Weak Interactions with Lepton-Hadron Symmetry," Phys. Rev. D **2**, 1285-1292 (1970)

[126] C. Jarlskog, "A Basis Independent Formulation of the Connection Between Quark Mass Matrices, CP Violation and Experiment," Z. Phys. C **29**, 491-497 (1985); "Commutator of the Quark Mass Matrices in the Standard Electroweak Model and a Measure of Maximal CP Violation," Phys. Rev. Lett. **55**, 1039 (1985).

[127] P. H. Frampton and C. Jarlskog, "Systematics of Quark Mass Matrices in the Standard Electroweak Model," Phys. Lett. B **154**, 421-424 (1985)

[128] A. E. Nelson, D. B. Kaplan and A. G. Cohen, Nucl. Phys. B **373**, 453-478 (1992) doi:10.1016/0550-3213(92)90440-M

[129] K. Funakubo, "CP violation and baryogenesis at the electroweak phase transition," Prog. Theor. Phys. **96**, 475-520 (1996) [arXiv:hep-ph/9608358 [hep-ph]].

[130] G. R. Farrar and M. E. Shaposhnikov, Phys. Rev. Lett. **70**, 2833-2836 (1993) [erratum: Phys. Rev. Lett. **71**, 210 (1993)] [arXiv:hep-ph/9305274 [hep-ph]]; Phys. Rev. D **50**, 774 (1994) [arXiv:hep-ph/9305275 [hep-ph]].

[131] D. A. Kirzhnits and A. D. Linde, "Macroscopic Consequences of the Weinberg Model," Phys. Lett. B **42**, 471-474 (1972)

[132] L. Dolan and R. Jackiw, "Symmetry Behavior at Finite Temperature," Phys. Rev. D **9**, 3320-3341 (1974)

[133] S. Weinberg, "Gauge and Global Symmetries at High Temperature," Phys. Rev. D **9**, 3357-3378 (1974)

[134] M. E. Carrington, "The Effective potential at finite temperature in the Standard Model," Phys. Rev. D **45**, 2933-2944 (1992)

[135] P. Meade and H. Ramani, "Unrestored Electroweak Symmetry," Phys. Rev. Lett. **122**, no.4, 041802 (2019) [arXiv:1807.07578 [hep-ph]].

[136] I. Baldes and G. Servant, “High scale electroweak phase transition: baryogenesis \& symmetry non-restoration,” JHEP **10**, 053 (2018) [arXiv:1807.08770 [hep-ph]].

[137] M. Carena, C. Krause, Z. Liu and Y. Wang, “New approach to electroweak symmetry nonrestoration,” Phys. Rev. D **104**, no.5, 055016 (2021) [arXiv:2104.00638 [hep-ph]].

[138] W. Chao, H. K. Guo and X. F. Li, “First Order Color Symmetry Breaking and Restoration Triggered by Electroweak Symmetry Non-restoration,” [arXiv:2112.13580 [hep-ph]].

[139] M. Dine, R. G. Leigh, P. Y. Huet, A. D. Linde and D. A. Linde, “Towards the theory of the electroweak phase transition,” Phys. Rev. D **46**, 550-571 (1992) [arXiv:hep-ph/9203203 [hep-ph]].

[140] S. Kanemura, S. Kiyoura, Y. Okada, E. Senaha and C. P. Yuan, “New physics effect on the Higgs selfcoupling,” Phys. Lett. B **558**, 157-164 (2003) [arXiv:hep-ph/0211308 [hep-ph]].

[141] S. Kanemura, Y. Okada, E. Senaha and C. P. Yuan, “Higgs coupling constants as a probe of new physics,” Phys. Rev. D **70**, 115002 (2004) [arXiv:hep-ph/0408364 [hep-ph]].

[142] J. Braathen and S. Kanemura, “On two-loop corrections to the Higgs trilinear coupling in models with extended scalar sectors,” Phys. Lett. B **796**, 38-46 (2019) [arXiv:1903.05417 [hep-ph]]; “Leading two-loop corrections to the Higgs boson self-couplings in models with extended scalar sectors,” Eur. Phys. J. C **80**, no.3, 227 (2020) [arXiv:1911.11507 [hep-ph]].

[143] S. Kanemura, Y. Okada and E. Senaha, “Electroweak baryogenesis and quantum corrections to the triple Higgs boson coupling,” Phys. Lett. B **606**, 361-366 (2005) [arXiv:hep-ph/0411354 [hep-ph]].

[144] J. M. Cline and K. Kainulainen, “A New source for electroweak baryogenesis in the MSSM,” Phys. Rev. Lett. **85**, 5519-5522 (2000) [arXiv:hep-ph/0002272 [hep-ph]].

[145] G. D. Moore, “Sphaleron rate in the symmetric electroweak phase,” Phys. Rev. D **62**, 085011 (2000) [arXiv:hep-ph/0001216 [hep-ph]].

[146] B. Pontecorvo, “Mesonium and anti-mesonium,” Sov. Phys. JETP **6**, 429 (1957); “Inverse beta processes and nonconservation of lepton charge,” Zh. Eksp. Teor. Fiz. **34**, 247 (1957); “Neutrino Experiments and the Problem of Conservation of Leptonic Charge,” Zh. Eksp. Teor. Fiz. **53**, 1717-1725 (1967).

[147] Z. Maki, M. Nakagawa and S. Sakata, “Remarks on the unified model of elementary particles,” Prog. Theor. Phys. **28**, 870-880 (1962).

[148] S. M. Bilenky and S. T. Petcov, “Massive Neutrinos and Neutrino Oscillations,” Rev. Mod. Phys. **59**, 671 (1987) [erratum: Rev. Mod. Phys. **61**, 169 (1989); erratum: Rev. Mod. Phys. **60**, 575-575 (1988)].

[149] A. Gando *et al.* [KamLAND-Zen], "Search for Majorana Neutrinos near the Inverted Mass Hierarchy Region with KamLAND-Zen," Phys. Rev. Lett. **117**, no.8, 082503 (2016) [arXiv:1605.02889 [hep-ex]].

[150] P. Sikivie, L. Susskind, M. B. Voloshin and V. I. Zakharov, "Isospin Breaking in Technicolor Models," Nucl. Phys. B **173**, 189-207 (1980)

[151] H. E. Haber and A. Pomarol, "Constraints from global symmetries on radiative corrections to the Higgs sector," Phys. Lett. B **302**, 435-441 (1993) [arXiv:hep-ph/9207267 [hep-ph]].

[152] A. Pomarol and R. Vega, "Constraints on CP violation in the Higgs sector from the rho parameter," Nucl. Phys. B **413**, 3-15 (1994) [arXiv:hep-ph/9305272 [hep-ph]].

[153] J. M. Gerard and M. Herquet, "A Twisted custodial symmetry in the two-Higgs-doublet model," Phys. Rev. Lett. **98**, 251802 (2007) [arXiv:hep-ph/0703051 [hep-ph]].

[154] H. E. Haber and D. O'Neil, "Basis-independent methods for the two-Higgs-doublet model III: The CP-conserving limit, custodial symmetry, and the oblique parameters S, T, U," Phys. Rev. D **83**, 055017 (2011) [arXiv:1011.6188 [hep-ph]].

[155] B. Grzadkowski, M. Maniatis and J. Wudka, "The bilinear formalism and the custodial symmetry in the two-Higgs-doublet model," JHEP **11**, 030 (2011) [arXiv:1011.5228 [hep-ph]].

[156] M. Aiko and S. Kanemura, "New scenario for aligned Higgs couplings originated from the twisted custodial symmetry at high energies," JHEP **02**, 046 (2021) [arXiv:2009.04330 [hep-ph]].

[157] S. Kanemura, T. Kasai, G. L. Lin, Y. Okada, J. J. Tseng and C. P. Yuan, "Phenomenology of Higgs bosons in the Zee model," Phys. Rev. D **64**, 053007 (2001) [arXiv:hep-ph/0011357 [hep-ph]].

[158] L. Wolfenstein, "A Theoretical Pattern for Neutrino Oscillations," Nucl. Phys. B **175**, 93-96 (1980)

[159] V. D. Barger, J. L. Hewett and R. J. N. Phillips, "New Constraints on the Charged Higgs Sector in Two Higgs Doublet Models," Phys. Rev. D **41**, 3421-3441 (1990)

[160] Y. Grossman, "Phenomenology of models with more than two Higgs doublets," Nucl. Phys. B **426**, 355-384 (1994) [arXiv:hep-ph/9401311 [hep-ph]].

[161] M. Aoki, S. Kanemura, K. Tsumura and K. Yagyu, "Models of Yukawa interaction in the two Higgs doublet model, and their collider phenomenology," Phys. Rev. D **80**, 015017 (2009) [arXiv:0902.4665 [hep-ph]].

[162] K. Cheung and O. Seto, "Phenomenology of TeV right-handed neutrino and the dark matter model," Phys. Rev. D **69**, 113009 (2004) [arXiv:hep-ph/0403003 [hep-ph]].

[163] F. Zwicky, "Die Rotverschiebung von extragalaktischen Nebeln," Helv. Phys. Acta **6**, 110-127 (1933)

[164] E. Kolb, M. Turner, "The Early Universe", CRC press.

[165] S. Davidson and H. E. Haber, "Basis-independent methods for the two-Higgs-doublet model," Phys. Rev. D **72**, 035004 (2005) [erratum: Phys. Rev. D **72**, 099902 (2005)] [arXiv:hep-ph/0504050 [hep-ph]].

[166] A. G. Akeroyd, M. Aoki, A. Arhrib, L. Basso, I. F. Ginzburg, R. Guedes, J. Hernandez-Sanchez, K. Huitu, T. Hurth and M. Kadastik, *et al.* "Prospects for charged Higgs searches at the LHC," Eur. Phys. J. C **77**, no.5, 276 (2017) [arXiv:1607.01320 [hep-ph]].

[167] A. Arbey, F. Mahmoudi, O. Stal and T. Stefaniak, "Status of the Charged Higgs Boson in Two Higgs Doublet Models," Eur. Phys. J. C **78**, no.3, 182 (2018) [arXiv:1706.07414 [hep-ph]].

[168] G. Abbiendi *et al.* [ALEPH, DELPHI, L3, OPAL and LEP], "Search for Charged Higgs bosons: Combined Results Using LEP Data," Eur. Phys. J. C **73**, 2463 (2013) [arXiv:1301.6065 [hep-ex]].

[169] D. de Florian *et al.* [LHC HiAiggs Cross Section Working Group], "Handbook of LHC Higgs Cross Sections: 4. Deciphering the Nature of the Higgs Sector," [arXiv:1610.07922 [hep-ph]].

[170] A. M. Sirunyan *et al.* [CMS], "Search for charged Higgs bosons in the $\mathrm{H}^{\pm} \to \tau^{\pm}\nu_{\tau}$ decay channel in proton-proton collisions at $\sqrt{s} = 13$ TeV," JHEP **07**, 142 (2019) [arXiv:1903.04560 [hep-ex]].

[171] G. Aad *et al.* [ATLAS], "Search for charged Higgs bosons decaying into a top quark and a bottom quark at $\sqrt{\mathrm{s}} = 13$ TeV with the ATLAS detector," JHEP **06**, 145 (2021) [arXiv:2102.10076 [hep-ex]].

[172] M. Aaboud *et al.* [ATLAS], "Search for heavy particles decaying into top-quark pairs using lepton-plus-jets events in proton–proton collisions at $\sqrt{s} = 13$ TeV with the ATLAS detector," Eur. Phys. J. C **78**, no.7, 565 (2018) [arXiv:1804.10823 [hep-ex]].

[173] G. Aad *et al.* [ATLAS], "Search for heavy Higgs bosons decaying into two tau leptons with the ATLAS detector using *pp* collisions at $\sqrt{s} = 13$ TeV," Phys. Rev. Lett. **125**, no.5, 051801 (2020) [arXiv:2002.12223 [hep-ex]].

[174] T. Enomoto and R. Watanabe, "Flavor constraints on the Two Higgs Doublet Models of $\mathrm{Z}_2$ symmetric and aligned types," JHEP **05**, 002 (2016) [arXiv:1511.05066 [hep-ph]].

[175] J. Haller, A. Hoecker, R. Kogler, K. Mönig, T. Peiffer and J. Stelzer, "Update of the global electroweak fit and constraints on two-Higgs-doublet models," Eur. Phys. J. C **78**, no.8, 675 (2018) [arXiv:1803.01853 [hep-ph]].

[176] V. Khachatryan *et al.* [CMS and LHCb], "Observation of the rare $B_s^0 \to \mu^+\mu^-$ decay from the combined analysis of CMS and LHCb data," Nature **522**, 68-72 (2015) [arXiv:1411.4413 [hep-ex]].

[177] R. Aaij *et al.* [LHCb], "Measurement of the $B_s^0 \to \mu^+\mu^-$ branching fraction and effective lifetime and search for $B^0 \to \mu^+\mu^-$ decays," Phys. Rev. Lett. **118**, no.19, 191801 (2017) [arXiv:1703.05747 [hep-ex]].

[178] V. Andreev *et al.* [ACME], "Improved limit on the electric dipole moment of the electron," Nature **562**, no.7727, 355-360 (2018)

[179] M. Jung and A. Pich, "Electric Dipole Moments in Two-Higgs-Doublet Models," JHEP **04**, 076 (2014) [arXiv:1308.6283 [hep-ph]].

[180] K. Cheung, J. S. Lee, E. Senaha and P. Y. Tseng, "Confronting Higgcision with Electric Dipole Moments," JHEP **06**, 149 (2014) [arXiv:1403.4775 [hep-ph]].

[181] S. M. Barr and A. Zee, "Electric Dipole Moment of the Electron and of the Neutron," Phys. Rev. Lett. **65**, 21-24 (1990) [erratum: Phys. Rev. Lett. **65**, 2920 (1990)]

[182] C. Abel *et al.* [nEDM], "Measurement of the permanent electric dipole moment of the neutron," Phys. Rev. Lett. **124**, no.8, 081803 (2020) [arXiv:2001.11966 [hep-ex]].

[183] M. Pospelov and A. Ritz, "Neutron EDM from electric and chromoelectric dipole moments of quarks," Phys. Rev. D **63**, 073015 (2001) [arXiv:hep-ph/0010037 [hep-ph]].

[184] J. Hisano, J. Y. Lee, N. Nagata and Y. Shimizu, "Reevaluation of Neutron Electric Dipole Moment with QCD Sum Rules," Phys. Rev. D **85**, 114044 (2012) [arXiv:1204.2653 [hep-ph]].

[185] K. Fuyuto, J. Hisano, N. Nagata and K. Tsumura, "QCD Corrections to Quark (Chromo)Electric Dipole Moments in High-scale Supersymmetry," JHEP **12**, 010 (2013) [arXiv:1308.6493 [hep-ph]].

[186] T. Abe, J. Hisano, T. Kitahara and K. Tobioka, "Gauge invariant Barr-Zee type contributions to fermionic EDMs in the two-Higgs doublet models," JHEP **01**, 106 (2014) [erratum: JHEP **04**, 161 (2016)] [arXiv:1311.4704 [hep-ph]].

[187] S. Weinberg, "Larger Higgs Exchange Terms in the Neutron Electric Dipole Moment," Phys. Rev. Lett. **63**, 2333 (1989)

[188] D. A. Dicus, "Neutron Electric Dipole Moment From Charged Higgs Exchange," Phys. Rev. D **41**, 999 (1990)

[189] V. M. Khatsimovsky, I. B. Khriplovich and A. S. Yelkhovsky, "Neutron Electric Dipole Moment, $T$ Odd Nuclear Forces and Nature of CP Violation," Annals Phys. **186**, 1-14 (1988)

[190] M. E. Peskin and T. Takeuchi, “A New constraint on a strongly interacting Higgs sector,” Phys. Rev. Lett. **65**, 964-967 (1990); “Estimation of oblique electroweak corrections,” Phys. Rev. D **46**, 381-409 (1992).

[191] S. Kanemura, T. Kubota and E. Takasugi, “Lee-Quigg-Thacker bounds for Higgs boson masses in a two doublet model,” Phys. Lett. B **313**, 155-160 (1993) [arXiv:hep-ph/9303263 [hep-ph]].

[192] A. G. Akeroyd, A. Arhrib and E. M. Naimi, “Note on tree level unitarity in the general two Higgs doublet model,” Phys. Lett. B **490**, 119-124 (2000) [arXiv:hep-ph/0006035 [hep-ph]].

[193] I. F. Ginzburg and I. P. Ivanov, “Tree-level unitarity constraints in the most general 2HDM,” Phys. Rev. D **72**, 115010 (2005) [arXiv:hep-ph/0508020 [hep-ph]].

[194] S. Kanemura and K. Yagyu, “Unitarity bound in the most general two Higgs doublet model,” Phys. Lett. B **751**, 289-296 (2015) [arXiv:1509.06060 [hep-ph]].

[195] S. Nie and M. Sher, “Vacuum stability bounds in the two Higgs doublet model,” Phys. Lett. B **449**, 89-92 (1999) [arXiv:hep-ph/9811234 [hep-ph]].

[196] S. Kanemura, T. Kasai and Y. Okada, “Mass bounds of the lightest CP even Higgs boson in the two Higgs doublet model,” Phys. Lett. B **471**, 182-190 (1999) [arXiv:hep-ph/9903289 [hep-ph]].

[197] P. M. Ferreira, R. Santos and A. Barroso, “Stability of the tree-level vacuum in two Higgs doublet models against charge or CP spontaneous violation,” Phys. Lett. B **603**, 219-229 (2004) [erratum: Phys. Lett. B **629**, 114-114 (2005)] [arXiv:hep-ph/0406231 [hep-ph]].

[198] S. R. Coleman and E. J. Weinberg, “Radiative Corrections as the Origin of Spontaneous Symmetry Breaking,” Phys. Rev. D **7**, 1888-1910 (1973)

[199] S. Baum, M. Carena, N. R. Shah, C. E. M. Wagner and Y. Wang, “Nucleation is more than critical: A case study of the electroweak phase transition in the NMSSM,” JHEP **03**, 055 (2021) [arXiv:2009.10743 [hep-ph]].

[200] R. R. Parwani, “Resummation in a hot scalar field theory,” Phys. Rev. D **45**, 4695 (1992) [erratum: Phys. Rev. D **48**, 5965 (1993)] [arXiv:hep-ph/9204216 [hep-ph]].

[201] L. D. McLerran, E. Mottola and M. E. Shaposhnikov, “Sphalerons and Axion Dynamics in High Temperature QCD,” Phys. Rev. D **43**, 2027-2035 (1991)

[202] G. F. Giudice and M. E. Shaposhnikov, “Strong sphalerons and electroweak baryogenesis,” Phys. Lett. B **326**, 118-124 (1994) [arXiv:hep-ph/9311367 [hep-ph]].

[203] C. L. Wainwright, “CosmoTransitions: Computing Cosmological Phase Transition Temperatures and Bubble Profiles with Multiple Fields,” Comput. Phys. Commun. **183**, 2006-2013 (2012) [arXiv:1109.4189 [hep-ph]].

[204] G. D. Moore, "Computing the strong sphaleron rate," Phys. Lett. B **412**, 359-370 (1997) [arXiv:hep-ph/9705248 [hep-ph]].

[205] P. Huet and A. E. Nelson, "Electroweak baryogenesis in supersymmetric models," Phys. Rev. D **53**, 4578-4597 (1996) [arXiv:hep-ph/9506477 [hep-ph]].

[206] J. M. Cline and B. Laurent, "Electroweak baryogenesis from light fermion sources: A critical study," Phys. Rev. D **104**, no.8, 083507 (2021) [arXiv:2108.04249 [hep-ph]].

[207] M. Cepeda, S. Gori, P. Ilten, M. Kado, F. Riva, R. Abdul Khalek, A. Aboubrahim, J. Alimena, S. Alioli and A. Alves, *et al.* "Report from Working Group 2: Higgs Physics at the HL-LHC and HE-LHC," CERN Yellow Rep. Monogr. **7**, 221-584 (2019) [arXiv:1902.00134 [hep-ph]].

[208] K. Fujii, C. Grojean, M. E. Peskin, T. Barklow, Y. Gao, S. Kanemura, H. D. Kim, J. List, M. Nojiri and M. Perelstein, *et al.* "Physics Case for the International Linear Collider," [arXiv:1506.05992 [hep-ex]].

[209] P. Bambade, T. Barklow, T. Behnke, M. Berggren, J. Brau, P. Burrows, D. Denisov, A. Faus-Golfe, B. Foster and K. Fujii, *et al.* "The International Linear Collider: A Global Project," [arXiv:1903.01629 [hep-ex]].

[210] P. N. Burrows *et al.* [CLICdp and CLIC], "The Compact Linear Collider (CLIC) - 2018 Summary Report," [arXiv:1812.06018 [physics.acc-ph]].

[211] J. W. Martin, "Current status of neutron electric dipole moment experiments," J. Phys. Conf. Ser. **1643**, no.1, 012002 (2020)

[212] D. J. H. Chung, B. Garbrecht, M. J. Ramsey-Musolf and S. Tulin, "Lepton-mediated electroweak baryogenesis," Phys. Rev. D **81**, 063506 (2010) [arXiv:0905.4509 [hep-ph]].

[213] J. De Vries, M. Postma and J. van de Vis, "The role of leptons in electroweak baryogenesis," JHEP **04**, 024 (2019) [arXiv:1811.11104 [hep-ph]].

[214] K. P. Xie, "Lepton-mediated electroweak baryogenesis, gravitational waves and the $4\tau$ final state at the collider," JHEP **02**, 090 (2021) [arXiv:2011.04821 [hep-ph]].

[215] K. Enomoto, S. Kanemura and Y. Mura, work in progress.

[216] A. Riotto, "Towards a nonequilibrium quantum field theory approach to electroweak baryogenesis," Phys. Rev. D **53**, 5834-5841 (1996) [arXiv:hep-ph/9510271 [hep-ph]]; "Supersymmetric electroweak baryogenesis, nonequilibrium field theory and quantum Boltzmann equations," Nucl. Phys. B **518**, 339-360 (1998) [arXiv:hep-ph/9712221 [hep-ph]].

[217] E. Kou *et al.* [Belle-II], "The Belle II Physics Book," PTEP **2019**, no.12, 123C01 (2019) [erratum: PTEP **2020**, no.2, 029201 (2020)] [arXiv:1808.10567 [hep-ex]].

[218] R. Aaij *et al.* [LHCb], "Implications of LHCb measurements and future prospects," Eur. Phys. J. C **73**, no.4, 2373 (2013) [arXiv:1208.3355 [hep-ex]].

[219] M. Benzke, S. J. Lee, M. Neubert and G. Paz, "Long-Distance Dominance of the CP Asymmetry in $B \to X_{s,d} + \gamma$ Decays," Phys. Rev. Lett. **106**, 141801 (2011) [arXiv:1012.3167 [hep-ph]].

[220] S. Watanuki *et al.* [Belle], "Measurements of isospin asymmetry and difference of direct $CP$ asymmetries in inclusive $B \to X_s\gamma$ decays," Phys. Rev. D **99**, no.3, 032012 (2019) [arXiv:1807.04236 [hep-ex]].

[221] D. Jeans and G. W. Wilson, "Measuring the CP state of tau lepton pairs from Higgs decay at the ILC," Phys. Rev. D **98**, no.1, 013007 (2018) [arXiv:1804.01241 [hep-ex]].

[222] O. J. P. Eboli, G. C. Marques, S. F. Novaes and A. A. Natale, "TWIN HIGGS BOSON PRODUCTION," Phys. Lett. B **197**, 269-272 (1987)

[223] D. A. Dicus, C. Kao and S. S. D. Willenbrock, "Higgs Boson Pair Production From Gluon Fusion," Phys. Lett. B **203**, 457-461 (1988)

[224] E. W. N. Glover and J. J. van der Bij, "HIGGS BOSON PAIR PRODUCTION VIA GLUON FUSION," Nucl. Phys. B **309**, 282-294 (1988)

[225] T. Plehn, M. Spira and P. M. Zerwas, "Pair production of neutral Higgs particles in gluon-gluon collisions," Nucl. Phys. B **479**, 46-64 (1996) [erratum: Nucl. Phys. B **531**, 655-655 (1998)] [arXiv:hep-ph/9603205 [hep-ph]].

[226] A. Djouadi, W. Kilian, M. Muhlleitner and P. M. Zerwas, "Production of neutral Higgs boson pairs at LHC," Eur. Phys. J. C **10**, 45-49 (1999) [arXiv:hep-ph/9904287 [hep-ph]].

[227] X. Li and M. B. Voloshin, "Remarks on double Higgs boson production by gluon fusion at threshold," Phys. Rev. D **89**, no.1, 013012 (2014) [arXiv:1311.5156 [hep-ph]].

[228] D. Gonçalves, T. Han, F. Kling, T. Plehn and M. Takeuchi, "Higgs boson pair production at future hadron colliders: From kinematics to dynamics," Phys. Rev. D **97**, no.11, 113004 (2018) [arXiv:1802.04319 [hep-ph]].

[229] E. Asakawa, D. Harada, S. Kanemura, Y. Okada and K. Tsumura, "Higgs boson pair production in new physics models at hadron, lepton, and photon colliders," Phys. Rev. D **82**, 115002 (2010) [arXiv:1009.4670 [hep-ph]].

[230] R. Apreda, M. Maggiore, A. Nicolis and A. Riotto, "Gravitational waves from electroweak phase transitions," Nucl. Phys. B **631**, 342-368 (2002) [arXiv:gr-qc/0107033 [gr-qc]].

[231] C. Grojean and G. Servant, "Gravitational Waves from Phase Transitions at the Electroweak Scale and Beyond," Phys. Rev. D **75**, 043507 (2007) [arXiv:hep-ph/0607107 [hep-ph]].

[232] M. Kakizaki, S. Kanemura and T. Matsui, "Gravitational waves as a probe of extended scalar sectors with the first order electroweak phase transition," Phys. Rev. D **92**, no.11, 115007 (2015) [arXiv:1509.08394 [hep-ph]].

[233] P. Amaro-Seoane *et al.* [LISA], "Laser Interferometer Space Antenna," [arXiv:1702.00786 [astro-ph.IM]].

[234] N. Seto, S. Kawamura and T. Nakamura, "Possibility of direct measurement of the acceleration of the universe using 0.1-Hz band laser interferometer gravitational wave antenna in space," Phys. Rev. Lett. **87**, 221103 (2001) [arXiv:astro-ph/0108011 [astro-ph]].

[235] V. Corbin and N. J. Cornish, "Detecting the cosmic gravitational wave background with the big bang observer," Class. Quant. Grav. **23**, 2435-2446 (2006) [arXiv:gr-qc/0512039 [gr-qc]].

[236] G. Aad *et al.* [ATLAS], "Searches for electroweak production of supersymmetric particles with compressed mass spectra in $\sqrt{s} = 13$ TeV $pp$ collisions with the ATLAS detector," Phys. Rev. D **101**, no.5, 052005 (2020) [arXiv:1911.12606 [hep-ex]].

[237] G. Aad *et al.* [ATLAS], "Search for electroweak production of charginos and sleptons decaying into final states with two leptons and missing transverse momentum in $\sqrt{s} = 13$ TeV $pp$ collisions using the ATLAS detector," Eur. Phys. J. C **80**, no.2, 123 (2020) [arXiv:1908.08215 [hep-ex]].

[238] G. Aad *et al.* [ATLAS], "Search for direct stau production in events with two hadronic $\tau$-leptons in $\sqrt{s} = 13$ TeV $pp$ collisions with the ATLAS detector," Phys. Rev. D **101**, no.3, 032009 (2020) [arXiv:1911.06660 [hep-ex]].

[239] A. M. Baldini *et al.* [MEG], "Search for the lepton flavour violating decay $\mu^+ \to \mathrm{e}^+\gamma$ with the full dataset of the MEG experiment," Eur. Phys. J. C **76**, no.8, 434 (2016) [arXiv:1605.05081 [hep-ex]].

[240] B. Aubert *et al.* [BaBar], "Searches for Lepton Flavor Violation in the Decays tau+- $\to$ e+- gamma and tau+- $\to$ mu+- gamma," Phys. Rev. Lett. **104**, 021802 (2010) [arXiv:0908.2381 [hep-ex]].

[241] U. Bellgardt *et al.* [SINDRUM], "Search for the Decay mu+ $\to$ e+ e+ e-," Nucl. Phys. B **299**, 1-6 (1988)

[242] K. Hayasaka, K. Inami, Y. Miyazaki, K. Arinstein, V. Aulchenko, T. Aushev, A. M. Bakich, A. Bay, K. Belous and V. Bhardwaj, *et al.* "Search for Lepton Flavor Violating Tau Decays into Three Leptons with 719 Million Produced Tau+Tau-Pairs," Phys. Lett. B **687**, 139-143 (2010) [arXiv:1001.3221 [hep-ex]].

[243] A. M. Sirunyan *et al.* [CMS], "Search for lepton flavour violating decays of the Higgs boson to $\mu\tau$ and $e\tau$ in proton-proton collisions at $\sqrt{s} = 13$ TeV," JHEP **06**, 001 (2018) [arXiv:1712.07173 [hep-ex]].

[244] V. Khachatryan *et al.* [CMS], "Search for lepton flavour violating decays of the Higgs boson to $e\tau$ and $e\mu$ in proton–proton collisions at $\sqrt{s} = 8$ TeV," Phys. Lett. B **763**, 472-500 (2016) [arXiv:1607.03561 [hep-ex]].

[245] W. H. Bertl *et al.* [SINDRUM II], "A Search for muon to electron conversion in muonic gold," Eur. Phys. J. C **47**, 337-346 (2006)

[246] M. Aoki, S. Kanemura, K. Sakurai and H. Sugiyama, "Testing neutrino mass generation mechanisms from the lepton flavor violating decay of the Higgs boson," Phys. Lett. B **763**, 352-357 (2016) [arXiv:1607.08548 [hep-ph]].

[247] M. Aoki, S. Kanemura and K. Yagyu, "Triviality and vacuum stability bounds in the three-loop neutrino mass model," Phys. Rev. D **83**, 075016 (2011) [arXiv:1102.3412 [hep-ph]].

[248] G. Passarino and M. J. G. Veltman, "One Loop Corrections for e+ e- Annihilation Into mu+ mu- in the Weinberg Model," Nucl. Phys. B **160**, 151-207 (1979)

[249] M. Srednicki, R. Watkins and K. A. Olive, "Calculations of Relic Densities in the Early Universe," Nucl. Phys. B **310**, 693 (1988)

[250] P. Gondolo and G. Gelmini, "Cosmic abundances of stable particles: Improved analysis," Nucl. Phys. B **360**, 145-179 (1991)

[251] H. Y. Cheng and C. W. Chiang, "Revisiting Scalar and Pseudoscalar Couplings with Nucleons," JHEP **07**, 009 (2012) [arXiv:1202.1292 [hep-ph]].

[252] E. Aprile *et al.* [XENON], "Dark Matter Search Results from a One Ton-Year Exposure of XENON1T," Phys. Rev. Lett. **121**, no.11, 111302 (2018) [arXiv:1805.12562 [astro-ph.CO]].

[253] A. M. Baldini *et al.* [MEG II], "The design of the MEG II experiment," Eur. Phys. J. C **78**, no.5, 380 (2018) [arXiv:1801.04688 [physics.ins-det]].

[254] A. Blondel, A. Bravar, M. Pohl, S. Bachmann, N. Berger, M. Kiehn, A. Schoning, D. Wiedner, B. Windelband and P. Eckert, *et al.* "Research Proposal for an Experiment to Search for the Decay $\mu \to eee$," [arXiv:1301.6113 [physics.ins-det]].

[255] K. Arndt *et al.* [Mu3e], "Technical design of the phase I Mu3e experiment," Nucl. Instrum. Meth. A **1014**, 165679 (2021) [arXiv:2009.11690 [physics.ins-det]].

[256] K. Abe *et al.* [Hyper-Kamiokande], "Hyper-Kamiokande Design Report," [arXiv:1805.04163 [physics.ins-det]].

[257] D. S. Akerib *et al.* [LZ], "LUX-ZEPLIN (LZ) Conceptual Design Report," [arXiv:1509.02910 [physics.ins-det]].

[258] J. Aalbers *et al.* [DARWIN], "DARWIN: towards the ultimate dark matter detector," JCAP **11**, 017 (2016) [arXiv:1606.07001 [astro-ph.IM]].

[259] J. R. Espinosa, M. Quiros and F. Zwirner, "On the nature of the electroweak phase transition," Phys. Lett. B **314**, 206-216 (1993) [arXiv:hep-ph/9212248 [hep-ph]].